STRENGTH AND DURABILITY PROPERTIES OF SELF-COMPACTING CONCRETE INCORPORATING COPPER SLAG

A Thesis
Submitted in fulfillment of the requirement
for the award of the degree of

DOCTOR OF PHILOSOPHY
IN
CIVIL ENGINEERING

by

NIKITA GUPTA
Registration No. 901702002

Under the Supervision of

DR. RAFAT SIDDIQUE
Senior Professor of Civil Engineering &
Dean, Research and Sponsored Projects

DEPARTMENT OF CIVIL ENGINEERING
THAPAR INSTITUTE OF ENGINEERING & TECHNOLOGY
PATIALA, PUNJAB (INDIA)
SEPTEMBER 2020

CERTIFICATE

This is to certify that thesis entitled, **"Strength and Durability Properties of Self-Compacting Concrete Incorporating Copper Slag"**, submitted by Miss Nikita Gupta in partial fulfillment of the requirements, for the award of degree of Doctor of Philosophy in Civil Engineering submitted in the Department of Civil Engineering, Thapar Institute of Engineering & Technology, Patiala, is a record of the candidate original research work carried out by her under the guidance and supervision. The matter embodied in this thesis has not been submitted in part or full to any other University or Institute for the award of any degree.

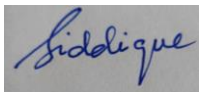

(Dr. Rafat Siddique)

Senior Professor of Civil Engineering &

Dean, Research and Sponsored Projects

Thapar Institute of Engineering & Technology Patiala-147004, India

DECLARATION

I hereby certify that the work which is being presented in the thesis entitled, **"Strength and Durability Properties of Self-Compacting Concrete Incorporating Copper Slag"** being in partial fulfillment of the requirements for the award of degree of Doctor of Philosophy in Civil Engineering submitted in the Department of Civil Engineering, Thapar Institute of Engineering & Technology, Patiala, is an authentic record of my own work carried out by me under the guidance of Dr. Rafat Siddique and refers other researcher's work duly listed in the reference section.

The matter presented in this thesis has not been submitted in part or full to any other University or Institute for the award of any degree in India or Abroad.

(Nikita Gupta)

ACKNOWLEDGEMENT

- Foremost, I thank the almighty whose blessing have enabled me to accomplish this research work.
- I would like to express my sincere gratitude to my advisor Dr. Rafat Siddique, Sr. Professor, Department of Civil Engineering & DRSP, Thapar Institute of Engineering & Technology, Patiala for his invaluable guidance, moral support, and encouragement throughout my Ph.D. journey. I could not have imagined having a better advisor and mentor.
- I would like to extend my acknowledgement to my advisory committee members Dr. Shweta Goyal, Dr. Shruti Sharma, Dr. Puneet Sharma, and Dr. A.B. Danie Roy for their valuable suggestions and feedback. The inputs provided by Dr. Prem Pal Bansal, Head, Department of Civil Engineering, his interest and critical appraisal during the early stage of this research are invaluable. I would like express my gratitude to Dr. Kulvir Singh for his guidance and valuable suggestions.
- The help and support provided by technical staff Er. Varinder Sharma and Mr. Ram Sumiran during the entire research period are greatly appreciated. I am grateful to Er. M.P Singh, Assistant Engineer, Er. Gagan, Senior Section Engineer for their help and support.
- I would like thank my sister Dr. Ankita Gupta for helping me in the statistical analysis of my research.
- I am grateful to my senior research fellow Dr. Ashutosh, Dr. Malkit Singh and Mr. Kirti for their help and encouragement throughout the research period.
- I also acknowledge the support of SAIF Facility, Punjab University and SAI labs, Thapar Institute of Engineering & Technology, Patiala for SEM and XRD analysis.
- Special thanks to my father Mr. Ashok K Gupta, my mother Mrs. Neena Gupta and my brother Mr. Devansh Gupta for their patience, understanding and constant support during the whole research program.

(Nikita Gupta)

PUBLICATIONS

Research Publications

1. Gupta, N., and Siddique, R. Sulfate Resistance and Drying Shrinkage of Self-Compacting Concrete incorporating Copper Slag. **Journal of Materials in Civil Engineering (ASCE). 2020. DOI: 10.1061/(ASCE)MT.1943-5533.0003501.**

2. Gupta, N., and Siddique, R. Durability characteristics of self-compacting concrete made with copper slag**. Construction and Building Materials (Elsevier), Vol. 247, June 2020, Pages 118580.**

3. Gupta, N., and Siddique, R. Strength and micro-structural properties of self-compacting concrete incorporating copper slag. **Construction and Building Materials (Elsevier), Vol. 224, November 2019, Pages 894-908**.

4. Gupta, N., Siddique, R. and Belarbi, R. Sustainable and Greener Self-Compacting Concrete incorporating Industrial By-Products: A Review. **Journal of Cleaner Production. 2020 (Accepted).**

Conference Publications

1. Gupta, N., and Siddique, R. Utilization of Copper Slag in Self-compacting Concrete-Strength and Permeation Properties. In Rheology and Processing of Construction Materials. 2019. pp. 544-551. Springer, Cham **(Paper Presented).**

2. Gupta, N., and Siddique, R. Utilization of Industrial By-Products in Self-Compacting Concrete. The 34th International Conference on Solid Waste Technology and Management, Annapolis (Washington, D.C. Area) U.S.A., March 31- April 3, 2019 **(Paper Accepted).**

3. Gupta, N., and Siddique, R. Utilization of Copper Slag in Self-Compacting Concrete: An Overview. 10th International Concrete Congress, Bursa, Turkey, May 2-4, 2019 **(Paper Presented).**

ABSTRACT

Copper manufacturing industry produces abundant quantity of copper slag as an industrial by-product. Its management and disposal poses a major challenge for the environment, thus an urgent need for its potential alternative is recommended. Also, the high excavation cost of natural sand, its scarcity in the environment along with its ever increasing demand has urged the concrete industry to look for some low-cost and abundantly available alternatives. A sustainable approach is required to conserve the environment as well preserve the natural resources at the same time. The consumption of copper slag as sand replacement in concrete serves to be a viable option for progressing towards a sustainable development.

The intent of the current research work is to design self-compacting concrete (SCC) mixes incorporating copper slag as fine aggregate replacement. SCC mixes were designed to have 28 days compressive strength in the range of 20-40 MPa. SCC mixes incorporated 20% fly ash as cement substitution and copper slag varying from 0% to 60% as sand replacement. A total of seven SCC mixes were developed- 0CS-SCC, 10CS-SCC, 20CS-SCC, 30CS-SCC, 40CS-SCC, 50CS-SCC and 60CS-SCC. 0CS-SCC mix was developed with 0% copper slag, 10CS-SCC for SCC mix with 10% copper slag, 20CS-SCC for SCC mix with 20% copper slag, 30CS-SCC for SCC mix with 30% copper slag, 40CS-SCC for SCC mix with 40% copper slag, 50CS-SCC for SCC mix with 50% copper slag, and 60CS-SCC for SCC mix with 60% copper slag. The fresh properties included the slump flow, V-funnel, L-box, U-box and sieve segregation resistance of SCC. The strength properties included the compressive strength and splitting tensile strength of SCC. The durability properties included the water absorption, sorptivity, chloride ion permeability, drying shrinkage and sulfate resistance of SCC made with copper slag. The strength and durability properties of SCC were performed and analysed for up to one year. The microstructural analysis included Scanning electron microscopy (SEM), Energy dispersive spectroscopy (EDS) and X-ray diffraction (XRD) of SCC mixes at all ages of curing. Statistical analysis was conducted to study the correlations amongst various properties of SCC. The statistical significance of the strength and durability properties was evaluated using Analysis of Variance (ANOVA). Multiple

comparison analysis was conducted to compare different SCC mixes using the Post Hoc Tukey test.

Test results indicated that all the mixes were in good accordance with the classifications prescribed in the European code. Copper slag was effective in enhancing the filling ability, viscosity, passing ability and sieve segregation resistance of SCC mixes. The compressive strength of SCC mixes incorporating up to 60% copper slag showed almost similar/higher results in comparison with a concrete mix containing 100% sand. The strength of SCC mixes increased with the increase in curing age. The 28 days compressive strength of SCC mix incorporating 10, 20, 30, 40 and 50% copper slag achieved 6.97, 8.19, 4.20, 0.97 and 0.04% higher compressive strength as compared to control SCC mix (35.63 MPa). An insignificant decrease of 0.09% was observed in SCC mix with 60% copper slag in comparison to control SCC mix at 28 days. The splitting tensile strength of SCC mixes increased with the increase of copper slag content from 0 to 60% and also with the increase in curing age. At 28, 90 and 365 days, splitting tensile strength of SCC mixes with copper slag (0 to 60%) increased from 2.56 to 3.43, 3.65 to 4.23, 3.86 to 4.47 MPa as compared to 2.13, 3.11 and 3.42 MPa, respectively, of control mix without slag.

A reduction in water absorption and volume of permeable voids was obtained in SCC mixes incorporating up to 60% copper slag. With age, reduction in water absorption and volume of permeable voids was significantly achieved. Incorporation of copper slag up to 60% exhibited reduced sorptivity values of SCC mixes up to 365 days. SCC mixes incorporating copper slag showed improved resistance to chloride ion permeability. The drying shrinkage of SCC mixes decreased on the addition of copper slag up to 60% at all curing ages. Even after one year of sulfate exposure to SCC mixes, no major catastrophic damage was visible. Copper slag was successful in improving the overall sulfate resistance of SCC mixes. The microstructure of SCC incorporating up to 60% copper slag showed the formation of calcium silicate hydrate layers under SEM analysis giving the concrete matrix a denser and homogenous structure. SCC mixes showed a crystalline behaviour up to 365 days. No major phase change was indicated while increasing the percentages of copper slag in SCC.

CONTENTS

LIST OF FIGURES

LIST OF TABLES

LIST OF UNITS

Units		**Word(s)**
Kg	-	Kilogram
g	-	Gram
mg	-	Milligram
˚C	-	Degree Celsius
˚/sec	-	Degree per second
%	-	Percentage
m	-	Meter
cm	-	Centimeter
mm	-	Millimeter
µm	-	Micrometer
mA	-	Milliampere
N	-	Newton
MPa	-	Mega Pascal
GPa	-	Giga Pascal
Kg/m^3	-	Kilogram per cubic meter
cm^2/g	-	Centimeter square per gram
m^2/kg	-	Meter square per kilogram
N/mm^2	-	Newton per square millimeter
$litres/m^3$	-	Litres per cubic meter
kN	-	Kilo Newton
kV	-	Kilovolt
hr	-	Hour
min	-	Minute

sec	-	Second
m/s	-	Meter per second
km/s	-	Kilometer per second
θ	-	Theta
W/m.K	-	Watts per meter-kelvin
$mm/sec^{1/2}$	-	Millimeter per square root of second
Å	-	Angstrom

ABBREVIATIONS

Abbreviations		Word(s)
A	-	Anorthite
AASC	-	Alkali-Activated Slag Concrete
ACI	-	American Concrete Institute
Alb	-	Albite
ANOVA	-	Analysis of Variance
ASH	-	Aluminium Silicate Hydrate
ASTM	-	American Society for Testing Materials
BIS	-	Bureau of Indian Standards
C	-	Calcium Hydroxide
CA	-	Coarse Aggregate
CaS	-	Calcium Silicate
CBA	-	Coal Bottom Ash
CI	-	Calcium Iron Oxide
CRTG	-	Cathode Ray Tube Funnel Glass
CS	-	Copper Slag
CSH	-	Calcium Silicate Hydrate
EDS	-	Energy Dispersive X-ray Spectroscopy
EFNARC	-	European Federation of Specialist Construction Chemicals and Concrete Systems
F	-	Hematite
FESEM	-	Field Emission Scanning Electron Microscopy

$\bar{F}$	-	Magnetite
G	-	Gismondine
H	-	Hedenbergite
Ha	-	Halloysite
HCL	-	Hindustan Copper Limited
HS	-	Hydrogen Silicate Hydrate
IS	-	Iron Silicon
JCPD	-	Joint Committee of Powder Diffraction Standards
L	-	Laumontite
M	-	Muscovite
OPC	-	Ordinary Portland Cement
P	-	Portlandite
PA	-	Passing Ability Class
PC	-	Portland Cement
Q	-	Quartz
RCPT	-	Rapid Chloride Permeability Test
RHA	-	Rice Husk Ash
RILEM	-	International Union of Laboratories and Experts in Construction Materials, Systems and Structures
S	-	Silicon Oxide
SCC	-	Self-Compacting Concrete
SEM	-	Scanning Electron Microscopy
SF	-	Slump Flow

SP	-	Superplasticizer
SR	-	Segregation Class
UPV	-	Ultrasonic Pulse Velocity
VS	-	Viscosity Class Expressed by T_{500}
VF	-	Viscosity Class Expressed by V-Funnel Time
WFS	-	Waste Foundry Sand
WG	-	Waste Glass
WTR	-	Waste Tire Rubber
w/c	-	Water to Cement Ratio
XRD	-	X-ray Diffraction

CHAPTER-1
INTRODUCTION

This unit deals with the basic introduction of self-compacting concrete, including its constituents, parameters, mechanism and advantages. The mix design theories studied by various researchers, along with the requirements of SCC in the fresh state, has been mentioned. The types of industrial by-products, their physical and chemical characteristics are studied. Copper slag and fly ash have been discussed in detail pertaining to their manufacture, production, physical and chemical characteristics. The significance of conducting this research, research gap and the objectives of the study has been stated. Lastly, the methodology of this research is mentioned in brief in addition to the outline of the entire thesis work.

1.1 DEFINITION OF SELF-COMPACTING CONCRETE

Self-compacting concrete (SCC) is the most recent concrete invention that elucidated the difficulty of compaction and good concreting in areas of congested reinforcements. SCC is defined as an innovative concrete that is able to compact under its weight without causing segregating or bleeding and thereby eliminating the prerequisite of external vibration (Salhi et al., 2020, Mohseni et al., 2017). This concrete revolution took place in the late 1980s (Saeedian et al., 2017). The lack of vibrations in areas of congested reinforcement (post-tensioning ducts) and uneven compaction in concreting while giving external or internal vibrations exhibits a negative impact on the permeability as well as durability of concrete. To eliminate these shortcomings and to offset the growing shortage of skilled labour in Japan, SCC was first time introduced by Okamura (1997) and Ozawa (1989). Primarily, development of SCC took place in chemistry incorporated in concrete (Okamura, 1997) and then was extended into constituent materials employing various mineral additives and industrial by-products.

1.1.1 Constituents of SCC

SCC is composed of a combination of cementitious materials including few additions, sand, coarse aggregates, water, superplasticizer and sometimes a viscosity modifying agent. The additions can be classified into inert or pozzolanic or hydraulic depending on

their reactivity with water, as shown in Fig. 1.1. Fly ash and silica fume are effective in improving cohesion between particles. Silica fume also helps to improve the resistance to segregation. The size of aggregates used in the design of SCC should be limited to 20 mm (EFNARC, 2005). The influence of fine aggregate is much more significant than coarse aggregate in terms of SCC. Admixtures are used to facilitate the appropriate dispersion of constituents in the fresh state as well as during its transport (Kapoor et al., 2020). Viscosity modifying admixtures are added to improve cohesion without influencing fluidity of SCC. The stability of SCC is defined essentially by four important parameters:

a) Flowability
b) Viscosity
c) Passing ability
d) Segregation

Based on these parameters, the fresh properties of SCC are further classified into various classes (EFNARC, 2005).

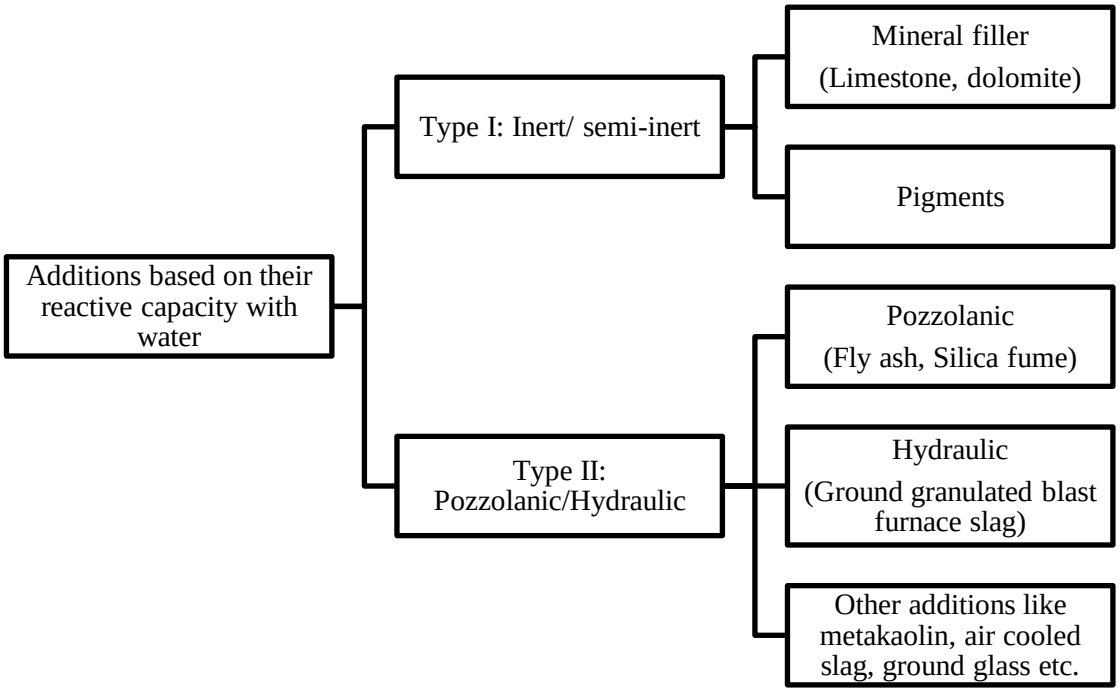

Fig. 1.1: Type of Additions in SCC

1.1.2 Requirements of SCC

The main four important parameters for designing SCC are its flowability, viscosity, passing ability and segregation resistance. The fresh performance of SCC depends on many factors including the degree of reinforcement congestion, placement method, requires surface finish, labour skill, level of quality assurance and quality control (Bartos et al., 2002). Flowability is the ease of flow of fresh concrete unconstrained by formwork (EFNARC, 2005). Passing ability is the property of fresh concrete to pass through congested reinforcements (EFNARC, 2005). The ability of fresh concrete to maintain homogeneity without getting segregated is termed as segregation resistance. Fig. 1.2 gives a summary of the fresh properties of SCC.

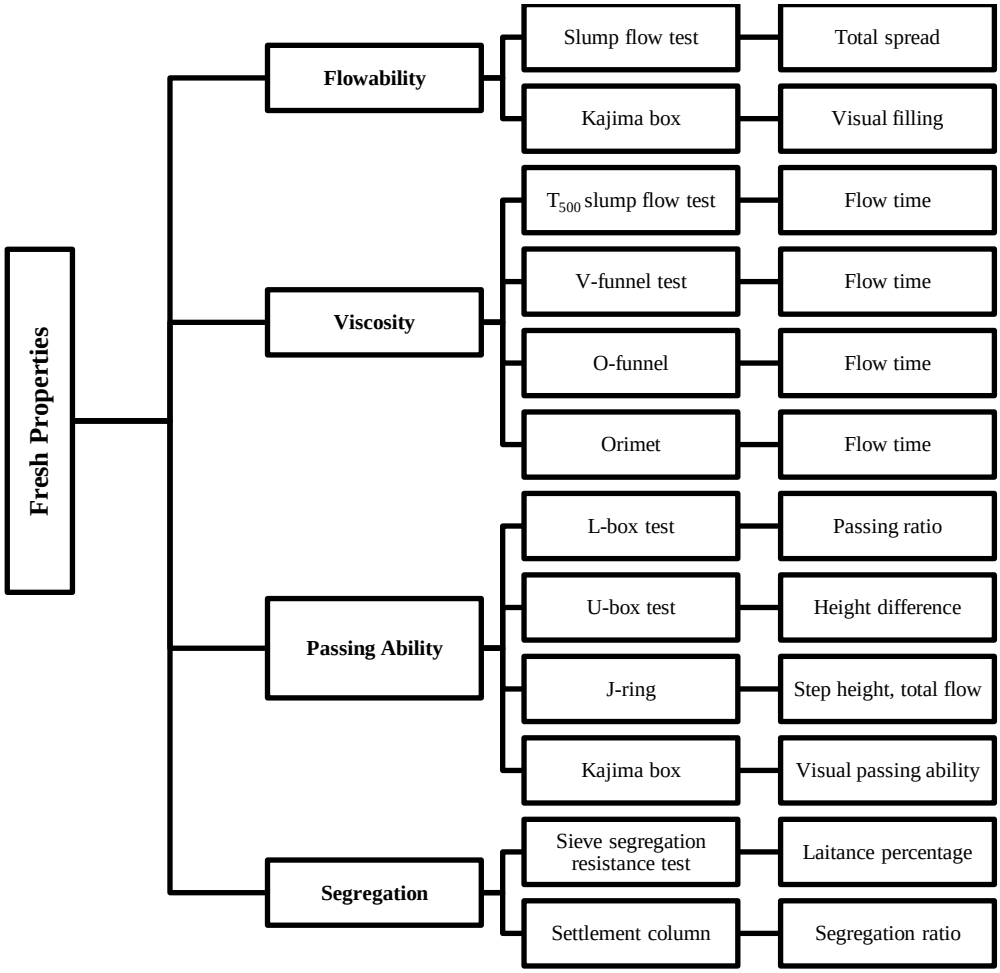

Fig. 1.2: Fresh Properties of SCC

A slump flow test evaluates the flowability of SCC without obstructions as per EFNARC (2005). It also determines the filling ability of SCC. For checking the filling ability of SCC, the maximum size of aggregate must not exceed 40 mm. The permissible values of slump flow, as well as its applications, are given in Fig. 1.3. To measure the viscosity and the filling ability of SCC, V-funnel test is suitable as per EFNARC (2005). The viscosity class is sub-divided into two main categories: VS1/VF1 and VS2/VF2. VS1/VF1 exhibited good ability in congested reinforcement. The class VS2/VF2 has more flow time range, thus can improve segregation resistance. The passing ability of SCC is determined with the help of L-box test, J-ring and U-box test as specified by EFNARC (2005). SCC is allowed to flow through obstructions in the form of congested reinforcements without segregating. This test consists of L-box shaped equipment stipulated with three or two reinforcing bars. Three bars simulate a congested reinforcement set up to study the passing ability more significantly. Passing ability PA1 and PA2 are the two main categories. PA1 class is preferred for constructions with a gap of 80 to 100 mm and generally used for vertical, housing structures. Class PA2 is preferred for structures having a gap of 60 to 80 mm and used for all civil engineering structures. The maximum value of U-box height is 30 mm as per EFNARC (2002). Sieve segregation test determines the segregation resistance of SCC as per EFNARC (2005). SR1 and SR2 are the categories of sieve segregation resistance test. The permissible values of the fresh properties as defined in EFNARC are given in a flow chart shown in Fig. 1.4.

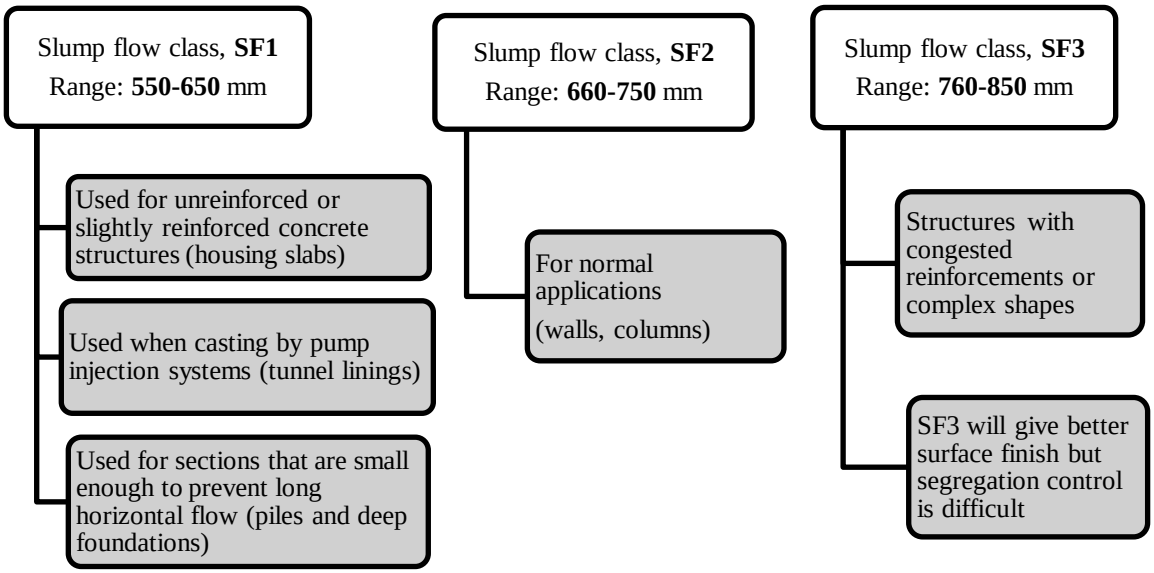

Fig. 1.3: Slump Flow Classes (EFNARC, 2005)

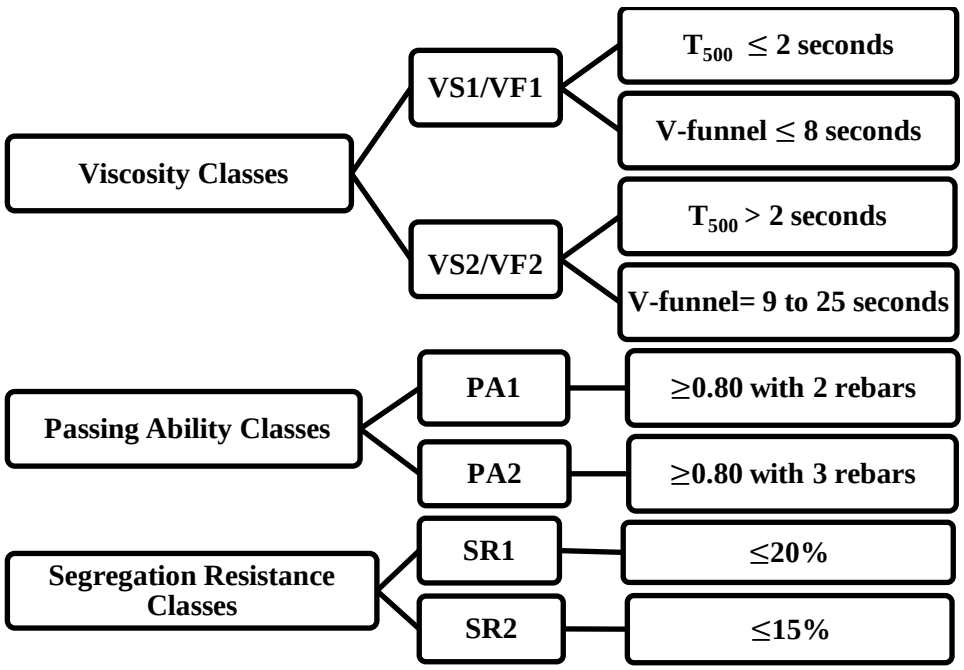

Fig. 1.4: Classes of Fresh properties (EFNARC, 2005)

1.1.3 Mechanism of SCC

The main parameters defining SCC and comparing it with normally vibrated concrete are:

(a) Limited coarse aggregate content

(b) Increased paste content

(c) Low water to cement ratio

(d) Use of superplasticizer

(e) Sometimes a viscosity modifying agent (EFNARC, 2005)

While the concrete is deformed, the frequency of collision of aggregates rises as the distance amid particles reduces. This then leads to an increase in internal stress. This internal stress consumes the energy required by concrete for flowing and thus leads to the blocking of aggregate particles. Apart from this, a highly viscous paste is needed to elude segregation of particles, as shown in Fig. 1.5 (Okamura and Ouchi, 2003). The paste volume should be more than the void volume of aggregate so that individual aggregate is completely surrounded by the paste (EFNARC, 2005). Also, superplasticizer or viscosity modifying agents help in decreasing segregation and sensitivity of the concrete. Accurate diffusion of flocculated particles and wetting or binding of water should take place (RILEM Technical Committee, 2006). Earlier, 1^{st} and 2^{nd} generation superplasticizer based on Melamine and Naphthalene was used. But now 3^{rd} generation superplasticizer based on poly-carboxylic ether have been incorporated (RILEM Technical Committee, 2006).

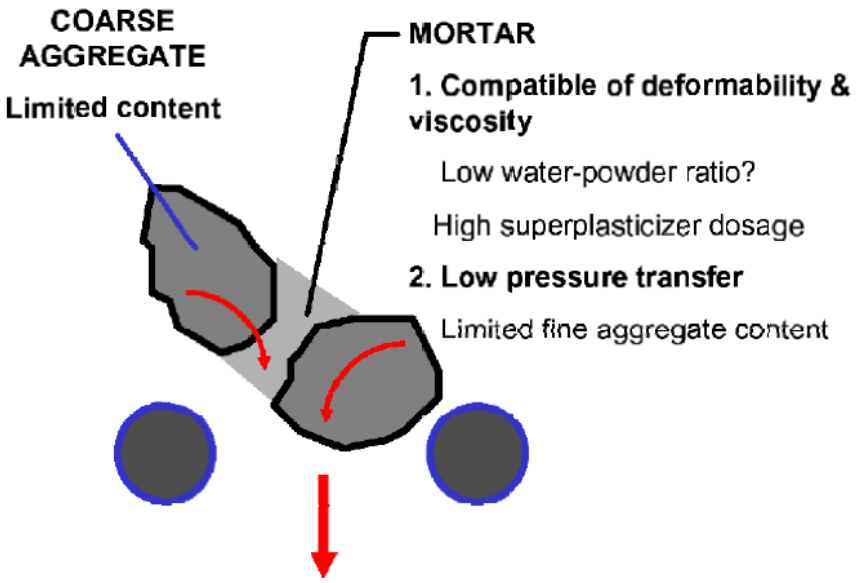

Fig. 1.5: Mechanism of SCC (Okamura and Ouchi, 2003)

1.1.4 Mix Design Procedures

The mix design of SCC is selected such that it achieves all the properties in the fresh and hardened state. Researchers and engineers have given various mix design approaches since 1992. Few mix design approaches have been explained here.

1.1.4.1 Mix Design Approach (Okamura, 1997)

A mix design proposed by Okamura (1997) suggested that the correct w/c ratio and optimum dosage of superplasticizer can be effective in achieving self-compatibility of concrete for a fixed amount of aggregate. The coarse aggregate content is retained at 50% to that of solid volume; fine aggregate is kept at 50% of that of mortar volume, as shown in Fig. 1.6. Pertaining to the content and type of cement required, w/c ratio by volume is assumed to be 0.9-1.0.

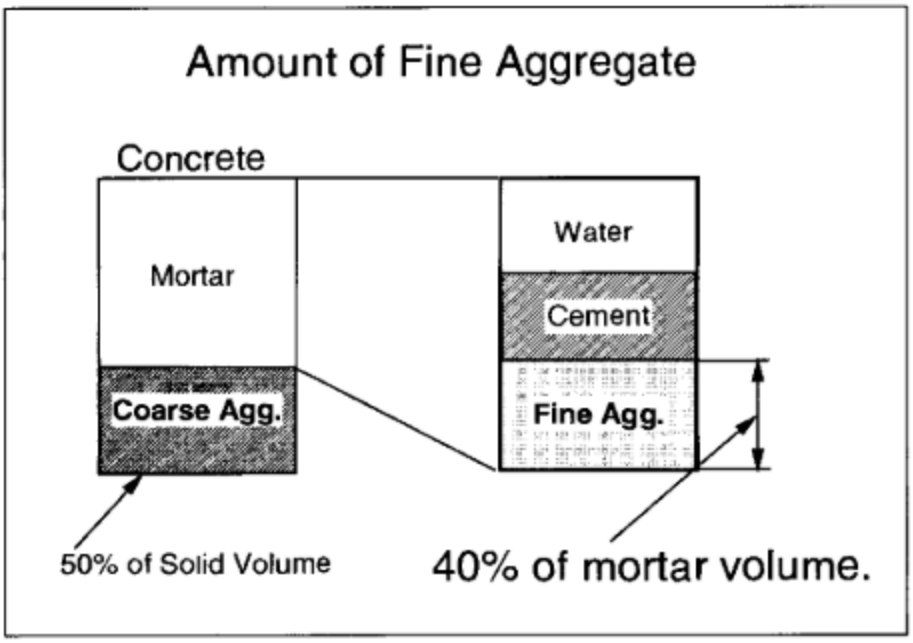

Fig. 1.6: Content of Fine Aggregate for Designing SCC (Okamura, 1997)

1.1.4.2 Japanese Method (Domone et al., 1999)

The mix design proposed was an extended study of that published by Okamura and Ozawa (1995). Self-compacting concrete mixes have been designed from the materials available in the UK. A linear optimization technique was considered, which gave the results of the optimized mix design proportions used in SCC.

a) Value of air-content is chosen (1-1.5% for a non-air-entrained mix)
b) Estimation of coarse aggregate content
c) Powder composition is chosen
d) Maximum water to powder ratio is obtained
e) The volume of sand in the mortar is chosen
f) Paste content is designed
g) The water and powder content is evaluated
h) Estimation of superplasticizer is made by testing on mortar
i) A trial mix design of concrete is then made on the same terms as the mortar was designed

1.1.4.3 Simple Mix Design for SCC (Su et al., 2001)

A simple mix design method for SCC was designed, which considered the filling of the voids of aggregates by the paste of binders (Su et al., 2001) and tested in Taiwan. The amount of required coarse aggregate is evaluated first and the paste is filled into the voids of aggregate. The volume ratio of aggregates considered here is 52-58%, which meant that the volume of loose aggregate is 42-48%. The packing factor is determined and is defined as the ratio of the mass of aggregate in a tightly packed state to that of loosely packed state. SCC designed by this method contains less coarse aggregate content and more sand; thereby increasing the passing ability, flowability, segregation resistance and thus achieving medium-range compressive strength of SCC (Fig. 1.7). However, the elastic modulus of SCC might get affected; therefore needs to pay special attention. Also, the volume of sand to mortar is about 54-60%. This method considered low content of binders as compared to other design approaches and thus reducing the cost of SCC. The step-wise mix design for SCC is as follows:

a) Estimation of coarse and fine aggregate content
b) Estimation of cement content
c) Estimation of mixing water required by the cement
d) Estimation of fly ash and ground granulated blast furnace slag
e) Estimation of mixing water content required in SCC
f) Estimation of superplasticizer content
g) Adjusting the water content required for SCC
h) Conducting trial mixes and then the tests on SCC
i) If a test fails, re-adjustment of mix proportions

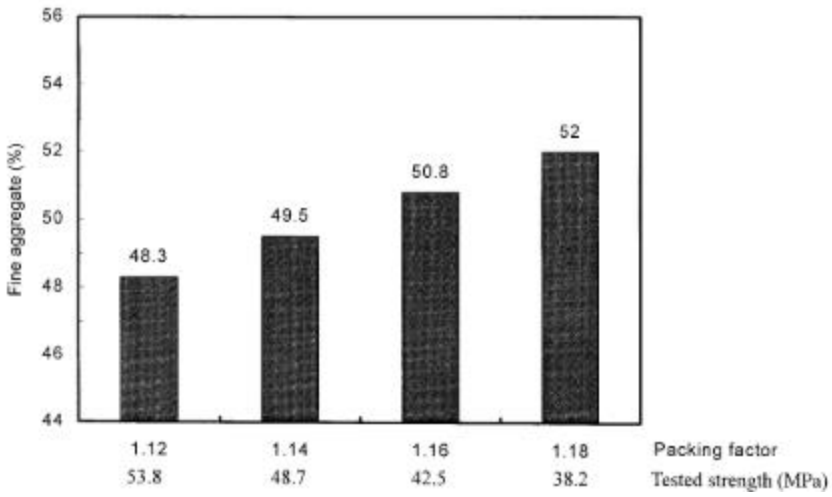

Fig. 1.7: Relation between Packing Factor, Compressive Strength and Fine Aggregate Volume Ratio (Su et al., 2001)

1.1.5 Advantages and Applications of SCC

SCC mixes gives better durability, enhances surface finish, easy placing and paves a way to faster construction times. Reduction in manpower is one of the primary advantages of SCC which caters the need of shortage of skilled labour. The noise of vibrators at the construction site gets reduced with the introduction of SCC and thus offering a safer working environment. There are many practical application of SCC worldwide since its development. SCC has found its applicability in the construction industry and used for the construction of bridges, in pre-cast structures, tunnel construction, highways, high-rise buildings, production of architectural and texture surfaces, containment vessels, chimneys, nuclear reactors, water tanks etc. The early stages included the construction of two anchorages of Akashi-Kaikyo Bridge (Ouchi, 2000). Another application of SCC that completed in 1998 was the construction of the wall of a large LNG tank (Ouchi, 2000). The main highlight observed was that the construction time decreased from 22 to 18 months. SCC eliminated the noise of vibration that helped in improving the working environment at the plants and thus made it possible for the concrete production plants to be installed in urban areas (Ouchi, 2000). Ouchi et al. (2003) reported several case studies relevant to the application of SCC in Japan and Europe. This included the Ritto Bridge of Japan, Higashi-Oozu Viaduct located in Japan and Sodra Lanken Project

located in Sweden. The Burj Khalifa referred to as World's tallest building with a height of 828 m and 166 stories, was inaugurated in 2010. SCC was used in the development of pile structure. The Kiaga-4, nuclear power reactor located in Karnataka, India incorporated SCC for ease laying and compaction works. Delhi Metro Project in India has used SCC for improving durability and saving the construction time. The use of high content of fine aggregates and other chemical admixtures makes it different from normally vibrated concrete. The only disadvantage of SCC is its high cost due to the constituents involved in its production.

1.2 COPPER SLAG

Copper slag is an industrial by-product of copper producing industry (Singh and Singh, 2020a). The method of matte smelting, in conjunction with the refining of copper, generates copper slag. Sulphides and oxides of iron and copper are the major elements of a copper smelting charge; other constituents include SiO_2, Al_2O_3, CaO and MgO (Mavroulidou, 2017). Copper-rich matte and copper slag are the discrete phases being formed. Because of the high density of the copper-rich matte liquid, it settles down. Particles of copper slag stay on the surface, which is then separated and cooled (Mavroulidou, 2017). Depending on the rapid or slow cooling, copper slag grains formed are amorphous or crystalline.

Around 2.2 to 3 tonnes of copper slag is formed with every ton of copper being generated (Gorai et al., 2003). Copper slag is debarred from the hazardous waste lists of materials (Shi et al., 2008). Copper slag has been successfully utilized in concrete as cement or fine aggregate substitute depending on the fineness and the physical properties of the slag available (Resende et al., 2008). Properties like strength, creep, shrinkage and modulus of elasticity are improved on the addition of copper slag up to 40-50% in concrete (Dhir et al., 2016a, Dhir et al., 2016b).

1.2.1 Production

Fig. 1.8 shows the copper smelter production globally in the year 2018. China produced approximately 8500 thousand metric tonnes of copper smelter in 2018. Based on 2018 figures, China is estimated to generate almost 40% of the total world copper smelter

production, followed by Japan (8%), Chile (6%) and Russian Federation (5%) (International Copper Study Group, 2019).

While in India, the metal content out of total copper resources is 12.16 million tonnes, of which 2.73 million tonnes constitute reserves. Rajasthan has the highest reserve of copper ore (813 million tonnes). Other leading states are Jharkhand (295 million tonnes) and Madhya Pradesh (283 million tonnes). Rest of the states that included Andhra Pradesh, Gujarat, Haryana, Karnataka, Maharashtra, Meghalaya, Nagaland, Odisha, Sikkim, Tamil Nadu, Telangana, Uttarakhand and West Bengal constitute remaining 7.9% of the total reserved in India.

In India, there are main three industries that are the chief producers of copper metal. These are Hindustan Copper Limited (HCL) in Jharkhand and Maharashtra, Hindalco Industries Limited in Gujarat and Vedanta Limited in Tamil Nadu. HCL is the only company that has its mining of ore, smelting and refining plant in India. However, the latter two companies are dependent on imported copper concentrated. HCL operates four underground mines and one opencast mine, with a total production capacity of 3.5 million tonnes per year. The various mines and plants operating in India along with their capacity are given in Fig. 1.9.

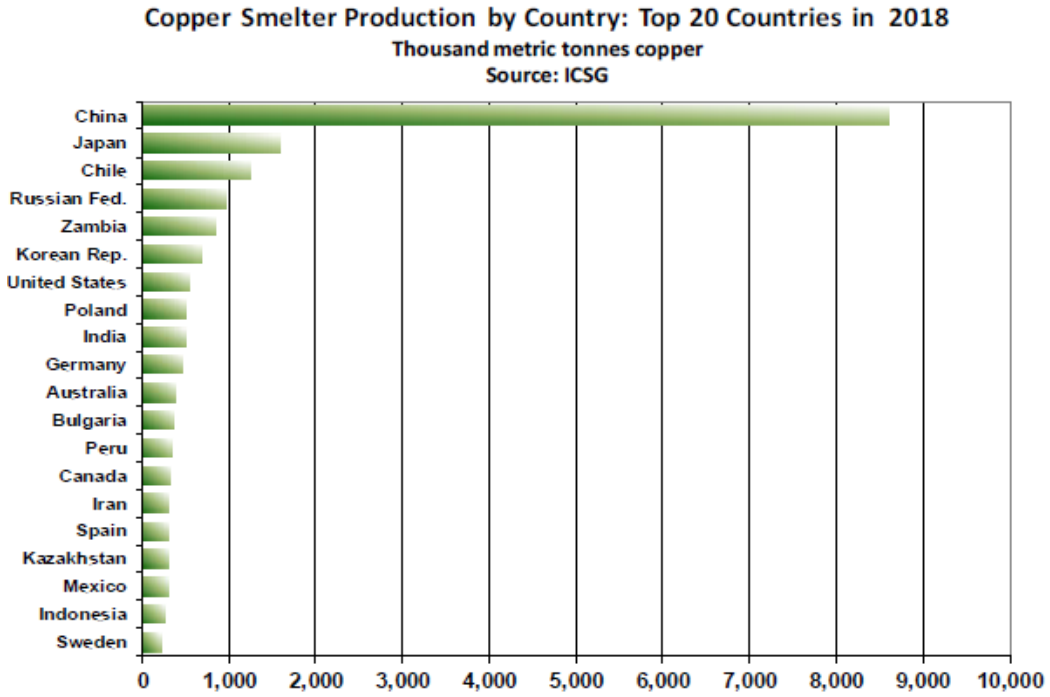

Fig. 1.8: Copper Smelter Production (International Copper Study Group, 2019)

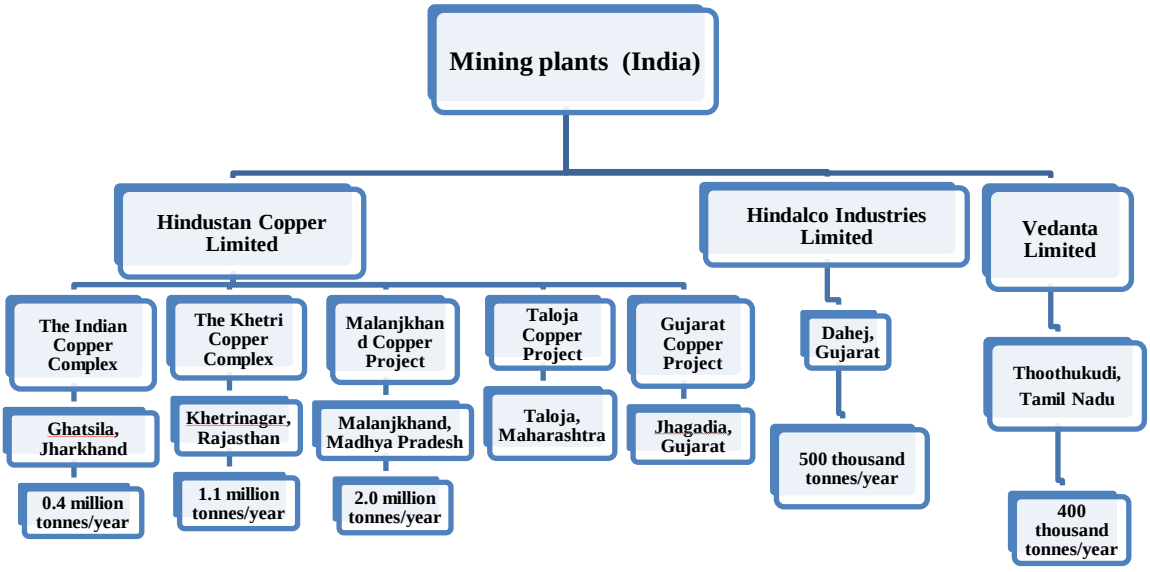

Fig. 1.9: Mining Plants of India (Indian Minerals Yearbook, 2019)

1.3 RESEARCH SIGNIFICANCE

Worldwide problem that has caused a major challenge is the generation as well as disposal of enormous amount of industrial by-products. Due to limited space for landfilling and thereby its escalating cost; attention has been made to recycle or reuse them. Also, the high excavation cost of natural sand, its scarcity in the environment along with its ever increasing demand has urged the concrete industry to look for some low-cost and abundantly available alternatives (Tang et al., 2020). A sustainable approach is required to conserve the environment as well preserve the natural resources at the same time. The utilization of industrial by-products in SCC optimises the solution for this problem (Sormunen and Kärki, 2019, Contrafatto et al., 2020). The economic benefit of utilizing industrial by-products usually attributes to the reduction of environment wastes as well as it saves the landfill expenses and resulting in lesser material being dumped in landfills. This step will also help in reducing the cost of concrete manufacturing while protecting the environment from possible pollution effects (Singh and Singh, 2018). Copper manufacturing industry produces abundant quantity of copper slag as an industrial by-product. The use of copper slag in SCC would give a solution to the environmental threats as well as provide with the technical benefits. The consumption of copper slag as sand replacement in SCC serves to be a viable option for progressing towards a sustainable development.

1.4 RESEARCH GAP

Copper slag is available in varied sizes, thus making it suitable for use in SCC either as cement or aggregate replacement. Researchers have explored the possibility of using copper slag in normally vibrated and high-performance concrete. However, limited research is available on the properties of SCC incorporating copper slag as a replacement of fine aggregate. Research needs to be directed much more towards the long term strength and durability properties of SCC incorporating copper slag.

1.5 RESEARCH OBJECTIVES

The objectives of the proposed work are:

- Fresh properties of self-compacting concrete made with copper slag as partial replacement of fine aggregate.
- Strength properties of self-compacting concrete made with copper slag as partial replacement of fine aggregate.
- Durability properties of self-compacting concrete made with copper slag as partial replacement of fine aggregate.
- Microstructural studies of the self-compacting concrete mixes.

1.6 METHODOLOGY

Initially, testing of the raw materials or the constituents of concrete was done to understand the basic behaviour of these materials. This included the initial testing of cement, fine aggregates, coarse aggregates, copper slag and fly ash. Fine aggregate was replaced with copper slag by weight in varying percentages ranging from 0 to 60% with an increment of 10%. The mix design of SCC was then chosen, targeting the fresh and strength properties. The fresh properties like flowability, passing ability, viscosity and segregation resistance followed EFNARC specifications. The strength and durability properties of SCC incorporating copper slag were studied for a period of up to one year. The results obtained were compared with the research already published to draw some relevant inferences. The microstructure of SCC was analyzed using SEM, Energy dispersive spectroscopy (EDS) and XRD techniques. Statistical analysis was studied with the help of ANOVA for finding out the statistical significance of the research conducted.

1.7 OUTLINE OF THESIS

The entire thesis has been divided into five chapters. Each chapter is sub-divided into a number of sections to cover the idea behind the comprehensive scientific work.

Chapter-1 Introduces about self-compacting concrete including its constituents, parameters, mechanism and advantages, copper slag, its properties, fly ash, its properties.

Chapter-2 Describes the literature review on the utilization of industrial by-products in SCC.

Chapter-3 Gives information about the various materials and the methods being used in this research. The experimental procedures for conducting the fresh, strength and durability properties of SCC are explained.

Chapter-4 Presents the results obtained after analyzing the fresh, strength and durability properties of SCC. The results are followed by discussions owing to the reasons responsible for the development patterns.

Chapter-5 Concluded the results obtained after carrying out the entire scientific program.

A list of references is given in the end after chapter-5. After the list of references, appendix (A to E) is given.

CHAPTER-2
LITERATURE REVIEW

This chapter deals with the literature review of the utilization of industrial by-products in SCC. The chapter included the basic introduction of industrial by-products: their physical, chemical properties and microstructure. The fresh, strength and durability of SCC made with industrial by-products like waste foundry sand (WFS), coal bottom ash (CBA), waste tire rubber, waste glass, iron slag and copper slag (CS) are reviewed based on published literature.

2.1 WASTE FOUNDRY SAND (WFS)

2.1.1 Properties of Waste Foundry Sand

Waste foundry sand (WFS) is a by-product of metal casting industries (Parashar et al., 2020). The ferrous and non- ferrous metal casting industries produce a large amount of WFS which cannot be further recycled and used (Siddique et al., 2011). The worldwide casting production increased by 5.3% in the year 2017 and was 109.8 million metric tonnes as per Modern Casting Census of World Casting Production. Russia showed the highest growth, with an increase of 8.3%. The global production rate of casting production in the US and India increased by 4% and 6.2%, respectively, in the year 2017.

Waste foundry sand exhibited carbon black coloured appearance having spherical, rough-textured and angular particles (Sandhu and Siddique, 2019). Table 2.1 gives the physical properties of WFS as studied by various researchers. Şahmaran et al. (2011) studied both angular and rounded shaped particles of WFS having smooth texture under scanning electron microscopy (SEM) analysis (Fig. 2.1). Guney et al. (2010) studied the sub-angular to round-shape particles of WFS (Fig. 2.1). Sua-iam et al. (2019) studied the irregular shape of foundry sand particles, as shown in Fig. 2.1. The crystalline phases of WFS was studied by Parashar et al., (2020); wherein the main phases were found to be that of Quartz and Albite under X-ray diffraction (XRD) analysis (Fig. 2.2). Silica is the main constituent found in WFS (Table 2.2). Other constituents present were mainly alumina, iron oxide, magnesium oxide, calcium oxide, sodium oxide and minute traces of sulphur oxide, potassium oxide and titanium oxide.

Table 2.1: Physical Properties of Waste Foundry Sand

Property	Bhat and Lovell (1996)	Naik et al. (2001)	Siddique et al. (2009)	Guney et al. (2010)	Basar and Aksoy (2012)	Siddique and Sandhu (2013)	Prabhu et al. (2014)	Gurumoorthy and Arunachalam (2016)	Torres et al. (2017)	Smarzewski (2020)
Specific gravity	2.66	2.44	2.20	2.45	-	2.43	2.24	2.32	2.45	2.45
Water absorption (%)	0.50	-	1.30	-	0.90	1.21	1.13	-	1.40	1.40
Moisture content (%)	-	0.25	-	3.25	-	-	-	-	-	-
Fineness modulus	-	2.32	1.60	-	-	1.23	-	1.72	1.70	1.80
Unit weight (kg/m^3)	-	1784	1520	-	1160	-	1576	-	1536	1521
Clay lumps and friable particles (%)	-	0.40	0.90	-	-	-	-	-	-	-
Materials finer than 75 µm (%)	-	1.08	8.00	24.00	-	-	-	-	9.00	-
Active clay content (< 2 µm) (%)	-	-	-	5.00	-	-	-	-	-	-

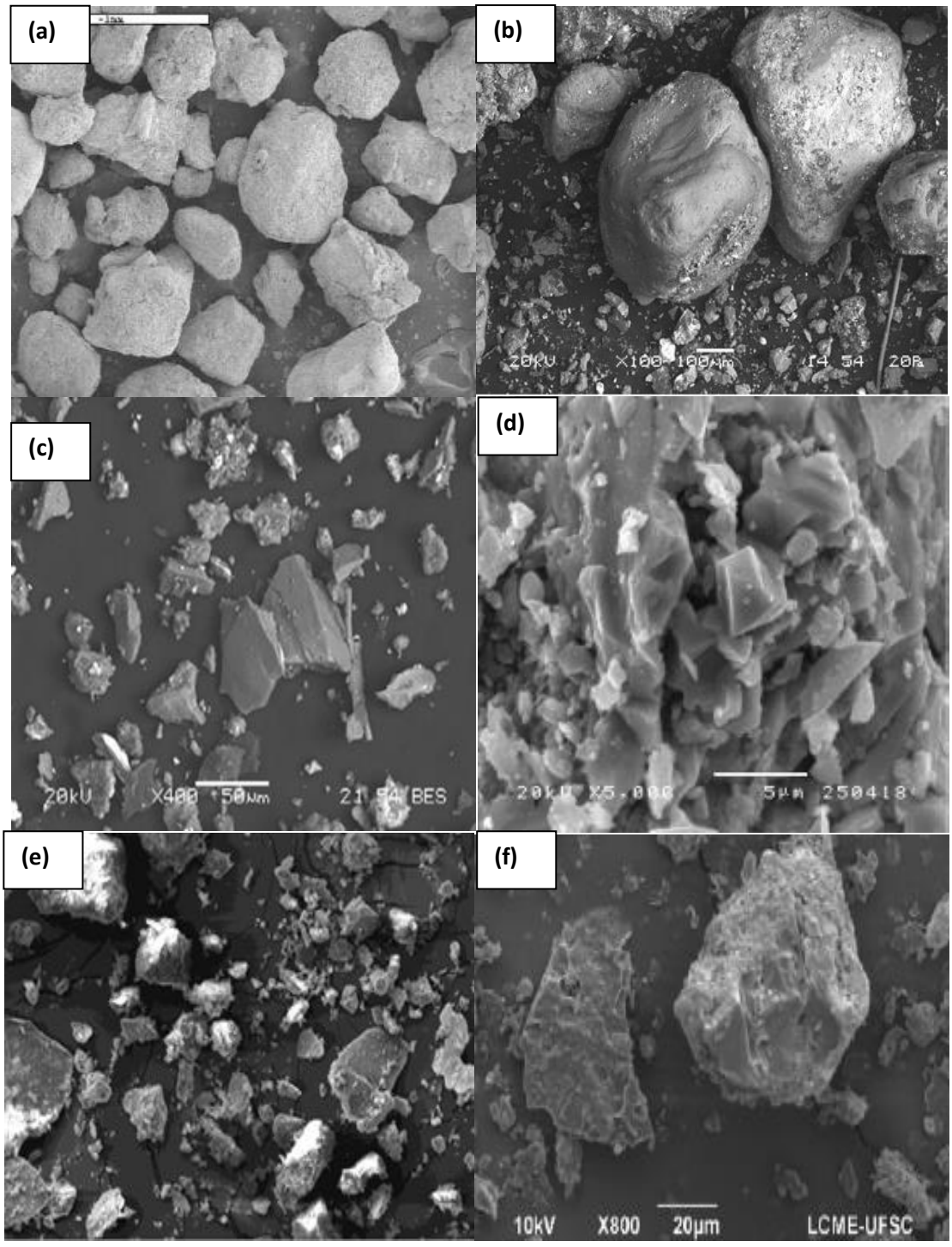

Fig. 2.1: SEM Image of WFS by (a) Guney et al. (2010) (b), (c) Şahmaran et al. (2011) (d) Sua-iam et al. (2019) (e) Parashar et al. (2020) (f) de Matos et al. (2020)

Table 2.2: Chemical Composition of Waste Foundry Sand

Chemical compounds (%)	Siddique et al. (2009)	Guney et al. (2010)	Şahmaran et al. (2011)	Singh and Siddique (2012)	Basar and Aksoy (2012)	Aggarwal and Siddique (2014)	Torres et al. (2017)	Sua-iam et al. (2019)	Sandhu and Siddique (2019)	Smarzewski (2020)
SiO_2	87.91	98.00	76.00	83.80	81.851	78.81	94.10	19.84	86.44	95.30
Al_2O_3	4.70	0.800	4.45	0.81	10.412	6.32	1.70	4.21	4.31	1.90
Fe_2O_3	0.94	0.250	5.06	5.39	1.818	4.83	5.80	3.19	2.74	0.70
MgO	0.30	0.023	1.98	0.86	1.974	1.95	0.00	1.25	0.88	-
CaO	0.14	0.035	3.56	1.42	1.210	1.88	0.20	68.02	0.98	0.35
Na_2O	0.19	0.040	0.38	0.87	0.764	-	-	0.18	0.39	-
SO_3	0.09	0.010	-	0.21	0.842	0.05	-	3.57	0.19	-
K_2O	0.25	0.040	1.20	1.14	0.494	-	0.00	-	0.28	-
TiO_2	0.15	-	0.17	0.22	-	-	0.00	-	0.17	-
P_2O_5	0.00	-	0.04	-	-	-	0.00	-	0.00	-
MnO	-	-	0.46	-	-	-	0.00	-	-	-
Cr_2O_3	-	-	0.04	-	0.025	-	-	-	-	-
V_2O_5	-	-	< 0.01	-	-	-	-	-	-	-
Mn_2O_3	0.02	0.010	-	-	-	-	-	-	0.04	-
Mn_3O_4	-	-	-	0.047	-	-	-	-	-	-
SrO	0.03	-	-	-	0.005	-	-	-	0.03	-
NiO	-	-	-	-	0.005	-	-	-	-	-
ZnO	-	-	-	-	0.018	-	-	-	-	-
Cl	-		-	-	0.071	0.04	-	-	-	-
Loss on ignition	5.15	-	5.85	-	6.93	2.15	-	0.92	3.55	-

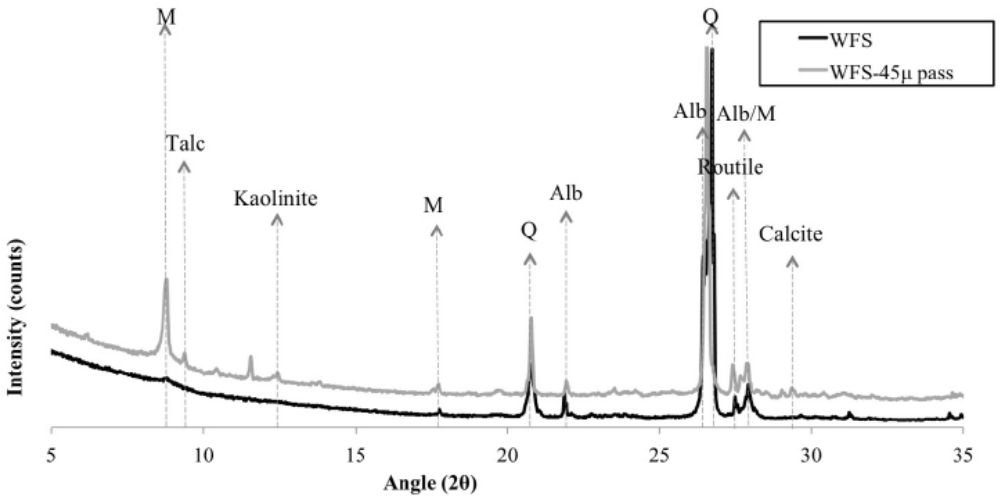

Fig. 2.2: XRD of WFS as Received and WFS after Passing 45-Micron Sieve (M-Muscovite, Q- Quartz, Alb- Albite) (Parashar et al., 2020)

2.1.2 Fresh Properties of SCC made with WFS

Sandhu and Siddique (2019) conducted an extensive laboratory study on SCC mixes incorporating up to 30% WFS at 0.36 w/c ratio. A reduction in workability was studied with the increase in WFS content owing to the rough, spherical and angular shape of particles present that created hindrance in a smooth flow (Table 2.3). Increase in superplasticizer content was observed with the rise in WFS content for a constant amount of fly ash quantity (Şahmaran et al., 2011, Sua-iam et al., 2019).

2.1.3 Mechanical Properties of SCC made with WFS

Şahmaran et al. (2011) evaluated SCC mixes incorporating WFS (0, 25, 50 and 100%) as a sand substitute in combination with fly ash (FA) (0, 30, 50 and 70%) as cement replacement. A reduction in strength was reported in SCC mixes made with WFS at all ages. An opposite trend was observed by Sua-iam et al. (2019); wherein they studied the effect of WFS as a sand replacement (0, 30 and 50%) and rice husk ash (RHA) varying from 0 to 20% as a cement substitute. An increase in compressive strength was observed in SCC mixes containing RHA and WFS. Incorporation of 10% RHA with 30% WFS resulted in the highest strength. Sandhu and Siddique (2019) reported a decline in

splitting tensile strength of SCC mixes with the increasing amount of WFS at all curing ages up to 365 days.

2.1.4 Durability Properties of SCC made with WFS

An insignificant change in the volume of permeable pores was studied on the addition of WFS up to 50% (Şahmaran et al., 2011). Concerning fly ash variation, the volume of permeable pores reduced as the fly ash content increased. Makul (2019) reported the properties of SCC incorporating WFS as a sand replacement (30 and 50%) and rice husk ash as cement replacement (10 and 20%). The water permeability values decreased with the addition of WFS up to 20%. Drying shrinkage increased during the initial curing days and the rate of increase was more significant up to 56 days owing to the presence of capillary pores and voids that contained water. Shrinkage strains became constant during later stages of curing form 90 to 180 days.

Table 2.3: Fresh Properties of SCC Incorporating Waste Foundry Sand

Author	Replacement Material (%)		w/c	Super Plasticizer (%)	Slump Flow (mm)	V-Funnel Time (sec)	T_{500} Slump Flow (sec)	L-Box	U-Box (mm)
	Sand by WFS	Cement by Fly Ash							
Şahmaran et al. (2011)	0 25 50 100	0	0.40	Requirement increased with increase in WFS content	605 657 655 675	7.7 5.6 7.3 9.0	3.83 2.02 2.71 1.70	-	-
	0 25 50 100	30			707 710 685 745	2.6 4.6 3.1 7.0	3.10 1.50 0.91 1.10	-	-
	0 25 50 100	50			612 605 717 739	3.5 5.5 1.9 6.5	1.60 2.20 1.10 1.30	-	-
	0 25 50 100	70			695 615 702 710	2.5 3.5 2.4 2.5	1.20 1.50 0.90 0.90	-	-
Sandhu and Siddique (2019)	0 5 10 15 20 25 30	7.41	0.36	1.17	774 762 747 665 640 623 608	6.84 7.33 8.27 9.12 12.29 11.96 14.15	2.14 2.38 2.73 3.25 3.46 3.69 3.98	0.96 0.92 0.93 0.87 0.89 0.81 0.85	0 0 5 12 15 20 27

w/c- water to cement ratio

2.2 COAL BOTTOM ASH (CBA)

2.2.1 Properties of Coal Bottom Ash

Coal bottom ash (CBA) is an industrial by-product produced from coal-fired electric power plants. During burning of coal in furnace of large thermal power plant, a large quantity of coal ash is generated. The bottom ash is generated when ash particles soften and stick to furnace walls and boiler tubes. These particles agglomerate and fall on hoppers that are situated at the base of the furnace. These are then collected and transported for further disposal.

Coal bottom ash is blackish with a fineness modulus of 1.60 as studied by Siddique (2013). CBA appeared porous and contained rough texture. Field emission scanning electron microscopic (FESEM) image of CBA reflected spherical, irregular shaped porous particles, as shown in Fig. 2.3 (Rafieizonooz et al., 2016). The production of CBA from the year 2000-2018 as reported by American Coal Ash Association has been given in Fig. 2.4. XRD analysis of CBA showed the presence of two major phases-Quartz and Mullite (Andrade et al., 2007) as given in Fig. 2.5. Table 2.4 and 2.5 presents the physical properties and chemical composition as studied by various researchers.

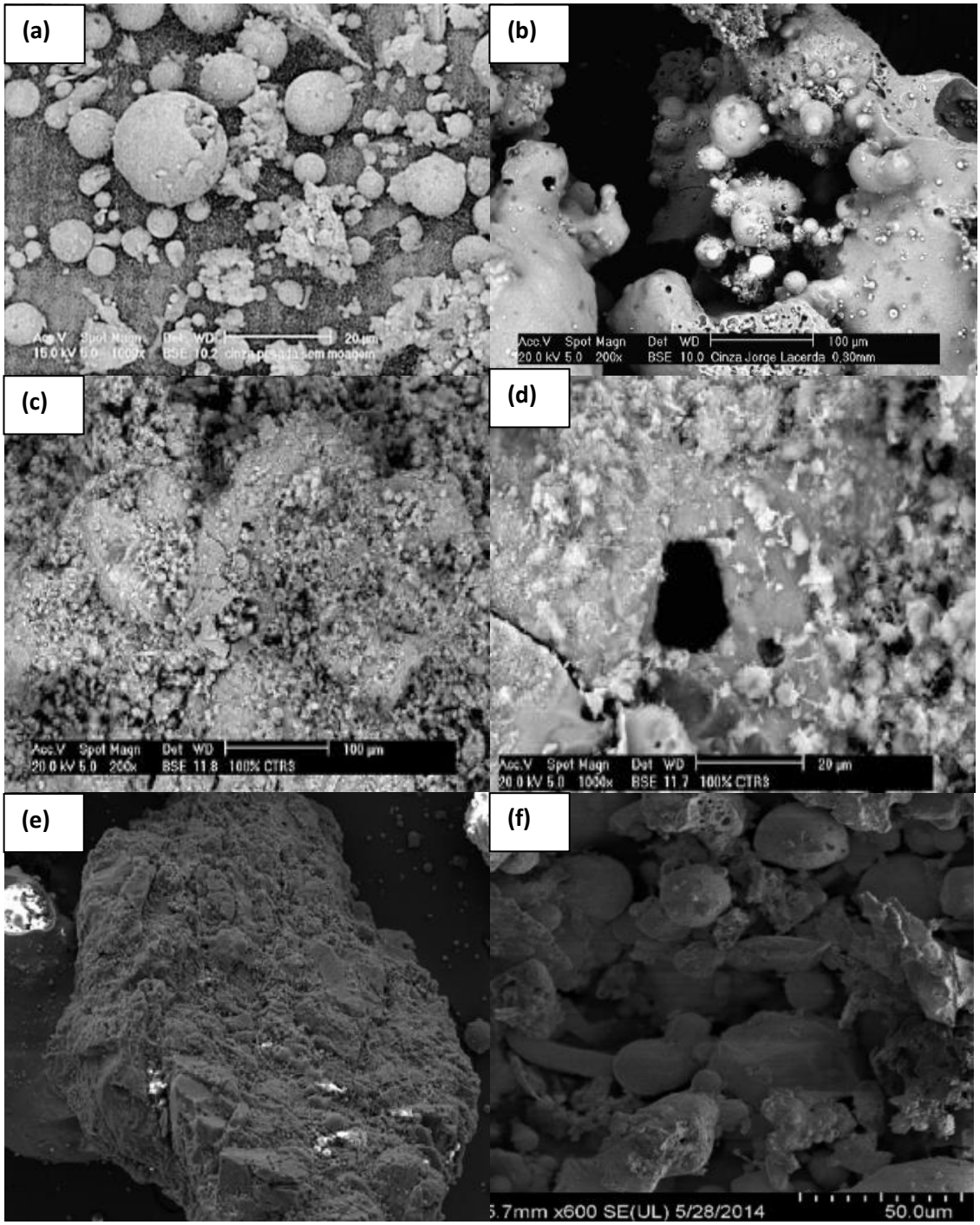

Fig. 2.3: Morphology of Coal Bottom Ash (a) Cheriaf et al. (1999) (b) Andrade et al. (2007) (c), (d) Andrade et al. (2009) (d) Kim et al. (2012) (e), (f) Rafieizonooz et al. (2016)

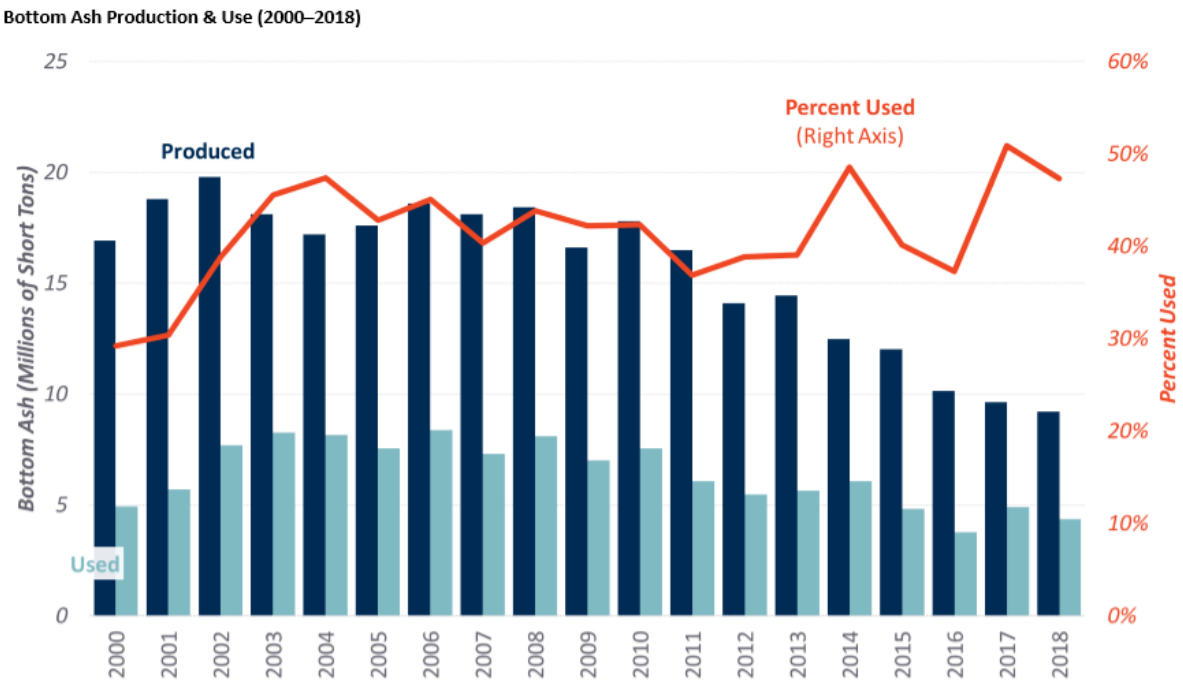

Fig. 2.4: Coal Bottom Ash Production from 2000-2018 (American Coal Ash Association)

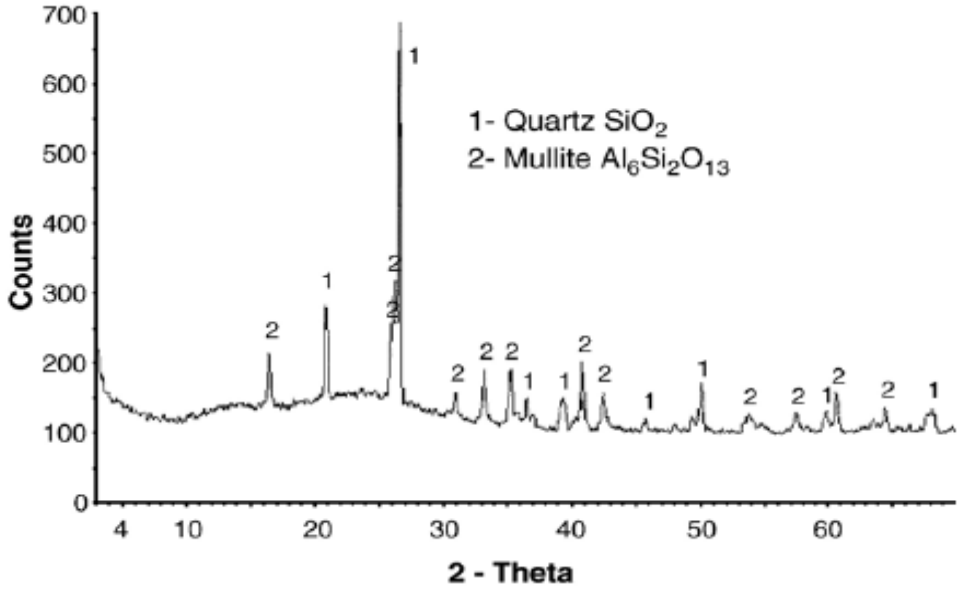

Fig. 2.5: XRD of Coal Bottom Ash (Andrade et al., 2007)

Table 2.4: Physical Properties of Coal Bottom Ash

Property	**Canpolat et al. (2004)**	**Bai et al. (2005)**	**Yüksel et al. (2007)**	**Andrade et al. (2009)**	**Kim et al. (2012)**	**Siddique (2013)**	**Singh and Siddique (2014b)**	**Rafieizonooz et al. (2016)**	**Singh et al. (2019)**
Specific gravity	2.39	1.50	1.39	1.674	1.87	1.93	1.39	1.88	2.08
Water absorption (%)	18.00	32.20	12.10	-	5.45	-	31.58	11.61	6.80
Fineness modulus	2.96	-	-	-	2.34	1.60	1.37	3.44	1.50
Bulk density, loose (kg/ m^3)	-	-	-	-	-	776	-	-	-
Bulk density, compacted (kg/ m^3)	-	-	-	-	-	948	-	-	-
Specific surface area (cm^2/kg)	830	-	-	-	-	-	-	-	-
Clay lumps and friable particles (%)	-	-	2.40	-	-	-	-	-	-

Table 2.5: Chemical Composition of Coal Bottom Ash

Chemical compounds (%)	Canpolat et al. (2004)	Bai et al. (2005)	Andrade et al. (2007)	Andrade et al. (2009)	Wongkeo and Chaipanich (2010)	Kim et al. (2012)	Singh and Siddique (2015)	Rafieizonooz et al. (2016)	Hashemi et al. (2019)
SiO_2	44.26	61.80	50.46	56.00	42.51	34.00	56.44	45.30	50.49
Al_2O_3	21.48	17.80	28.35	26.70	23.52	36.00	29.24	18.10	27.56
Fe_2O_3	6.40	6.97	10.69	5.80	10.20	16.80	8.44	19.84	10.93
MgO	1.29	1.34	-	0.60	2.45	-	0.40	0.97	1.24
CaO	17.57	3.19	2.07	0.80	12.55	2.40	0.75	8.70	4.19
Na_2O	0.29	0.95	-	0.20	2.20	-	0.09	-	0.57
SO_3	2.17	0.79	0.34	0.10	-	-	0.24	0.35	0.10
K_2O	0.77	2.00	3.81	2.60	2.12	5.90	1.29	2.48	0.82
TiO_2	-	0.88	1.57	1.30	0.41	3.80	3.36	3.27	2.23
P_2O_5	-	0.20	-	-	0.17	-	-	0.35	0.24
MnO	-	-	0.07	-	0.05	-	-	0.25	0.08
BaO	-	-	-	-	-	-	-	0.31	-
ZrO_2	-	-	0.18	-	-	-	-	-	-
V_2O_5	-	-	0.09	-	-	-	-	-	-
ZnO	-	-	0.03	-	-	-	-	-	-
SrO	-	-	0.03	-	-	-	-	-	0.12
ZrO_2	-	-	-	-	-	-	-	-	0.11
Y_2O_3	-	-	0.03	-	-	-	-	-	-
Free CaO	0.32	-	-	-	-	-	-	-	-
Others	-	0.49	-	-	-	-	-	-	-
Loss on ignition	-	3.61	2.30	4.60	3.82	-	0.89	-	1.10

2.2.2 Fresh Properties of SCC with CBA

Siddique (2013) reported the properties of SCC mixes made with CBA (0, 10, 20 and 30%) as a sand substitute and fly ash replacing cement (15%). As the content of CBA increased, the w/c ratio increased. However, it would be right to conclude that the quantity of superplasticizer reduced to achieve the fresh properties of SCC. Ibrahim et al. (2015) evaluated SCC mixes incorporating CBA varying from 0 to 30% with an increment of 10% as fine aggregate. As the percentage of CBA increased, the slump flow, L-box ratio and segregation resistance of SCC mix decreased.

2.2.3 Mechanical Properties of SCC with CBA

The compressive strength of SCC reduced with the increase in the percentage of CBA up to 30% as studied by Siddique (2013). Concerning the age of curing, compressive strength enhanced up to 365 days for each percentage of replacement. The splitting tensile strength reduced from 2.96 (control concrete) to 2.26 MPa for SCC mix incorporating 30% CBA at 365 curing days (Siddique, 2013).

2.2.4 Durability Properties of SCC with CBA

Water absorption and sorptivity of SCC mixes increased with the addition of CBA up to 30% (Siddique, 2013). Water absorption varied from 5.8 to 7.1% for all SCC mixes with and without CBA. Compressive strength of SCC reduced on the addition of CBA. The values of sorptivity varied from 0.055 to 0.0145 $mm^3/mm^2/min^{0.5}$ for all SCC mixes with and without CBA. SCC mixes incorporating CBA increased charge passed in coulombs at 90 and 365 days (Siddique, 2013). Though the charge passed in all SCC mixes corresponded to “very low permeability” as the charge passed was less than 1000 coulombs. With the increase in the content of CBA, there was an increase in depth of wear at 60 min time. Thus, abrasion resistance of SCC reduced with increase in CBA percentage (Siddique, 2013).

2.3 WASTE TIRE RUBBER (WTR)

2.3.1 Properties of Waste Tire Rubber

The annual production of tires is approximately 1.5 billion globally, whereas 1000 million of waste tire rubbers are generated that has created havoc (Azevedo et al., 2012). More than half of waste tire rubber is dumped into landfills creating environmental problems (Roychand et al., 2020). The long term buried tire would cause anti-leakage cover of the burial ground. While the exposed buried waste will pave the way for bacteria, insect breeding to grow, thus causing adverse effects on the environment (Youssf et al., 2020). Waste tires also generate a large number of toxic gases in case of fire, thus leading to pollution (Dhir et al., 2001). Therefore, recycling and reusing waste tire rubber prompts an urgent need (Yung et al., 2013). The chemical composition and physical properties of waste tire rubber are given in Table 2.6 and 2.7, respectively.

Table 2.6: Composition of Waste Tire Rubber (Sukontasukkul, 2009)

Composition	**Weight (%)**
Natural rubber	23.10
Synthetic rubber	17.90
Carbon black	28.00
Steel	14.50
Ash content	5.10
Fabric, fillers, accelerators etc.	16.50

Table 2.7: Physical Properties of Waste Tire Rubber

`Property	Savas et al. (1997)	Bignozzi and Sandrolini (2006)	Najim and Hall (2012)	Yung et al. (2013)	Hilal (2017)	Aslani et al. (2018)	Li et al. (2019)
Initial elastic modulus (MPa)	-	-	-	-	-	-	3.40
Tensile strength (MPa)	-	-	4.2 - 15	-	-	-	8.00
Specific gravity	1.14	-	1.12	0.95	0.50, 0.67	-	1.00
Apparent density (kg/m^3)	-	-	489	-	-	-	-
Approx. specific surface area (m^2/g)	2.2	-	-	-	-	-	-
Thermal conductivity (W/ m K)	-	-	0.11	-	-	-	-
Speed of combustion	-	-	Very low	-	-	-	-
Fineness modulus	-	-	-	2.17, 1.56	-	-	-
Size of rubber (mm)	0.058	0.50-2.00 0.05-0.70	-	0.60 0.30	< 1.0 1.0-4.0	1.0-3.0 2.0-5.0 5.0-10.0	2.0-4.0 1.0-2.0 0.0-0.3

2.3.2 Fresh Properties of SCC with WTR

Bignozzi and Sandrolini (2006) reported the influence of waste tire rubber in SCC. Slump flow diameter of more than 600 mm reported. SCC mixes incorporating waste tire rubber showed good flowability and passing ability in congested reinforcement. Similar results inferred by Topçu and Bilir (2009); workability of SCC mixes improved by using various viscosity modifying agents. Ismail and Hassan (2016) studied SCC incorporating up to

50% crumb rubber as a fine aggregate replacement; while replacing cement with fly ash, metakaolin and ground granulated blast furnace slag with different air-entraining admixtures. Metakaolin improved the passing ability and strength of SCC mixes. Aslani and Khan (2019) reported the study of SCC mixes incorporating crumb rubber varying in proportions of 10, 20, 30 and 40% exposed to elevated temperatures of 20°, 100°, 300° and 600°. Increase in superplasticizer content observed in SCC mixes made with crumb rubber. The fluidity of SCC mixes improved on the addition of crumb rubber; though segregation observed. However, an opposing trend was reported by few researchers. A decrease in flowability and passing ability concluded with the increase in waste tire aggregate content as well as a reduction of waste tire aggregate size (Li et al., 2019). Increase in T_{500} value and decrease in slump flow observed on adding waste tire rubber aggregate in SCC mix. A decline in L-box values with increase in waste tire rubber aggregate was concluded. This owed to the rise in inter-particle friction arising due to the rough texture of rubber aggregate (Batayneh et al., 2008, Taha et al., 2008, Guo et al., 2017). The reduced aggregate size increased the specific surface area; leading to more inter-particle friction and decrease in flowability (Youssf et al., 2014).

2.3.3 Mechanical Properties of SCC with WTR

Hilal (2017) evaluated SCC mixes incorporating three different sizes of crumb rubber aggregate as fine and coarse aggregate (5, 10, 15, 20 and 25% by volume). The one size was that passing through 1 mm sieve (No. 18) and the other was retained on 1 mm sieve and passing through 4 mm sieve (No. 5); while the third size of aggregate included the one that contained 40% No. 18 and 60% No. 5 crumb rubber aggregate. SCC mixes contained 520 kg/m^3 of cementitious content with 30% fly ash replacing cement at 0.35 w/c ratio. The compressive strength of SCC mixes decreased as the content of crumb rubber aggregate increased. Li et al. (2019) concluded the compressive strength (56 days) of SCC mixes decreased with the increasing rubber aggregate. With the increase in crumb rubber content, the splitting tensile strength decreased. SCC with 5 mm crumb rubber aggregates as fine aggregate yielded the maximum splitting tensile strength whereas SCC with 10 mm crumb rubber as coarse aggregate gave the lowest strength values (Aslani et

al., 2018). Similar results were shown by Hilal (2017); wherein the splitting tensile strength decreased on the addition of crumb rubber.

2.3.4 Durability Properties of SCC with WTR

Yung et al. (2013) studied that the ultrasonic pulse velocity of SCC mixes was 4000 m/s on the addition of 5% waste tire rubber powder. However, for all other mixes, the velocity exceeded 4000 m/s. The shrinkage of SCC was less with the addition of rubber powder. Ridgley et al. (2018) studied the abrasion resistance of SCC incorporating crumb rubber in combination with acoustic emission monitoring. The results showed declining effects on abrasion resistance on the addition of crumb rubber only. Water absorption, chloride ion permeability and sorptivity tend to decrease with an increase in waste tire rubber aggregate (Li et al., 2019).

2.4 WASTE GLASS (WG)

2.4.1 Properties of Waste Glass

Glass is formed by melting several constituents like silica, soda ash, calcium carbonate at very high temperatures and then cooling it. While cooling, solidification of glass takes places without crystallization (Siddique, 2007). Glass is manufactured in various forms depending on the requirement of the glass industry like flat glass, container glass, bulb glass, cathode ray tube glass. Colored and colorless glass waste is produced during its manufacture by the glass industry. The colored glass waste poses a stern risk to the environment as it is non-biodegradable. Dumping of colored waste glass into a landfill creates great havoc to the landfilling site. Thus, an environmentally safe way out is desired to recycle or reuse glass. Recycled waste glass bottles (beverages bottles) used in SCC consisted of 30% colorless, 40% green and 30% brown-coloured bottles that were provided by the Environmental Protection Department of Hong Kong (Kou and Poon, 2009). The liquid crystal glass was used in place of aggregates in SCC (Wang and Huang, 2010a). Waste LCD glass is hydrophobic and consists of smooth particles, as shown in Fig. 2.6. XRD analysis showed predominantly amorphous behaviour of recycled glass aggregate as given in Fig. 2.7. Table 2.8 and 2.9 provides a compiled result of the physical properties and chemical composition of the waste glass, respectively.

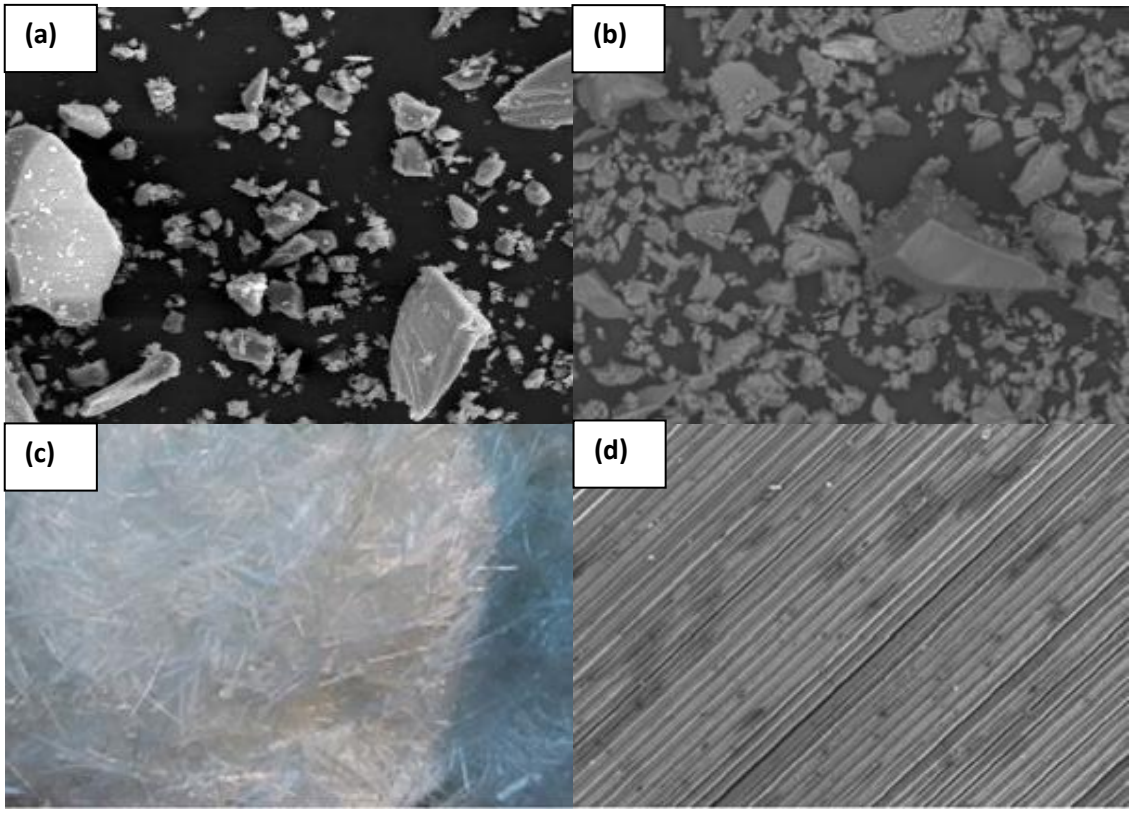

Fig. 2.6: Picture of (a) SEM image of glass aggregate (Nunes et al., 2013) (b) SEM image of glass powder (Afshinnia and Rangaraju, 2016) (c) Glass fibres used (Ahmad and Umar, 2018) (d) SEM image of glass fibres at 160 x (Ahmad and Umar, 2018)

Table 2.8: Physical Properties of Waste Glass

Property	**Kou and Poon (2009)**	**Wang and Huang (2010)**	**Liu (2011)**	**Ali and Al-Tersawy (2012)**	**Ling et al. (2012)**	**Sharifi et al. (2013)**	**Al-Bawi et al. (2017)**	**Ouldkhaoua et al. (2020)**
Specific gravity	2.49	2.45	2.40	2.20	2.49	-	2.53	-
Water absorption (%)	0.36	0.40	-	0.57	0.00	-	-	0.00
Fineness modulus	4.25	3.37	-	-	3.33	-	4.03	2.16
Bulk density (kg/m^3)	-	680	-	1340	-	2500	-	2750
Clay and fine dust content (%)	-	-	-	0.42	-	-	-	-

Table 2.9: Chemical Composition of Waste Glass

Chemical compounds (%)	Wang and Huang (2010)	Ali and Al-Tersawy (2012)	Sharifi et al. (2013)	Matos et al. (2016)	Al-Bawi et al. (2017)	Rehman et al. (2018)	Hendi et al. (2019)
SiO_2	62.48	67.72	70.50	72.69	71.91	74.30	73.00
Al_2O_3	16.76	3.40	2.60	0.67	-	0.15	2.00
Fe_2O_3	9.41		-	0.47	0.01	0.08	-
MgO	0.20	6.00	2.90	3.70	15.60	3.91	5.00
CaO	2.70	6.90	5.70	8.72		8.79	8.00
Cr_2O_3	-	-	-	-	0.30	-	-
Na_2O	0.64	10.75	16.30	12.22	9.58	11.6	11.00
K_2O	1.37		1.20	0.21	0.53	0.03	1.00
SO_3	-	0.17	0.20	1.30	0.22	0.10	-
TiO_2	0.01	-	-	< 0.04	0.06	-	-
P_2O_5	0.01	-	-	< 0.03	0.06	-	-
SrO	-	-	-	-	0.01	-	-
MnO	-	-	-	< 0.02	-	-	-
Other oxides	-	-	-	-	1.72	-	-
All of the alkali content	-	-	-	-	-	-	12.00
Insoluble residue	-	-	-	-	-	-	100.00
Loss on ignition	-	-	-	0.69	-	-	-

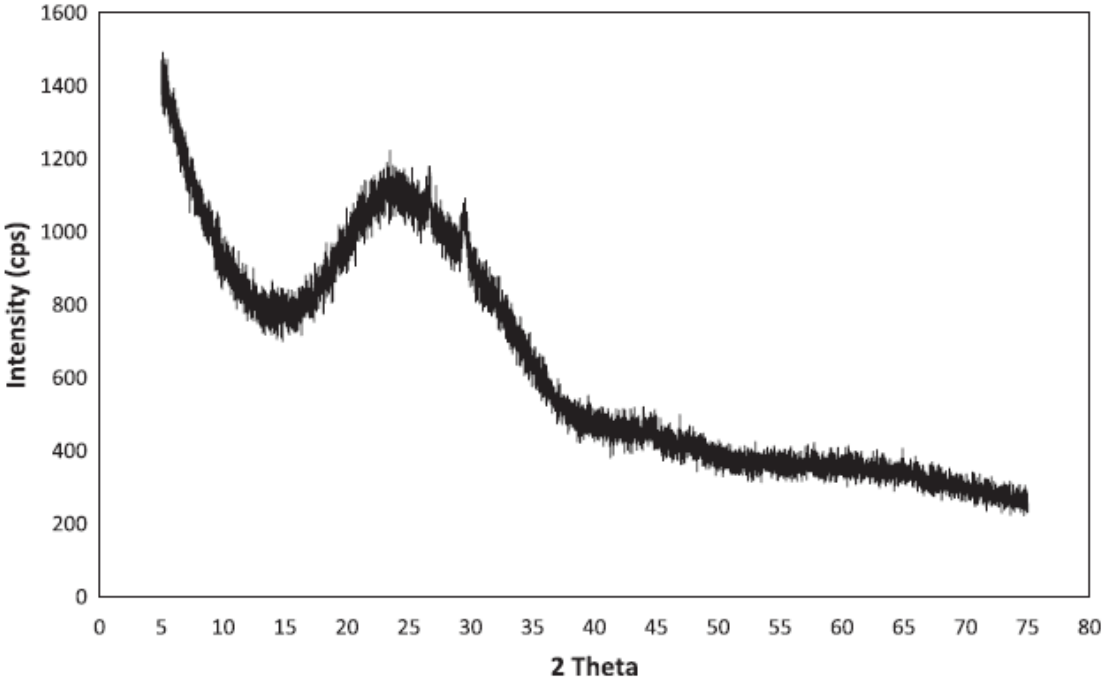

Fig. 2.7: XRD Pattern of Glass (Arabi et al., 2019)

2.4.2 Fresh Properties of SCC with WG

The slump flow obtained initially in SCC mixes incorporating glass cullet was analogous to that of control concrete mix (Kou and Poon, 2009) as given in Table 2.10. Cathode ray tube funnel glass (CRTG) utilized as a sand replacement (0, 10, 20, 30, 40 and 50%) and metakaolin (5, 10 and 15%) used to partially replace cement in SCC to develop a sustainable mixture (Ouldkhaoua et al., 2020). Slump flow decreased in mixes incorporating 15% metakaolin while SCC mixes made with CRTG showed improvement in slump flow even up to 50% replacement. V-funnel times prolonged with the rise in glass content due to lesser unit weight of SCC mixes made with glass (Wang and Huang, 2010b). U-box values remained unchanged on the addition of liquid waste glass in SCC (Table 2.10). However, these results opposed by the research findings of Sharifi et al. (2013); V-funnel time reduced with the addition of recycled glass. Analogous results reported by Ouldkhaoua et al. (2020); the flow times and V-funnel time reduced with the addition of cathode ray tube glass. The blocking ratio varied from 0.84 to 0.88 for all

SCC mixes with and without glass (Kou and Poon, 2009). L-box ratio decreased with glass addition probably due to sharp edges of glass that led to difficulty in passing between the reinforcing bars present in L-box equipment (Sharifi et al., 2013).

2.4.3 Mechanical Properties of SCC with WG

Kou and Poon (2009) reported a decrease in compressive strength of SCC mix incorporating recycled glass. A decrease in compressive strength of SCC containing LCD glass up to 30% observed (Wang and Huang, 2010a). Similar results followed by Ali and Al-Tersawy (2012). The effect of substitution of sand with glass (30, 50, 70 and 100%) and cement with polypropylene fibres (0, 0.5, 1 and 1.5%) in SCC mixes at a constant w/c ratio was considered by Fathi et al. (2017). The loss of compressive strength due to glass aggregate addition was more than that of glass fibres. A decrease of 5% splitting tensile strength was reported in SCC mixes containing up to 50% waste glass (Sharifi et al., 2013). There was a reduction in flexural strength in SCC mixes incorporating up to 30% waste glass (Wang and Huang, 2010a). A reduction in flexural strength was studied in SCC mixes incorporating up to 50% waste glass except for the mix made with 10% glass (Sharifi et al., 2013). This may be probably due to adhesion developed between glass and cement initially by adding 10% glass.

2.4.4 Durability Properties of SCC with WG

Sulfate resistance in terms of weight loss was observed by (Wang and Huang, 2010a). Weight loss ranged from 2.43 to 2.913% after eight cycles of sulfate exposure to SCC mixes incorporating up to 30% LCD glass. The results of Chloride ion permeability showed a reduction on the addition of recycled glass cullet in SCC mixes. The drying shrinkage values decreased with the addition of glass in SCC owing to the hydrophobic nature of glass cullet (Kou and Poon, 2009, Wang and Huang, 2010a). Chloride ion permeability enhanced with the addition of metakaolin and CRTG in SCC mixes (Ouldkhaoua et al., 2020).

Table 2.10: Fresh Properties of SCC Incorporating Waste Glass

Author	Replacement Material (%)		w/c	SP (%)	SP (kg/m^3)	SF (mm)	SF Time (sec)	V-Funnel Time (sec)	L-Box	U-Box (mm)	Air Content (%)	Wet Density (kg/m^3)
	Sand by Glass	Cement by										
Kou and Poon (2009)	0 10 20 30	25 (Fly ash)	0.37	-	8.5 8.2 8.0 7.8	755 750 760 750	42.5 42.0 43.0 41.0	-	0.88 0.87 0.86 0.84	-	3.1 2.6 2.7 2.9	2,290 2,280 2,260 2,250
Wang and Huang (2010b)	0 10 20 30	20 (Fly ash)	0.28	-	7.2	680 720 770 810	-	5.00 6.00 7.00 10.00	-	340[a] 340 340 340	2.9 2.8 2.6 2.0	2,410 2,395 2,380 2,369
	0 10 20 30	~20 (Fly ash)	0.32	-	6.5	610 620 680 750	-	4.00 6.00 7.00 9.00	-	340 340 340 340	2.8 2.7 2.5 1.9	2,393 2,380 2,374 2,363
	0 10 20 30	20 (Fly ash)	0.36	-	5.7	555 570 630 660	-	4.00 5.00 5.50 7.00	-	340 340 340 340	2.5 2.3 2.1 1.3	2,380 2,369 2,353 2,347
Ali and Al-Tersawy (2012)	0 10 20 30 40 50	10 (Silica fume)	0.40	1.50 1.30 1.20 1.20 1.10 1.10	-	640 670 710 730 860 880	-	7.00 8.00 6.00 6.00 5.00 4.00	0.86 0.83 0.84 0.85 0.87 0.89	-	-	-
Sharifi et al. (2013)	0 10 20 30 40 50	1.36 (Silica fume)	0.52	2.50 2.50 2.80 2.90 3.00 3.10	-	695 710 720 725 735 655	-	18.95 11.50 16.33 15.31 13.24 12.58	0.94 0.84 0.82 0.81 0.80 0.82	-	-	-

w/c- water to cement ratio; a-According to JSCE R2 acceptance criterion; SP-superplasticizer; SF-slump flow; SR-segregation ratio

2.5 IRON SLAG

2.5.1 Properties of Iron Slag

Blast furnace slags generally include both the iron and steel slag that is generated during the melting and reducing of iron ore in a blast furnace. During the production of iron, the blast furnace is provided with iron ore, fluxing agents like limestone and reducing agent like coke. Due to its low specific gravity, the molten slag rises above the pig iron, allowing it to be separated and collected easily.

Iron slag is black and has a glassy appearance. Iron slag is brittle in comparison to natural sand (Singh and Siddique, 2016a). The physical properties and chemical composition of iron slag are given in Table 2.11 and 2.12, respectively. The XRD pattern of iron slag has been studied by Sheikh et al. (2010) as provided in Fig. 2.8.

Table 2.11: Physical Properties of Iron Slag

Property	**Raharjo et al. (2013)**	**Singh and Siddique (2016a)**	**Ouda and Gawwad (2017)**
Specific gravity	-	2.49	2.71
Water absorption (%)	-	18.54	-
Fineness modulus	-	2.72	-
Unit weight (kg/m^3)	1809	2000	1870
Clay and fine material (%)	-	-	19.60

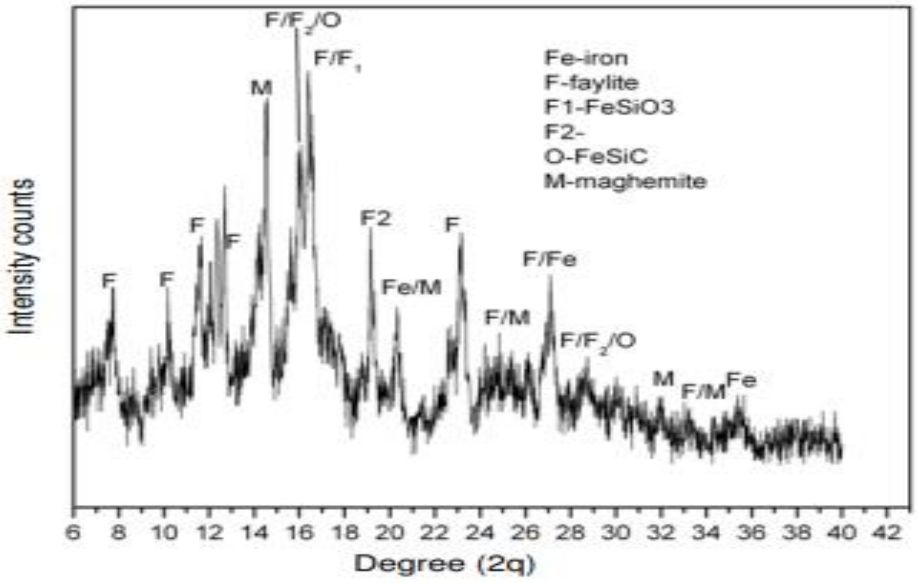

Fig. 2.8: XRD Pattern of Iron Slag (Sheikh et al., 2010)

2.5.2 Fresh Properties of SCC with IS

Singh and Siddique (2016a) studied SCC mixes incorporating iron slag as sand replacement in the range of 0, 10, 25 and 40% at 0.44 w/c ratio. SCC design mix contained superplasticizer at 1.2% by weight of the total cementitious mixture. Slump flow values ranged between 680 and 780 mm and followed EFNARC requirements. A decrease in slump flow values was studied on the addition of iron slag due to the rough texture and complicated shape of iron slag particles. The results of V-funnel indicated an increase in values on the addition of iron slag in SCC mixes. The value of U-box was less than 35 mm for all SCC mixes.

Table 2.12: Chemical Composition of Iron Slag

Chemical compounds (%)	**Monshi and Asgarani (1999)**	**Raharjo et al. (2013)**	**Singh and Siddique (2016a)**	**Saleh et al. (2019)**	**Zhang et al. (2019)**
SiO_2	36.80	35.67	6.98	28.00	25-45
Al_2O_3	9.84	3.62	2.94	16.40	0-10
Fe_2O_3	1.50	41.39	66.88	4.99	10-30
MgO	11.93	4.27	-	10.10	3.5-15
CaO	35.80	6.12	0.80	32.90	30-50
CO_2	-	-	22.40	-	-
SO_3	-	1.83	-	0.87	-
MnO	1.88	-	-	3.05	-
K_2O	0.15	0.43	-	0.55	-
Na_2O		0.81	-	-	
TiO_2	4.81	-		2.00	-
H_2O	-	0.82	-	-	-
V_2O_5	0.17	-	-	-	-
Others	-	-	-	-	< 5
Loss on ignition	-	4.45	-	-	-

2.5.3 Mechanical Properties of SCC with IS

An increase in compressive strength and splitting tensile strength was inferred on the addition of iron slag from 0 to 40% at all curing days (Singh and Siddique, 2016a). The flexural strength of SCC mixes improved with the addition of iron slag. Modulus of elasticity significantly increased on the addition of iron slag in SCC (Singh and Siddique, 2016a).

2.5.4 Durability Properties of SCC with IS

Water absorption found to reduce with the increasing content of iron slag up to 365 days (Singh and Siddique, 2016b). SCC mixes were exposed to magnesium sulfate to access the extent of damage caused. No mass loss reported in all SCC mixes. When compared to water cured samples, SCC mixes showed not more than 5% loss of compressive strength at 28 days immersion in sulfate. The results of chloride ion permeability showed a decrease in values with the addition of iron slag at 28, 91 and 365 curing days (Singh and Siddique, 2016b). The value of pulse velocity was more than 4000 m/s that depicted an excellent quality of concrete.

2.6 COPPER SLAG (CS)

2.6.1 Properties of Copper Slag

Copper slag is a safe industrial by-product, according to the Basel Convention, 1996 (Lye et al., 2015). It consists of fine material having black glassy colour and hardness of 7 Moh's scale. It has very low water absorption characteristic that makes it's unique from other types of by-products as can be seen from Table 2.13. Concrete mixes produced with high percentages of copper slag as fine aggregate results into a higher density. Its low water absorption property benefits the workability parameter. Much of the free water is available during the mixing of concrete and hence its leads to increase in slump flow and other flow properties. The specific gravity of copper slag ranges from 3.37 to 4.12, fineness modulus in the range of 2.61-3.50 and bulk density has a range from 1870-2310 kg/m^3 as per the published research. Copper slag mainly consists of silica (35-40%) and iron oxide (30–40%) as reported by various researchers. Traces of other compounds like

alumina, magnesium oxide, calcium oxide, copper oxide can be seen as given in Table 2.14. Due to its close gradation with sand, researchers have explored the possibility of utilizing copper slag in concrete as sand replacement.

2.6.2 Fresh Properties of SCC with CS

Sharma and Khan (2017a) reported the fresh properties of SCC made with copper slag (0, 20, 40, 60, 80 and 100%) as sand replacement. Workability enhanced on the addition of copper slag. Slump flow varied between 705 to 735 mm for all SCC mixes; conforming to the requirements of EFNARC (2005). The filling ability of SCC mixes enhanced significantly by adding copper slag. A decrease in V-funnel time values on the addition of copper slag from 0 to 100%.

2.6.3 Mechanical Properties of SCC with CS

Sharma and Khan (2017a) studied the effect of copper slag on the strength and durability properties of SCC mixes at 7, 28, 90 and 120 days. An increase in compressive strength and splitting tensile strength was observed in SCC incorporating up to 60% copper slag. The maximum compressive strength was observed in SCC mix with 20% copper slag.

2.6.4 Durability Properties of SCC with CS

Sharma and Khan (2017b) concluded a decrease in sorptivity and initial surface absorption values of SCC on the addition of copper slag up to 60%. Increase in weight and compressive strength loss was observed in SCC with copper slag exposed to sulfate solution (Sharma and Khan, 2017b). The electrical resistivity and ultrasonic pulse velocity (UPV) increased up to 60% copper slag addition. UPV values resulted in an excellent quality of concrete at later curing ages. Carbonation depth of SCC reduced with copper slag addition up to 100% copper slag.

Table 2.13: Physical Properties of Copper Slag

Property	**Khanzadi and Behnood (2009)**	**Wu et al. (2010)**	**Al-Jabri et al. (2011)**	**Afshoon and Sharifi (2014)**	**Ambily et al. (2015)**	**Murari et al. (2015)**	**Mithun and Narasimhan (2016)**	**Mavroulidou (2017)**	**Sharma and Khan (2017a)**
Specific gravity	3.59	3.66	3.40	-	3.37	3.50	3.60	-	3.51
Water absorption (%)	0.40	-	0.17	0.20	0.3-0.4	< 0.10	0.50	0.11	0.36
Fineness modulus	-	1.78	-	-	3.43	3.50	2.61	2.97	3.33
Bulk density, loose (kg/ m^3)	-	3660	-	-	2080	1870	-	3730	-
Specific surface area (cm^2/g)	-	-	-	2245	-	-	-	-	-

Table 2.14: Chemical Composition of Copper Slag

Chemical Compounds (%)	Khanzadi and Behnood (2009)	Wu et al. (2010)	Al-Jabri et al. (2011)	Afshoon and Sharifi (2014)	Murari et al. (2015)	Mithun and Narasimhan (2016)	Mirhosseini et al. (2017)	Sharma and Khan (2017a)
SiO_2	27.80	31.92	33.05	34.00	32.00	32.74	28.83	30.53
Al_2O_3	7.80	2.52	2.79	2.00	2.00	6.06	3.71	2.80
Fe_2O_3	52.50	59.11	53.45	48.78	43.00	49.30	46.37	57.82
MgO	1.2	1.65	1.56	1.23	0.80	0.20	-	1.48
FeO	-	-	-	-	-	-	-	-
CaO	4.60	1.25	6.06	4.89	1.50	0.84	5.80	1.60
Na_2O	-	1.40	0.28	0.63	-	0.14	-	0.34
SO_3	0.98	1.34	1.89	1.83	0.1	0.13	3.26	1.59
K_2O	1.6	0.81	0.61	0.87	-	0.03	1.15	0.71
TiO_2	1.49	-	0.00	-	-	-	0.34	0.26
P_2O_5	-	-	-	-	-	-	-	-
CuO	1.2	-	0.46	-	0.60	-	-	0.64
MnO	-	-	-	-	-	-		-
Cu	-	-	-	-	-	-	0.54	-
ZnO	0.84	-	-	-	-	-	-	-
Mn_2O_3	-	-	0.06	-	-	-	-	-
Insoluble residue	-	-	-	-	-	17.97	-	-
Loss on ignition	-	-	-	-	-	0.25	5.73	-

CHAPTER-3
EXPERIMENTAL PROGRAM

This chapter gives a detailed study of the materials used in the development of SCC incorporating copper slag. This included the laboratory procedure for carrying out the fresh properties, strength, durability properties and the microstructural analysis. The fresh properties included the slump flow, V-funnel, L-box, U-box, segregation resistance of SCC. The strength properties included the compressive strength and splitting tensile strength of SCC. The durability properties included the water absorption, sorptivity, chloride ion permeability, drying shrinkage and sulfate resistance of SCC made with copper slag.

3.1 MATERIALS USED

3.1.1 Cement

Ordinary Portland cement (OPC) grade 43 was procured from Shree Cement Company. OPC was tested for its physical properties according to the Indian standard specification, BIS: 8112-2013. Table 3.1 presented the results of physical properties that included the consistency, initial and final setting time, specific gravity and soundness of OPC. Table 3.2 gave the chemical composition of OPC. The SEM and EDS analysis of cement are given in Fig. 3.1 and 3.2 respectively.

Table 3.1: Physical Properties of Ordinary Portland Cement

Physical Properties	**Results**
Colour	Grey
Initial Setting time (min)	80
Final Setting time (min)	226
Specific gravity	3.01
Consistency (%)	29
Soundness (mm)	1

Table 3.2: Chemical Composition of Ordinary Portland Cement

Composition	**Compound (%)**
Calcium oxide (CaO)	64.67
Silica (SiO_2)	21.45
Aluminium oxide (Al_2O_3)	6.87
Iron oxide (FeO)	3.17
Total sulfate (SO_3)	1.95
Magnesium oxide (MgO)	1.16
Potassium oxide (K_2O)	0.60
Sodium oxide (Na_2O)	0.13

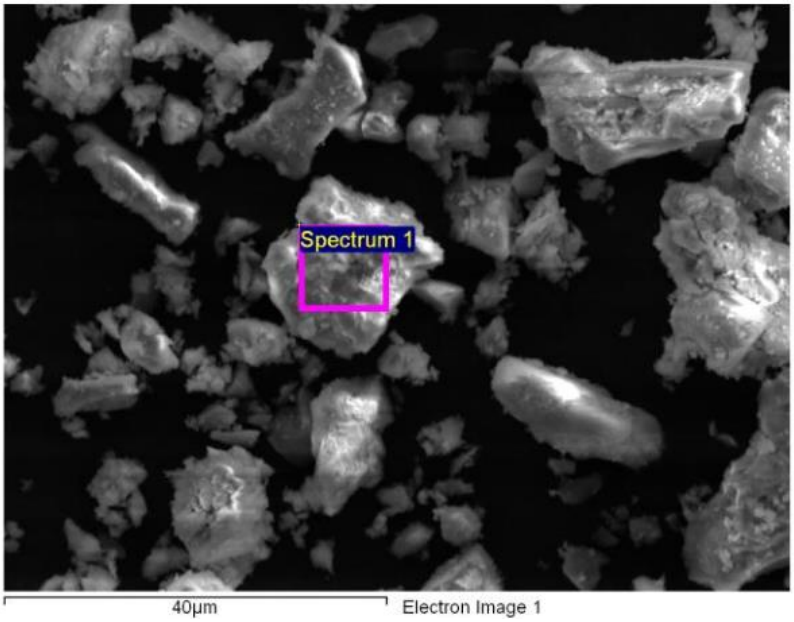

Fig. 3.1: SEM Image of Ordinary Portland Cement

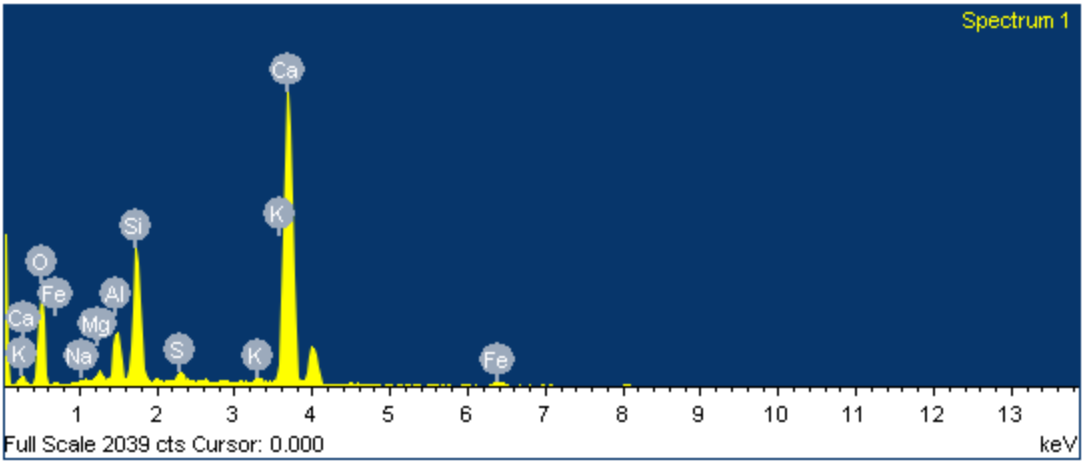

Fig. 3.2: EDS Spectrum of Ordinary Portland Cement

3.1.2 Fly Ash

Class F-Fly ash collected from an adjacent thermal power plant located in Ropar, Punjab, India was used. Fly ash appeared somewhat grey and the particle size was less than 45 micron. The physical properties of fly ash are given in Table 3.3. The sum of constituents SiO_2, Al_2O_3 and Fe_2O_3 were found to be higher than 70%, which confirms the criterion of class F fly ash as per ASTM C 618 (2005) as shown in Table 3.4. Pozzolanic additions like fly ash or silica fume are added in SCC to maintain the cohesion and segregation resistance of concrete matrix (EFNARC, 2005). Fig. 3.3 shows the SEM images of fly ash at 500, 1000 and 2500 magnification. Fig. 3.4 presents the EDS spectrum of fly ash.

Table 3.3: Physical Properties of Fly Ash

Physical Properties	**Results**
Colour	Grey
Specific gravity	2.13

Table 3.4: Chemical Composition of Fly Ash

Composition	**Compound (%)**
Calcium oxide (CaO)	0.58
Silica (SiO_2)	56.26
Aluminium oxide (Al_2O_3)	40.34
Iron oxide (FeO)	0.86
Total sulfate (SO_3)	1.95
Magnesium oxide (MgO)	0.42
Potassium oxide (K_2O)	1.52

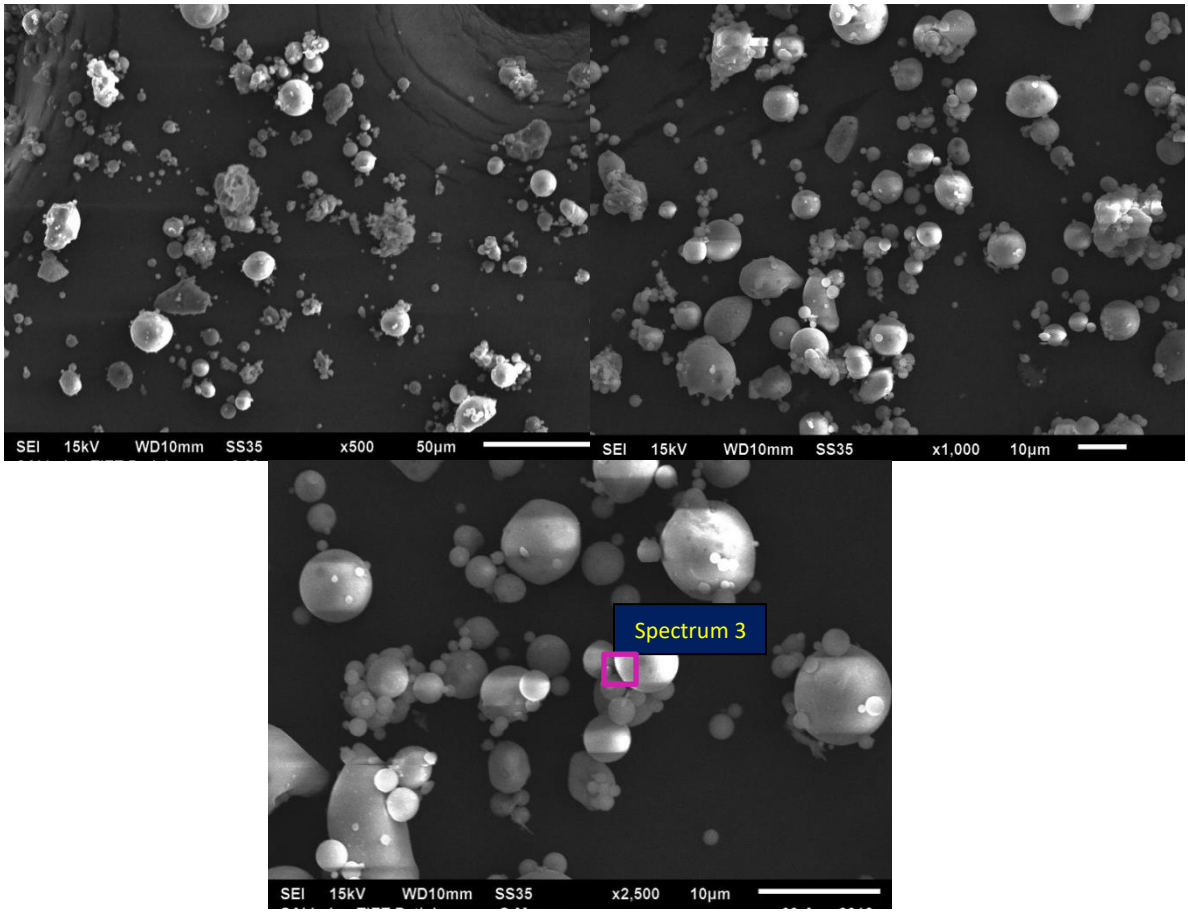

Fig. 3.3: SEM Image of Fly Ash

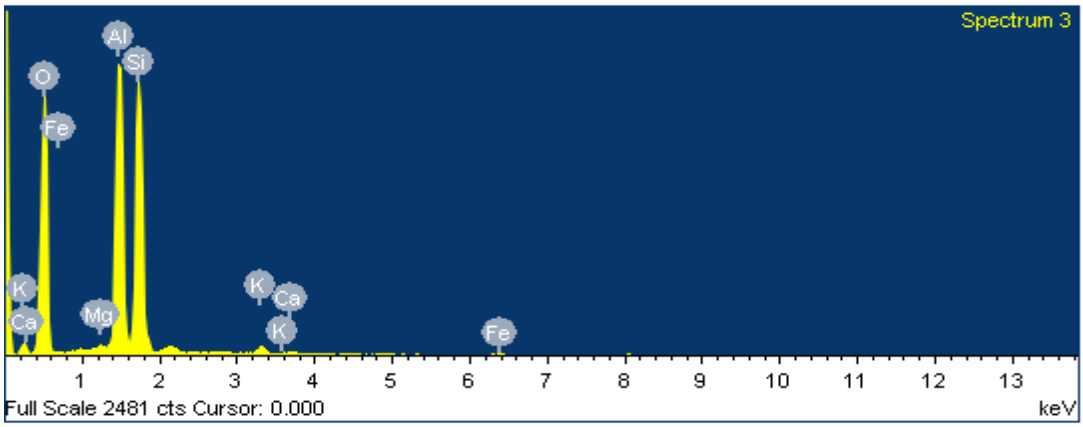

Fig. 3.4: EDS Spectrum of Fly Ash

3.1.3 Fine Aggregate

River sand was obtained from Pathankot, India, conformed to zone II as per BIS: 383-2016. The maximum size of fine aggregates used was 4.75 mm. Table 3.5 presented the physical properties of fine aggregates. Sieve analysis was performed for evaluating the fineness modulus of sand, as shown in Table 3.6. The fineness modulus of sand was 2.19.

Table 3.5: Physical Properties of Fine Aggregate

Property	**Results**
Appearance	Light grey
Specific gravity	2.55
Fineness modulus	2.19
Water absorption (%)	3.65
(Loose) Bulk density (Kg/m^3)	1236
(Compacted) Bulk weight (Kg/m^3)	1470
Moisture content (%)	Nil

Table 3.6: Sieve Analysis of Fine Aggregate

Weight of the sample taken = 1.0 kg

I.S. Sieve Size	Weight Retained (Kg)	Weight Retained (%)	Cumulative Weight Retained (%)	Percentage Passing	BIS: 383-2016 The Requirement For Zone II
10 mm	0.00	0	0	100	100
4.75 mm	0.00	0	0	100	90-100
2.36 mm	0.09	9	9	91	75-100
1.18 mm	0.10	10	19	81	55-90
600 micron	0.12	12	31	69	35-59
300 micron	0.39	39	70	30	8-30
150 micron	0.20	20	90	10	0-10
Pan	0.10	10	100	0	--

Fineness modulus of fine aggregate = 2.19

3.1.4 Coarse Aggregate

The maximum size of coarse aggregate used for SCC was 12.5 mm (EFNARC, 2005). The physical properties and sieve analysis of coarse aggregates are given in Table 3.7 and 3.8 respectively.

Table 3.7: Physical Properties of Coarse Aggregate

Property	**Results**
Maximum size (mm)	12.5
Specific gravity	2.65
Fineness modulus	6.09
Water absorption (%)	1.31
(Loose) Bulk density (Kg/m^3)	1710
(Compacted) Bulk weight (Kg/m^3)	1884
Moisture content (%)	Nil

Table 3.8: Sieve Analysis of Coarse Aggregate

Weight of the sample taken= 5.0 kg

I.S. Sieve Size	**Weight Retained (Kg)**	**Weight Retained (%)**	**Cumulative Weight Retained (%)**	**Percentage Passing**
20 mm	0.00	0.00	0.00	100
12.5 mm	0.00	0.00	0.00	100
10 mm	1.26	25.20	25.20	74.80
4.75 mm	2.97	59.40	84.60	15.40
Pan	0.77	15.40	100	0.00

Fineness modulus of coarse aggregate = 6.09

3.1.5 Copper Slag

Copper slag was purchased from Taj Abrasive Industries located at Fatehpur Road, Rajasthan, India. Fig. 3.5 presented SEM image of copper slag grains showing angular and smooth particles. The EDS spectrum of copper slag is shown in Fig. 3.6. XRD pattern of copper slag reports the amorphous nature of slag with 90% amorphous and contains traces of iron oxide and calcium magnesium iron silicate is shown in Fig. 3.7. Singh and Singh (2020) reported the amorphous nature of copper slag with traces of crystalline peaks of Fayalite and Clinoferrosilite. Table 3.9 presented the physical properties of copper slag. Sieve analysis test conducted to determine the fineness modulus of copper slag and the results are given in Table 3.10. Based on this, particle size distribution curves of sand and copper slag are shown in Fig. 3.8. The fineness modulus of copper slag was 3.11. The major constituents of copper slag are iron oxide and silica, as shown in Table 3.11.

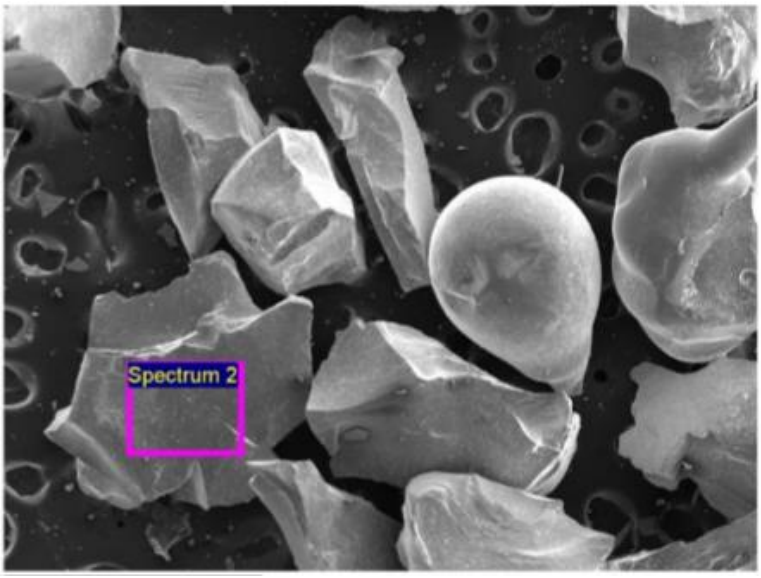

Fig. 3.5: SEM Image of Copper Slag

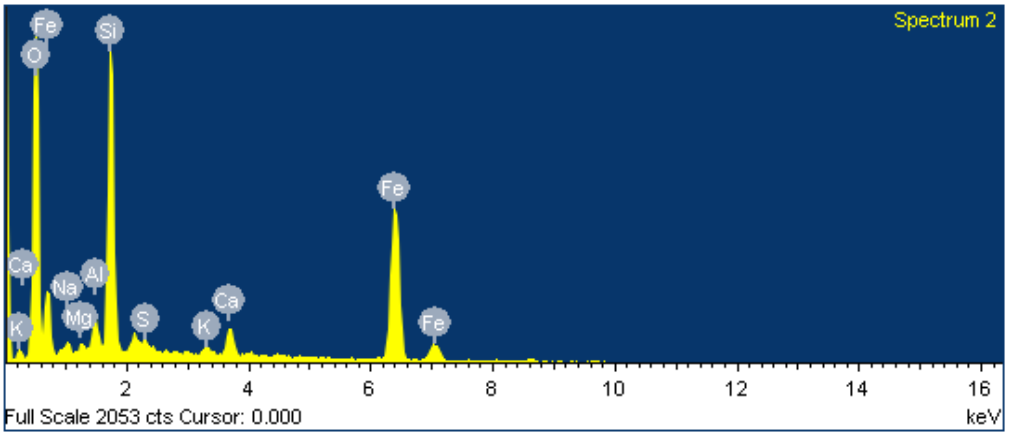

Fig. 3.6: EDS Spectrum of Copper Slag

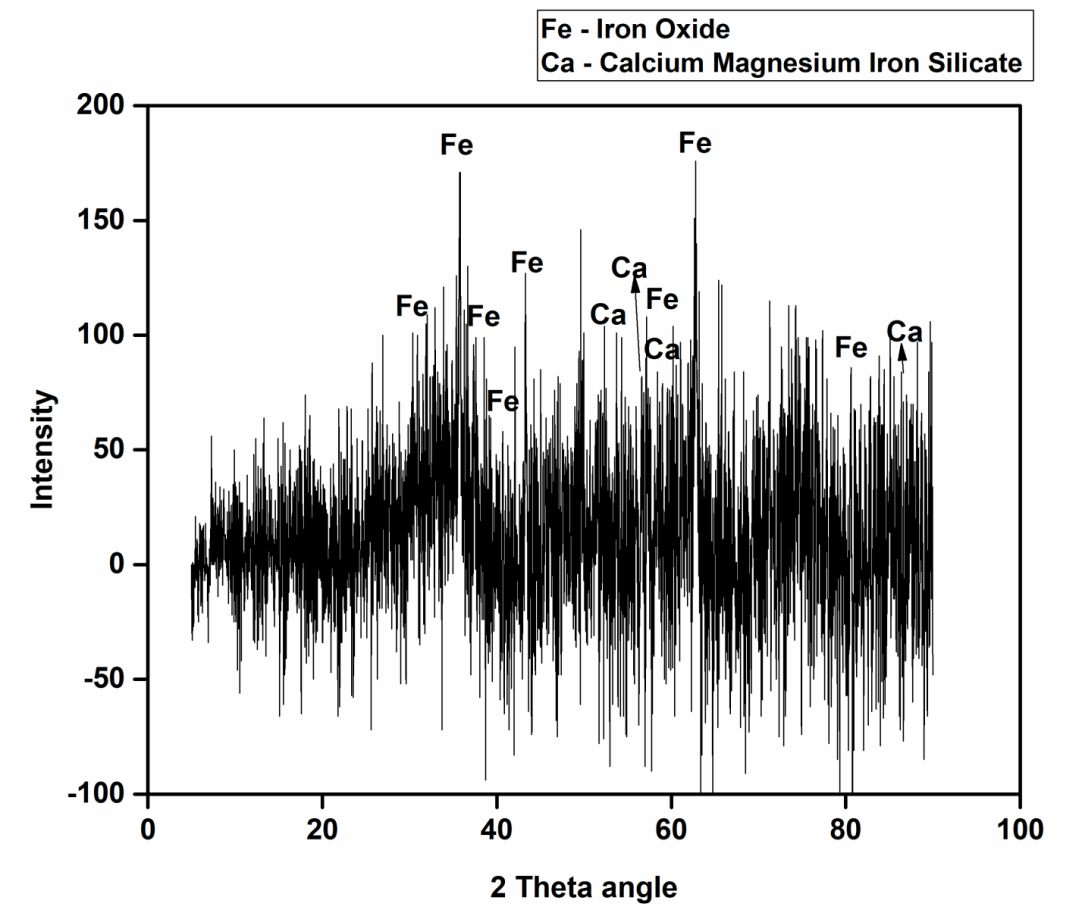

Fig. 3.7: XRD Analysis of Copper Slag

Table 3.9: Physical Properties of Copper Slag

Property	**Results**
Appearance	Black, Glassy texture
Specific gravity	3.51
Fineness modulus	3.11
Water absorption (%)	0.36
Unit weight (Kg/m^3)	2000

Table 3.10: Sieve Analysis of Copper Slag

Weight of the sample taken=1 kg

I.S. Sieve Size	**Weight Retained (Kg)**	**Weight Retained (%)**	**Cumulative Weight Retained (%)**	**Percentage Passing**
10 mm	0	0	0	100
4.75 mm	0	0	0	100
2.36 mm	0.014	1.4	1.4	98.6
1.18 mm	0.334	33.4	34.8	65.2
600 micron	0.456	45.6	80.4	19.6
300 micron	0.147	14.7	95.1	4.9
150 micron	0.041	4.1	99.2	0.8
Pan	0.008	0.8	100	0

Fineness modulus of copper slag = 3.11

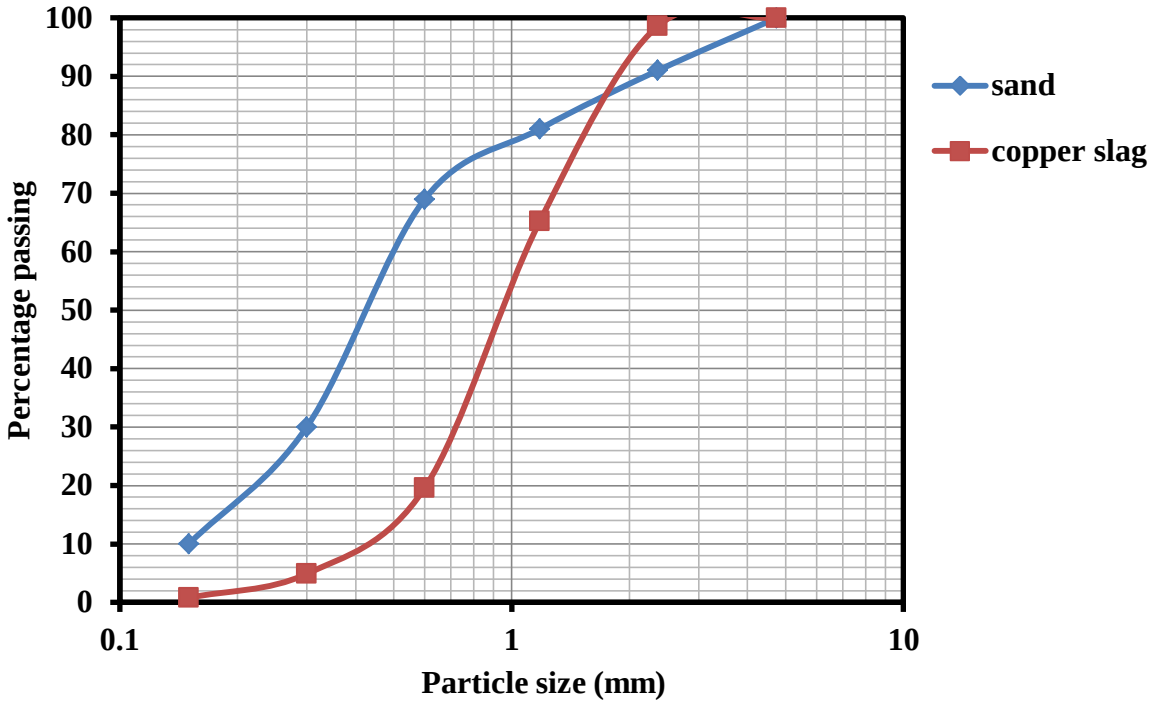

Fig. 3.8: Particle Size Distribution Curve of Sand and Copper Slag

Table 3.11: Chemical Composition of Copper Slag

Composition	**Compound (%)**
Calcium oxide (CaO)	3.31
Silica (SiO_2)	33.62
Aluminium oxide (Al_2O_3)	3.65
Iron oxide (FeO)	55.60
Total sulfate (SO_3)	1.12
Magnesium oxide (MgO)	1.51
Potassium oxide (K_2O)	0.82
Sodium oxide (Na_2O)	0.37

3.1.6 Superplasticizer

Auramix-400 was used as a superplasticizer in the design mix of SCC. It was bought from Fosroc Chemicals (India) Private Limited located in Chandigarh, India. It is a low viscosity and high water-reducing admixture that is based on polycarboxylic ether polymer along with long lateral chains. It has a light yellow coloured appearance and a minimum pH of 6. The alkali content is generally less than 1.5 g Na_2O equivalent/ litre of admixture. The volumetric mass of Auramix-400 is 1.09 kg/litre and contained a nil amount of chloride content.

3.1.7 Water

Tap water used for mixing concrete constituents and curing of samples as per BIS: 456-2000.

3.2 MIX DESIGN PRINCIPLE

The stability of SCC is defined essentially by four important parameters: Flowability, Viscosity, Passing ability and Segregation. The basic mix design principle, as suggested by EFNARC (2005), is explained. The fluidity and viscosity of the paste are adjusted by:

(a) Careful selection and proportioning of cement and additions
(b) Limiting water to cement ratio
(c) Adding the appropriate type and amount of superplasticizer and/ viscosity modifying agent

The additions are classified into inert or pozzolanic or hydraulic depending on their reactivity with water. Fly ash and silica fume are effective in improving cohesion between particles. The size of aggregates should be limited to 12-20 mm (EFNARC, 2005). The influence of fine aggregate is much more significant than coarse aggregate in terms of SCC (Niewiadomski et al., 2018). Admixtures are used to facilitate the appropriate dispersion of constituents in the fresh state as well as during its transport. Viscosity modifying admixtures are added to improve cohesion without influencing fluidity of SCC. The pozzolanic additions are required to control the temperature rise and

thermal shrinkage cracking. The ratio of coarse aggregate to fine aggregate is reduced to achieve a good flowability of SCC. There is as such no standard method for designing SCC. However, some guidelines given under the European project: The European Federation of Specialist Construction Chemicals and Concrete Systems (EFNARC, 2005) for the mix design procedure of SCC are shown in Table 3.12.

Table 3.12: Typical Range of Constituents of SCC (EFNARC, 2005)

Constituents	**Typical Range by Mass (Kg/m^3)**	**Typical Range by Volume ($litres/m^3$)**
Fine powder	380-600	-
Paste content	-	300-380
Water	150-210	150-210
Coarse aggregate	750-1000	270-360
Fine aggregate	The fine aggregate content depends on other materials, usually using 48-55% of the total aggregate weight	
Water to fine powder ratio by volume	-	0.85-1.10

3.2.1 Mixture Proportions

Several trials were produced to assure the requirements of SCC as per EFNARC (2005). SCC mixes incorporated 20% fly ash as cement substitution and copper slag varying from 0 to 60% as sand replacement. Fixed parameters considered were the quantities of cement as 400 kg/m^3, fly ash as 100 kg/m^3, coarse aggregate as 760 kg/m^3, 0.42 as water-cement ratio and admixture used was 1.2% of the weight of total cementitious powder. The final mix design of SCC is given in Table 3.13. Compressive strength of SCC mix carrying 100% sand was 35.63 MPa after 28 days curing.

Table 3.13: Design Mix of SCC

Mix	Cement (kg/m^3)	Fly Ash (kg/m^3)	Sand (kg/m^3)	CS (%)	CS (kg/m^3)	CA (kg/m^3)	w/c	SP (%)
0CS-SCC	400	100	960	0	0	760	0.42	1.2
10CS-SCC	400	100	864	10	96	760	0.42	1.2
20CS-SCC	400	100	768	20	192	760	0.42	1.2
30CS-SCC	400	100	672	30	288	760	0.42	1.2
40CS-SCC	400	100	576	40	384	760	0.42	1.2
50CS-SCC	400	100	480	50	480	760	0.42	1.2
60CS-SCC	400	100	384	60	576	760	0.42	1.2

CS-Copper Slag (0, 10, 20, 30, 40, 50 and 60 are the percentages of replacement of copper slag with sand), CA- coarse aggregate, w/c- water to cement ratio, SP- superplasticizer

3.3 PREPARATION, CASTING AND TESTING OF SPECIMENS

Before casting of samples, all the equipment's were cleaned and checked thoroughly for any opening or gap. The fresh property measuring instruments like slump cone, V-funnel, L-box, U-box were appropriately checked for any discrepancy or leakage from any point. Each ingredient was measured using a weighing balance and mixed in the pan mixture. Firstly, the dry materials like sand, copper slag, coarse aggregates added in a pan mixture (Fig. 3.9). After this, cement and fly ash were added in the mixer. Then, 60% of water was introduced and the pan mixture was rotated for about 2 minutes till a proper homogeneity was achieved. Rest 40% of the water was added along with the dosage of superplasticizer and mixed for another 2 minutes. Immediately after SCC mixes were prepared in the mixer, the fresh properties were determined and checked with the EFNARC (2005) requirements for all the batch of SCC mixes. Once the fresh property criterion was satisfied, casting of specimen for testing the hardened concrete properties then initiated (Fig. 3.10). Fig. 3.11 shows the curing of SCC samples. Table 3.14 gives the details of the casting of SCC fresh and hardened properties.

Fig. 3.9: Mixing of Constituents of SCC in a Pan Mixture

Fig. 3.10: Casting of SCC Samples

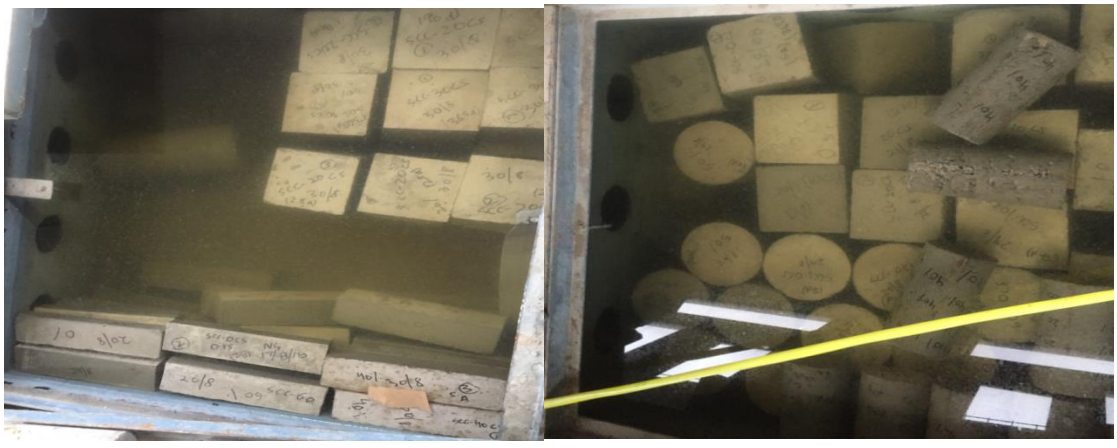

Fig. 3.11: Curing of SCC Samples

Table 3.14: Details of the Casting of SCC samples

Fresh Properties			
Property	**Reference Code**		**Testing Age**
Slump flow	EFNARC (2005)		Before casting samples
T_{500} slump flow	EFNARC (2005)		
V-funnel	EFNARC (2005)		
L-box	EFNARC (2005)		
U-box	EFNARC (2002)		
Segregation resistance	EFNARC (2005)		
Strength Properties			
Property	**Reference Code**	**Testing Age (Days)**	**Sample Details**
Compressive strength	BIS: 516-1959	7, 28, 90 and 365	150 mm cubes
Splitting tensile strength	BIS: 5816-1999		150 mm diameter and 300 mm length cylinder
Microstructure (SEM, EDS)	-	28, 90 and 365	Fracture sample from inner core of SCC after compressive strength test
XRD phase identification			Powder sample from inner core of SCC after compressive strength test
Durability Properties			
Property	**Reference Code**	**Testing Age (Days)**	**Sample Details**
Water absorption	ASTM C 642 (2013)	28, 90 and 365	100 mm diameter and 50 mm thick cylinder
Sorptivity	ASTM C 1585 (2004)		
Rapid chloride permeability	ASTM C 1202 (2010)		
Drying shrinkage	ASTM C 157 (2008)	Up to 448	(285 x 75 x 75) mm prism
Sulfate resistance Compressive strength Length variation	BIS: 516-1959 ASTM C 1012 (2010)	28, 90 and 365 Up to 365	150 mm cubes (285 x 75 x 75) mm prism

3.4 FRESH PROPERTIES OF SCC

3.4.1 Slump Flow and T_{500} Slump Flow Time

Slump flow test and T_{500} time determines the flowability and flow rate of SCC without obstructions using EFNARC (2005). The main principle is as follows: The fresh SCC is poured into the slump cone that is placed on a base plate of 1 x 1 m dimensions (Fig. 3.12). Concrete is then allowed to stand in the cone for not more than 30 seconds while the excess concrete is removed. The cone is uplifted vertically without disturbing the concrete spread. The time from commencing the cone upwards till concrete has spread to a diameter of 500 mm is denoted as T_{500} time. Then, the largest spread of concrete is noted without disturbing the baseplate and concrete and referred to as d_m. The spread diameter perpendicular to d_m is recorded and referred to as d_r. The average of d_m and d_r gives the value of the slump flow of SCC as given in equation 1.

$$Slump\ flow = \frac{dm+dr}{2} \quad (1)$$

Where;

dm= diameter of the largest spread of concrete; dr= diameter perpendicular to dm

SCC is checked for any segregation. If an accumulation of coarse aggregate is visible at the centre of the spread, the experiment is repeated while checking the constituents of the mix.

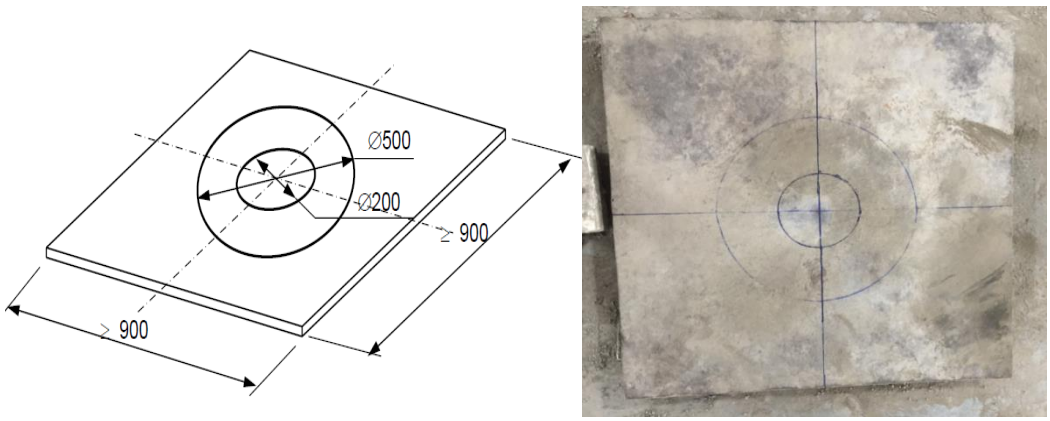

Fig. 3.12: Base Plate Used in Slump Flow Test (EFNARC, 2005)

3.4.2 V-Funnel

V-funnel test is suitable for measuring the viscosity and the filling ability of SCC as per EFNARC (2005). It consists of V-shaped funnel equipment having a bottom gate and a container is kept below the V-funnel. Around 12 litres of SCC is poured into the V-funnel while closing the bottom gateway and allowing to concrete to stand for 10 ± 2 seconds (Fig. 3.13). The time from opening the gate till the whole concrete is poured into the container is recorded and referred to as V-funnel time.

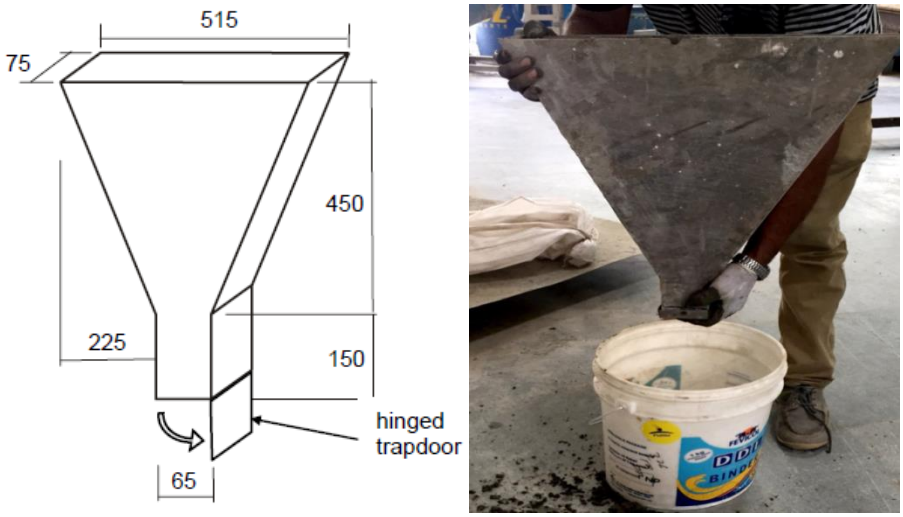

Fig. 3.13: V-Funnel Test as per EFNARC (2005)

3.4.3 L-Box

The passing ability of SCC is determined by the L-box test as specified by EFNARC (2005). SCC is allowed to flow through obstructions in the form of congested reinforcements without segregating. This test consists of L-box shaped equipment stipulated with three or two reinforcing bars (Fig. 3.14). Three bars simulate a congested reinforcement set up to determine the passing ability more significantly. Designing of reinforcing bars are as follows: two reinforcing bars of diameter 12 mm with a gap of 59 mm and three reinforcing bars of 12 mm diameter with 41 mm spacing. Approximately

17 litres of fresh concrete is poured in the vertical compartment of L-box while keeping the gate between horizontal and vertical chamber closed. The concrete is allowed to stand for 60 ± 10 seconds and segregation if any is recorded. The gate is lifted and the concrete flows into the horizontal compartment of L-box. When the movement of concrete has ceased to flow, measure the height difference between the top of the horizontal section of L-box and top of concrete at three different locations equally spaced across the width and find it's mean and refer it as H_2. The height difference between the top of the vertical section of the L-box and the top level of concrete is noted and its mean referred to as H_1. The ratio of H_2 and H_1 gives the passing ability of SCC.

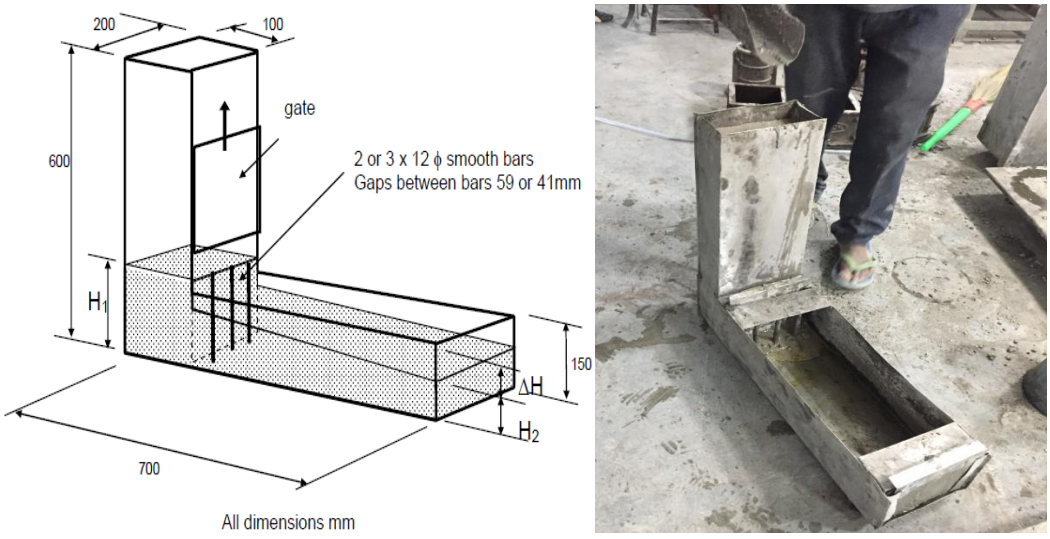

Fig. 3.14: L-Box Test Conducted as per EFNARC (2005)

3.4.4 U-Box

U-box test is conducted to study the passing ability of SCC as per EFNARC (2002). U-box apparatus is divided by a sliding gate that is supported by three reinforcing bars of 13 mm diameter with a centre to centre spacing of 50 mm (Fig. 3.15). About 20 litres of fresh concrete is poured in left compartment of U-box and retained for about a minute. The sliding gate is lifted and concrete is allowed to flow into the right chamber; passing

through the bars. Let the concrete come to rest and then measure the height of concrete in the filled compartment from two places and determine its mean (H_1). The height of the remaining concrete in the other chamber is measured and indicated as H_2. The filling height is calculated by their difference (H_1-H_2). If the concrete flows freely as water, then it will be horizontal at rest and the filling height will be zero. This indicates that values closer to this will give the better passing ability of fresh SCC.

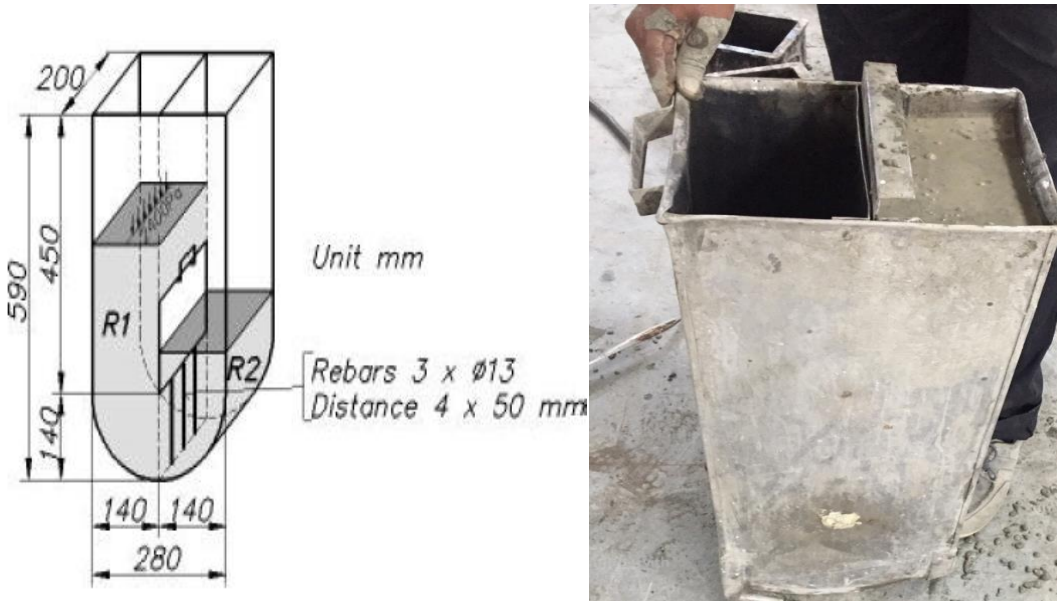

Fig. 3.15: U-Box Test Conducted as per EFNARC (2002)

3.4.5 Sieve Segregation Resistance

Sieve segregation resistance test is used to evaluate the segregation resistance of SCC as per EFNARC, (2005). Fresh SCC (about 10 litres) is poured into a container with lid having 300 mm diameter and capacity of about 12 litres; while it is allowed to stand for some time. A perforated sieve of 5 mm square aperture and sieve receiver is placed on the weighing machine. The mass of sieve receiver is recorded as W_p. About 4.8 kg of concrete is poured from the top of the sample container at a height of 500 mm above sieve. The mass of concrete retained on the sieve is recorded as W_c. The concrete is then

allowed to stand for almost 120 seconds and the sieve is lifted. The mass of the receiver along with the concrete passed in the receiver is measured as W_{ps}. The segregation portion is calculated using equation 2.

$$Segreagtion\ portion\ (\%) = \frac{Wps - Wp}{Wc} * 100 \quad (2)$$

Where;

W_{ps}= mass of sieve receiver and the concrete passed in the receiver; W_p= mass of the sieve receiver; W_c= mass of concrete retained on the sieve

3.5 STRENGTH PROPERTIES

3.5.1 Compressive Strength

After performing fresh properties of SCC, the casting of specimens for evaluating the strength and durability properties initiated. The compressive strength test is executed as per BIS: 516-1959. Cubes of dimensions 150 x 150 x 150 mm used to test the compressive strength of SCC. Cube moulds are stouted adequately to prevent any distortion and proper oiling is done before filling the concrete into the mould. Each cube mould is attached with a base plate that is having a plane surface. After the preparation of SCC in the pan mixture, it is filled in the cube moulds without providing any compaction. Test specimens are left for 24 hours and covered with a plastic sheet to prevent any moisture loss. After this, test specimens are taken out from the mould and marked for later identification. Test specimens are immediately cured in water until taken out before testing. Compression testing machine is used for testing the compressive strength of SCC (Fig. 3.16). At the age of 7, 28, 90 and 365 days, the test specimen is taken out of the water and immediately tested for the compressive strength; while wiping off excess water and grit from the surface. At least three samples tested for each concrete mix. The load is applied without shock and increased continuously at the rate of approximately 140 kg/cm^2/min till the specimen breaks down. The maximum load until failure is reported. The maximum load divided by the area of the sample determines the compressive strength of the concrete, as shown in equation 3. Average of three values is chosen for

determining the compressive strength provided the individual variation was not more than ±15% of the average.

$$fc = \frac{P}{A} \tag{3}$$

Where; f_c = *compressive strength (N/mm^2); P = maximum load (N); A = cross-sectional area of the specimen (mm^2)*

Fig. 3.16: Compressive Strength Test

3.5.2 Splitting Tensile Strength

Splitting tensile strength test is performed using BIS: 5816-1999. The test is an indirect test for measuring the tensile strength of concrete by compressing a cylinder through a line load applied along its length. Cylindrical specimens of diameter 150 mm and length 300 mm were cast. After casting, they were left for 24 hours covered with a plastic sheet to prevent moisture loss. The cylinders are then taken out of the mould and marked for later identification. Cylinders are kept under water curing till the age of testing (7, 28, 90 and 365 days). Splitting tensile strength is measured on compression testing machine as shown in Fig. 3.17. The load is applied without shock and is increased continuously at a rate of 1.2 to 2.4 N/ mm^2/ min until the failure of the specimen. Maximum load until failure is reported and splitting tensile strength is calculated by using equation 4. Average of three values is chosen as the desired splitting strength of SCC.

$$ft = \frac{2P}{\Pi ld} \quad (4)$$

Where;

f_t = splitting tensile strength (N/mm^2); P= maximum load (N); l= length of cylinder (mm); d= diameter of cylinder (mm)

Fig. 3.17: Splitting Tensile Strength Test

3.6 DURABILITY PROPERTIES

3.6.1 Water Absorption

Water absorption test of SCC performed on cylinders of 100 mm diameter and 50 mm thickness as per ASTM C 642-13. This measures the absorption and volume of voids present in the hardened SCC matrix. The procedure for carrying out this test is as follows. Report the mass of specimen initially and put it in an oven to dry at 110 ± 5 °C for about 24 hours. The sample is taken out of the oven and allowed to cool and the mass is noted. If the difference between the consecutive masses is more than 0.5% of the lower value, the specimen is kept back to the oven for drying for another 24 hours. The process is repeated until the difference between successive masses becomes less than 0.5% of that of lower value. The final value of oven-dried mass is reported as A. The sample is allowed to cool and then immersed in water at approximately 21 °C for about 48 hours. The sample is then taken out of water and surface dried. Mass of the sample is reported and if the difference between the successive masses is more than 0.5% of the larger value; the sample is put in water for another 24 hours. The process is repeated until the difference between consecutive masses becomes less than 0.5% of the larger value. The final surface-dried mass after immersion is reported as B. The specimen is then put in a covered receptacle filled with water and boiled for 5 hours. The sample is allowed to cool naturally by loss of heat for more than 14 hours to a temperature of 20-25 °C. The mass of the specimen is noted after removing the surface moisture with a towel. The mass of the soaked and boiled sample is denoted as C. Suspend the concrete specimen in a water bucket at a constant water level and report the apparent mass as D. The calculations are made according to the following equations:

$$Absorption\ after\ immersion\ (\%) = \frac{(B-A)}{A} * 100 \quad (5)$$

$$Absorption\ after\ immersion\ and\ boiling\ (\%) = \frac{(C-A)}{A} * 100 \quad (6)$$

$$Bulk\ density, dry = \frac{(A)}{C-D} * \rho \quad (7)$$

$$Bulk\ density\ after\ immersion = \frac{B}{C-D} * \rho \quad (8)$$

$$Bulk\ density\ after\ immersion\ and\ boiling = \frac{C}{C-D} * \rho \quad (9)$$

$$Volume\ of\ permeable\ voids\ (\%) = \frac{C-A}{C-D} * 100 \quad (10)$$

Where;

A= oven-dried mass of sample in the air (g)

B= surface-dried mass of sample in the air after immersion (g)

C= surface-dried mass of sample in the air after immersion and boiling (g)

D= apparent mass of sample in water after immersion and boiling (g)

ρ= density of water= 1g/cm^3

3.6.2 Sorptivity

One of the essential durability tests includes the testing of sorptivity of concrete samples. Sorptivity test performed as per ASTM C 1585-04. The test determines the rate of absorption of water when only one side of a concrete specimen is immersed in water while other surfaces are sealed. The exposed surface is immersed in water and water ingress of unsaturated concrete is determined mainly by capillary action. Test specimens are cores of size 100 mm diameter and 50 mm length cut from a cylinder of 100 mm diameter and 200 mm length. Test specimens are stored in an environmental chamber at a temperature of 50 ± 2 °C and relative humidity of 80 ± 3% for three days. Each sample is then stored in a separate sealable container for at least 15 days at around 23 ± 2 °C for maintaining the equilibrium of moisture distribution. This procedure is referred to as conditioning of the sample. The samples are taken out of the containers and their mass recorded. The average diameter of the surface of the sample exposed to water noted. The sides of the specimen are sealed with some sealing material like epoxy (Fig. 3.18). The surface that is not exposed to water is covered with a plastic sheet. The mass of the sealed specimen is recorded before its exposure to water and is denoted as initial mass. A support system is placed at the bottom of the pan. The pan is filled with water level such

that it is 1 to 3 mm above the top of the support system (Fig. 3.18). The stopwatch is started and the test surface of the specimen is placed on the support system. The mass of the sample is recorded at various intervals. The time and tolerances for the measurement schedule of sorptivity are given in Table 3.15.

Table 3.15: Time and Tolerances for the Measurements Schedule of Sorptivity (ASTM C 1585, 2004)

Time	**Tolerances**
60 seconds	2 seconds
5 min	10 seconds
10 min	2 minutes
20 min	2 minutes
30 min	2 minutes
60 min	2 minutes
Every hour up to 6 hours	5 minutes
Once a day up to 9 days	2 hours

The rate of absorption of water is calculated by dividing the change in mass by the product of cross-sectional area and density of water as given in equation 11.

$$I = \frac{mt}{a*\rho} \tag{11}$$

Where *I = absorption (mm);* m_t *= change in mass (g) at time t, a = exposed cross-sectional area of the specimen (*mm^2*);* ρ*= density of water (g/*mm^3*)*

The initial and secondary rate of absorption is obtained by plotting the values of absorption to the square root of time. The initial and secondary rate of absorption given by the slope of the line that is the best fit to absorption (I) plotted against the square root of time ($s^{1/2}$). Using linear regression, values of absorption from time 1 minute to 6 hours gives the initial rate of absorption ($mm/sec^{1/2}$) and values of absorption from 1 day to 7 days determines the secondary rate of absorption ($mm/sec^{1/2}$).

Fig. 3.18: Sorptivity Test

3.6.3 Rapid Chloride Permeability Test

The rapid chloride permeability test is conducted as per the specifications given in ASTM C 1202-10. The method provides a measure of the electrical conductance of concrete to determine the resistance of concrete to chloride ion penetration. Test specimens are cores of size 100 mm diameter and 50 mm length cut from a cylinder of 100 mm diameter and 200 mm length. Moist curing for about 28 days is necessary for carrying out this test. The specimen is placed in a desiccator such that both the sides of the specimen are exposed (Fig. 3.19). The desiccator is sealed and the vacuum pump is started keeping the pressure less than 50 mm mercury within a few minutes. The vacuum is maintained for three hours. Fill a separatory funnel with de-aerated water. When the vacuum pump is still on,

open the water stopcock and let sufficient quantity of water drain in to cover the specimen with water. The stopcock is then closed and the vacuum pump is run for an additional one hour. The vacuum line stopcock is closed and the pump is turned off. The specimens are submerged in water for at least 18 ±2 hours. By following these steps, the conditioning of samples is completed. The specimen is removed from the desiccator after this time and excess water cleaned. The sample is inserted between the two halves of the cell. One side of the cell filled with 3% sodium chloride (this side connected to the negative terminal of the power supply). In contrast, the other half filled with 0.3 normality sodium hydroxide (this side connected to the positive terminal of the power supply). The lead wires are attached to the banana post. Electrical connections are made properly at a voltage of 60 ± 0.1 V and the power turned on (Fig. 3.20). The initial reading of the charge passed in coulombs recorded. The reading is noted after every 30 minutes up to 6 hours. The test is closed at 6 hours and the specimen removed from the cell. The cell immediately cleaned with tap water for re-use. The total charge passed in coulombs is reported at the end of 6 hours test conducted (Fig. 3.21). It will give the measure of chloride ion permeability as per the specification given in Table 3.16 below.

Table 3.16: Measure of Chloride Ion Permeability (ASTM C 1202, 2010)

Charge Passed (Coulombs)	**Chloride Ion Permeability**
>4000	High
2000-4000	Moderate
1000-2000	Low
100-1000	Very low
<100	Negligible

Fig. 3.19: SCC Samples in a Desiccator

Fig. 3.20: Rapid Chloride Permeability Test

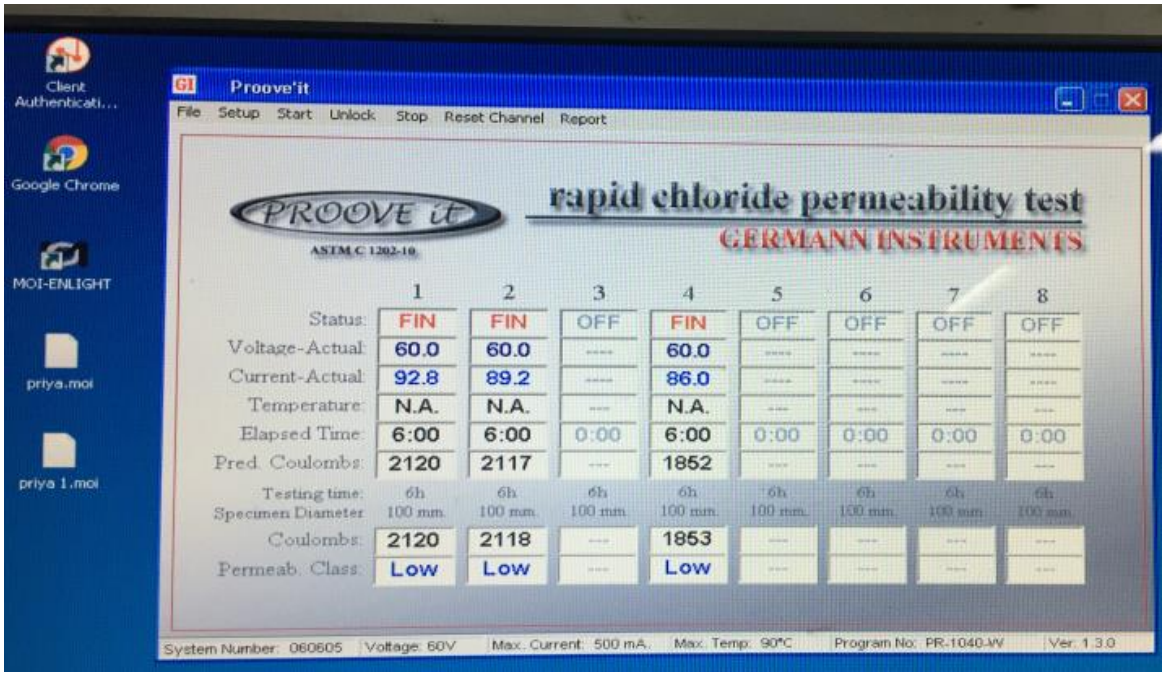

Fig. 3.21: Result Display of RCPT

3.6.4 Drying Shrinkage

Drying shrinkage of concrete has been conducted as per ASTM C 157-08. Volumetric changes are measured through this test by forces other than applied loads or temperature changes. Test specimen consists of a prism of square cross-section 75 x 75 mm and a length of 285 mm (Fig. 3.22). The size of the sample is one of the main factors influencing the length of prism, so the test specimens must maintain the same dimensions. The concrete is filled in two layers in the prism mould without giving compaction. The specimen mould is covered with a plastic sheet to prevent moisture loss for 24 hours. Remove the specimen from the mould without giving a jerk with the help of a demoulding device. Centerline marks are placed and positioned at both the ends of specimen for further identification with graphite using a pencil or waterproof ink only. The initial comparator reading is taken just after 24 hours of adding water to the cement during mixing of SCC. The specimens are stored in water for 28 days. A second comparator reading is recorded after 28 days. The samples stored in a drying room (with a relative humidity of 50 ± 4%). The readings recorded at 4, 7, 14, 28 days and after 8,

16, 32 and 64 weeks. The samples stored in such a way that they have 25 mm clearance on all sides and maintained at a temperature of 23 ± 2 °C. The length change is calculated using equation 12.

$$\Delta l = \frac{CRD - Initial\ CRD}{G} * 100 \quad (12)$$

Where;

Δl= change in length at any age (%); CRD= difference between comparator reading of the specimen and the reference bar at any age; G=the gauge length (mm)

Fig. 3.22: Drying Shrinkage Test

3.6.5 Sulfate Resistance

Sulfate resistance test is assessed by computing the changes in the length of the prisms, variation in compressive strength and gain in the mass of concrete cubes for up to one year. For measuring the length changes, prisms of dimensions 75 x75 x 285 mm are cast and cured for 28 days under water. The changes in mass and compressive strength are observed for cube specimens of size 150 mm (Fig. 3.23). The samples are initially cured under water for 28 days and then immersed in a 5% (Na_2SO_4) sulfate solution for up to one year. The sulfate solution is changed each month to maintain the homogeneity of the solution and pH is maintained between 6 to 8 each time the solution is prepared. Before immersing the prisms in sulfate solution, an initial comparator reading is recorded. The readings of the comparator are then noted after immersion in sulfate solution at 1, 2, 3, 4, 8, 13 and 15 weeks. Subsequent readings recorded at 4, 6, 9 and 12 months. The variations in length reported as per the procedure given in ASTM C 1012-10. The change in length of prisms immersed in sulfate is calculated by using equation 13. The compressive strength test is carried out as per BIS: 516-1959. The compressive strength test conducted at 28, 90 and 365 days of immersion of sulfate solution after the initial 28 days water curing.

$$\Delta l = \frac{lx - li}{G} * 100 \quad (13)$$

Where;

Δl= change in length at x age (%); lx= comparator reading of the specimen at x age; li= initial comparator reading of the specimen; G=the gauge length (mm)

Fig. 3.23: SCC Samples (150 mm Cubes) for Sulfate Resistance Test

3.7 MICROSTRUCTURAL ANALYSIS

3.7.1 Scanning Electron Microscopy and Energy Dispersive Spectroscopy

Scanning electron microscopy (SEM) is used for the characterization of materials. The Scanning electron microscope is an instrument used to analyze the microstructure of a sample by means of a finely focussed beam of energetic electrons. An electron-optical system is used to form an electron probe that is scanned through the sample (raster pattern). Different types of signals are produced during the interaction of this beam with the sample. Detectors then collect the signals. The signal amplitude at each position in the raster pattern is compiled to form an image. The SEM consists of (a) Illuminating system or Imaging system that includes an electron gun and magnetic lenses (b) Information system (c) Display system and (d) Vacuum system. The information system consists of two types of interactions: elastic and inelastic collisions. The elastic collisions are the electron-nucleus interactions that produce the backscattered electron, which provides the topographic and composition information. The inelastic collisions are the electron-electron interactions that form the secondary electrons, X-rays and photons. The signals

that are derived from electron-sample interactions reveal the information about the sample like its morphology and chemical composition. SEM is applied to study morphology, topography, composition and crystallographic information of a sample. SEM has a large depth of field that allows a large sample to be focussed at one time and provides a larger magnification. The sample used in SEM is mounted on a conductive substrate such as aluminium stub and gold platted in a vacuum. The gold coated samples are kept at the sample stage of the microscope. In this research, the sample is obtained from the inner core of the concrete matrix after performing the compression strength test. The fracture surface of the sample is gold-coated before analyzing for SEM to make tit electrically active. Fig. 3.24 shows the image of a scanning electron microscope. The SEM of the concrete, in general, reflects the combination of calcium hydroxide, ettringites (calcium sulfoaluminate), calcium silicate hydrate (CSH), fine and coarse aggregate and the interfacial transition zone between the hydrated cement matrix and the aggregates. SEM is used for elemental analysis and chemical mapping of surfaces using energy dispersive spectroscopy (EDS). X-ray spectroscopy is a method to study the qualitative and quantitative analysis of the chemical composition by exciting atoms and detection of their characteristic x-ray. EDS is one of the methods used to identify x-ray emission.

Fig. 3.24: Scanning Electron Microscope

3.7.2 X-Ray Diffraction

The powder X-ray diffraction (XRD), also known as the Debye-Scherrer method, is one of the most powerful techniques used for the characterization of crystalline materials. XRD is also used to identify mixed phases present in the material. The method involves diffraction of monochromatic X-ray by a powdered sample. X-ray diffractometer is an instrument used for the analysis. It consists of an X-ray tube, a sample holder and an X-ray detector. The characteristic X-rays are produced by heating a filament in a cathode ray tube. The sample to be investigated is powdered and placed in a sample holder (small disc-like container) and the surface is flattened. The X-rays are collimated and directed onto the sample. The fundamental concept which governs the XRD is known as Braggs law which follows the equation:

$$2 d \sin \theta = n \lambda \quad (14)$$

Where d is the inter-planar spacing, λ is the wavelength of X-ray, θ is the scattering angle, n is an integer representing the order of diffraction peak.

The interaction of X-ray with the sample generated constructive interference when conditions follow the Braggs law and get diffracted in the form of a cone. The diffracted X-rays are detected and processed. The resultant diffraction peaks give information regarding the peak intensities, the position of diffraction maxima and intensity distribution in the form of diffraction angle. The results are processed in the form of an XY plot known as diffractogram, which plots the intensity (y-axis) and 2θ values (x-axis). The analysis of XRD is carried out with the help of software like The X'Pert high score plus. The results are compared with the known ASTM (American Society for Testing and Materials) or JCPD (Joint Committee of Powder Diffraction Standards) cards. In the present research, XRD technique was carried out to identify different phases present in hardened SCC mixes containing copper slag varying from 0% to 60%. Powder samples were taken from hardened concrete samples after performing the compressive strength test at 28, 90 and 365 curing days. The sample is sieved through 90 μm sieve and the sieved sample is used for XRD analysis. The XRD was conducted using a Panalytical X'Pert Pro device located at SAI labs, Thapar Institute of Engineering and Technology,

Patiala, India. The following parameters were fixed: monochromatic Cu kα radiation of 1.5418 Å wavelength in the range of 5-90° of 2θ range, step size of 0.02° and a scan rate of 0.097°/sec, functioning at 45 kV and 40 mA.

3.8 STATISTICAL ANALYSIS

SPSS version 20 is used for determining the statistical analysis of the present research work. Descriptive data is calculated for each group of samples pertaining to the strength and durability properties. Analysis of variance (ANOVA) used to compare different SCC mixes at 7, 28, 90 and 365 days of curing age. Post hoc Tukey test used for multiple comparisons between SCC mixes varying from 0% to 60%. The values of multiple comparison analysis of different SCC mixes are given in detail in appendix (A-E).

CHAPTER -4
RESULTS AND DISCUSSION

This chapter deals with the results of the fresh, mechanical and durability properties of SCC incorporating copper slag. The microstructural analysis included Scanning electron microscopy (SEM), Energy dispersive spectroscopy (EDS) and X-ray diffraction (XRD) of SCC mixes at all ages of curing. Statistical analysis was conducted to study the correlations amongst various properties of SCC. The statistical significance of the strength and durability properties was evaluated using Analysis of Variance (ANOVA). Multiple comparison analysis was conducted to compare different SCC mixes using the Post Hoc Tukey test.

4.1 FRESH PROPERTIES OF SCC

The fresh properties were performed to assess the flowability, the passing ability, the viscosity and segregation resistance of SCC; the key principals of designing SCC. Table 4.1 defined the various classes of SCC as per EFNARC (2005). From the results, it was inferred that there was an improvement in workability on the addition of copper slag up to 60%. All the mixes were in good accordance with the classifications prescribed in the European code.

4.1.1 Slump Flow and T_{500} Slump Flow

Table 4.2 presents the results of fresh properties of SCC incorporating copper slag. Slump flow diameters in the range of 685-750 mm were observed for SCC mixes and categorised under the slump flow class SF2; well within the range as required by EFNARC (2005). Fig. 4.1 presented the slump flow of all mixes studied in this research. The slump flow value of SCC mix containing 100% sand was 685 mm, which lies under the class SF2. The slump flow value augmented as the content of copper slag increased; reached 750 mm for the mix incorporating 60% copper slag. The increment in slump flow owed to the smooth, glassy texture and low water absorption characteristic of slag grains that increased the flowability of SCC mixes. These results were in concomitance with the research studies of Mavroulidou (2017), Al-Jabri et al. (2011), dos Anjos et al.

(2017), Sharma and Khan (2017a), Madheswaran et al. (2014); wherein they reported improvement in workability as the percentage of copper slag increased. Though, signs of bleeding and segregation were observed for mixes containing more than 40% copper slag. A greater amount of bleeding was seen with the increment of copper slag due to heavy specific weight and glassy texture of copper slag grains (Shoya et al., 1997). A sieve segregation resistance test thus was conducted for SCC mixes incorporating higher percentages of copper slag to access the resistance of SCC mixes to segregation. Fig. 4.2 presented the results of the T_{500} slump flow test. All the values were in the permissible range as per EFNARC (2005). The time taken by SCC mixes to reach 500 mm diameter mark decreased as there was an increase in copper slag content. This could be attributed to the lack of cohesion of the components of SCC (Gesoglu et al., 2009). Fig. 4.3 shows the picture of the slump flow of SCC mix.

Table 4.1: Classification of Fresh Properties of SCC (EFNARC, 2005)

Test	**Property**	**Range**	**Class**
Slump flow (EFNARC, 2005)	Consistency	550-650 mm 660-750 mm 760-850 mm	SF1 SF2 SF3
T_{500} slump flow (EFNARC, 2005)	Viscosity	≤ 2 s > 2 s	VS1 VS2
V-funnel (EFNARC, 2005)	Viscosity	≤ 8 s 9 to 25 s	VF1 VF2
L-box (EFNARC, 2005)	Passing ability	≥ 0.8 (2 rebars) ≥ 0.8 (3 rebars)	PA1 PA2
U-box (EFNARC, 2002)	Passing ability	0 to 30 mm	-
Sieve segregation resistance (EFNARC, 2005)	Segregation	≤ 20% ≤ 15%	SR1 SR2

Table 4.2: Results of Fresh Properties of SCC

Mix	Slump Flow (mm)	T_{500} Slump Flow (s)	V-Funnel (s)	L-Box	U-Box (mm)	Sieve Segregation Ratio (%)
0CS-SCC	685	3.01	7.55	0.82	20	3.75
10CS-SCC	727	2.78	7.04	0.85	17	4.5
20CS-SCC	730	2.32	6.78	0.85	16	5.5
30CS-SCC	730	2.1	6.34	0.91	15	7.5
40CS-SCC	735	1.71	5.78	0.95	15	10
50CS-SCC	740	1.69	5.46	0.96	18	11.5
60CS-SCC	750	1.21	5.01	0.98	20	12.5

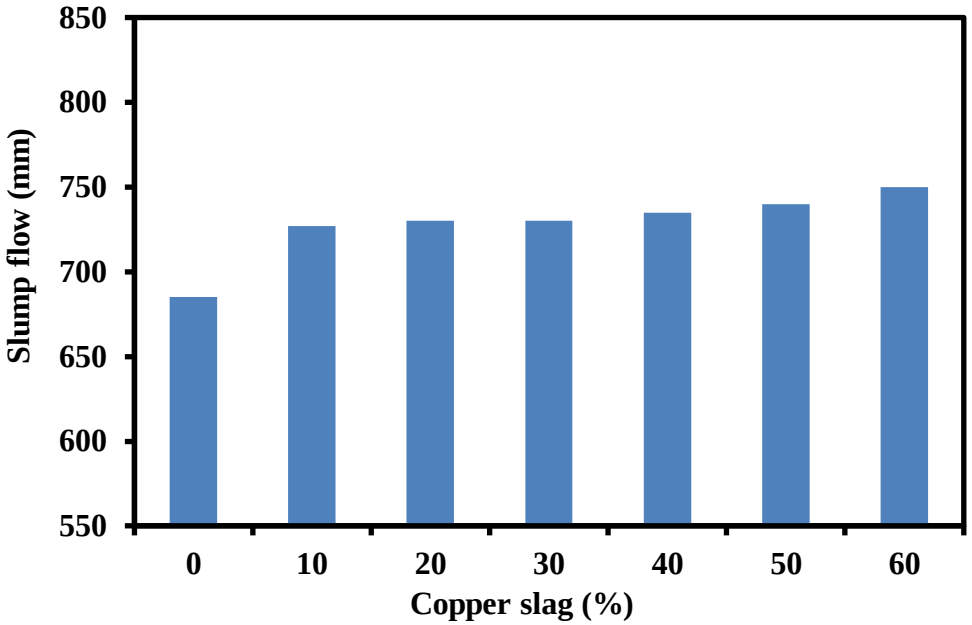

Fig. 4.1: Effect of Copper Slag on Slump Flow of SCC

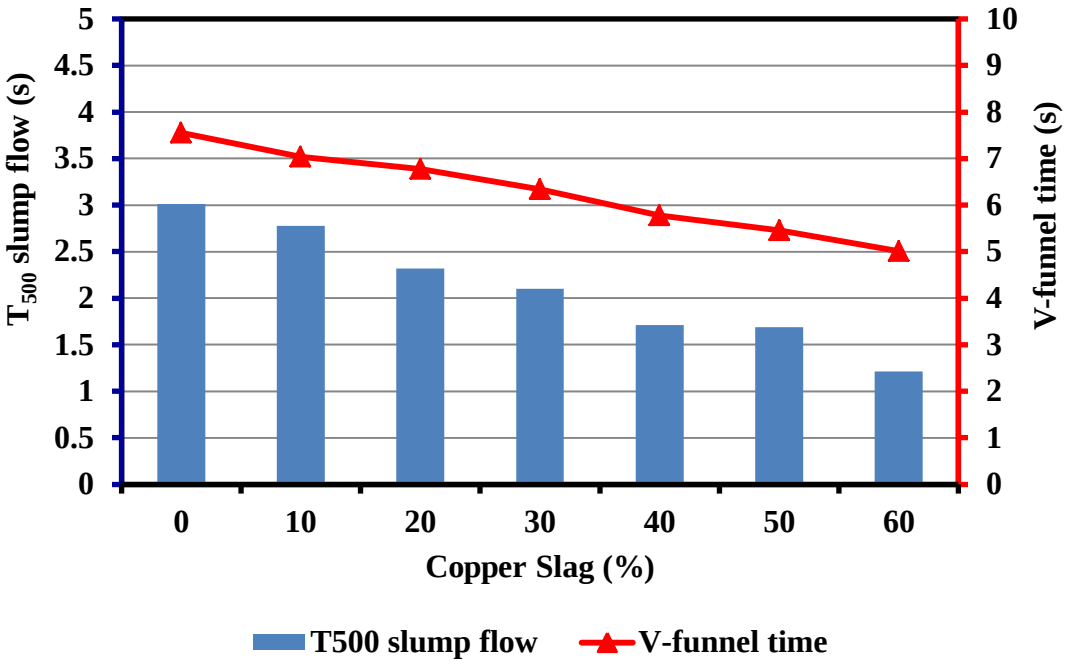

Fig. 4.2: Effect of Copper Slag on T_{500} Slump Flow and V-Funnel Time of SCC

Fig. 4.3: Slump Flow of SCC

4.1.2 V-Funnel

Fig. 4.2 shows the results of V-funnel test conducted on SCC mixes incorporating copper slag. It was inferred from the V-funnel test that the time taken to empty the funnel was maximum for the concrete mix having 0% copper slag. It decreased with the increasing content of copper slag. All the mixes were under the viscosity class VF1 as per the requirements of EFNARC (2005). Due to the smooth and glassy surface of copper grains, the viscosity reduced and hence the time taken to empty the funnel was less with the increasing copper slag content. The control concrete mix with 100% sand has V-funnel time more than all other mixes. V-funnel time decreased from 7.55 to 5.01 seconds as the amount of copper slag increased from 0 to 60% as given in Table 4.2. Afshoon and Sharifi (2014) observed that the V-funnel time decreased as the copper slag content escalated. Sharma and Khan (2017a) inferred the value of V-funnel in the range of 8.55 to 6.43 s while testing the SCC mixes containing 0 to 100% copper slag.

4.1.3 L-Box

The L-box test determined the passing ability of SCC mix, which enables the flow through tight openings and congested reinforcements. This test consisted of two main variations; one with two rebars and the other with three rebars. In the present study, the test was conducted with three rebars to stipulate the more congested type of reinforcement. The value of the blocking ratio generally lies from 0.8 to 1.0. In the present research, L-box ratio ranged from 0.82 to 0.98 for SCC mixes containing 0 to 60% copper slag (Fig. 4.4 and Table 4.2). All the mixes were categorized under class PA2 as per EFNARC (2005); test with three rebars. The results indicated that SCC mixes have been prepared with sufficient passing ability and could be used effectively.

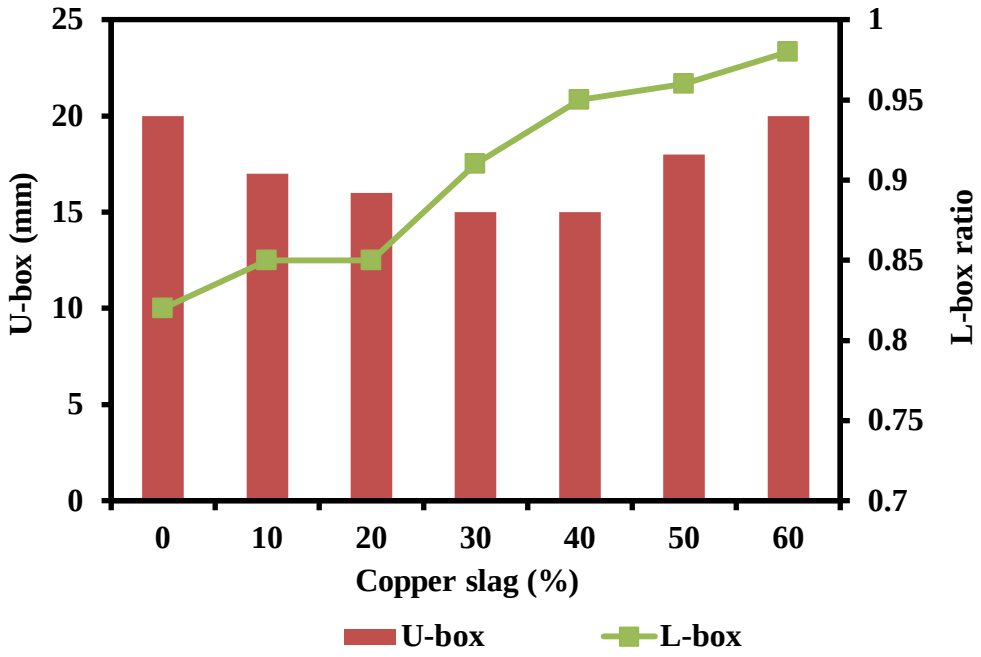

Fig. 4.4: Effect of Copper Slag on L-Box and U-Box Values of SCC

4.1.4 U-Box

The value of U-box ranged from 15-25 mm for SCC mixes; satisfying the criterion of EFNARC (2002) as presented in Table 4.2. The filling height of mix with 0% copper slag was 20 mm; this difference was somewhat decreased as copper slag augmented up to 40%. However, with further increase in copper slag percentage, signs of bleeding and segregation were observed due to which the filling height increased. Due to excess water being present in the mix that arises, the copper slag particles along with aggregates settle down due to their heavy weight; thereby increasing the filling height.

4.1.5 Sieve Segregation Resistance

SCC mixes were found to be stable with a segregation ratio of less than 15% and thus conforming to the guidelines of EFNARC (2005) as given in Table 4.2. The segregation ratio was 3.75, 4.5, 5.5 and 7.5% for SCC mixes incorporating 0%, 10%, 20% and 30% copper slag, respectively. While, the segregation ratio for SCC mix incorporating 40%,

50% and 60% copper slag came out to be 10, 11.5 and 12.5%, respectively; categorised under the segregation class SR2.

4.2 STRENGTH PROPERTIES OF SCC

4.2.1 Compressive Strength

The results of the compressive strength of SCC mixes incorporating up to 60% copper slag are given in Table 4.3. For each mix, the average of the three samples has been designated as its compressive strength value. Fig. 4.5 presented the effect of copper slag on the compressive strength of SCC mixes. The compressive strength of SCC mixes incorporating copper slag showed almost similar/higher results in comparison with a concrete mix containing 100% sand. The results were identical to the research findings of Hwang and Laiw (1989), Ayano and Sakata (2000), Shoya et al. (1997). As the content of copper slag increased in SCC mixes, the setting time of concrete got delayed. However, it did not have any noteworthy consequence on the properties of concrete (Ayano and Sakata, 2000). At 7 days curing age, SCC mixes incorporating 10, 20, 30, 40, 50 and 60% copper slag gained 2.86, 14.01, 16.88, 10.91, 6.64 and 6.40% compressive strength, respectively, in comparison to the control SCC mix without copper slag (20.54 MPa). The 28 days compressive strength of SCC mix incorporating 10, 20, 30, 40 and 50% copper slag achieved 6.97, 8.19, 4.20, 0.97 and 0.04% higher compressive strength, respectively, as compared to control SCC mix (35.63 MPa). An insignificant decrease of 0.09% was observed in SCC mix with 60% copper slag in comparison to control SCC mix at 28 days. A similar trend was followed for SCC mixes incorporating copper slag up to 60% at 90 and 365 days. At 90 days, SCC mixes incorporating 10, 20, 30, 40 and 50% copper slag gained 0.04, 6.89, 5.06, 0.49 and 0.26% compressive strength, respectively, in comparison to the SCC mix without copper slag (43.78 MPa). An insignificant decrease of 0.19% was observed in SCC mix with 60% copper slag in comparison to control SCC mix at 90 days. At 365 days, SCC mix incorporating 10, 20, 30, 40 and 50% copper slag achieved 1.14, 5.38, 4.10, 1.18 and 0.18% higher compressive strength, respectively, as compared to control SCC mix (45.56 MPa). An insignificant decrease of 0.07% was observed in SCC mix with 60% copper slag in comparison to control SCC mix at 365 days.

Maximum enhancement in strength of about 8.2% was observed for SCC incorporating 20% copper slag compared to control concrete at 28 days curing. This strength gain was attributed mainly to the physical properties of copper slag. Copper slag grains were effective in improving the stress concentration of the concrete matrix due to the enhanced compressibility of slag particles in comparison to sand (Wu et al., 2010). Due to the sharp edges of slag particles, it helps in improving the cohesion of the concrete matrix (Al-Jabri et al., 2011). However, an insignificant reduction in strength was observed beyond 30% copper slag replacement; though the strength was comparable with that of SCC mix with 100% sand. The major reason for the decrease in strength was the glassy texture and low water absorption property of copper slag, which led to excess water (Al-Jabri et al., 2011). The presence of ettringite and voids in the concrete matrix observed under SEM further confirmed the decrease in strength. With an increase in curing age, SCC mixes gained higher compressive strength, as shown in Fig. 4.6. The compressive strength of SCC mix with 0% copper slag increased from 20.54 to 45.56 MPa (121.60%) with the increase in curing age from 7 to 365 days curing. The compressive strength of SCC incorporating 10% copper slag increased by 118.16% with an increase in curing age from 7 to 365 days. The compressive strength of SCC mix incorporating 20, 30, 40, 50 and 60% copper slag increased by about 105.06, 97.59, 102.40, 108.43 and 108.37%, respectively, as the curing period increased from 7 to 365 days.

Hwang and Laiw (1989) concluded that compressive strength results are almost alike to that of control concrete for mixes up to 80% copper slag substitution as sand. Wu et al. (2010) suggested that incorporating copper slag content less than 40% as sand substitution will attain high strength concrete. Al-Jabri et al. (2011) concluded that the compressive strength of concrete incorporating up to 50% copper slag was similar to the strength of concrete mix incorporating 100% sand. Sharma and Khan (2017a) studied self-compacting mixes incorporating copper slag (0% to 100%) as sand replacement. The maximum increase in strength observed at 20% copper slag replacement. Hence, it can be concluded that the compressive strength of SCC mixes incorporating up to 60% copper slag showed either higher or comparable results as compared to control SCC. Also, with an increase in curing age, SCC mixes gained higher compressive strength.

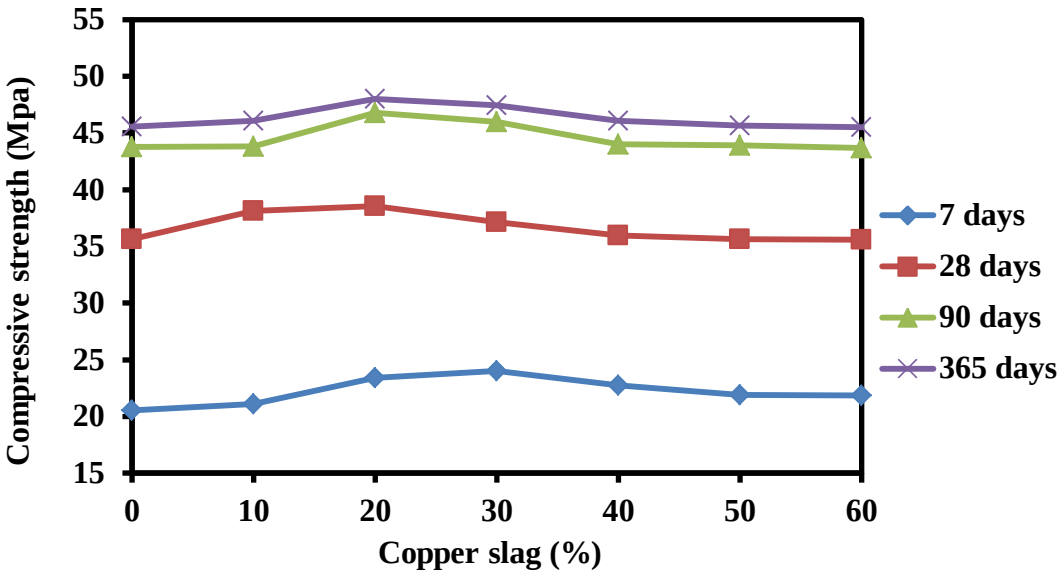

Fig. 4.5: Effect of Copper Slag on Compressive Strength of SCC

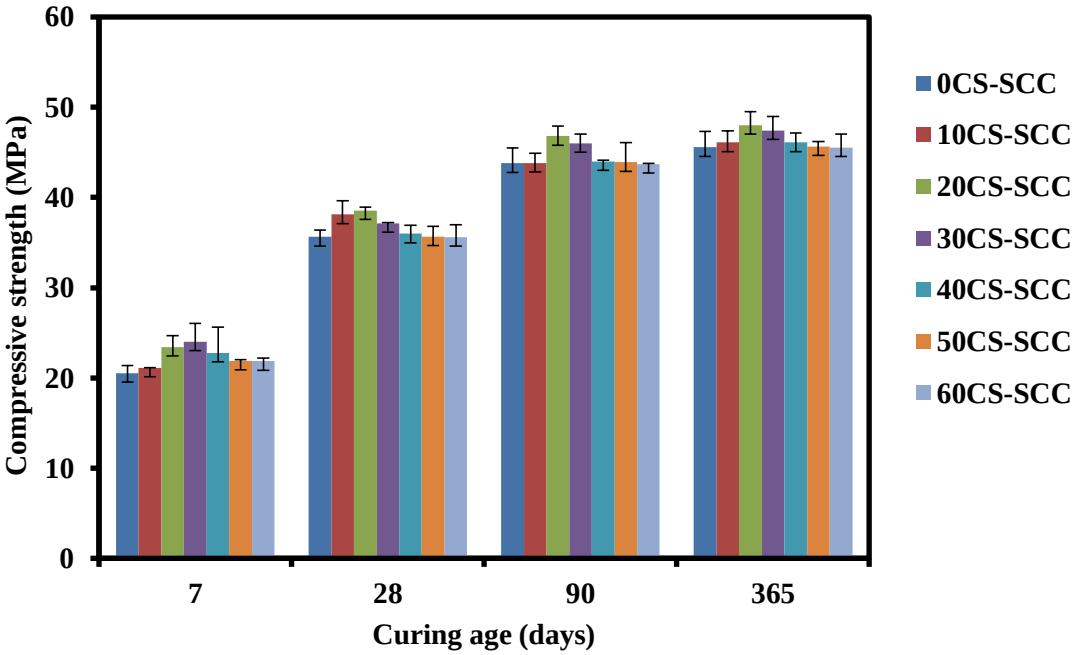

Fig. 4.6: Compressive Strength of SCC versus Age

Table 4.3: Compressive Strength of SCC

Type of Mix	7 Days				28 Days				90 Days				365 Days			
	1	**2**	**3**	**Avg.**	**1**	**2**	**3**	**Avg.**	**1**	**2**	**3**	**Avg.**	**1**	**2**	**3**	**Avg.**
0CS-SCC	19.70	21.37	20.54	***20.54***	34.90	35.60	36.40	***35.63***	42.09	45.48	43.78	***43.78***	47.40	45.40	43.89	***45.56***
10CS-SCC	21.12	21.11	21.14	***21.12***	36.59	39.64	38.12	***38.12***	42.70	43.80	44.90	***43.80***	46.18	44.76	47.31	***46.08***
20CS-SCC	23.86	24.38	22.00	***23.41***	38.20	38.55	38.90	***38.55***	45.70	46.80	47.90	***46.80***	49.10	48.60	46.34	***48.01***
30CS-SCC	25.60	21.70	24.70	***24.00***	37.20	37.13	37.06	***37.13***	46.00	45.00	47.00	***46.00***	48.60	45.69	48.00	***47.43***
40CS-SCC	26.02	20.68	21.63	***22.78***	36.50	36.52	34.92	***35.98***	43.90	44.00	44.10	***44.00***	47.20	46.00	45.10	***46.10***
50CS-SCC	21.80	22.00	21.90	***21.90***	35.68	34.50	36.76	***35.65***	42.59	42.70	46.40	***43.90***	44.98	45.98	45.98	***45.65***
60CS-SCC	22.20	21.85	21.50	***21.85***	34.20	35.60	37.00	***35.60***	43.76	43.64	43.70	***43.70***	44.48	44.90	47.21	***45.53***

Avg. refers to the average value obtained.

4.2.2 Splitting Tensile Strength

The results of splitting tensile strength are presented in Table 4.4. The effect of copper slag on the splitting tensile strength of SCC mixes incorporating copper slag is shown in Fig. 4.7. Utilization of copper slag in SCC mixes increased splitting tensile strength up to 60% replacement at curing ages from 7 to 365 days as presented in Fig. 4.8. The maximum strength was observed in SCC mix with 60% copper slag replacement at all curing ages. The splitting tensile strength of control SCC mix was 1.37 MPa at 7 days curing age. The strength increased by about 5.82, 45.63, 60.68, 61.41, 74.75 and 71.60% for SCC mix incorporating 10, 20, 30, 40, 50 and 60% copper slag, respectively. At 90 days, the splitting tensile strength of control SCC was 3.11 MPa which escalated by about 17.36, 23.26, 24.76, 25.08, 32.58 and 35.91% in SCC mix with 10, 20, 30, 40, 50 and 60% copper slag, respectively. The splitting tensile strength of control SCC mix was 3.43 MPa at 365 days curing age. The strength increased by about 12.54, 17.59, 19.34, 22.16, 26.43 and 30.22% for SCC mix incorporating 10, 20, 30, 40, 50 and 60% copper slag, respectively, at 365 days. Enhancement in strength was due to the angular edges of copper slag grains that led to an improvement in the cohesion of the concrete matrix. Sharma and Khan (2017a) inferred similar results wherein; the splitting tensile strength increased up to 80% copper slag addition.

An increase in splitting tensile strength was observed for SCC mixes with and without copper slag with the increase in curing age (Fig. 4.8). The splitting tensile strength of control SCC mix at 7 days curing age was 1.37 MPa and at 28, 90 and 365 days curing age, the result value increased about 55.90, 126.45 and 149.7%, respectively. With 10% copper slag in SCC mix, the value at 7 days curing was 1.45 MPa and the value increased by about 75.91, 155.14 and 165.59% at 28, 90 and 365 days curing age, respectively. The splitting tensile strength of SCC mix with 20% slag increased by about 45.00, 91.67 and 101.67% at 28, 90 and 365 days, respectively, as compared to the 7 days value of SCC mix (2.00 MPa). With the increase of copper slag from 20 to 30%, the splitting tensile strength value of SCC mix was 2.21 MPa at 7 days while this value increased by about 55.58, 75.83 and 85.49% at 28, 90 and 365 days curing age, respectively. Furthermore, the splitting tensile strength of SCC mix with 40, 50 and 60% slag was 2.22, 2.40 and

2.36 MPa, respectively, at 7 days. The strength of SCC with 40% copper slag increased by about 53.53, 75.48 and 89.02% at 28, 90 and 365 days, respectively. While the splitting tensile strength of SCC mix incorporating 50% copper slag increased by about 38.19, 71.80 and 80.69% at 28, 90 and 365 days, respectively. Also, the splitting tensile strength of SCC mix incorporating 60% copper slag increased by about 45.54, 79.34 and 89.53% at 28, 90 and 365 days, respectively.

It can be concluded that the utilization of copper slag in SCC mixes increased the splitting tensile strength up to 60% replacement. Also, an increase in splitting tensile strength was observed for SCC mixes with and without copper slag with the increase in curing age.

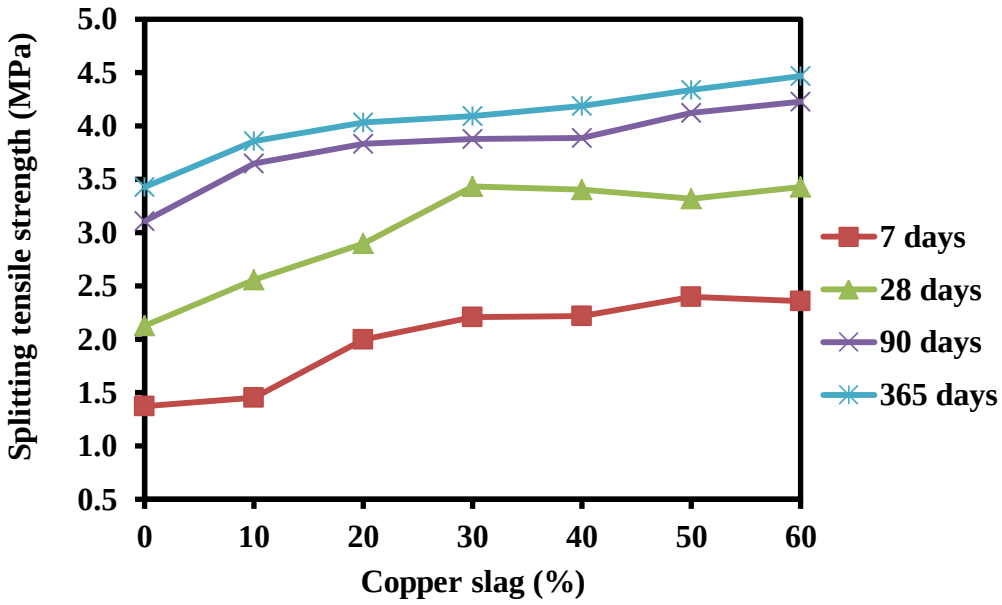

Fig. 4.7: Effect of Copper Slag on Splitting Tensile Strength of SCC

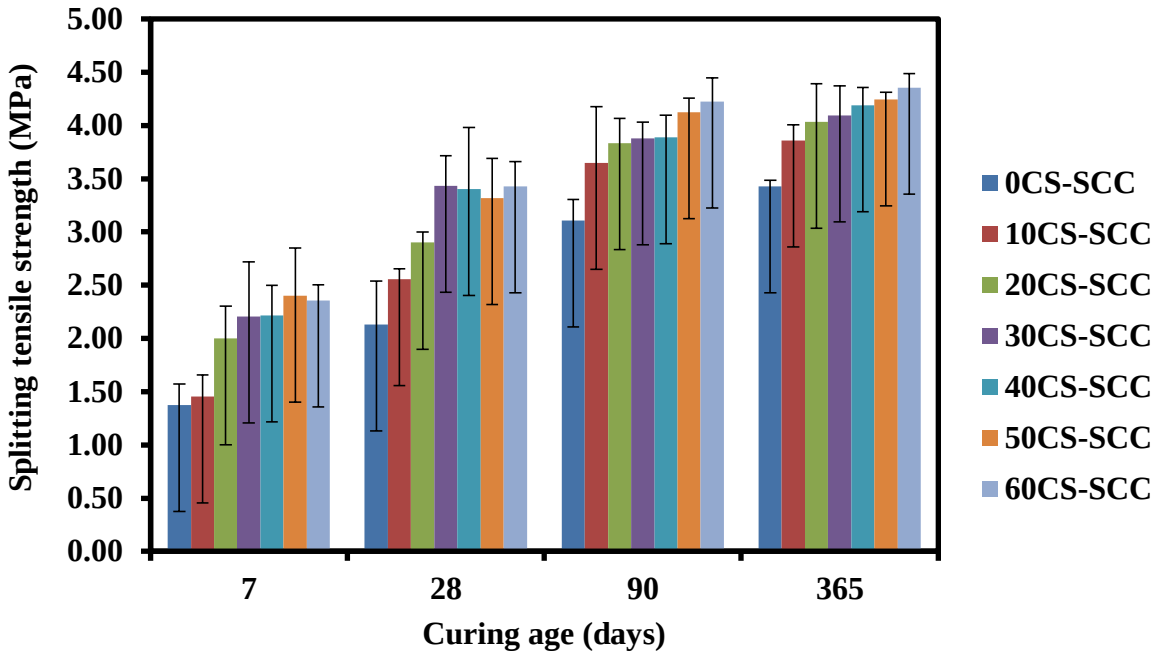

Fig. 4.8: Splitting Tensile Strength of SCC versus Age

4.3 DURABILITY PROPERTIES OF SCC

4.3.1 Water Absorption

Water absorption test evaluates the absorption value as well as the permeable voids present in the hardened concrete when it is subjected to aggressive environments. Table 4.5 shows the results of water absorption of SCC incorporating copper slag. Fig. 4.9 and 4.10 show the values of absorption with respect to copper slag percentage and curing ages, respectively.

As the percentage of copper slag increased in SCC mixes, the values of water absorption were found to reduce at all curing ages. Water absorption of SCC mixes was found to be less than 6.5% at all curing ages. A significant reduction in absorption was studied for SCC mixes incorporating up to 30% copper slag. At 28 days curing age, water absorption of control SCC mix was 6.30%. The results reduced by about 3.17, 9.40, 6.88, 6.35, 2.17 and 0.53%, respectively, for SCC mix incorporating 10, 20, 30, 40, 50 and 60% copper slag. The water absorption of control SCC mix was 5.72% at 90 days curing age. The

results reduced about 4.72, 11.42, 7.98, 6.63, 3.32 and 0.99%, respectively, for SCC mix incorporating 10, 20, 30, 40, 50 and 60% copper slag. At 365 days, water absorption of control SCC mix was 5.18%. The results reduced about 6.52, 13.15, 9.48, 9.15, 5.43 and 2.21%, respectively, for SCC mix incorporating 10, 20, 30, 40, 50 and 60% copper slag. The absorption value was lowest for SCC mixes with 20% slag replacement at curing ages up to 365 days. It was because of the enhancement in particle packing of aggregates that led to the reduction of pores (Obe et al., 2016). A slight increase in water absorption value was found in the concrete mix with the further addition of copper slag; although that was less than that of control SCC mix. It was attributed to the rise in free water content, which led to the creation of new voids in SCC mixes with higher copper slag percentages (Al-Jabri et al., 2011). The values became analogous to the control concrete when copper slag increased beyond 30% in SCC.

SCC mixes with copper slag showed lower water absorption value at all curing ages, as shown in Fig. 4.10. Water absorption of control SCC at 28 days curing age was 6.30%. This reduced by about 9.15 and 17.76% at 90 and 365 days curing age, respectively. The water absorption of SCC mix with 10 and 20% copper slag was 6.10 and 5.71%, respectively, at 28 days. The results decreased by about 10.60 and 20.60% for SCC mix with 10% copper slag at 90 and 365 days, respectively. Further, water absorption of SCC mix incorporating 20% slag reduced by about 11.18 and 21.16% at 90 and 365 days, respectively. The water absorption value of SCC mix with 30, 40, 50 and 60% copper slag was 5.87, 5.90, 6.16 and 6.27%, respectively, at 28 days. The results decreased by about 10.23 and 20.06% for SCC mix with 30% slag at 90 and 365 days, respectively. Further, the water absorption of SCC incorporating 40% copper slag reduced by 9.42 and 20.22% at 90 and 365 days curing age, respectively. Likewise, the absorption of SCC incorporating 50% copper slag reduced by 10.22 and 20.50% at 90 and 365 days, respectively. With the further increase in copper slag from 50 to 60% in SCC, the decrease in water absorption was about 9.57 and 19.15% at 90 and 365, days curing age, respectively.

Table 4.4: Splitting Tensile Strength of SCC

Type of Mix	7 Days				28 Days				90 Days				365 Days			
	1	**2**	**3**	**Avg.**	**1**	**2**	**3**	**Avg.**	**1**	**2**	**3**	**Avg.**	**1**	**2**	**3**	**Avg.**
0CS-SCC	1.55	1.41	1.16	***1.37***	1.9	2.6	1.89	***2.13***	2.90	3.28	3.15	***3.11***	3.38	3.49	3.42	***3.43***
10CS-SCC	1.25	1.66	1.45	***1.45***	2.5	2.5	2.67	***2.56***	3.78	3.07	4.10	***3.65***	3.70	3.89	3.99	***3.86***
20CS-SCC	1.75	1.91	2.34	***2.00***	3	2.9	2.8	***2.90***	3.85	4.06	3.59	***3.83***	3.69	4.41	4.00	***4.03***
30CS-SCC	1.67	2.69	2.26	***2.21***	3.74	3.38	3.18	***3.43***	4.01	3.92	3.71	***3.88***	4.18	4.32	3.78	***4.09***
40CS-SCC	2.1	2.01	2.54	***2.22***	3.67	2.74	3.8	***3.40***	3.76	4.13	3.78	***3.89***	4.22	4.34	4.01	***4.19***
50CS-SCC	2.78	2.52	1.9	***2.40***	3.43	2.9	3.62	***3.32***	4.24	3.98	4.15	***4.12***	4.34	4.47	4.20	***4.34***
60CS-SCC	2.19	2.46	2.42	***2.36***	3.45	3.65	3.19	***3.43***	4.43	3.99	4.26	***4.23***	4.43	4.42	4.55	***4.47***

Avg. refers to the average value obtained.

The percentage permeable voids present in SCC mixes are presented in Fig. 4.11. SCC mixes incorporating up to 60% copper slag showed a reduction in permeable voids percentage. A significant reduction was observed for the volume of permeable voids (%) in SCC as copper slag content augmented up to 30% at 28, 90 and 365 days curing. The permeable voids (%) in hardened SCC mix incorporating 100% sand were 13.59, 13.44 and 13.09% at 28, 90 and 365 days curing, respectively. This reduced to 13.18, 12.96 and 12.53% for 30% copper slag SCC mixes at 28, 90 and 365 days, respectively. With the increase in copper slag from 40 to 60%, the results of permeable voids became comparable to that of control SCC mix. The results of permeable voids in SCC mix incorporating 60% slag were 13.50, 13.25 and 12.99% at 28, 90 and 365 days curing age, respectively. These results could be related closely with compressive strength of SCC. This research was in agreement with the result findings of Al-Jabri et al. (2009), Al-Jabri et al. (2011). Al-Jabri et al. (2011) reported a decrease in water absorption values up to 40% copper slag replacement as fine aggregate in normally vibrated concrete mixes. The value became comparable on further addition of copper slag till 100% replacement in the concrete mix. Prem et al. (2018) reported an improvement in water absorption even at 100% copper slag substitution at 0.37, 0.47 and 0.57 w/c ratios. A decrease in water absorption value for concrete mixes containing up to 15% copper slag as cement substitution (Afshoon and Sharifi, 2017). However, the value increased when the replacement was more than 15%. Rajasekar et al. (2019) concluded that water absorption decreased up to 60% copper slag substitution in ultra-high-strength concrete.

With the incorporation of copper slag in SCC mixes, water absorption and volume of permeable voids reduced as concluded from the results. SCC mixes with and without copper slag showed lower water absorption value at all curing ages up to 365 days.

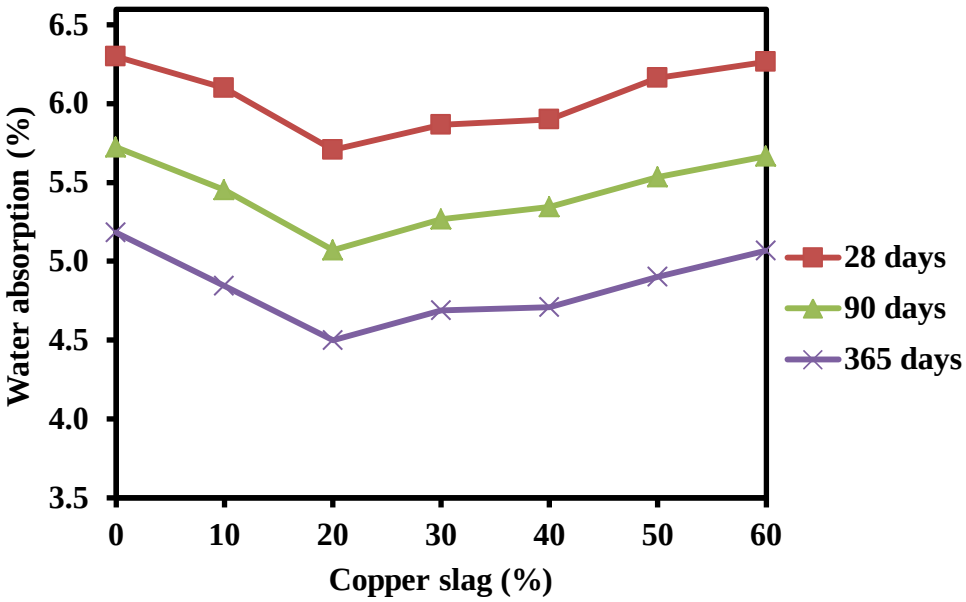

Fig. 4.9: Effect of Copper Slag on Water Absorption of SCC

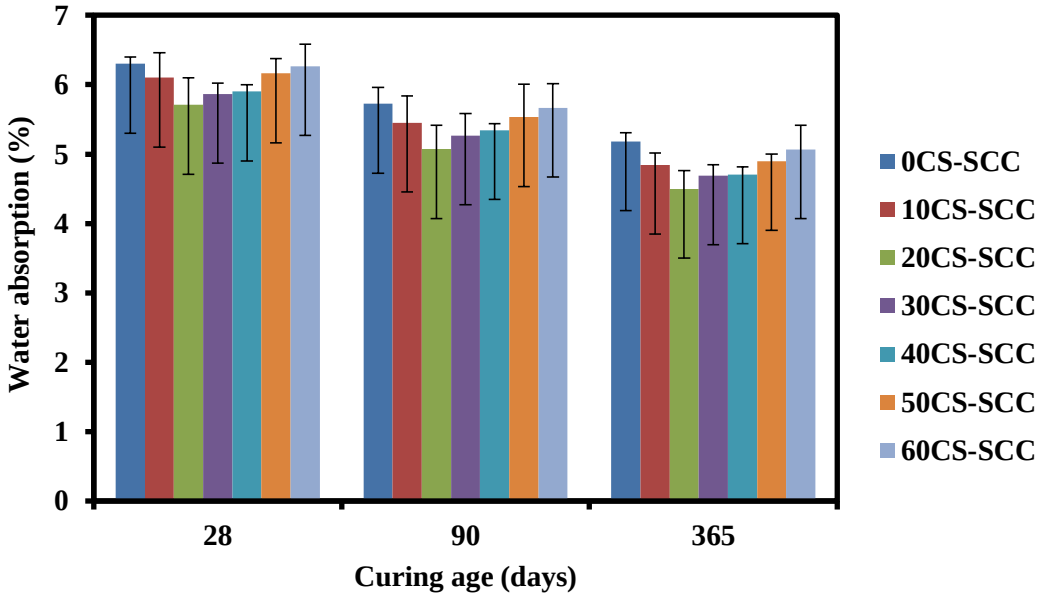

Fig. 4.10: Water Absorption of SCC versus Age

Table 4.5: Water Absorption Values of SCC

Type of mix	28 Days				90 Days				365 Days			
	1	**2**	**3**	**Avg.**	**1**	**2**	**3**	**Avg.**	**1**	**2**	**3**	**Avg.**
0CS-SCC	6.20	6.40	6.30	***6.30***	5.57	6.00	5.60	***5.72***	5.04	5.30	5.20	***5.18***
10CS-SCC	6.20	5.70	6.40	***6.10***	5.89	5.30	5.17	***5.45***	4.98	4.90	4.65	***4.84***
20CS-SCC	6.00	5.27	5.86	***5.71***	4.98	4.78	5.45	***5.07***	4.80	4.40	4.30	***4.50***
30CS-SCC	5.9	5.7	6.0	***5.87***	5.40	4.90	5.50	***5.27***	4.60	4.87	4.60	***4.69***
40CS-SCC	6.0	5.8	5.9	***5.90***	5.26	5.45	5.32	***5.34***	4.70	4.82	4.60	***4.71***
50CS-SCC	6.40	6.10	5.99	***6.16***	5.90	5.70	5.00	***5.53***	4.80	4.90	5.00	***4.90***
60CS-SCC	6.50	6.40	5.90	***6.27***	5.70	5.30	6.00	***5.67***	5.40	4.70	5.10	***5.07***

Avg. refers to the average value obtained.

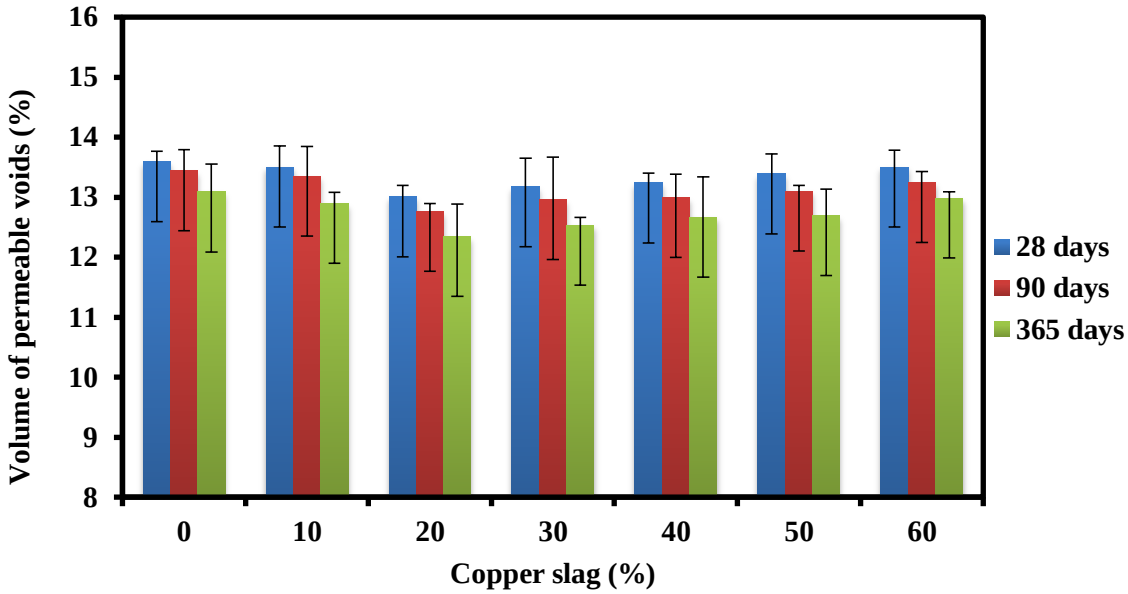

Fig. 4.11: Effect of Copper Slag on Volume of Permeable Voids of SCC

4.3.2 Sorptivity

Sorptivity mainly determines the exposure of unsaturated concrete to the permeation of water, as explained in ASTM C1585-04. It mainly depends on concrete mix proportions, type of admixture, supplementary cementitious materials, physical characteristics of the aggregates and placement method (Öz et al., 2016). Fig. 4.12 shows the plot of sorptivity coefficient (mm/sec$^{1/2}$) with respect to SCC mixes. The joint effect of copper slag and fly ash was successful in lowering down the sorptivity values of SCC mixes. Sorptivity value of control SCC mix at 28 days curing age was 0.0056 mm/sec$^{1/2}$. The value reduced by about 9.52, 20.83, 19.64, 14.29, 11.90 and 8.33% for SCC mix incorporating 10, 20, 30, 40, 50 and 60% copper slag SCC mix at 28 days curing age, respectively. The value of sorptivity of control SCC was 0.0049 mm/sec$^{1/2}$ and 0.0044 mm/sec$^{1/2}$ at 90 and 365 days curing age, respectively. The value reduced by about 9.59, 25.34, 22.60, 15.07, 13.70 and 8.90% for SCC mix incorporating 10, 20, 30, 40, 50 and 60% copper slag, respectively, at 90 days curing age. Also, the sorptivity value reduced by about 12.12, 28.79, 22.73, 18.18, 11.36 and 3.79% for SCC mix incorporating 10, 20, 30, 40, 50 and 60% copper slag, respectively, at 365 days curing age. It can be observed that the lowest value of

sorptivity was observed for 20% copper slag SCC mix at 28, 90 and 365 days. A similar trend was observed for the other durability properties, including water absorption and rapid chloride permeability. Sorptivity exhibited a marked decrease in SCC mixes, incorporating copper slag up to 30%. The sorptivity value of SCC mixes containing beyond 30% slag became almost equivalent to control concrete. The reason for the reduced values of sorptivity may be attributed to the contribution of fly ash and copper slag leading to enhancement of the pore structure of the SCC matrix. This further resulted in the transformation of large permeable pores into smaller and less permeable pores (Lotfy et al., 2016). With the increase in age of concrete, the reaction concerning fly ash and calcium hydroxide became much more significant, giving rise to a denser concrete (Lotfy et al., 2016). The findings are in line with the results of water absorption of SCC mixes; thereby significantly increasing the compressive strength up to 30% copper slag.

With the increase in curing age, a significant reduction in the sorptivity values of SCC mixes was observed. The value of sorptivity of control SCC mix was 0.0056 mm/sec$^{1/2}$ at 28 days. A decrease of about 12.50 and 27.27% was studied for control SCC mix at 90 and 365 days curing age, respectively. The sorptivity values of SCC mix incorporating 10% copper slag reduced by about 13.16 and 29.91% at 90 and 365 days, respectively, as compared to 28 days results. The value of sorptivity of SCC mix incorporating 20, 30, 40, 50 and 60% slag was 0.0045, 0.0044, 0.0048, 0.0049 and 0.0051 mm/sec$^{1/2}$, respectively, at 28 days. The results reduced by about 15.56 and 32.35% for SCC mix with 20% slag at 90 and 365 days, respectively. Further, the value of sorptivity of SCC mixes with 30% copper slag reduced by 18.18 and 41.94% at 90 and 365 days, respectively. Also, the values of sorptivity of SCC mix with 40% copper slag reduced by 14.58 and 33.33% at 90 and 365 days, respectively. The values of sorptivity of SCC mix with 50% copper slag reduced by 14.29 and 25.64% at 90 and 365 days, respectively. Further, the values of sorptivity of SCC mix with 60% copper slag reduced by 13.73 and 21.43% at 90 and 365 days, respectively.

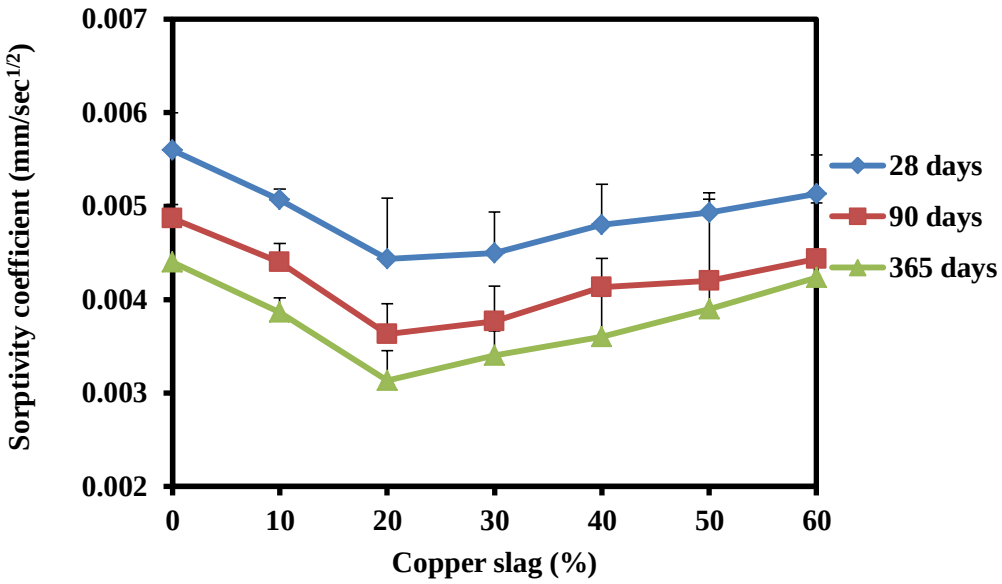

Fig. 4.12: Effect of Copper Slag on Sorptivity of SCC

For copper slag SCC mixes, the initial rate of water absorption decreased with the increase in replacement level of sand up to 30%. An insignificant increase in absorption was observed in SCC mixes incorporating copper slag beyond 30%; although that was less than that of control SCC mix. However, the secondary rate of water absorption for all SCC mixes was identical. The cumulative absorption of water was lower for SCC mixes incorporating copper slag up to 30% than that of SCC mix without copper slag. Sharma and Khan (2017b) reported a decrease in sorptivity values up to 60% copper slag replacement at 120 days of curing. Rajasekar et al. (2019) reported a decline in sorptivity values for ultra-high-strength concrete incorporating copper slag up to 60%; thus making concrete highly impermeable. The results of compressive strength were following the durability results obtained.

Hence, it can be concluded that the combined effect of copper slag and fly ash was successful in lowering down the sorptivity values of SCC mixes. With the increase in curing age, a significant reduction in the sorptivity values of SCC mixes was observed.

4.3.3 Rapid Chloride Permeability Test

The results of rapid chloride ion permeability (RCP) are presented in Table 4.6. A reduction in chloride permeability values in SCC mixes incorporating up to 60% copper slag was studied. A substantial decrease in RCP was observed in SCC mixes containing up to 30% copper slag at 28, 90 and 365 days (Fig. 4.13). The permeability of concrete reduced owing to the reduction of pores under the influence of copper slag (Thomas et al., 2013). This was validated from the results of water absorption; wherein the absorption got significantly reduced on the addition of slag up to 30%. At 28 days, the permeability values of SCC mixes incorporating 0, 10, 20, 30, 40, 50 and 60% copper slag was 1269, 1017, 876, 900, 1060, 1146 and 1229 coulombs, respectively. At 90 days, the permeability values of SCC mixes incorporating 0, 10, 20, 30, 40, 50 and 60% copper slag was 692, 624, 550, 593, 623, 651 and 668 coulombs, respectively. At 365 days, the permeability values of SCC mixes incorporating 0, 10, 20, 30, 40, 50 and 60% copper slag was 459, 438, 359, 386, 393, 406 and 443 coulombs, respectively. All SCC mixes were ranged under the category of very low to low chloride ion permeability at 28 days curing. At 90 and 365 days curing, the results of chloride ion permeability were much more significant than the results of 28 days curing. The values showed very low category of chloride ion permeability of SCC mixes at 90 and 365 days curing age. With the increase in age of curing, the chloride ion permeability values of SCC mixes reduced. The influence of slag on chloride ion permeability was much significant at later ages of curing. With the low penetration of chloride ions in concrete, long term durability of concrete structures could be achieved. The research findings were in concurrence with the results of Najimi et al. (2011), Brindha and Nagan (2011), Mithun and Narasimhan (2016), Thomas et al. (2013), Boakye and Uzoegbo (2014), Rajasekar et al. (2019). The influence of copper slag in concrete as cement replacement was higher at 90 days curing comparing to 28 days (Najimi et al., 2011). Brindha and Nagan (2011) reported the values of RCPT after 90 days curing period. The RCP value of copper slag admixed concrete was categorized as very low. Thomas et al. (2013) reported a decrease in chloride ion permeability value of concrete containing copper slag up to 30% at 0.4 and 0.5 w/c ratio. However, the decrease in permeability of concrete incorporating up to 40% copper slag substitution was studied at 0.45 w/c ratio. Boakye and Uzoegbo (2014)

concluded that chloride ion permeability decreased with the increase in copper slag up to 15% cement substitution owing to the improvement of the pore structure. Rajasekar et al. (2019) observed very low values of chloride ion permeability in ultra-high strength concrete (UHSC) incorporating copper slag up to 60%. However, some of the research findings showed that copper slag did not significantly affect the RCPT values of concrete mixes (Prem et al., 2018). The RCPT values of concrete mixes incorporating copper slag were categorized under moderate class (Prem et al., 2018) as per ASTM C1202-10.

The decrease in permeability values of SCC mixes incorporating copper slag indicated a denser microstructure with reduced voids. The permeability of SCC mixes with and without copper slag decreased with the increase in curing ages. The results of permeability are inter-related with the compressive strength of SCC mixes, as it can be seen that compressive strength increases and the permeability decreases.

Table 4.6: Charge Passed through SCC

Type of mix	Coulombs Passed at Different Curing Ages (Days)		
	28	**90**	**365**
0CS-SCC	1269	692	459
10CS-SCC	1017	624	438
20CS-SCC	876	550	359
30CS-SCC	900	593	386
40CS-SCC	1060	623	393
50CS-SCC	1146	651	406
60CS-SCC	1229	668	443

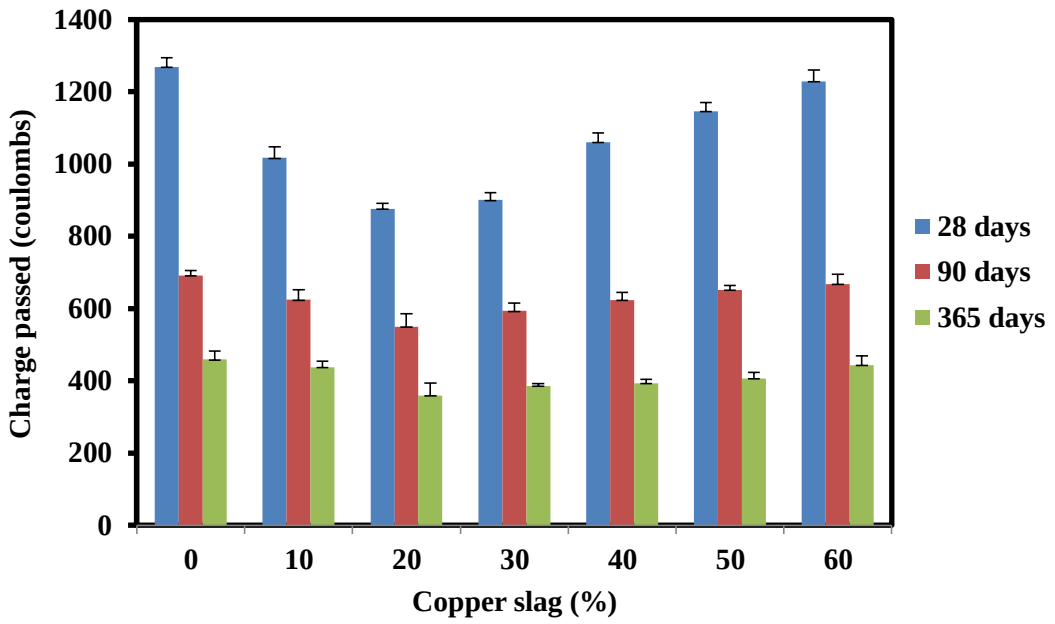

Fig. 4.13: Effect of Copper Slag on Chloride Ion Permeability of SCC

4.3.4 Drying Shrinkage

Concrete shrinkage is the main source of cracking in concrete structures; thus need to be studied cautiously. Reduction in volume due to the removal of water from concrete to the surroundings is known as the drying shrinkage of concrete (Tam et al., 2012). The tensile stresses developed in concrete are responsible for the cracking and thus affecting the service life of concrete members. This affects the load-carrying capacity of the structures and degrades the quality of concrete. Development of cracks opens a pathway to water and other chemical agents, which further disrupts the concrete cover initially and then the corrosion of reinforcements (Zhang et al., 2014). Experimental studies on triplicates of SCC samples containing copper slag (0-60%) have been conducted to observe the drying shrinkage phenomenon. Long-term drying shrinkage results of SCC mixes at various ages up to 448 days are demonstrated in Fig. 4.14. The drying shrinkage of SCC mixes decreased on the addition of copper slag and the least value of shrinkage was obtained for SCC mix incorporating 20% copper slag at all ages. In general, shrinkage strains were comparable at early ages up to 28 days; while clear distinction was observed after 28 days of drying period. The value of 28 days drying shrinkage of control SCC was 230

micro strain. The 28 days drying shrinkage of SCC made with 10, 20, 30, 40, 50 and 60% copper slag were 22.61, 32.61, 17.39, 13.04, 8.69 and 2.17%, respectively, lower than that of control SCC mix. The value of 56 days drying shrinkage of control SCC was 310 micro strain. At 56 days curing age, drying shrinkage of SCC made with 10, 20, 30, 40, 50 and 60% copper slag were 13.87, 25.16, 9.68, 10.32, 8.06 and 3.23%, respectively, lower than that of control SCC mix. At 90 days, the value of drying shrinkage strain was 380 micro strain. Reductions in strains was about 21.32, 33.16, 15.79, 15.79, 10.53 and 5.26% for SCC mix made with 10, 20, 30, 40, 50 and 60% copper slag, respectively. The value of 224 and 365 days drying shrinkage of control SCC was 500 and 513 micro strain, respectively. At 224 days, reduction in shrinkage strains were 11.00, 20.00, 8.00, 2.20, 1.00 and 0.40% for SCC mixes with 10, 20, 30, 40, 50 and 60% copper slag, respectively. At 365 days, reduction in shrinkage strains were 10.72, 16.57, 8.38, 3.70, 2.53 and 0.78%, respectively, for the same compositions of SCC mixes. At 448 days, reduction in shrinkage strains were 10.19, 16.35, 7.69, 4.23, 1.92 and 0.96%, respectively, for the same compositions of SCC mixes. This may be attributed to the loss of physically absorbed water from Calcium Silicate Hydrate (C–S–H), resulting in a shrinkage strain (Wong et al., 2007). The mutual effect of fly ash and copper slag was effective in lowering the shrinkage strains of copper slag SCC mixes. Long term drying shrinkage became stable for SCC mixes after 224 days. The research findings are in agreement with the research conducted by Thomas et al. (2013), Afshoon and Sharifi (2017), Ayano and Sakata (2000). Thomas et al. (2013) reported a decrease in drying shrinkage value up to 30% copper tailing replacement at 0.4 and 0.5 w/c ratio. When w/c ratio was 0.45, drying shrinkage reduced up to 20% copper tailing replacement from control concrete and gradually increased from 30 to 60% replacement. Ayano and Sakata (2000) concluded that copper slag admixed concrete resulted in lower drying shrinkage as compared with concrete with sand. Afshoon and Sharifi (2017) reported the drying shrinkage strains of SCC mix made with copper slag as cement replacement were comparable to control concrete at initial ages; the clear difference was observed at later ages of drying.

It can be concluded that the drying shrinkage of SCC mixes decreased on the addition of copper slag.

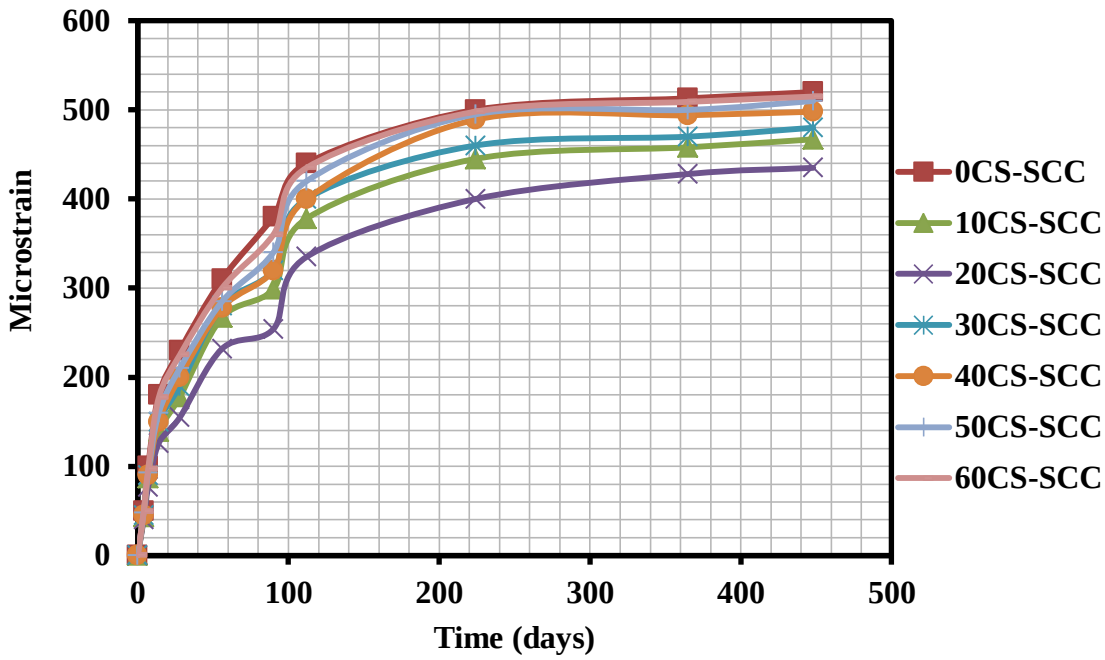

Fig. 4.14: Effect of Copper Slag on Drying Shrinkage of SCC

4.3.5 Sulfate Resistance

The most important durability property includes the sulfate attack as it may lead to deterioration of concrete (Cachim et al., 2010). The external factors of environment like sulfate attack, chloride ingress, acid attack results in the damaging of concrete (Singh et al., 2016). The phenomenon of deteriorating of normally vibrated concrete when exposed to sulfate has been studied by various researchers (Scherer, 1999, Neville, 2004, Tian and Cohen, 2000, Glasser et al., 2008, Yu et al., 2013, Al-Swaidani, 2019). Performance of SCC incorporating copper slag when exposed to aggressive environments like sulfate attack has been studied in detail. Sulfate resistance test is assessed by computing the changes in the length of the prisms, variation in compressive strength and gain in the mass of concrete cubes for up to one year.

4.3.5.1 Variation of Compressive Strength of SCC under Normal Curing

Fig. 4.15 represented the compressive strength results of SCC mixes under water (normal) curing at various ages for up to one year after initial curing of 28 days. The compressive strength of control SCC mix was 35.63 MPa under normal curing of 28 days. A marginal increase in strength of SCC mixes containing up to 30% copper slag was reported. A maximum increase of 7.2, 6.24 and 5.1% were observed in SCC mix incorporating 20% copper slag in comparison to control SCC mix under normal curing at 28, 90 and 365 days, respectively, after an initial 28 days curing. The reason for strength gain was the shape of copper slag particles which helped in improving the bond and overall cohesion of the concrete matrix. However, the compressive strength of SCC mixes incorporating beyond 30% slag became almost equivalent to that of control SCC mix at 28, 90 and 365 days.

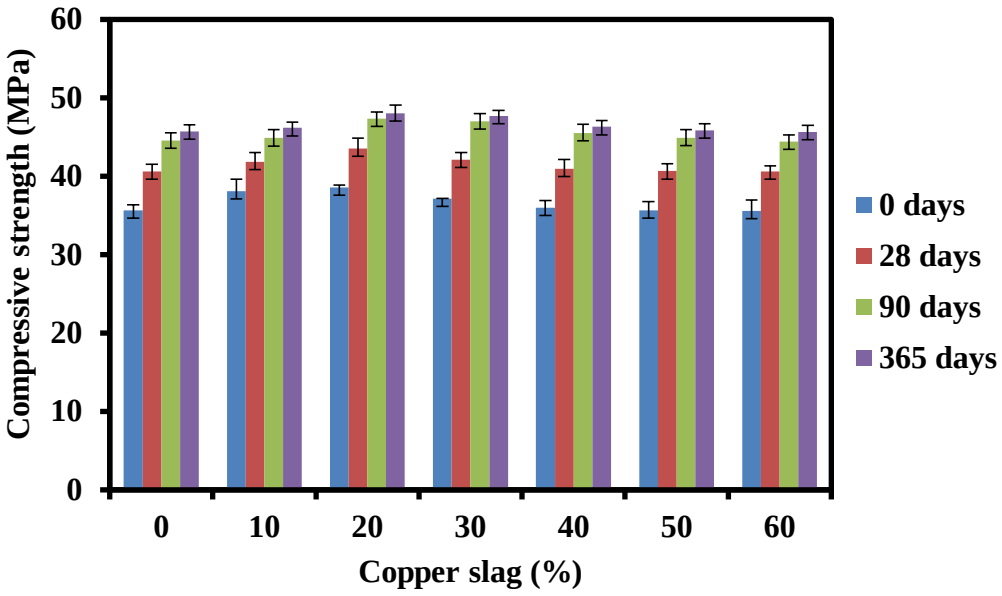

Fig. 4.15: Compressive Strength of SCC Immersed in Water after Initial Curing of 28 Days

4.3.5.2 Variation of Compressive Strength of SCC with respect to Copper Slag (%)

A marginal increase in the compressive strength of SCC containing up to 30% copper slag was observed at all ages, as shown in Fig. 4.16. The 28 days compressive strength of SCC mix incorporating 10, 20, 30, 40 and 50% copper slag achieved 6.15, 7.08, 4.62, 3.93 and 1.54% higher compressive strength, respectively, as compared to control SCC mix (32.50 MPa). An insignificant decrease of 0.14% was observed in SCC mix with 60% copper slag in comparison to control SCC mix at 28 days. A similar trend was followed for SCC mixes incorporating copper slag up to 60% at 90 and 365 days. At 90 days, SCC mixes incorporating 10, 20, 30, 40 and 50% copper slag gained 2.95, 3.54, 3.25, 1.08 and 0.54% compressive strength, respectively, in comparison to the SCC mix without copper slag (36.70 MPa). An insignificant decrease of 0.39% was observed in SCC mix with 60% copper slag in comparison to control SCC mix at 90 days. At 365 days, SCC mix incorporating 10, 20, 30, 40 and 50% copper slag achieved 4.61, 7.53, 2.93, 2.64 and 1.98% higher compressive strength, respectively, as compared to control SCC mix (34.10 MPa). An insignificant decrease of 0.30% was observed in SCC mix with 60% copper slag in comparison to control SCC mix at 365 days. The maximum increase in compressive strength was observed in SCC mixes made with 20% copper slag. Increase of 7.07, 3.54 and 7.53% was reported in SCC mix incorporating 20% copper slag at 28, 90 and 365 days, respectively, of sulfate exposure from control SCC mix. For SCC mixes made with 50 and 60% copper slag, the strength results became analogous to that of control SCC mix at 28, 90 and 365 days exposure to sulfate. The increase in strength may be attributed to the continuous hydration reactions taking place in the concrete matrix. Also, the low absorption characteristic of copper slag grains was responsible for reducing the permeability of concrete. This led to the reduction of pores and at the same time filling of voids with the reaction products in a concrete matrix. Penetration property of concrete is directly linked with the sulfate attack mechanism (Roy and Ldorn, 1982, Mehta, 1980). Due to low absorption of SCC mixes with copper slag, it led to low permeability to sulfate ions. This was further evident from the SEM and EDS results. It was understandable from the results mentioned above that SCC with copper slag performed better in sulfate as compared to SCC without slag. Similar observations

were observed by Mithun and Narasimhan (2016), Najimi et al. (2011). Mithun and Narasimhan (2016) reported an increase in the strength of alkali-activated slag concrete (AASC) mixes with sand/copper slag when exposed to sodium sulfate. In contrast, reduction in strength was observed for AASC mixes when immersed in a magnesium sulfate solution. The reason for the decrease in strength was due to the formations of gypsum and magnesium silicate hydrate instead of CSH layers; which further led to the cracking of concrete samples. Najimi et al. (2011) concluded that the concrete mixes made with copper slag (as cement replacement) resulted in superior performance when exposed to sulfate as a comparison to that of control concrete. Hwang and Laiw (1989) reported no significant changes in concrete mixes exposed to sodium sulfate solution. Sharma and Khan (2017b) reported significant mass gain and decrease in compressive strength of SCC mixes exposed to sulfate solution up to 120 days.

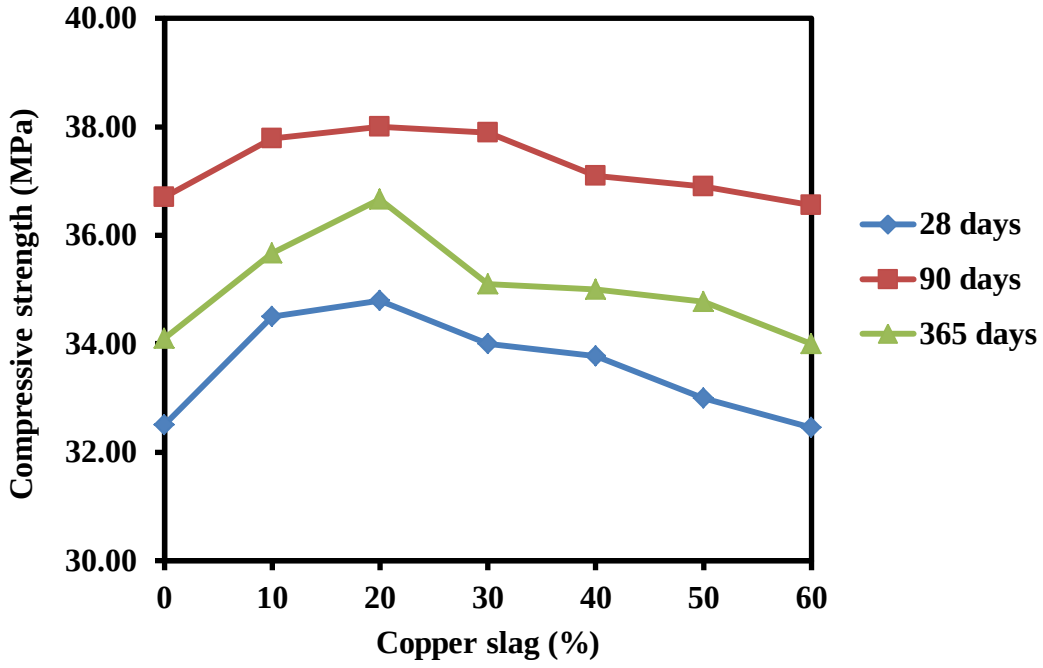

Fig. 4.16: Effect of Copper Slag on Compressive Strength of Sulfate Cured SCC

4.3.5.3 Variation of Compressive Strength of SCC with respect to Immersion Period of Sulfate Solution

The strength of control SCC mix was 32.50, 36.70 and 34.10 MPa at 28, 90 and 365 days of sulfate curing. The strength of SCC mix incorporating 10, 20 and 30% copper slag was 34.50 MPa, 34.80 MPa and 34.00 MPa, respectively, at 28 days curing age. The strength increased by about 12.92 and 4.92%, respectively, in SCC mix with 0% slag at 90 and 365 days of sulfate curing in comparison to SCC at 28 days. The strength increased by about 9.52 and 3.40%, respectively, in SCC mixes with 10% slag at 90 and 365 days of sulfate curing. The strength increase was about 9.20 and 5.36%, respectively, in SCC mixes with 20% slag at 90 and 365 days of sulfate curing. The compressive strength of SCC mix made with 30% slag increased by 11.45 and 3.24% at 90 and 365 days of sulfate curing, respectively. The compressive strength of SCC mix made with 40% slag increased by 9.83 and 3.62% at 90 and 365 days of sulfate curing, respectively, as compared to the strength of SCC mix at 28 days curing (33.78 MPa). The compressive strength of SCC mix with 50% slag increased by 11.81 and 5.38% at 90 and 365 days of sulfate curing, respectively, as compared to the strength of SCC mix at 28 days curing (33.00 MPa). The compressive strength of SCC mix made with 60% slag increased by 12.64 and 4.76% at 90 and 365 days of sulfate curing, respectively, as compared to the strength of SCC mix at 28 days curing (32.45 MPa). With respect to immersion in sulfate solution with curing ages, a marginal increase in compressive strength of SCC mixes was established from 28 to 90 days. A slight decrease in strength was observed after 90 days of immersion in sulfate, owing to the reaction between calcium hydroxide and sulfate ions present in the solution (Najimi et al., 2011). Reduction in strength was almost in the range of 3.5 to 7% for SCC mixes incorporating 0 to 60% copper slag at 365 days in comparison to 90 days. However, the strength of SCC at 365 days became almost equivalent to that of the strength of sulfate exposed SCC mixes at 28 days (Fig. 4.17). Even after one year of sulfate exposure to SCC mixes, no major catastrophic damage was visible. Depending on the strength requirements from the construction point of view, SCC can be developed using copper slag in selective percentages, especially in areas exposed to aggressive environments involving sulfate attack.

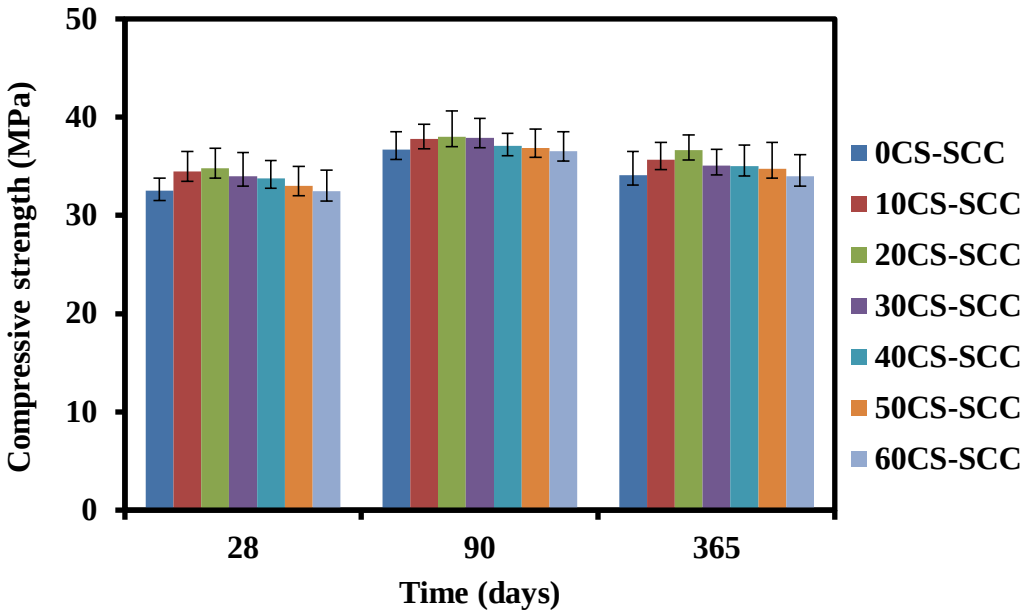

Fig. 4.17: Compressive Strength of SCC Exposed to Sulfate Solution

4.3.5.4 Comparison of Compressive Strength of SCC under Normal Curing and Sulfate Attack

The compressive strength of SCC mixes under sulfate exposure was compared with the results of the compressive strength of SCC mixes under normal curing. The compressive strength of SCC mixes exposed to sulfate showed a reduction when compared to the strength values of SCC mixes under normal curing at all ages. Fig. 4.18 presented the percentage loss of compressive strength of SCC mixes exposed to sulfate attack. A reduction of 20.01, 17.64 and 25.38% were observed in SCC mixes with 0% slag after immersion in sulfate solution at 28, 90 and 365 days, respectively. A reduction of 17.60, 15.80 and 22.74% were observed in SCC mixes with 10% slag after immersion in sulfate solution at 28, 90 and 365 days, respectively. A reduction of 20.09, 19.73 and 23.75% were observed in SCC mixes with 20% slag after immersion in sulfate solution at 28, 90 and 365 days, respectively. Further, a decline in compressive strength of SCC mixes with 30% slag was 19.30, 19.37 and 26.37% after immersion in sulfate solution at 28, 90 and 365 days, respectively. A reduction of 17.57, 18.46 and 24.41% were observed in SCC mixes with 40% slag after immersion in sulfate solution at 28, 90 and 365 days,

respectively. A reduction of 18.82, 17.82 and 24.18% were observed in SCC mixes with 50% slag after immersion in sulfate solution at 28, 90 and 365 days, respectively. A reduction of 20.07, 17.66 and 25.52% were observed in SCC mixes with 60% slag after immersion in sulfate solution at 28, 90 and 365 days, respectively. The average decrease in compressive strength of SCC mixes exposed to sulfate was around 19.07, 18.07 and 24.6%, respectively, in comparison to respective SCC mixes under normal curing conditions at 28, 90 and 365 days.

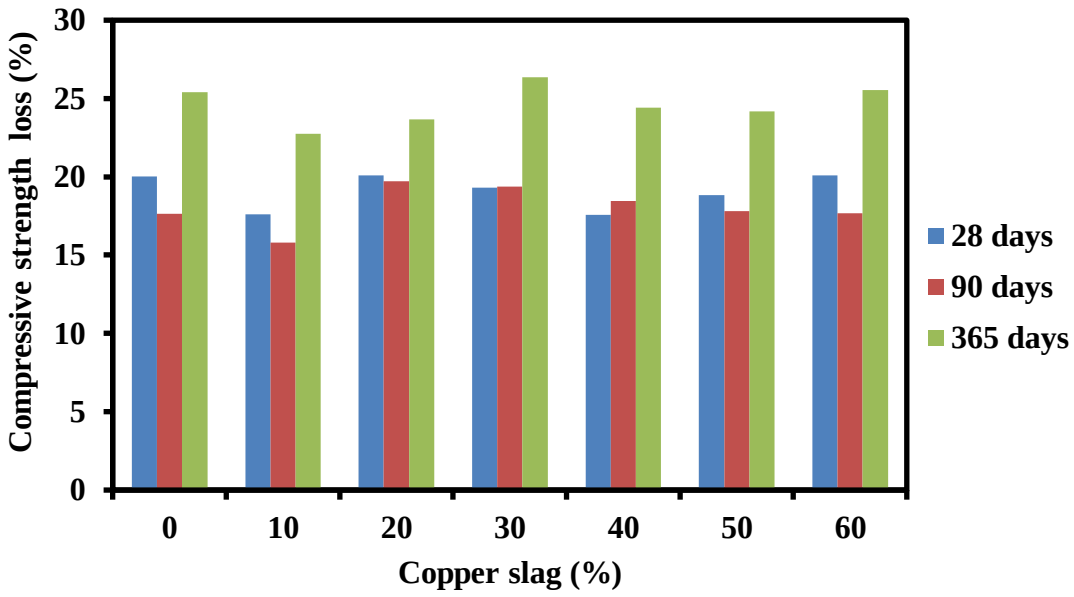

Fig. 4.18: Compressive Strength Loss (%) of SCC after Immersion in Sulfate

4.3.5.5 Microstructure Analysis

Fig. 4.19- 4.30 shows the SEM/EDS/XRD analysis of SCC mixes under normal curing as well as sulfate attack. Only those images are given in which major changes have been observed. Fig. 4.19 presented the microstructure of SCC matrix containing 0 and 20% copper slag under normal curing and sulfate attack at 28 days. Development of ettringite and voids was visible under SEM analysis of control SCC at 28 days normal curing. SEM analysis showed dense and homogenous formations of calcium silicate hydrate (CSH)

layers in SCC mixes with 20% copper slag under normal curing. Microstructure showing CSH layers along with ettringite formation inside the voids in SCC mixes with 40 and 60% copper slag under normal curing (Fig. 4.20). For sulfate exposed SCC mixes, improvement in microstructure as the immersion period increased from 28 to 365 days was visible. Few voids and micro-cracks were visible in SCC mix exposed to sulfate at 28 days. Detection of sulfur and aluminium under EDS spectrum in SCC mixes incorporating 20, 40 and 60% slag confirmed the formation of ettringite when the mixes were exposed to sodium sulfate solution for 28 days as shown in Fig. 4.21. Compact structure with homogenous CSH formations developed in SCC mixes at 90 and 365 days of sulfate immersion, as shown in Fig. 4.22, 4.23, 4.25 and 4.26. Fig. 4.22 and 4.23 showed the interface of copper slag aggregate with the concrete matrix in SCC mix with 20 and 60% copper slag at 90 days of sulfate immersion. Major peaks of calcium and silica were observed owing to the formation of CSH layers in SCC mixes, leading to strength gain as given in Fig. 4.24 and 4.27. With the increase in immersion period of sulfate from 28 to 90 days, gain in strength was observed in SCC mixes. No peak of sulfur was significant in EDS analysis for SCC mixes exposed to sulfate at 90 days. This accounted to the low penetrability of sulfur in SCC mixes and thus low permeability. On increasing the immersion time of sulfate further from 90 to 365 days, a minor decrease in strength was reported. This was evident from the presence of voids and cracks in the matrix seen in SEM images. EDS spectrum of all SCC mixes indicated the presence of major elements like that of Ca, Si, Mg, Fe, Na, k, Al and O. XRD analysis was conducted to detect the phases formed in SCC mixes up to 365 days immersion in sulfate. Fig. 4.28-4.30 gave a comparative analysis of the phases formed in SCC mixes incorporating 0, 20 and 60% copper slag under normal curing and sulfate exposure at 28, 90 and 365 days. XRD results confirmed the crystalline structure of the SCC matrix with well-defined peaks giving rise to various phases. The phases formed were mainly that of Quartz, Anorthite, Calcium Hydroxide and Calcium Silicate Hydrate. Other phases with low-intensity peaks were that of Gismondine, Hydrogen Silicate Hydrate and Hedenbergite. Apart from these, the peak of Laumontite having chemical formulae- $CaAl_2Si_4O_{12}(H_2O)_2$ and Halloysite with chemical formulae-$Al_2Si_2O_5(OH)_4 \cdot 2H_2O$ was observed in 60CS-

SCC. No major phase change was observed for SCC mixes under normal curing as well as under sulfate attack at 28, 90 and 365 days.

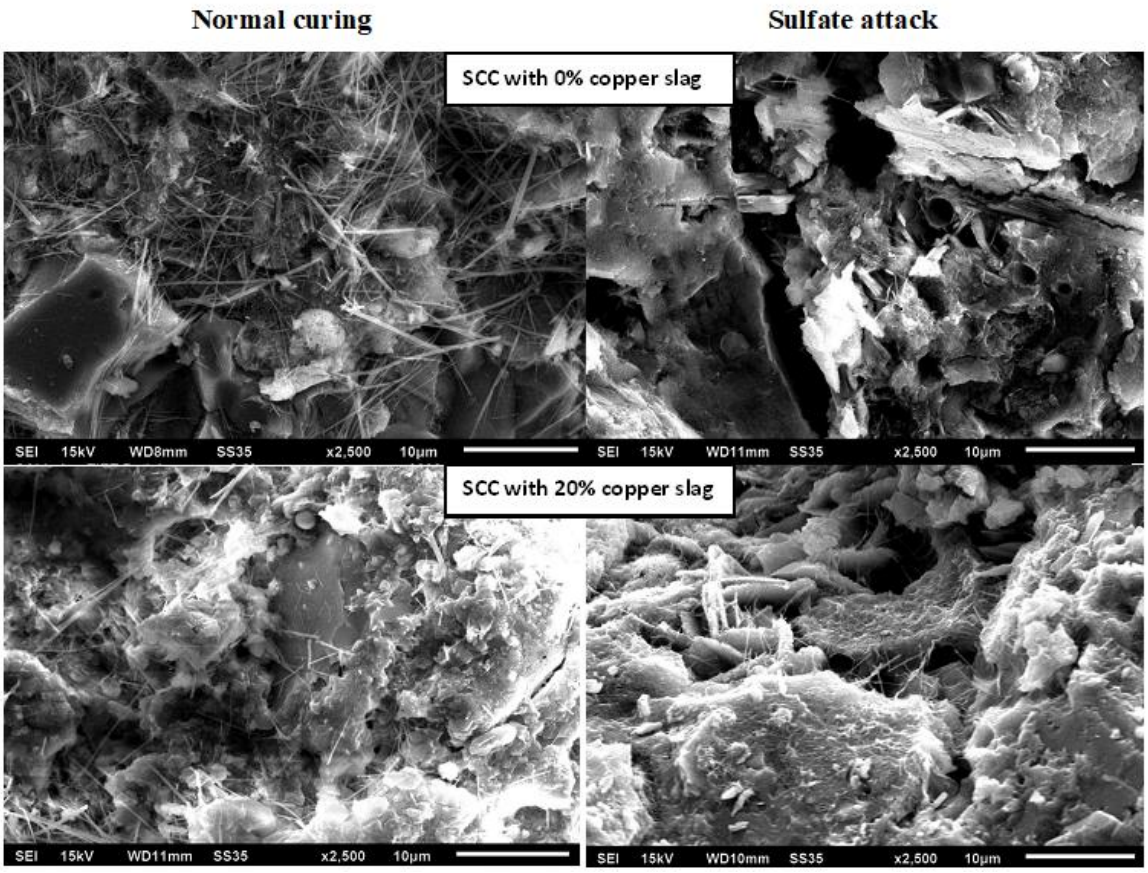

Fig. 4.19: Microstructure Comparison of SCC Incorporating 0% and 20% Copper Slag at 28 Days

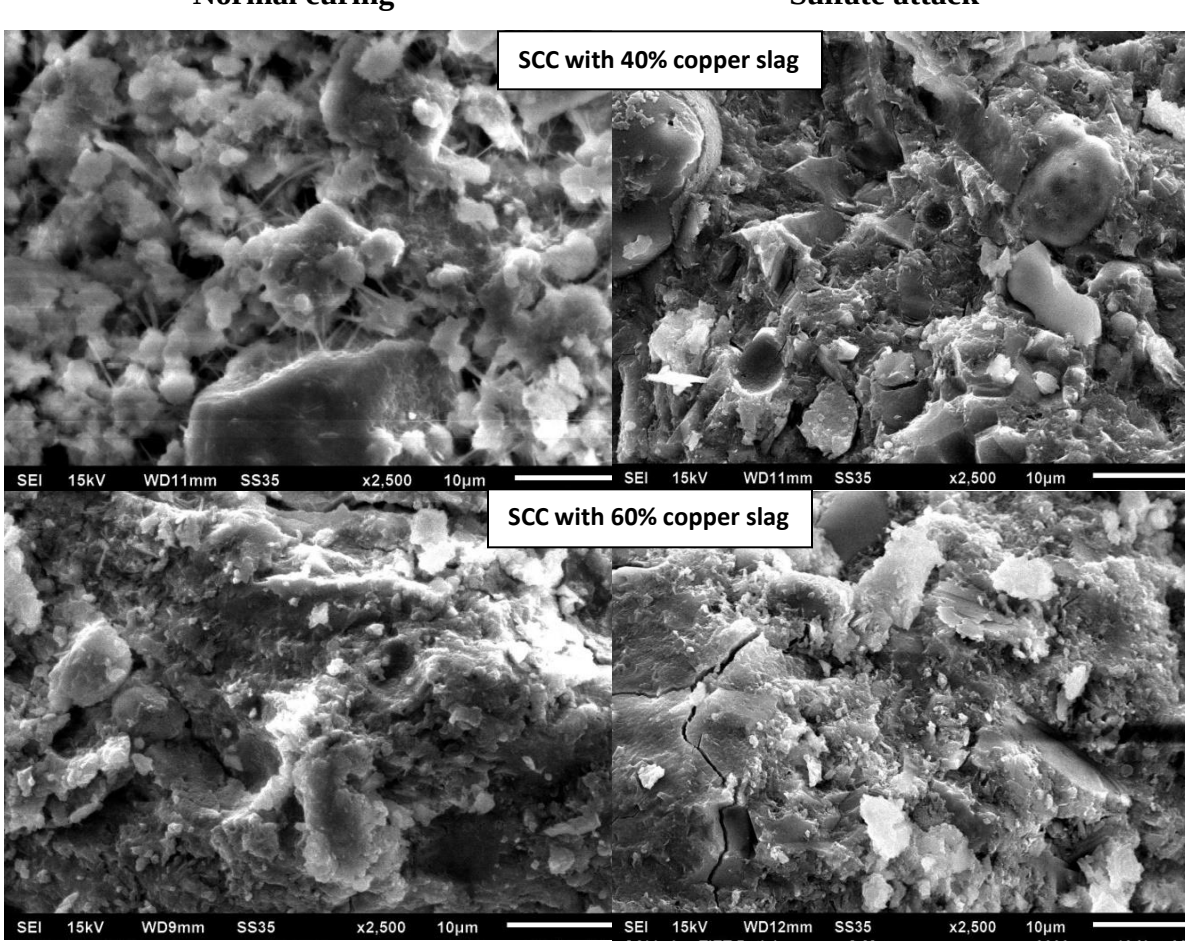

Fig. 4.20: Microstructure Comparison of SCC Incorporating 40% and 60% Copper Slag at 28 Days

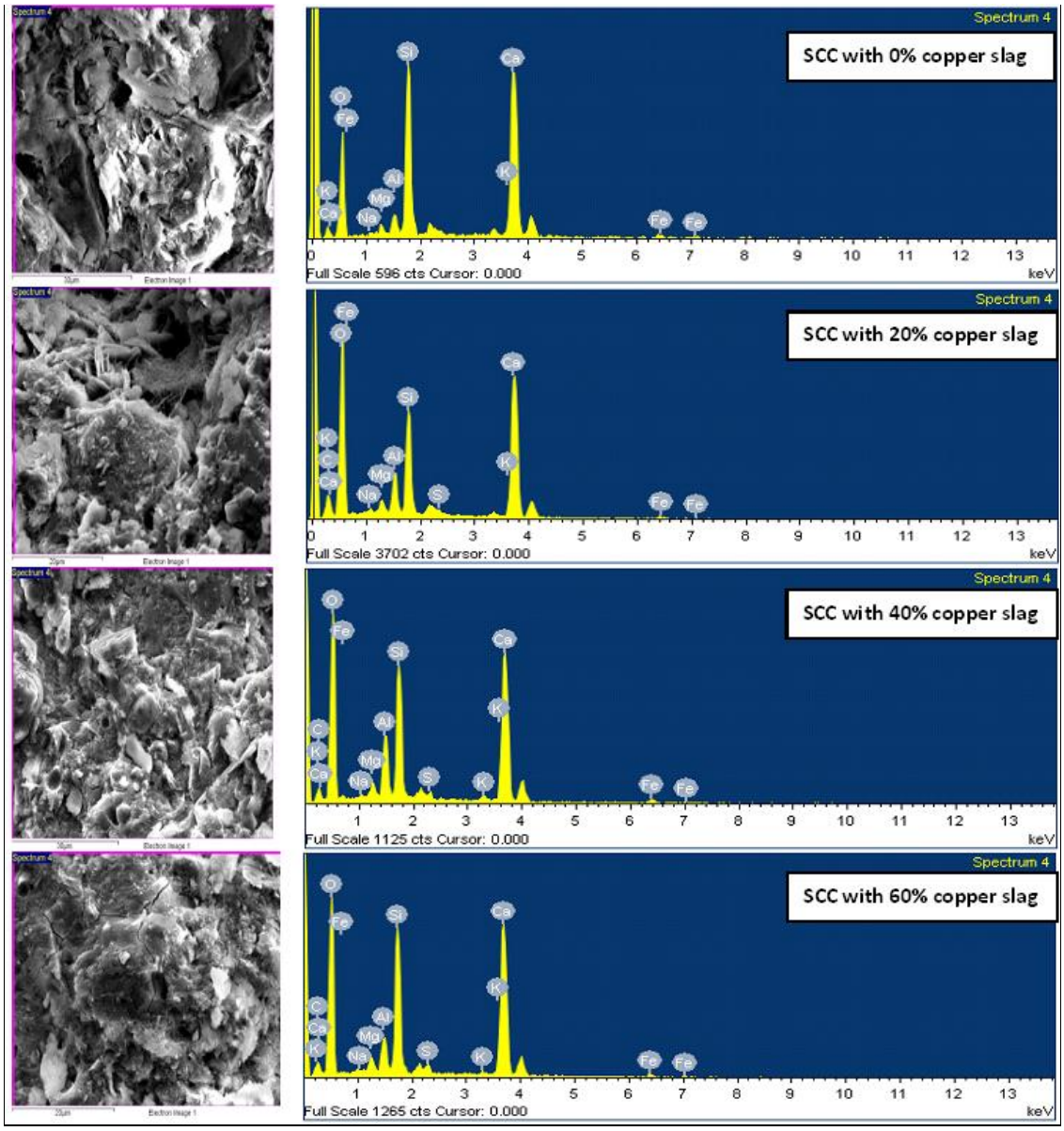

Fig. 4.21: EDS Spectrum of SCC Immersed in Sulfate Solution for 28 Days

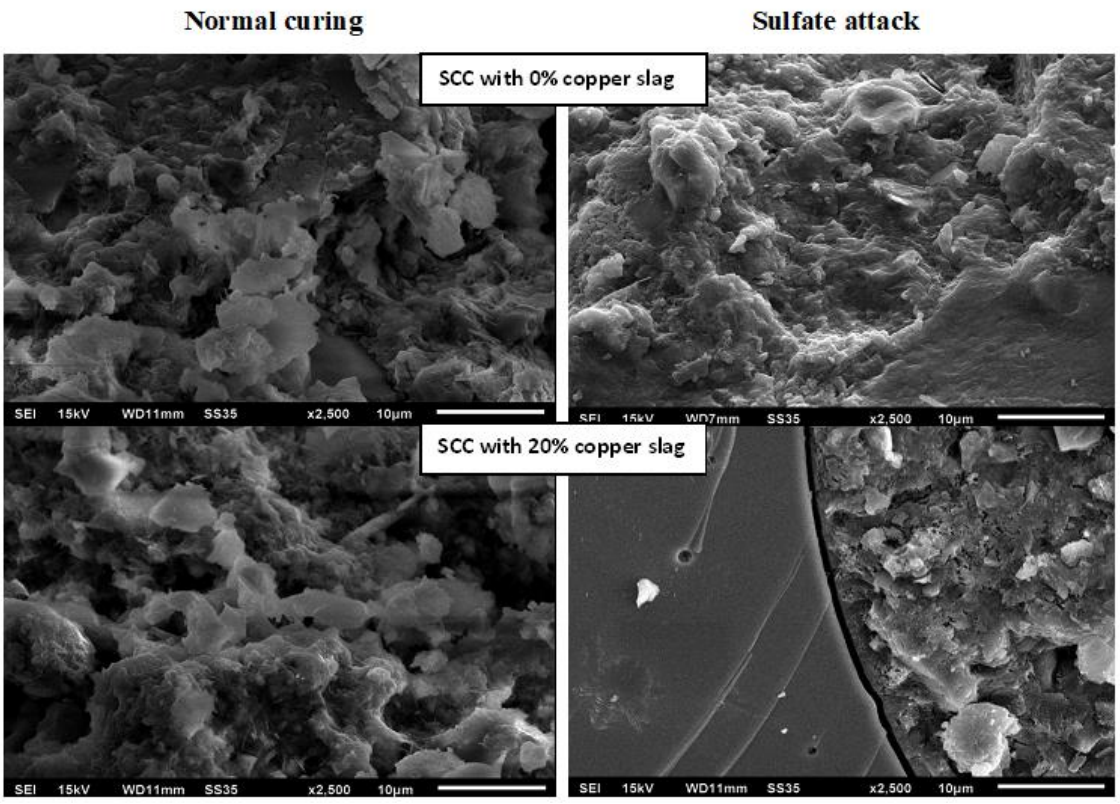

Fig. 4.22: Microstructure Comparison of SCC Incorporating 0% and 20% Copper Slag at 90 Days

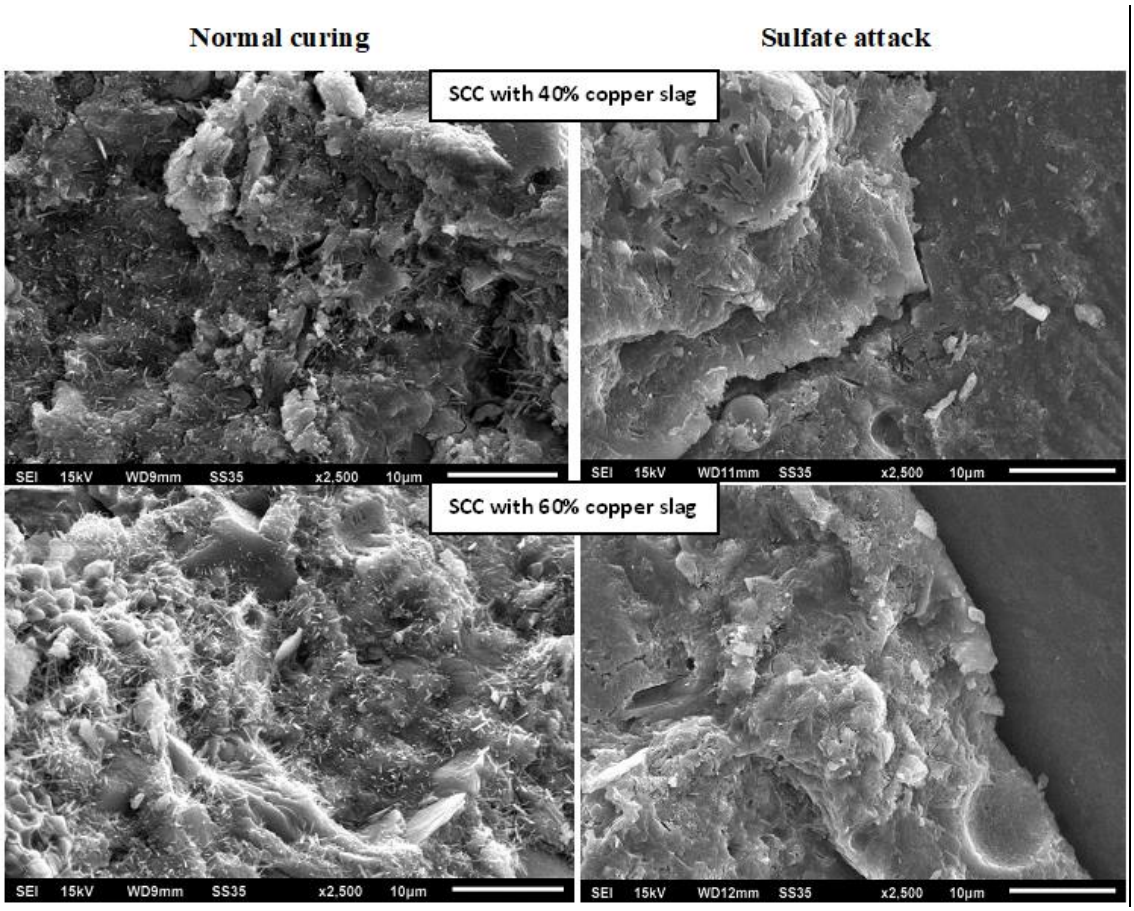

Fig. 4.23: Microstructure Comparison of SCC Incorporating 40% and 60% Copper Slag at 90 Days

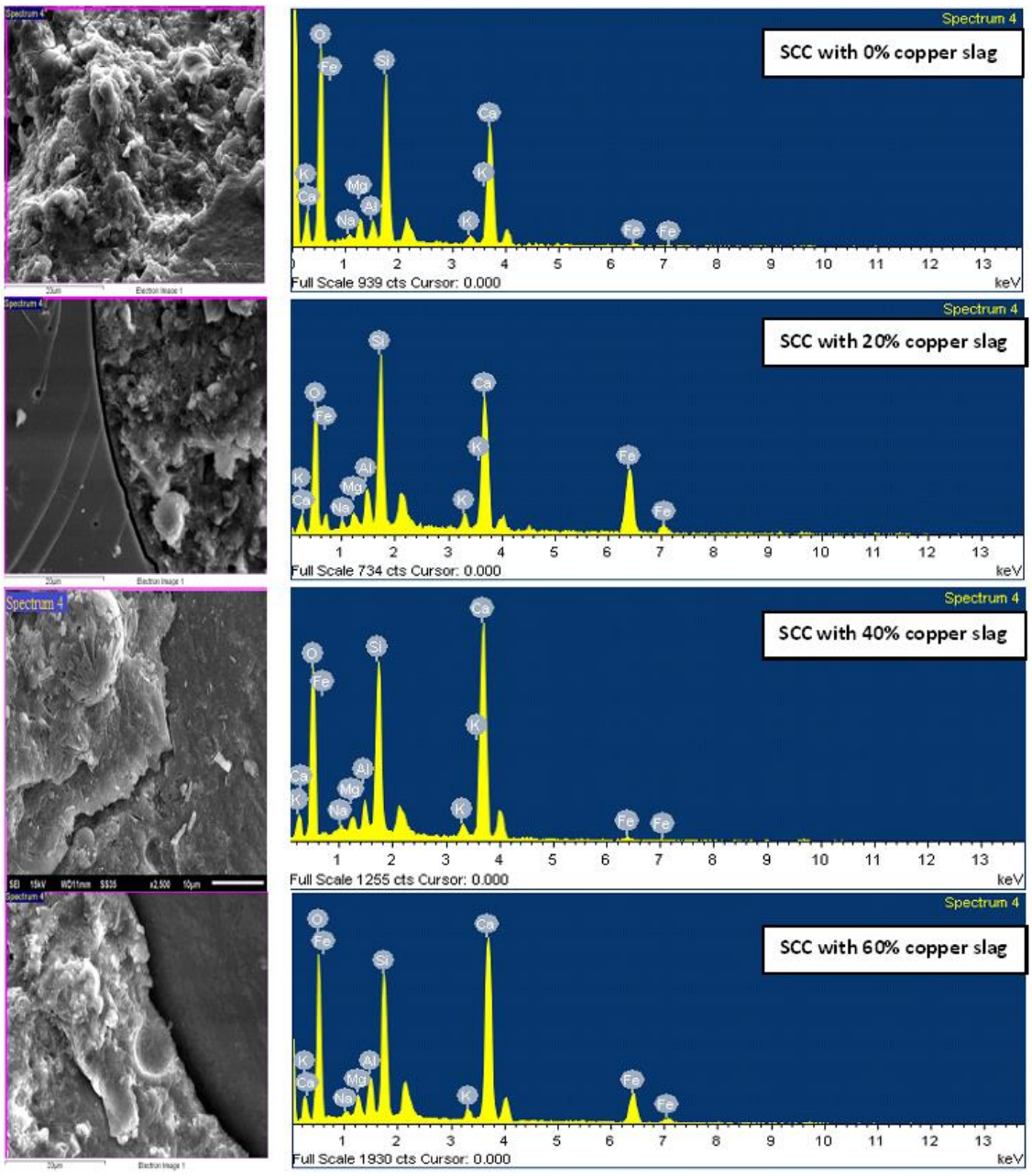

Fig. 4.24: EDS Spectrum of SCC Immersed in Sulfate Solution for 90 Days

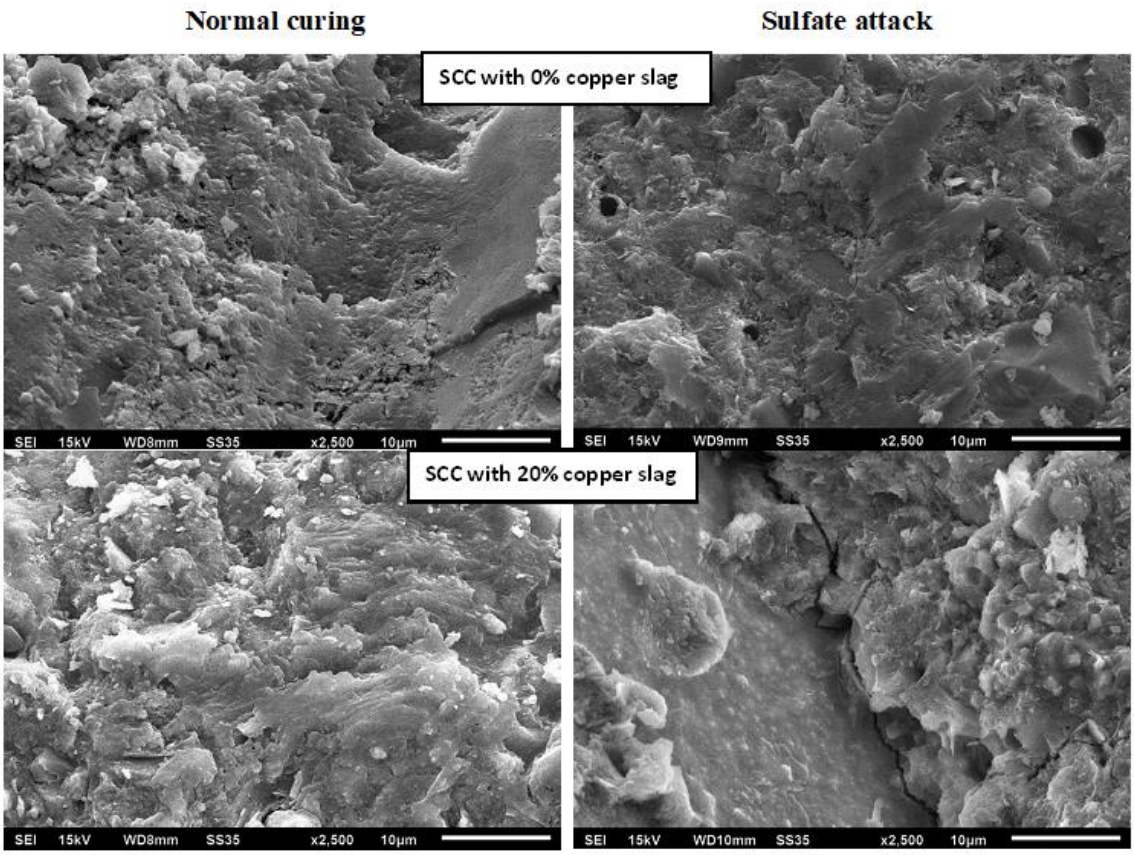

Fig. 4.25: Microstructure Comparison of SCC Incorporating 0% and 20% Copper Slag at 365 Days

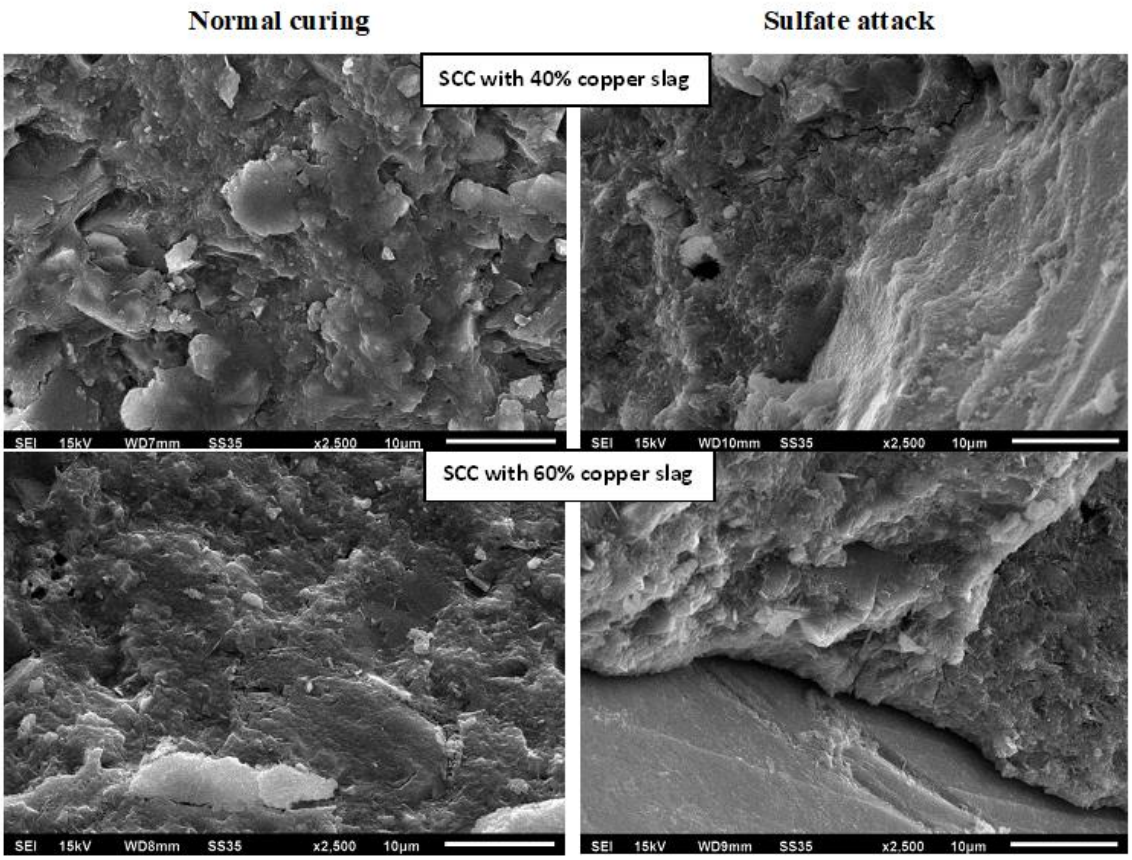

Fig. 4.26: Microstructure Comparison of SCC Incorporating 40% and 60% Copper Slag at 365 Days

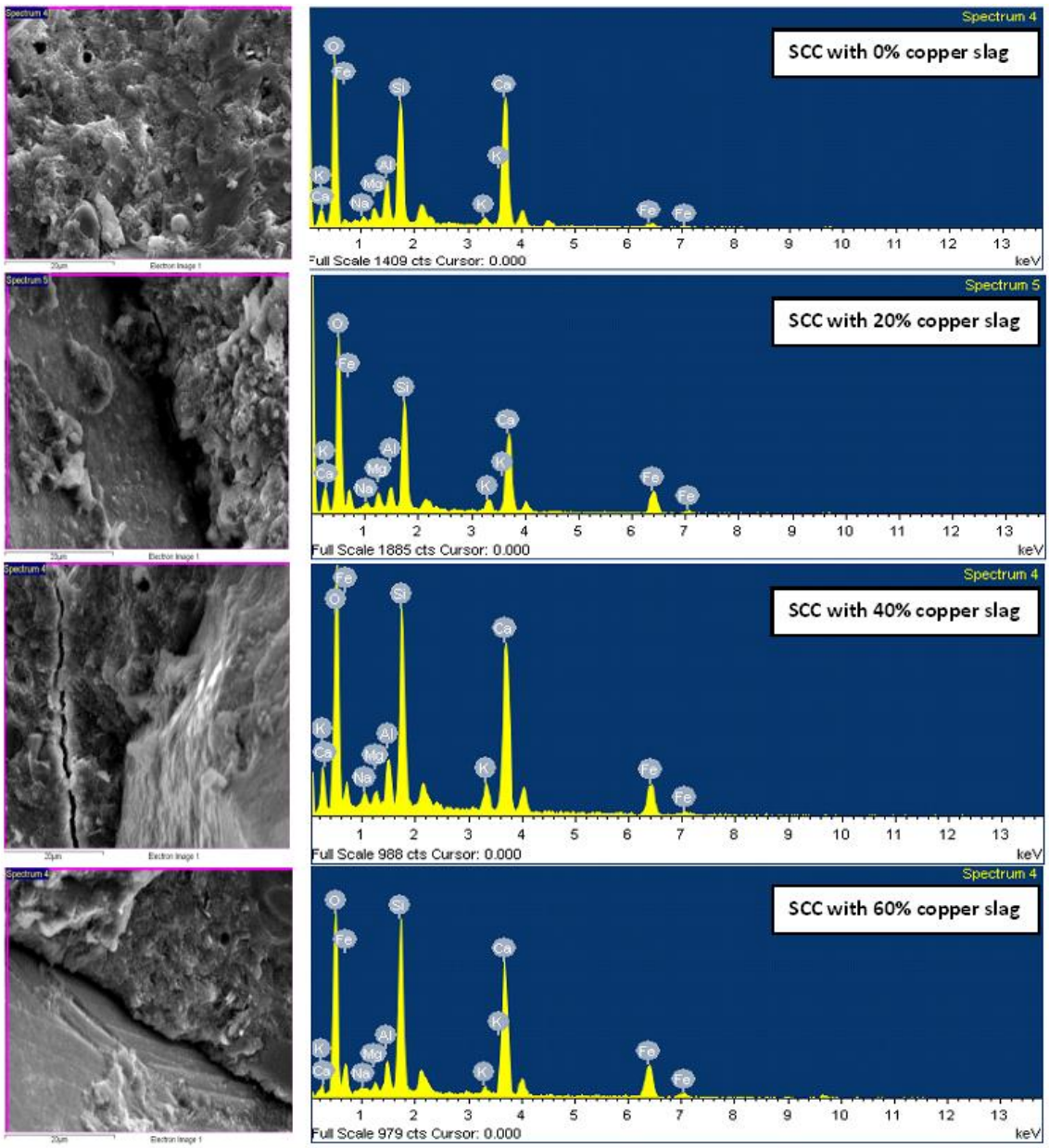

Fig. 4.27: EDS Spectrum of SCC Immersed in Sulfate Solution for 365 Days

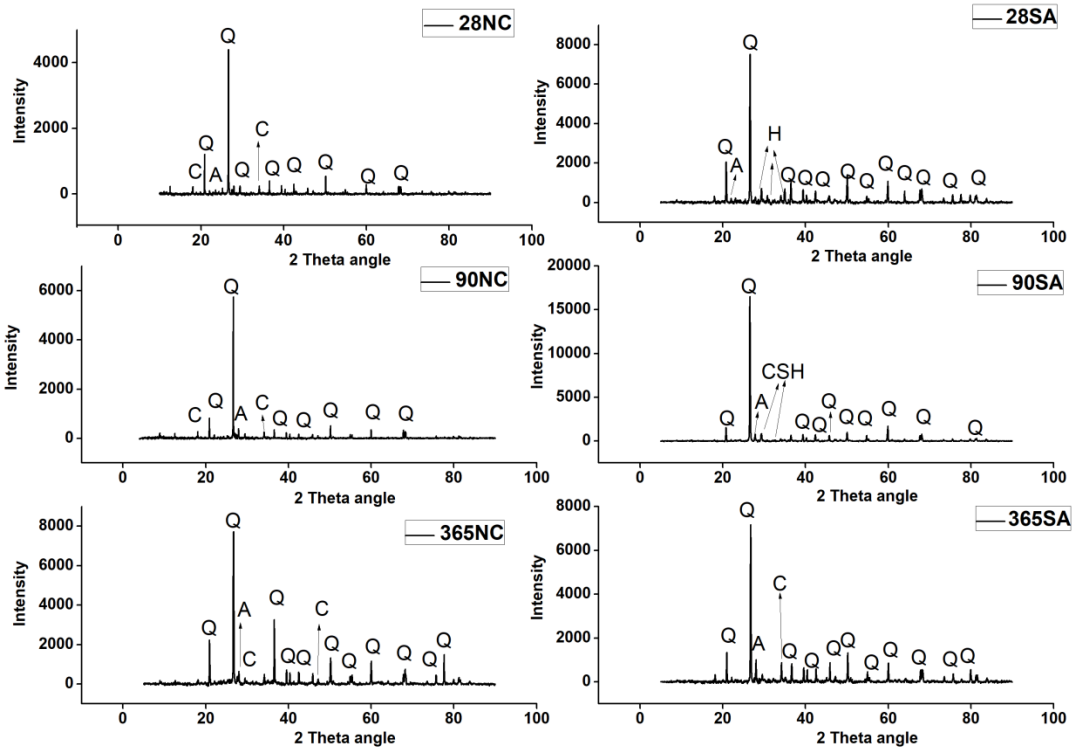

Fig. 4.28: Comparison of XRD Patterns of SCC Incorporating 0% Copper Slag Exposed to Normal Curing (NC) and Sulfate (SA) Solution (A-Anorthite; C-Calcium Hydroxide; CSH-Calcium Silicate Hydrate; H- Hedenbergite; Q-Quartz)

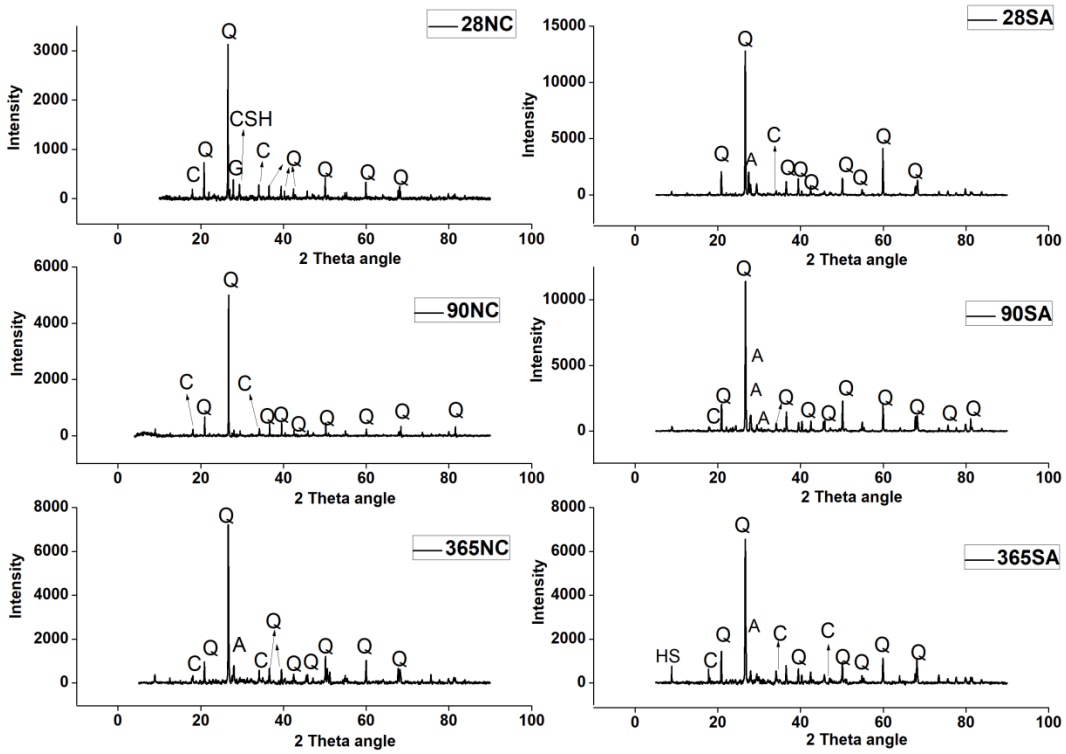

Fig. 4.29: Comparison of XRD Patterns of SCC Incorporating 20% Copper Slag Exposed to Normal Curing (NC) and Sulfate (SA) Solution (A-Anorthite; C-Calcium Hydroxide; CSH-Calcium Silicate Hydrate; G-Gismondine; HS-Hydrogen Silicate Hydrate; Q-Quartz)

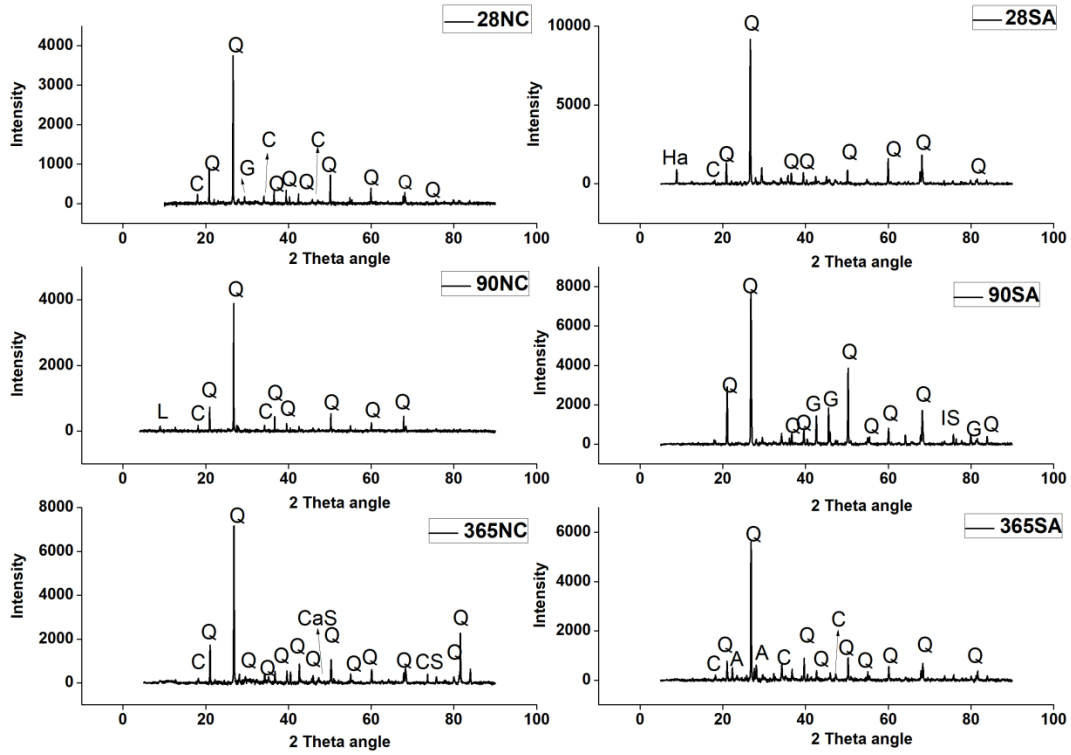

Fig. 4.30: Comparison of XRD Patterns of SCC Incorporating 60% Copper Slag Exposed to Normal Curing (NC) and Sulfate (SA) Solution (A-Anorthite; C-Calcium Hydroxide; CaS-Calcium Silicate; G-Gismondine; Ha-Halloysite; IS-Iron Silicon; L-Laumontite; Q-Quartz)

4.3.5.6 Expansion Measurements

Fig. 4.31 shows the expansion measurements of SCC exposed to sulfate solution for up to 365 days after the initial 28 days of water curing. Length of concrete prisms was recorded at various days of immersion in sulfate to study the long-term effect of sulfate on SCC incorporating copper slag, Changes in length (ΔL) (%), corresponding to expansion was then found out as given in ASTM C1012-10.

Minute expansions (less than 0.02%) were observed in SCC mixes under sulfate environment for up to 365 days. The maximum expansion of concrete prisms was reported for SCC mix with 0% slag at all days of sulfate immersion. SCC mixes

containing (10-60%) copper slag showed lower expansions in comparison with control SCC mix. With respect to immersion in sulfate solution, an insignificant increase in the value of expansion (%) was observed in SCC prisms incorporating 0 to 60% copper slag exposed to Sulfate solution after 90 days. The expansion values observed for 20% copper slag SCC mix exposed to sulfate solution from 90 to 365 days were 0.0034, 0.0039, 0.0043, 0.0049, 0.0053, 0.0059 and 0.006%, respectively. Najimi et al. (2011) concluded that expansions decreased in SCC mixes containing up to 5% copper slag; whereas for 10 and 15% copper slag replacements, expansions became almost equivalent.

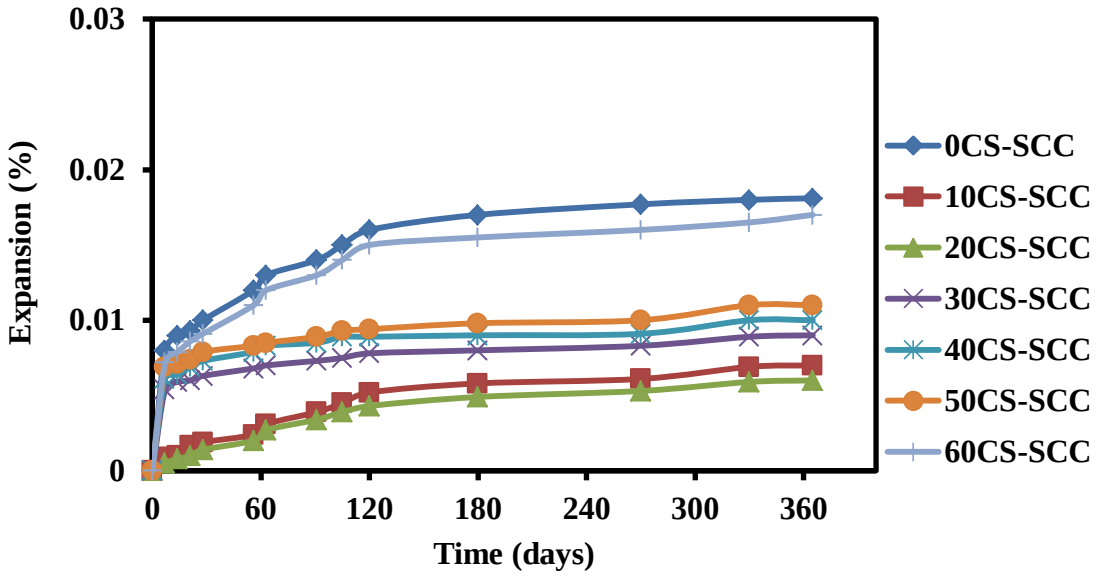

Fig. 4.31: Expansion Measurements of SCC in Sulfate Solution

4.3.5.7 Changes in Mass

The change in mass (%) of concrete cubes immersed in sulfate solution for up to 365 days after the initial 28 days of water curing was recorded and plotted in Fig. 4.32. The gain in mass (%) of all SCC mixes with the increasing immersion periods up to 365 days was studied. The increase in mass was less than 0.3% for mixes up to 365 days. SCC mixes incorporating 0% copper slag gave the lowest value of mass gain for up to 365

days; while the highest gain in mass was recorded for SCC mixes made with 60% copper slag. Increase in mass may be owed to the filling of sulfate ions into the pores of the SCC concrete matrix. This did not affect the compressive strength of SCC exposed to sulfate solutions.

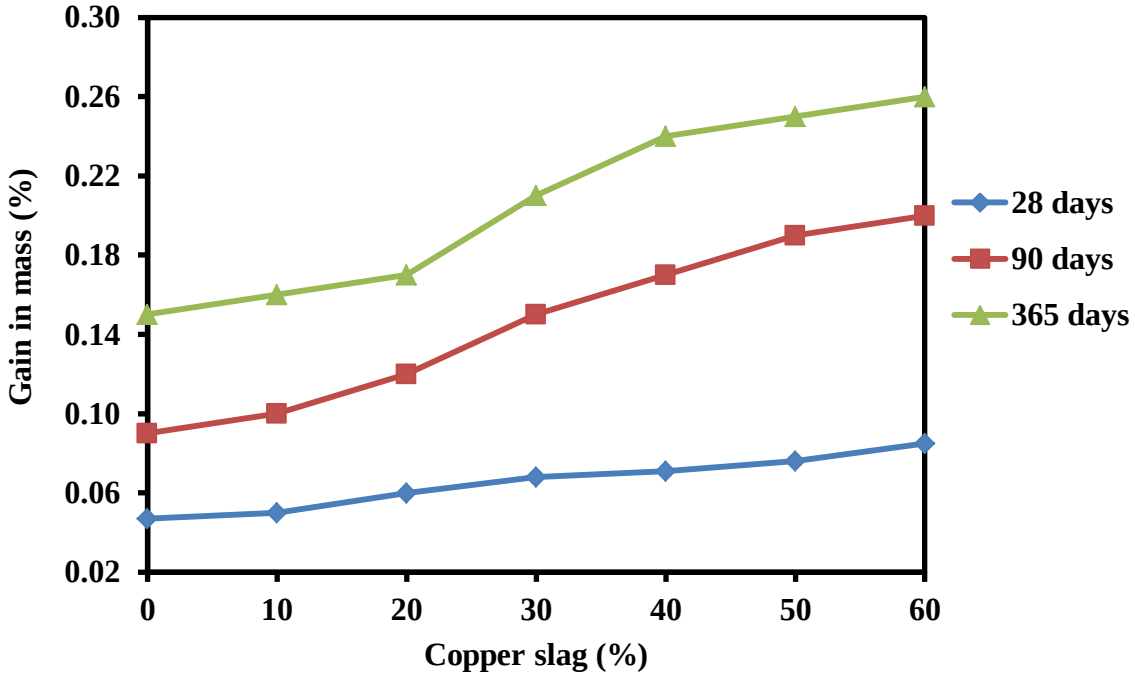

Fig. 4.32: Gain in the Mass of SCC in Sulfate Solution

4.4 MICRO-STRUCTURAL PROPERTIES OF SCC

4.4.1 Scanning Electron Microscopy and Energy Dispersive Spectroscopy

SEM analysis determines the microstructure of concrete matrix while Energy Dispersive Spectroscopy (EDS) determines the elemental composition of the concrete matrix. The microstructure of SCC mixes was studied using SEM and EDS techniques at 28, 90 and 365 days curing period. SEM, coupled with EDS, was performed on the gold-coated fracture surface of the sample obtained from the inner core of SCC after performing the compressive strength test. The development of microstructure of concrete from 28 to 365

days at 5000x magnification is shown in Fig. 4.33 to 4.37. In this research, the images presented are of those SCC mixes where slight visible changes have been investigated. The strength and the rheological properties of concrete mixes are significantly affected by its microstructural formations. The morphology of the concrete matrix is studied by SEM analysis. A comparison has been made to understand the changes in the microstructure of the SCC matrix at 28, 90 and 365 days curing. At 28 days, SCC mix made with 100% sand showed the formation of voids and micro-cracks. Also, development of needle-shaped ettringites was found in the initial stages of curing up to 28 days as visible in Fig. 4.33. As the curing age increased up to 90 days, the formation of uneven calcium silicate hydrate (CSH) layers was quite prominent. Further, as the curing age increased from 90 to 365 days, dense and homogenous layers of CSH were visible and no ettringites were seen. For SCC mix incorporating 20 and 30% copper slag, ettringites and voids could be seen at 28 days, as shown in Fig. 4.34 and 4.35. As the curing age increased up to 365 days, compact homogenous CSH layers were formed. This resulted in a refined structure with slag and fly ash filling the voids as well as giving rise to the increased strength. A similar type of morphology was observed in SCC mix incorporating 10% copper slag. For SCC mixes containing 40, 50 and 60% copper slag, voids and micro-cracks along with ettringite formations were formed in the concrete matrix. Due to low water absorption of copper slag, the excess water present resulted in the creation of voids and cracks and thus reduced the strength of the concrete matrix (Fig. 4.36 and 4.37). It can be concluded that the microstructure of SCC mixes improved and got denser with the addition of copper slag in SCC mixes at all ages of curing. Reduction of voids and improved compressive strength of SCC mixes gives a good effect to its durability properties. With the increase in curing period from 28 to 365 days, the formation of CSH layers in SCC mixes can be closely related to its improved compressive strength and reduced permeability.

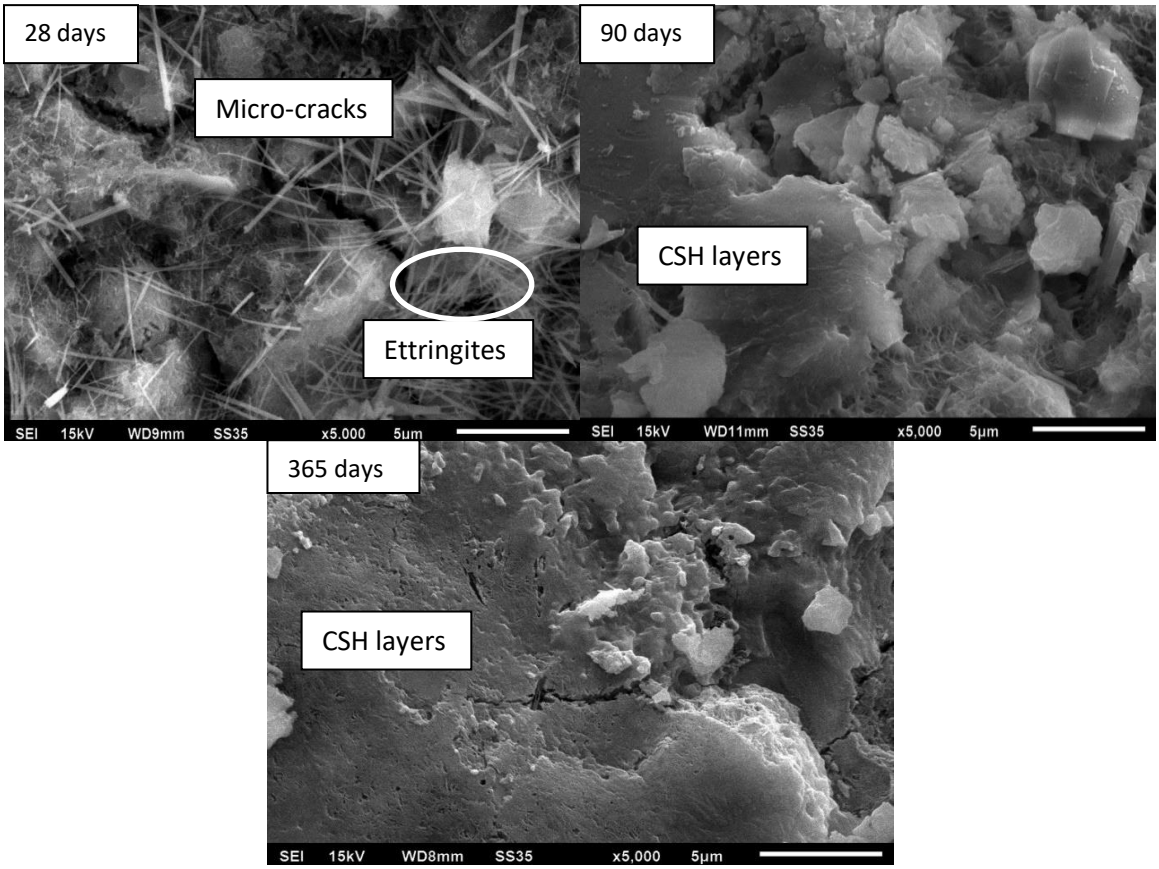

Fig. 4.33: Development of Microstructure of SCC with 0% Copper Slag

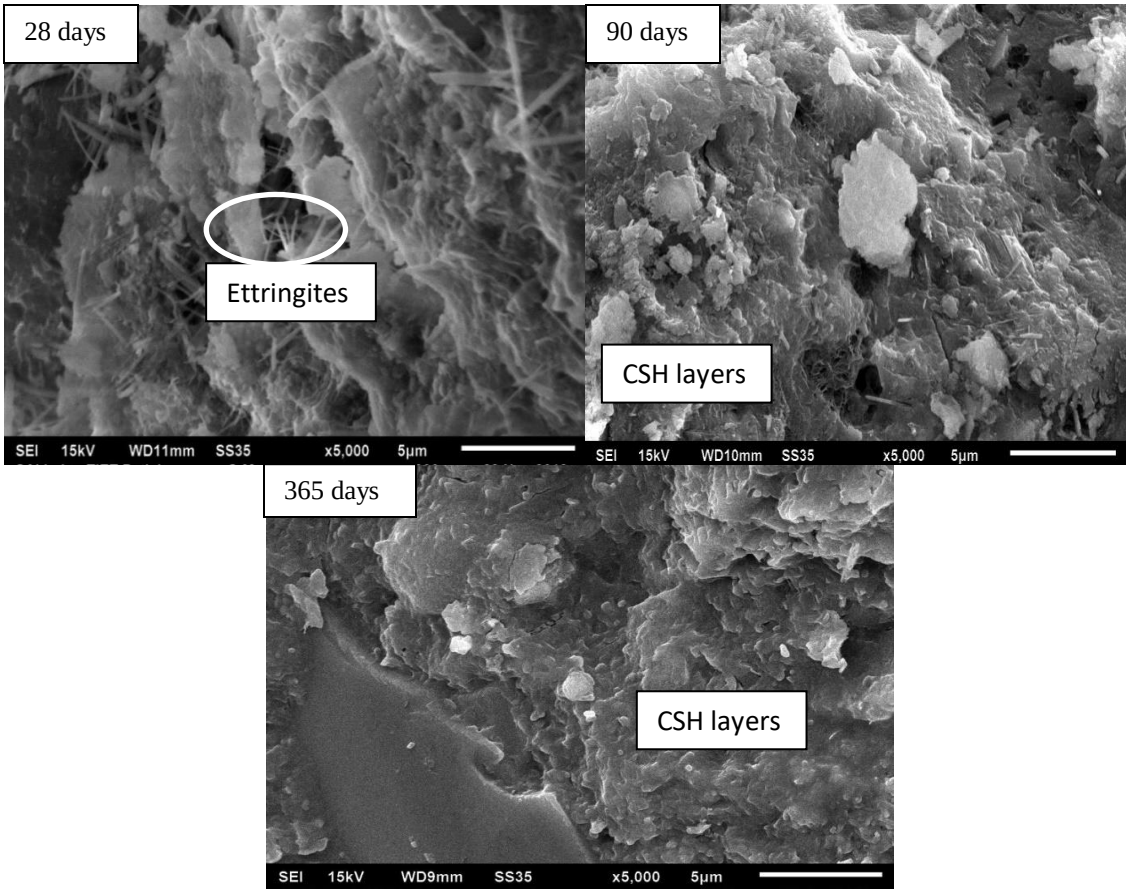

Fig. 4.34: Development of Microstructure of SCC with 20% Copper Slag

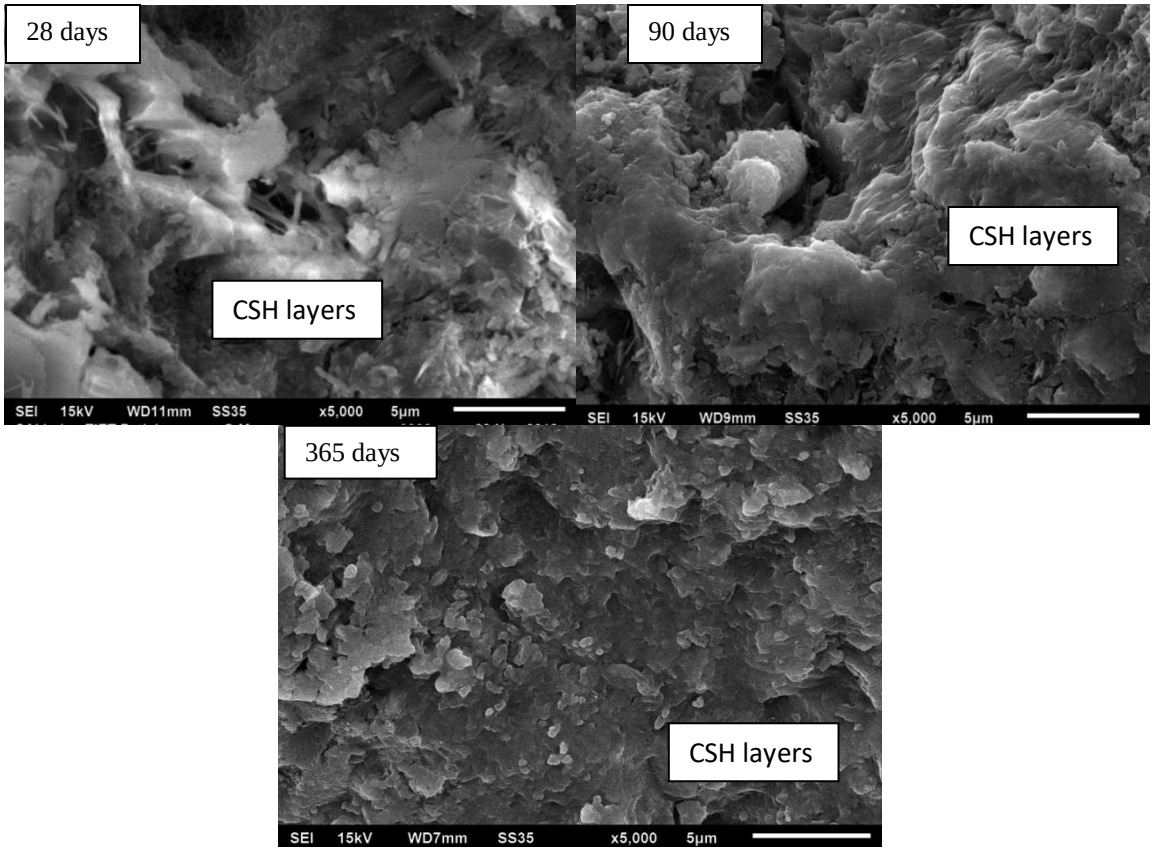

Fig. 4.35: Development of Microstructure of SCC with 30% Copper Slag

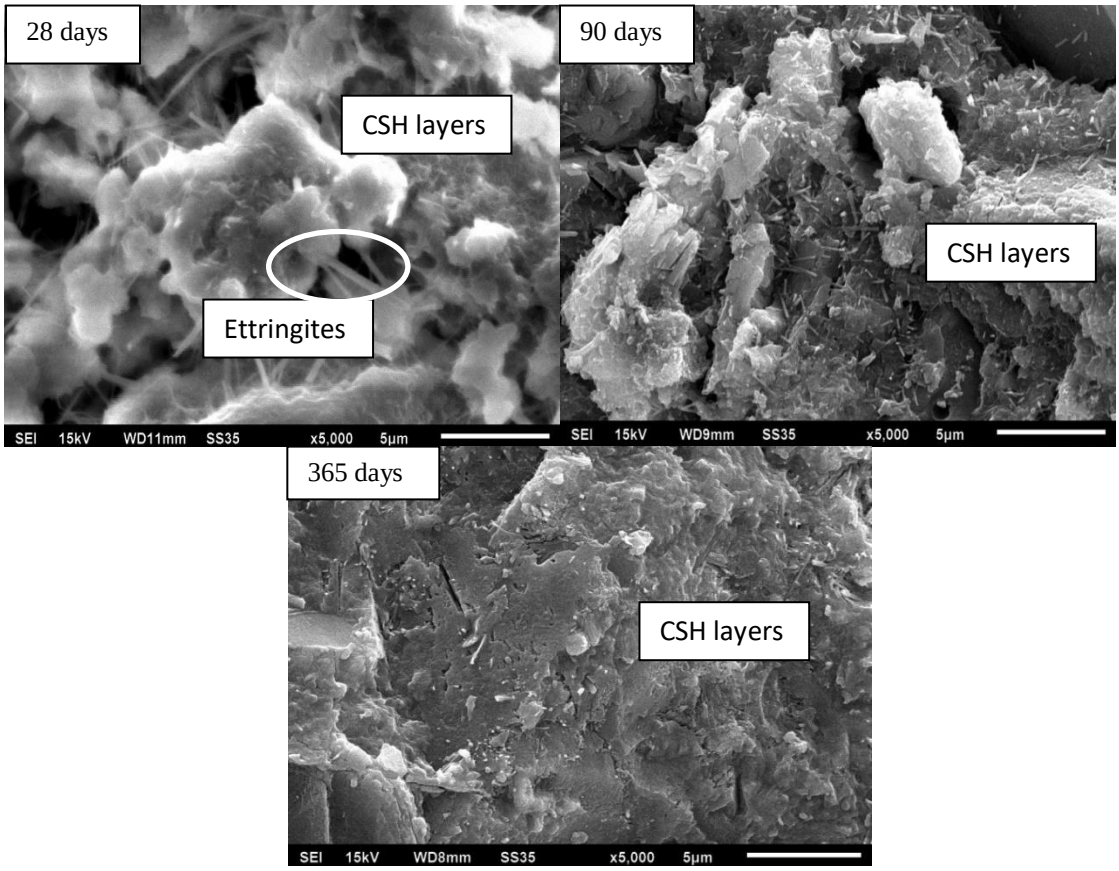

Fig. 4.36: Development of Microstructure of SCC with 40% Copper Slag

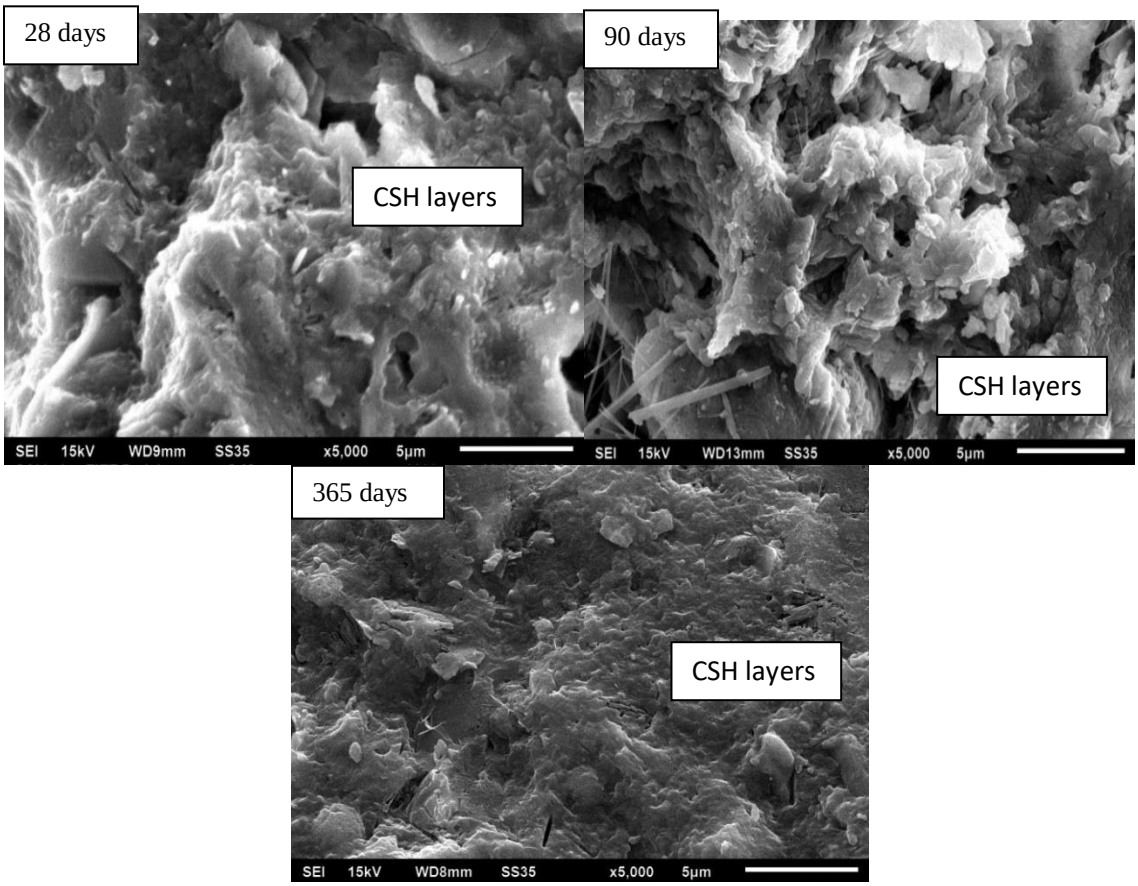

Fig. 4.37: Development of Microstructure of SCC with 60% Copper Slag

Further, the elemental composition of concrete mixes was studied under EDS and their spectrums at 28 and 90 days of curing age can be found in Fig. 4.38 to 4.45. It consisted of peaks of major elements like those of Ca, Si, Al, S, K, O, Fe, Na and Mg. Presence of Aluminium and sulfur in SCC mix without copper slag revealed the ettringite formation under EDS (Fig. 4.38). Peaks of Ca, Si, Fe, Al, O and S were observed in EDS analysis for SCC mixes containing 20% copper slag (Fig. 4.39). As the copper slag content increased further, dense layers of C-S-H gel were observed. From EDS analysis, peaks of Ca and Si further confirmed the development of calcium silicate hydrate gel in the concrete matrix. The accumulation of C-S-H layers makes the concrete matrix denser. Ettringite crystals along with voids were observed in SCC mix with 40% copper slag under SEM analysis. Also, peaks of Al and S further confirmed the formation of calcium alumino-sulfates in concrete (Fig. 4.40). EDS analysis of the SCC mixes at 365 days is

presented in Table 4.7. The highest amount of silica existed in 20% copper slag SCC mix. The ratio of Calcium to Silica was calculated for all mixes and was then related to compressive strength (Dadsetan and Bai, 2017). It can be related to the fact that the increasing silica content corresponds to the good pozzolanic reaction (Jawahar et al., 2013). The atomic Ca/Si ratios were investigated for SCC mixes incorporating copper slag at 365 days (Table 4.7). The Ca/Si ratio of SCC with 0, 10, 20, 30, 40, 50 and 60% copper slag was found to be 1.96, 2.0, 1.66, 1.70, 1.86, 1.99 and 2.31, respectively. Lower Ca/Si ratio of concrete corresponded to higher compressive strength. It could be due to the conversion of calcium hydrate into CSH layers, thus improving the total porosity and refinement of the concrete matrix (Jawahar et al., 2013, Poon et al., 2006, Kavitha et al., 2015).

Table 4.7: EDS Analysis of SCC at 365 Days

Chemical elements (Atomic %)	O	Ca	Si	Al	Mg	K	Na	Fe	Ca/Si
0CS-SCC	75.76	12.92	6.57	2.50	0.73	0.64	0.45	0.43	1.96
10CS-SCC	74.01	13.17	6.56	2.48	1.84	0.49	0.80	0.64	2.00
20CS-SCC	71.93	15.33	9.26	1.80	0.50	0.39	0.34	0.45	1.66
30CS-SCC	68.72	15.15	8.09	3.34	1.14	0.53	0.16	2.06	1.70
40CS-SCC	75.26	14.40	7.73	0.96	0.85	0.49	-	0.31	1.86
50CS-SCC	77.59	12.41	6.25	1.63	0.90	0.25	-	0.95	1.99
60CS-SCC	72.63	16.88	7.31	1.60	0.61	0.33	0.33	0.31	2.31

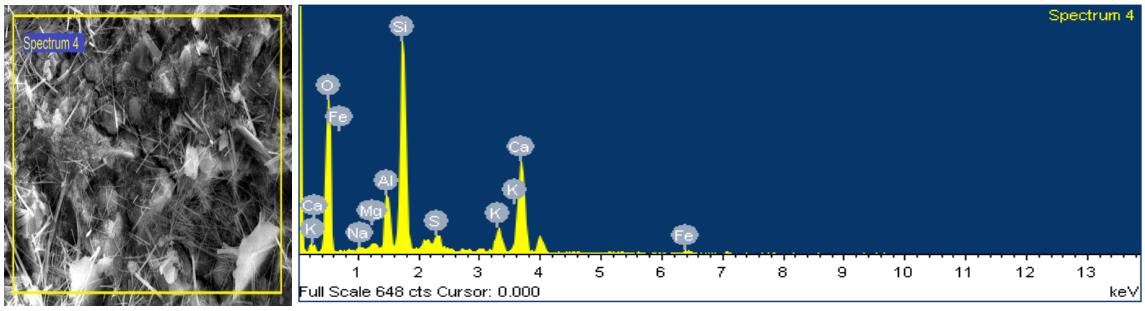

Fig. 4.38: EDS Analysis of SCC with 0% Copper Slag at 28 Days

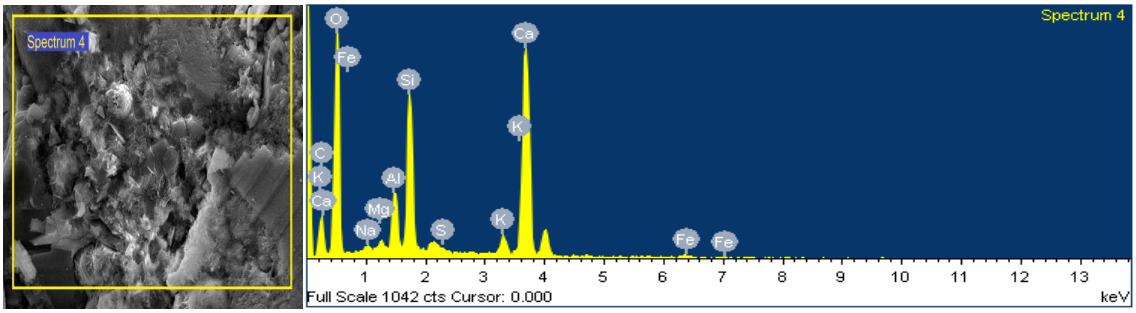

Fig. 4.39: EDS Analysis of SCC with 20% Copper Slag at 28 Days

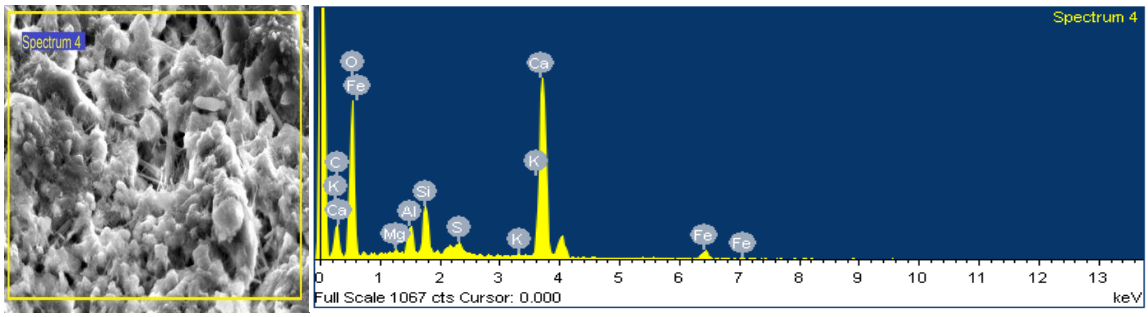

Fig. 4.40: EDS Analysis of SCC with 40% Copper Slag at 28 Days

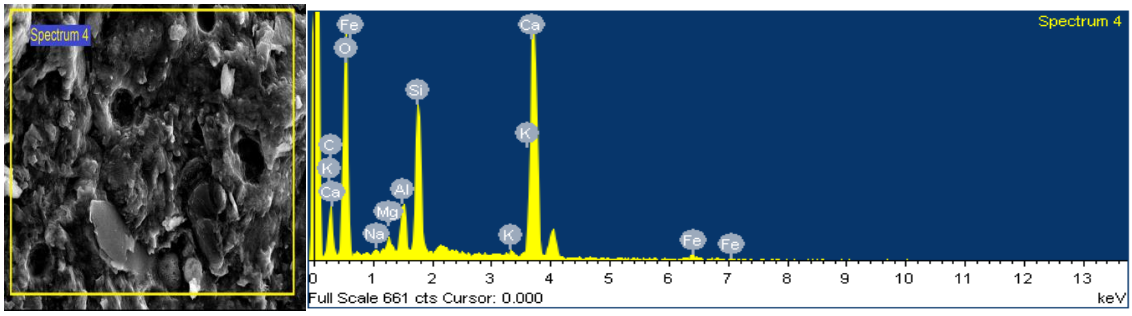

Fig. 4.41: EDS Analysis of SCC with 60% Copper Slag at 28 Days

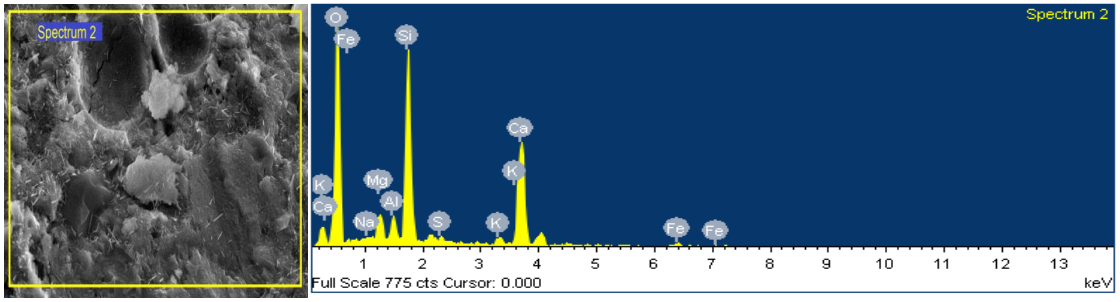

Fig. 4.42: EDS Analysis of SCC with 0% Copper Slag at 90 days

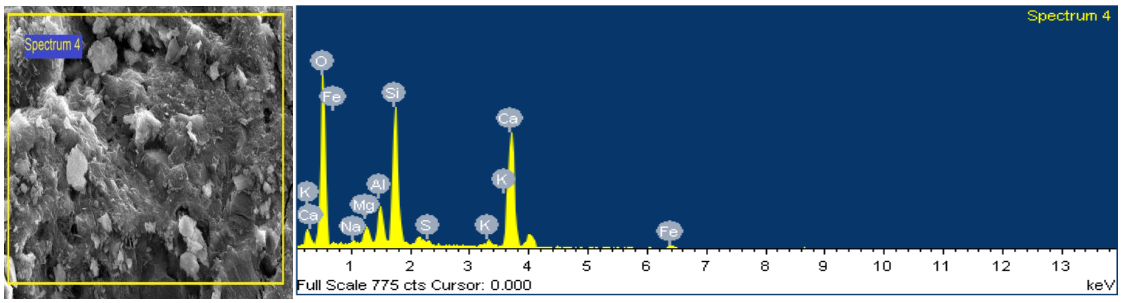

Fig. 4.43: EDS Analysis of SCC with 20% Copper Slag at 90 Days

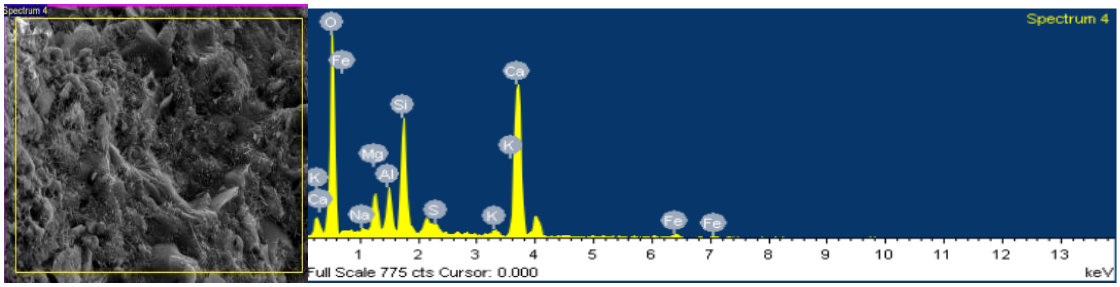

Fig. 4.44: EDS Analysis of SCC with 40% Copper Slag at 90 Days

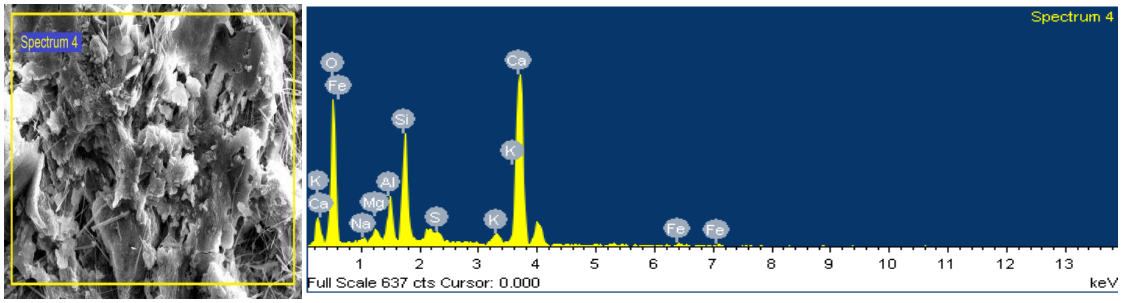

Fig. 4.45: EDS Analysis of SCC with 60% Copper Slag at 90 Days

4.4.2 X-Ray Diffraction

X-ray diffraction (XRD) technique was evaluated to spot different phases present in hardened SCC mixes containing copper slag varying from 0% to 60%. Powder samples were taken from hardened concrete samples with and without copper slag after performing the compressive strength test at 28, 90 and 365 curing days. The samples were sieved from 90 µm sieve and the sieved sample was used for XRD analysis. XRD patterns of SCC were recorded using X'Pert Pro device with the following parameters as a set: monochromatic Cu kα radiation of 1.5418 Å wavelength in the range of 5-90° of 2θ range, step size of 0.02° and a scan rate of 0.097°/sec, functioning at 45 kV and 40 mA.

Fig. 4.46 to Fig. 4.52 presented the XRD pattern of all SCC mixes varying from 0% to 60% at 28 days curing period. XRD patterns showed that the concrete mixes confirmed the crystalline structure at all replacement levels. SCC mixes with and without copper slag contained multi-phase peaks. The phases present in SCC mixes were: Quartz, Anorthite, Calcium Hydroxide, Calcium Silicate Hydrate (CSH), Gismondine, Portlandite and Silicon Oxide. XRD pattern of SCC mix without copper slag is shown in Fig. 4.46. The main peak with 2 Theta angle of 26.6633 degrees refers to the hexagonal crystal structure of Quartz-synthetic phase having ICSD- 01-085-1053. Apart from this, peaks of phases Anorthite and Calcium Hydroxide were also present. The phase Anorthite has the chemical formulae- $CaAl_2Si_2O_8$ and Calcium hydroxide as $Ca(OH)_2$. SCC mix incorporating 10% copper slag contained the main peak of Quartz alpha-syn, ICSD- 01-078-1253 having a hexagonal crystal structure. Phases of Calcium Silicate Hydrate and Calcium hydroxide were also observed; which further gives the proof of the increased strength of SCC mix. SCC mixes containing 40% copper slag showed the main peak of Quartz and Gismondine phase. Gismondine phase, ICSD- 00-020-0452 and chemical formula- $CaAl_2Si_2O_8.4H_2O$ represented the monoclinic crystal structure. No major phase changes were observed for SCC mixes.

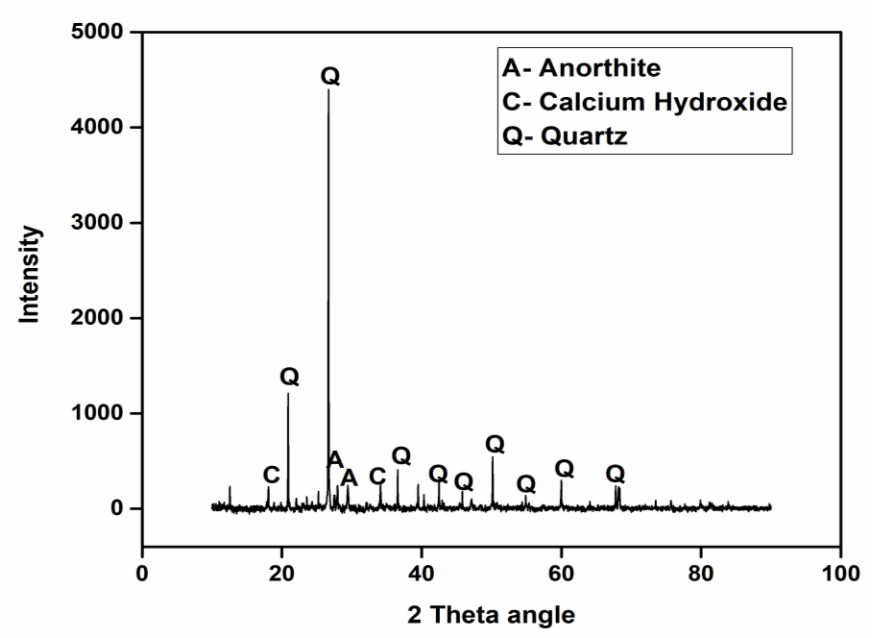

Fig. 4.46: XRD Analysis of SCC with 0% Copper Slag at 28 Days

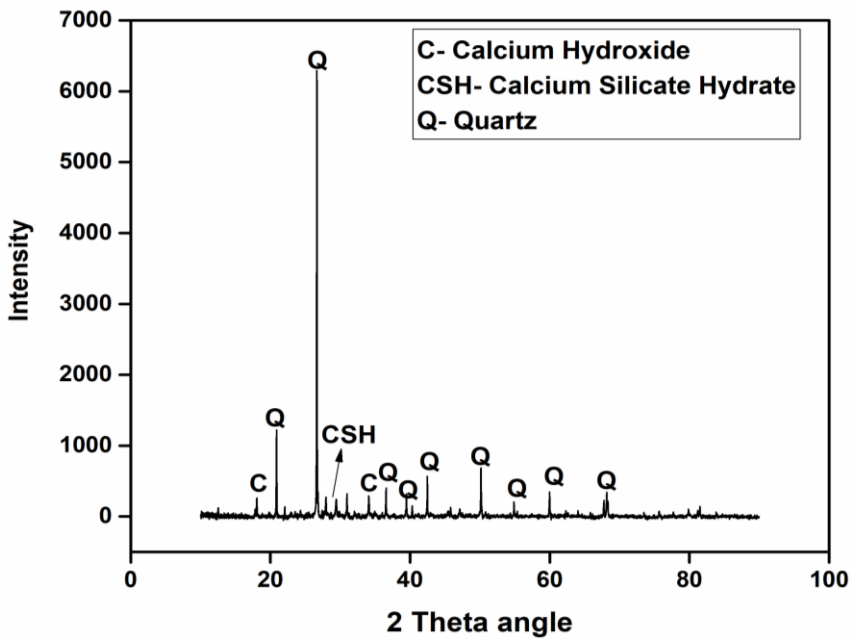

Fig. 4.47: XRD Analysis of SCC with 10% Copper Slag at 28 Days

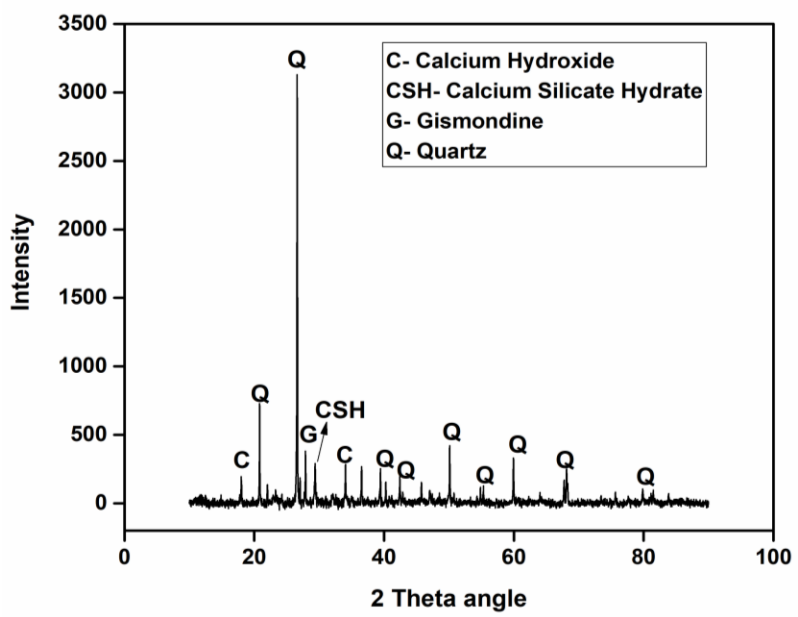

Fig. 4.48: XRD Analysis of SCC with 20% Copper Slag at 28 Days

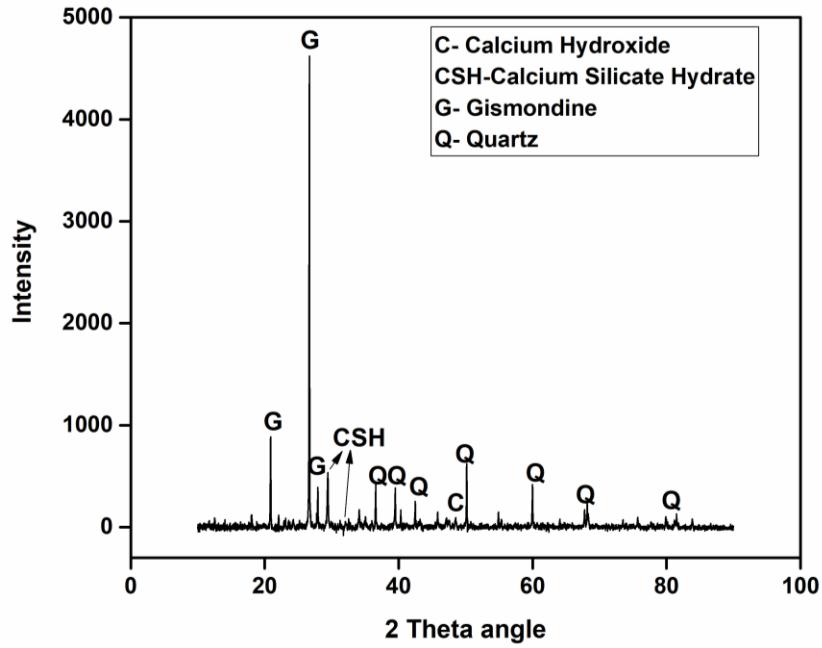

Fig. 4.49: XRD Analysis of SCC with 30% Copper Slag at 28 Days

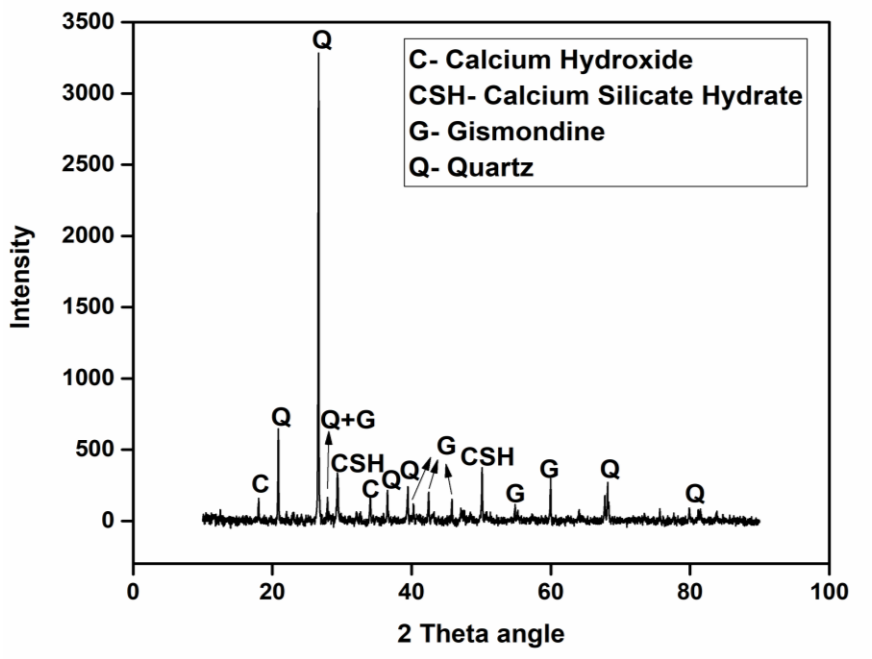

Fig. 4.50: XRD Analysis of SCC with 40% Copper Slag at 28 Days

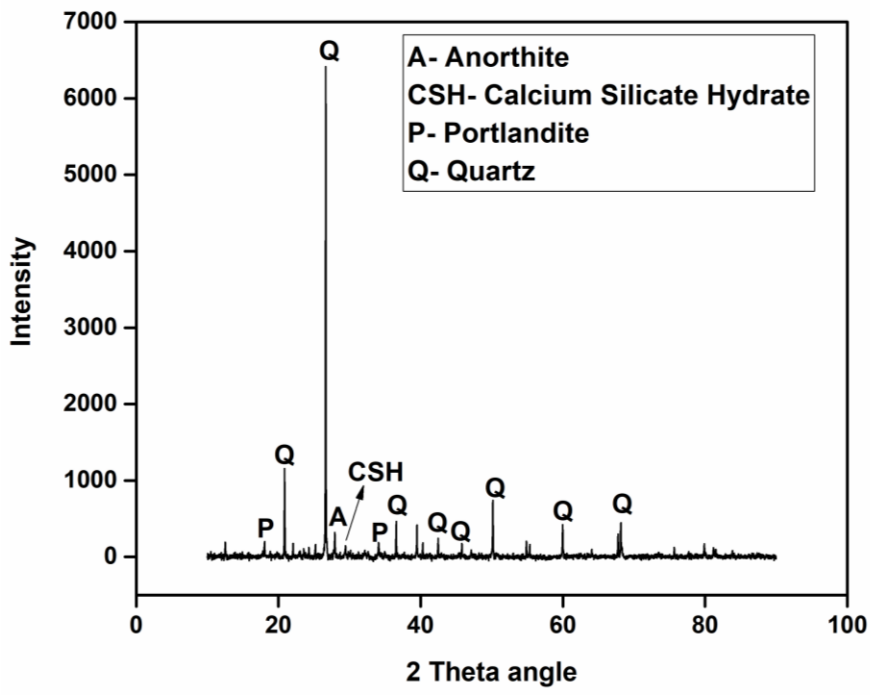

Fig. 4.51: XRD Analysis of SCC with 50% Copper Slag at 28 Days

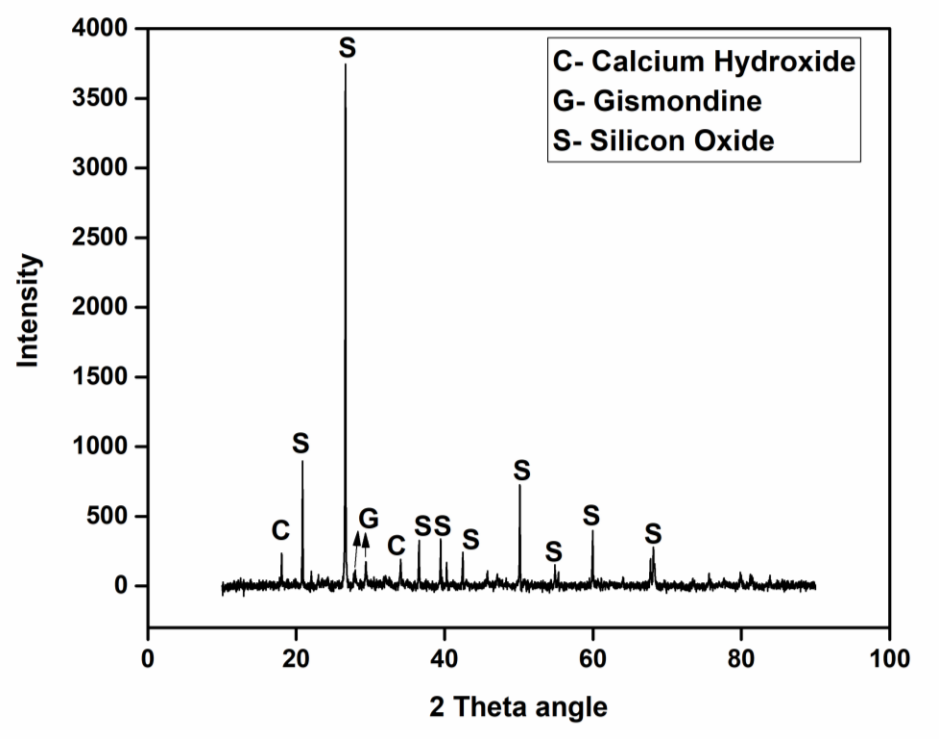

Fig. 4.52: XRD Analysis of SCC with 60% Copper Slag at 28 Days

XRD technique was evaluated to study the phases that were developed in the concrete matrix from 90 to 365 days. As can be seen from Fig. 4.53 and 4.54; SCC mixes showed a crystalline behaviour up to 365 days. No major phase change was indicated while increasing the percentages of copper slag in SCC. Major Peak of Quartz having hexagonal crystal structure was formed in SCC mixes up to 365 days. Other hydrated phases formed were that of Calcium Hydroxide, Anorthite, Aluminium Silicate Hydrate and Calcium Iron oxide at 90 days. In addition to these, traces of Gismondine, Calcium Silicide and Hedenbergite were formed in SCC mixes at 365 days. Hedenbergite phase having chemical formulae $CaFeSi_2O_6$ represented the monoclinic crystal system whereas Calcium Silicide with chemical formulae $CaSi_2$ represented the rhombohedral crystal structure. Also, small amounts of Calcium Iron Oxide and Hedenbergite phases existed in 50% copper slag SCC mix at 90 and 365 days, respectively.

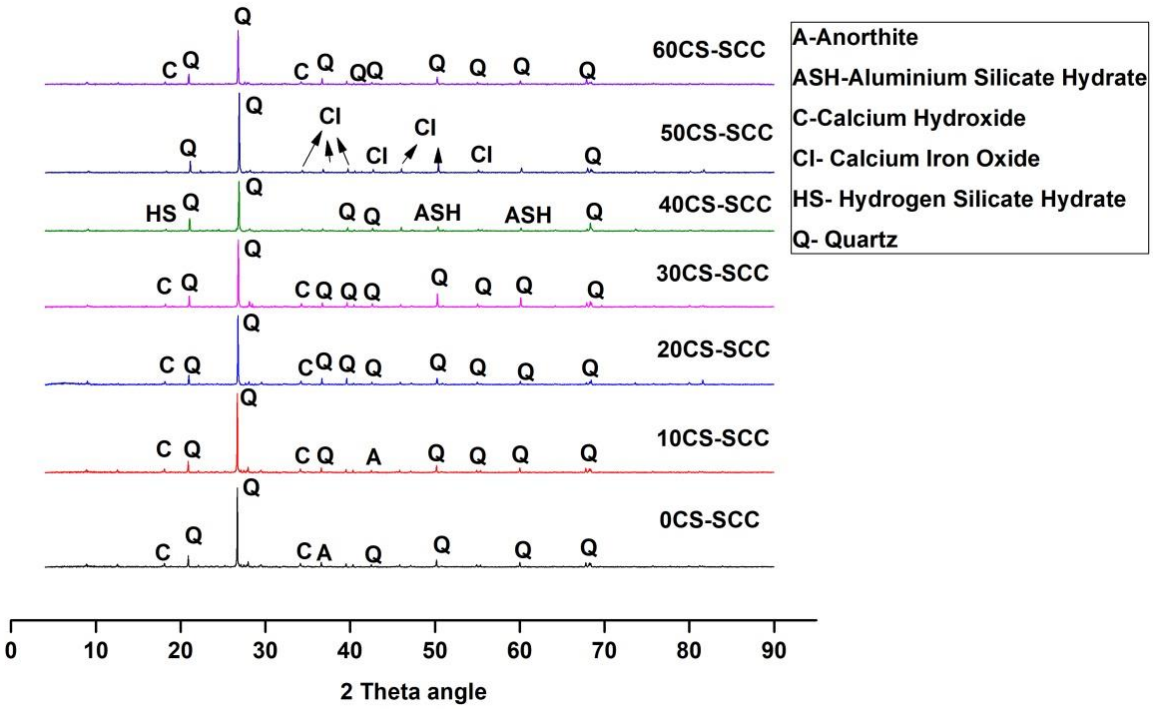

Fig. 4.53: XRD Analysis of SCC at 90 Days

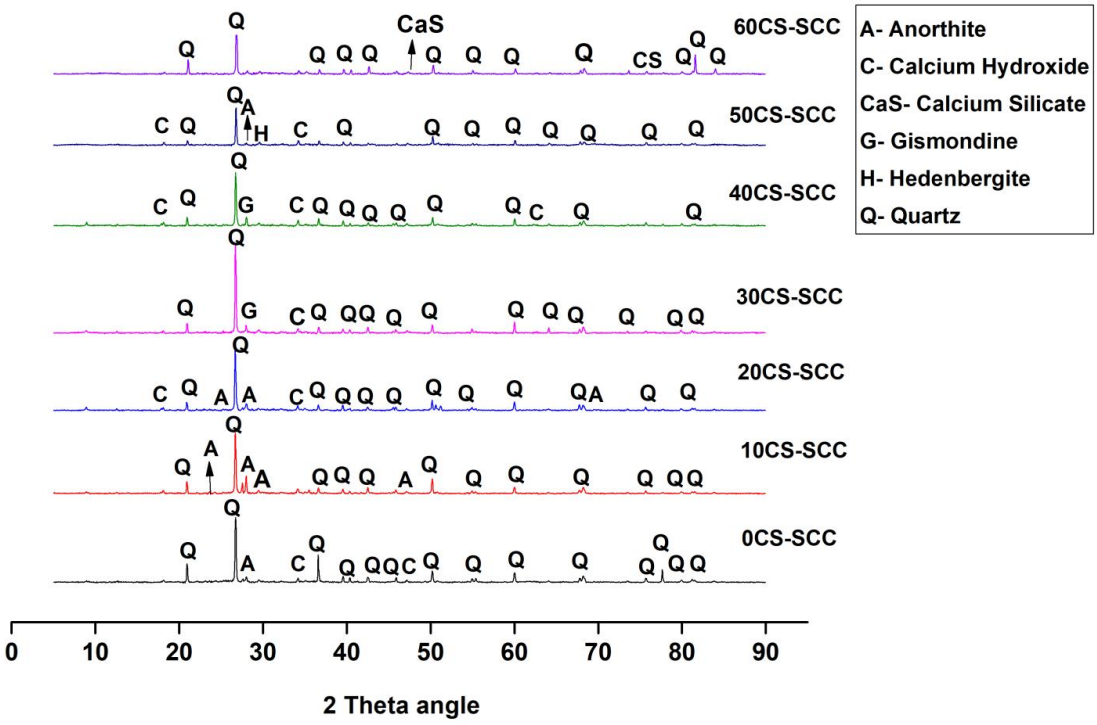

Fig. 4.54: XRD Analysis of SCC at 365 Days

4.5 STATISTICAL ANALYSIS

4.5.1 Correlations amongst Flow Properties

Linear regression analysis was used to discover the relation between flowability, passing ability and viscosity parameters of various SCC mixes. The linear regression coefficients (R^2) of the correlation between (1) slump flow and T_{500} slump flow (2) V-funnel time and T_{500} slump flow were investigated to be 0.71 and 0.97, respectively (Fig. 4.55). As slump flow increases, there is a linear decrease in T_{500} slump flow. Thus, validating an inverse relationship between flowability and viscosity of SCC mixes. On the contrary, T_{500} slump flow increases linearly with increase in V-funnel time. Likewise, a linear correlation established amongst V-funnel time and slump flow with regression coefficient, R^2=0.72. Behera et al. (2019) reported a linear correlation coefficient, R^2=0.5 between slump flow and T_{50} time and R^2=0.4 between slump flow and V-funnel time in case of SCC incorporating recycled fine aggregate. Further, a very strong correlation existed between V-funnel time and L-box ratio by regression coefficient, R^2=0.97 (Fig. 4.56).

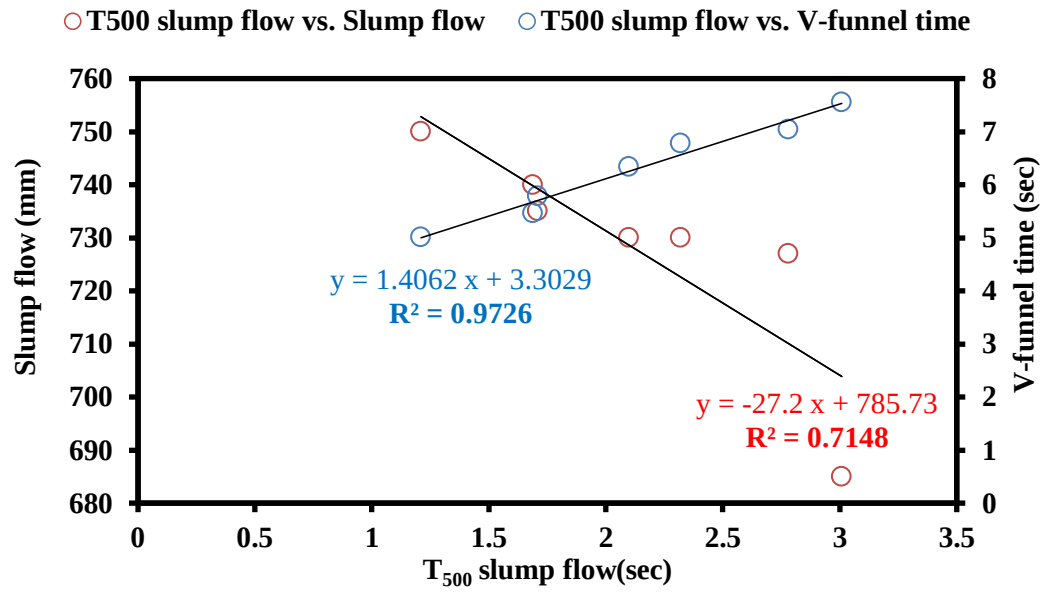

Fig. 4.55: Correlation of T_{500} Slump Flow of SCC with Slump Flow and V-Funnel Time

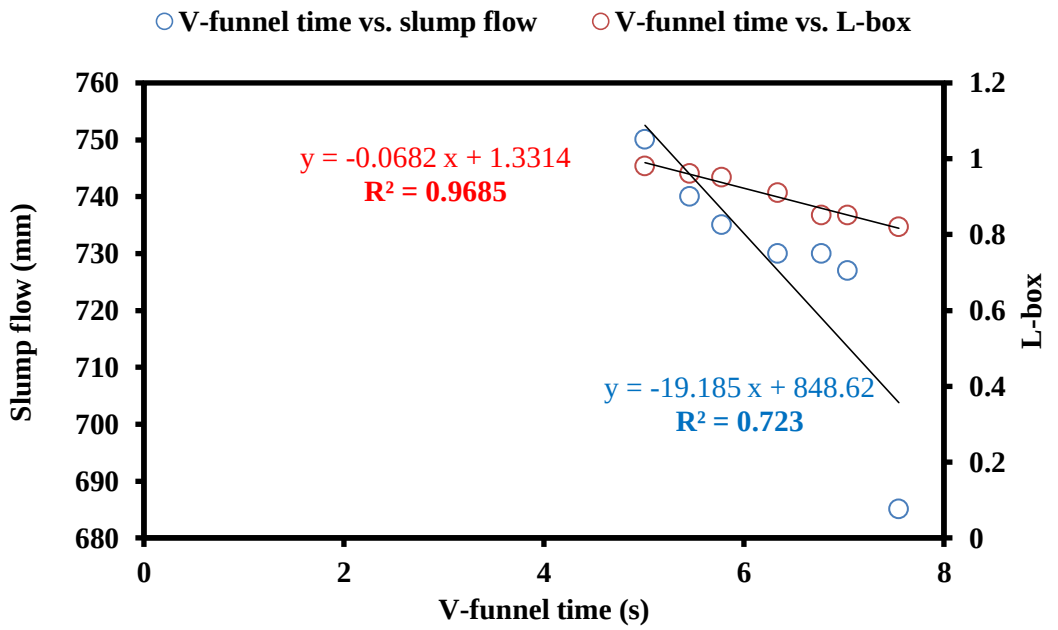

Fig. 4.56: Correlation of V-Funnel Time of SCC with Slump Flow and L-Box

4.5.2 Correlations amongst Compressive Strength and Durability Properties

To study the interdependence of compressive strength with RCP values (charge passed), water absorption and sorptivity of SCC mixes incorporating copper slag; linear regression analysis was conducted for the values up to 365 days curing. A strong declining linear correlation established amid compressive strength and water absorption with regression coefficient; R^2=0.84 as shown in Fig. 4.57. Also, a strong linear correlation was achieved among compressive strength and the charged passed with R^2=0.93 (Fig. 4.57). Both water absorption and RCP values showed an inverse relationship with compressive strength. A correlation coefficient with R^2=0.73 was established between compressive strength and sorptivity (Fig. 4.58). With the escalation of strength, durability properties like water absorption, chloride ion permeability and sorptivity decreases. This further validated the results obtained experimentally for strength and durability.

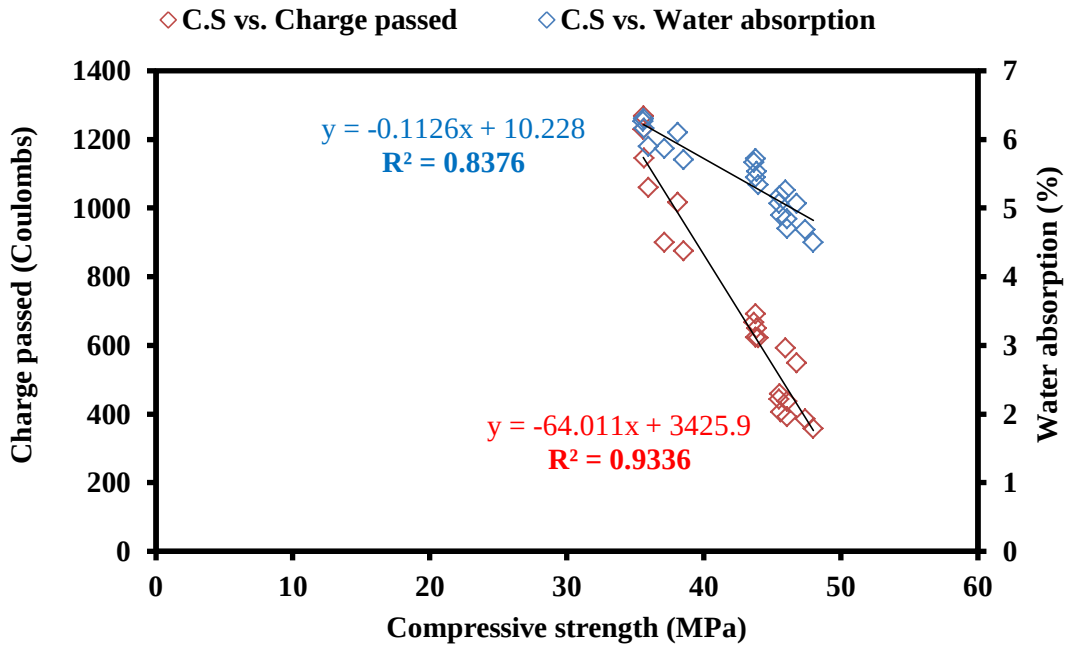

Fig. 4.57: Correlation of Compressive Strength of SCC with Charge Passed and Water Absorption

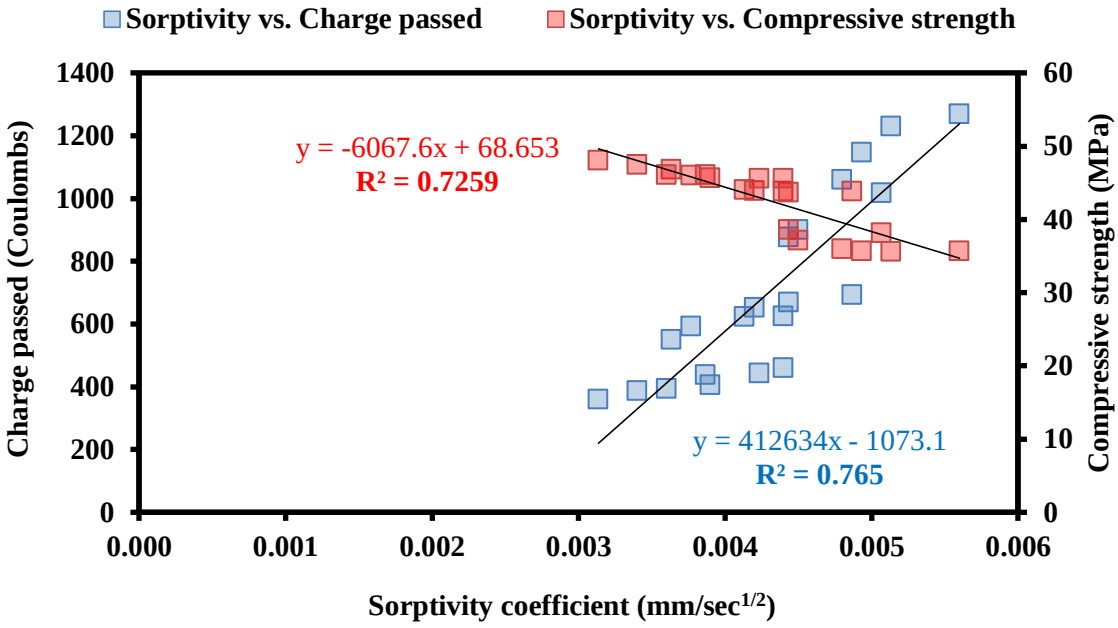

Fig. 4.58: Correlation of Sorptivity Coefficient of SCC with Charge Passed and Compressive Strength

The relationship between various durability properties was studied to understand the interdependency of their results. A direct linear correlation with a coefficient of 0.77 was established between sorptivity and charge passed in SCC mixes, as shown in Fig. 4.58. Water absorption of SCC mixes was plotted against RCPT (charge passed) values as well as sorptivity values for up to 365 days using linear regression analysis. As evident from Fig. 4.59, there is a direct linear correlation of water absorption with charge passed and sorptivity. The linear regression coefficients of the correlations between (a) water absorption with charge passed, (b) water absorption and sorptivity were 0.91 and 0.88, respectively. The decline in water absorption was related to the reduction of pores and voids of the concrete matrix. This could be owed to the filling effect of slag and fly ash; thereby decreasing the total chloride ion permeability. The porosity of SCC gets reduced and increases the strength of SCC mixes (Mehrinejad Khotbehsara et al., 2017).

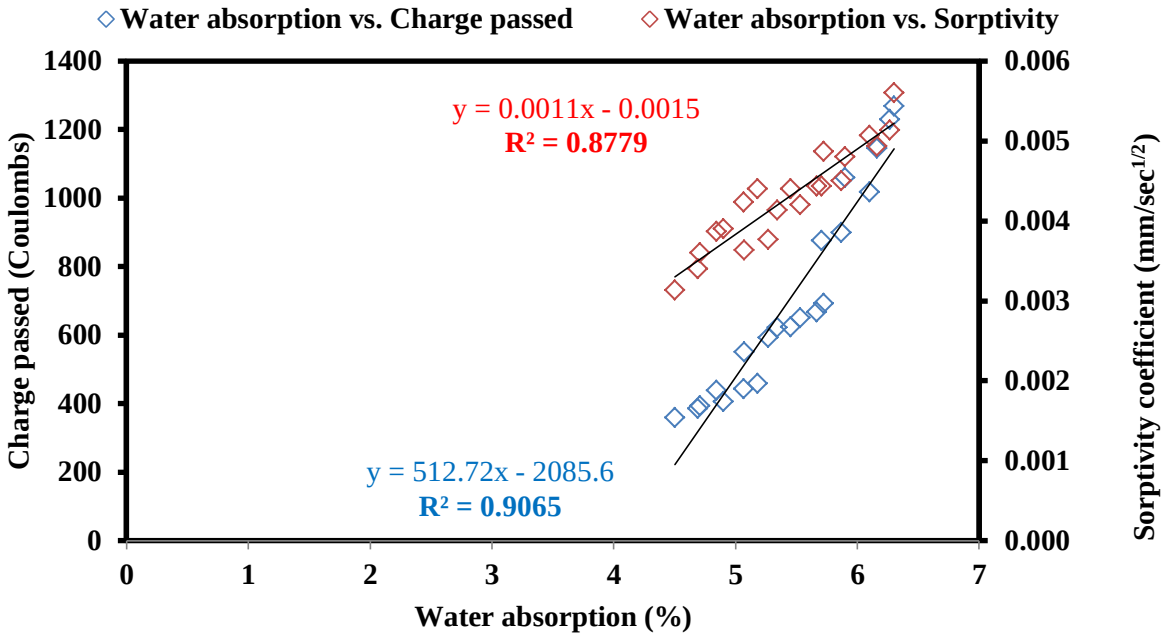

Fig. 4.59: Correlation of Water Absorption of SCC with Charge Passed and Sorptivity Coefficient

4.5.3 Statistical Significance

Method of Analysis of variance (ANOVA) was determined to study the statistical significance of the above reported experimental investigation. The influence of varying percentages of copper slag on the strength and durability properties of SCC mixes at different curing ages was studied. The mechanical properties included the compressive strength and splitting tensile strength and the durability properties included water absorption, sorptivity and rapid chloride permeability test.

4.5.3.1 Compressive Strength

Mean values of compressive strength reported from experimental data were considered. ANOVA test was performed at 0.05 level of significance. In the analysis, the compressive strength of SCC incorporating various percentages of copper slag from 0 to 60% was assigned as the independent variable. At the same time, the factor of curing age (7, 28, 90 and 365 days) was determined as the dependent variable. If the p-value was

less than or equal to 0.05, then the results were reported as statistically significant. The compressive strength of SCC mixes was found to be statistically significant with a p-value less than 0.05 at 28 and 90 curing days. When the ANOVA test was applied for 7 days and 365 days compressive strength, it was found out to be insignificant (p-value >0.05) as given in Table 4.8. Further, at 28 days and 90 days curing age, multiple comparison test was applied to check the significance between various percentages of SCC mixes using Post hoc Tukey test. The results of multiple comparison test are given in Appendix A. It was inferred that the compressive strength of SCC mix incorporating 0% and 20% copper slag were statistically significant at 28 days curing age. Also, the compressive strength of SCC mix with 20% copper slag was found to be statistically significant with SCC mix incorporating 50% and 60% copper slag at 28 days curing.

Table 4.8: Result of Analysis of Variance of SCC Based on Strength Properties

Curing Age (Days)	Compressive Strength		Splitting Tensile Strength	
	F	Significance (p-value)	F	Significance (p-value)
7	2.191	.106	5.037	.006*
28	4.725	.008*	7.044	.001*
90	3.104	.038*	5.545	.004*
365	1.593	.221	7.024	.001*

F- ANOVA value; *p value < 0.05 (significant)

4.5.3.2 Splitting Tensile Strength

Mean values of splitting tensile strength reported from experimental data were considered. ANOVA test was performed at 0.05 level of significance. In the analysis,

splitting tensile strength of SCC incorporating various percentages of copper slag from 0 to 60% was assigned as the independent variable. At the same time, the factor of curing age (7, 28, 90 and 365 days) was determined as the dependent variable. The splitting tensile strength of SCC mixes was found to be highly statistically significant with a p-value less than 0.05 at 7, 28, 90 and 365 curing days as given in Table 4.8. Further, a multiple comparison test was applied to check the significance between various percentages of SCC mixes using Post hoc Tukey test (Appendix B). It was inferred that the splitting tensile strength of SCC mix with 0% copper slag was found to be statistically significant with SCC mix incorporating 50% and 60% copper slag at 7 days curing. Also, SCC mix with 10% copper slag was statistically significant with the mix with 50% copper slag at 7 days. At 28 and 90 curing days, the splitting tensile strength of SCC mix without copper slag was found to be statistically significant with SCC mix incorporating 30, 40, 50 and 60% copper slag. At 365 days, the splitting tensile strength of SCC mix with 0% copper slag was found to be statistically significant with the values of SCC mix with 20, 30, 40, 50 and 60% copper slag.

4.5.3.3 Water Absorption

ANOVA test was performed at 0.05 level of significance based on the mean values of water absorption. In the analysis, values of water absorption of SCC mixes incorporating various percentages of copper slag from 0 to 60% were assigned as the independent variable. In contrast, the factor of curing age (28, 90 and 365 days) was determined as the dependent variable. The water absorption values of SCC mixes were found to be statistically significant, with a p-value less than 0.05 at 365 curing days as given in Table 4.9. Further, a multiple comparison test was applied to check the significance between various percentages of SCC mixes using Post hoc Tukey test (Appendix C). It was inferred that the water absorption values of SCC mix with 0% copper slag were found to be statistically significant with SCC mix incorporating 20% copper slag at 365 days curing. Also, SCC mix with 20% copper slag was found to be statistically significant with the mix with 60% copper slag at 365 days.

Table 4.9: Result of Analysis of Variance of SCC Based on Durability Properties

Curing Age (Days)	Water Absorption		Sorptivity		Rapid Chloride Permeability	
	F	Significance (p-value)	F	Significance (p-value)	F	Significance (p-value)
28	2.200	.105	-	-	109.831	.000*
90	1.417	.276	-	-	11.691	.000*
365	4.002	.015*	5.945	.003*	8.829	.000*

F- ANOVA value; *p value < 0.05 (significant)

4.5.3.4 Sorptivity

ANOVA test was performed at 0.05 level of significance based on the mean values of sorptivity. In the analysis, sorptivity values of SCC mixes incorporating various percentages of copper slag from 0 to 60% were assigned as the independent variable. In comparison, the factor of curing age (28, 90 and 365 days) was determined as the dependent variable. If the p-value was less than or equal to 0.05, then the results were reported as statistically significant. As the sorptivity coefficient values were very small, the results of ANOVA were not that much noteworthy. The sorptivity values of SCC mixes were found to be statistically significant, with a p-value less than 0.05 at 365 curing days as given in Table 4.9. Further, a multiple comparison test was applied to check the significance between various percentages of SCC mixes using Post hoc Tukey test (Appendix D). It was inferred that the sorptivity values of SCC mix with 0% copper slag were found to be statistically significant with SCC mix incorporating 20% and 30% copper slag at 365 days. Also, sorptivity values of SCC mix with 20% copper slag was found to be statistically significant with the mix incorporating 60% copper slag at 365 days.

4.5.3.5 Rapid Chloride Permeability

ANOVA test was performed to test the statistical significance of the durability property- rapid chloride ion permeability of SCC mixes. In the analysis, charge passed in SCC mixes incorporating various percentages of copper slag from 0 to 60% were assigned as the independent variable. In comparison, the factor of curing age (28, 90 and 365 days) was determined as the dependent variable. If the p-value was less than or equal to 0.05, then the results were reported as statistically significant. The chloride ion permeability values of SCC mixes were found to be highly statistically significant with a p-value less than 0.05 at 28, 90 and 365 curing days as given in Table 4.9.

Further, a multiple comparison test was applied to check the significance between various percentages of SCC mixes using Post hoc Tukey test (Appendix E). It was inferred that the charge passed in SCC mix with 0% copper slag was found to be statistically significant with SCC mix incorporating 20%, 30% and 40% copper slag at 365 days. Also, chloride permeability values of SCC mix with 10% copper slag was found to be statistically significant with the mix incorporating 20% copper slag at 365 days. The chloride ion permeability values of SCC mix with 20% copper slag was found to be statistically significant with the mix incorporating 60% copper slag at 365 days.

The results of statistical analysis were then evaluated and compared with the research findings of others. Statistical analysis was conducted to test the significance of the compressive strength results with factors like cement type; water to cement ratio and level of copper slag in concrete mixes incorporating copper slag as a fine aggregate replacement (Mavroulidou, 2017). ANOVA test was performed in addition to the Kruskal-Wallis non-parametric analysis. The ANOVA results indicated that water to cement ratio is the most statistically significant factor with p value= 2.493×10^{-6} and then comes the cement type with p value= 1.139×10^{-4}. In contrast to this, copper slag was found to have no statistically significant value with p-value =0.208. Moreover, no statistical significance was found among- cement type-w/c ratio, copper slag-w/c ratio and cement type-copper slag interactions. The non-parametric analysis inferred similar results (Mavroulidou, 2017). A general linear model of analysis of variance was studied

to test the statistical significance of compressive strength and drying shrinkage of SCC incorporating mineral admixtures (fly ash, silica fumes, ground granulated blast furnace slag and metakaolin) (Güneyisi et al., 2010). The compressive strength and drying shrinkage were considered to be dependent variables while types of admixtures were considered as factors. Statistical analysis was conducted in addition to the contribution effect of each kind of admixture on compressive strength and drying shrinkage was considered. The p-value of each admixture was less than 0.05 for drying shrinkage of SCC. Incorporation of silica fumes proved to be the most significant admixture on the drying shrinkage of SCC. However, the use of ground granulated blast furnace slag produced insignificant results on the compressive strength of SCC mixes. A general linear model of analysis was conducted to investigate the statistical significance of durability properties like water absorption, sorptivity and RCPT on SCC mixes (Gesolu and Güneyisi, 2011). The Minitab software was used to analyse the experimental results. The measured SCC properties like water absorption, sorptivity and RCPT were considered as dependent variables. In contrast, different systems like portland cement (PC) with crumb rubber, PC with fly ash and PC with fly ash and crumb rubber were considered as independent variables. The p-values of all systems were less than 0.05 giving significant statistical results. Also, the contribution of each of the modes on the measured test results was reported. The system PC-FA showed the lowest influence on the measured properties of SCC. A statistically significant effect of fibre volume and hybridization on the mechanical properties of high-strength SCC was reported (Hari and Mini, 2019).

CHAPTER-5
CONCLUSIONS

In the present research work, the effect of copper slag on the fresh, strength and durability properties of SCC mixes has been studied. The properties included the slump flow, T_{500} slump flow, V-funnel, L-box, U-box, segregation resistance, compressive strength, splitting tensile strength, water absorption, sorptivity, rapid chloride permeability, drying shrinkage and sulfate resistance. The microstructure and XRD analysis of SCC mixes have also been carried out.

Test results indicated that copper slag is a sustainable material which could be employed as fine aggregate in the production of SCC. Copper slag is a non-hazardous material. For the same water-cement ratio and a fixed quantity of superplasticizer, SCC mixes could be designed, resulting in similar or increased strength results. The incorporation of copper slag in SCC mixes improved its workability, strength and durability. This research will be valuable for the researchers working in areas pertaining to SCC as well as for the copper industry. Following conclusion can be drawn based on the research conducted.

5.1 FRESH PROPERTIES OF SCC

5.1.1 Slump Flow and T_{500} Slump Flow

The slump flow value of SCC mixes increased on the addition of copper slag from 0 to 60% at fixed water to cement ratio. Slump flow diameters in the range of 685-750 mm were observed for SCC mixes. The increase in slump flow owed to the smooth, glassy texture and low water absorption characteristic of slag grains that increased the flowability of SCC mixes. The time taken by SCC mixes to reach 500 mm diameter mark decreased as there was an increase in copper slag content. This could be attributed to the lack of cohesion of the components of SCC and low water absorption characteristic of copper slag grains.

5.1.2 V-Funnel

V-funnel test results of SCC mixes decreased with the increasing content of copper slag. V-funnel time decreased from 7.55 to 5.01 seconds as the amount of copper slag increased from 0 to 60%. Due to the smooth and glassy surface of copper grains, the viscosity reduced and hence the time taken to empty the funnel was less with the increasing copper slag content.

5.1.3 L-Box

L-box ratio ranged from 0.82 to 0.98 for SCC mixes containing 0 to 60% copper slag. The results indicated that SCC mixes have been prepared with sufficient passing ability and can be used effectively.

5.1.4 U-Box

The value of U-box ranged from 15-25 mm for SCC mixes incorporating up to 60% copper slag. The filling height of mix with 0% copper slag was 20 mm; this difference was somewhat decreased as copper slag augmented up to 40%. However, with further increase in copper slag percentage, signs of bleeding and segregation were observed due to which the filling height increased. Due to excess water being present in the mix that arises, the copper slag particles along with aggregates settle down due to their heavy weight; thereby increasing the filling height.

5.1.5 Sieve Segregation Resistance

SCC mixes were found to be stable with a segregation ratio of less than 15%. From the results, it was inferred that there was an improvement in workability values on the addition of copper slag. All the mixes were in good accordance with the classifications prescribed in the European code. The smooth, glassy texture and the low water absorption characteristic of copper slag grains led to improved fresh properties of SCC mixes. Copper slag was effective in enhancing the filling ability, viscosity, passing ability and segregation resistance of SCC mixes.

5.2 STRENGTH PROPERTIES OF SCC

5.2.1 Compressive Strength

The compressive strength of SCC mixes incorporating up to 60% copper slag showed almost similar/higher results in comparison with a concrete mix containing 100% sand.

The 28 days compressive strength of SCC mix incorporating 10, 20, 30, 40 and 50% copper slag achieved 6.97, 8.19, 4.20, 0.97 and 0.04% higher compressive strength as compared to control SCC mix (35.63 MPa). An insignificant decrease of 0.09% was observed in SCC mix with 60% copper slag in comparison to control SCC mix at 28 days. A similar trend was followed for SCC mixes incorporating copper slag up to 60% at 90 and 365 days.

Also, the compressive strength of SCC mixes with or without copper slag augmented with an increase in curing age.

5.2.2 Splitting Tensile Strength

Splitting tensile strength of SCC mixes increased with the increase of copper slag content from 0 to 60%. Also, the strength was found to increase with the increase in curing age.

At 28, 90 and 365 days, splitting tensile strength of SCC mixes with copper slag (0 to 60%) increased from 2.56 to 3.43, 3.65 to 4.23, 3.86 to 4.47 MPa as compared to 2.13, 3.11 and 3.42 MPa, respectively, of control mix without slag.

The strength enhancement was due to the angular edges of copper slag grains that led to the improvement in the cohesion of the concrete matrix.

5.3 DURABILITY PROPERTIES OF SCC

5.3.1 Water Absorption

As the percentage of copper slag increased, the value of water absorption and permeable voids decreased in all SCC mixes and at all curing ages. At 28 days curing age, water absorption of control SCC mix was 6.30%. The results reduced by about 3.17, 9.40, 6.88, 6.35, 2.17 and 0.53%, respectively, for SCC mix incorporating 10, 20, 30, 40, 50 and

60% copper slag. At 90 days, the water absorption of control SCC mix was 5.72%. The results reduced about 4.72, 11.42, 7.98, 6.63, 3.32 and 0.99%, respectively, for SCC mix incorporating 10, 20, 30, 40, 50 and 60% copper slag. At 365 days, water absorption of control SCC mix was 5.18%. The results reduced about 6.52, 13.15, 9.48, 9.15, 5.43 and 2.21%, respectively, for SCC mix incorporating 10, 20, 30, 40, 50 and 60% copper slag.

5.3.2 Sorptivity

A decrease in the sorptivity values was studied in SCC with the addition of copper slag. The combined effect of copper slag and fly ash was successful in lowering down the sorptivity values of SCC mixes. With the increase in curing age, a significant reduction in the sorptivity values of SCC mixes was observed.

Sorptivity value of control SCC mix at 28 days curing age was 0.0056 mm/sec$^{1/2}$. The value reduced by about 9.52, 20.83, 19.64, 14.29, 11.90 and 8.33% for SCC mix incorporating 10, 20, 30, 40, 50 and 60% copper slag SCC mix at 28 days curing age. The value of sorptivity was 0.0049 mm/sec$^{1/2}$ and 0.0044 mm/sec$^{1/2}$ in control SCC mix at 90 and 365 days curing age. The value reduced by about 9.59, 25.34, 22.60, 15.07, 13.70 and 8.90% for SCC mix incorporating 10, 20, 30, 40, 50 and 60% copper slag SCC mix at 90 days curing age. Also, the sorptivity value reduced by about 12.12, 28.79, 22.73, 18.18, 11.36 and 3.79% for SCC mix incorporating 10, 20, 30, 40, 50 and 60% copper slag SCC mix at 365 days curing age.

5.3.3 Rapid Chloride Permeability

SCC mixes incorporating copper slag showed improved resistance to chloride ion permeability. With the incorporation of copper slag up to 60% in SCC mixes, reduction in chloride ion permeability was obtained. All SCC mixes were ranged under the category of very low to low chloride ion permeability at 28 days curing (876-1269 coulombs). SCC mixes were categorized under ‘very low’ permeability at both 90 days (550-692 coulombs) and 365 days (359-459 coulombs). The influence of slag on chloride ion permeability was much significant at later ages of curing.

With the addition of copper slag in SCC mixes, a reduction in water absorption, permeable voids, sorptivity and chloride ion permeability was concluded. This may be attributed to the combined effect of fly ash and copper slag leading to enhancement of the pore structure of the SCC matrix. This further resulted in the transformation of large permeable pores into smaller and less permeable pores. With the increase in age of concrete, the reaction concerning fly ash and calcium hydroxide became much more significant, giving rise to a denser concrete. The decrease in permeability values of SCC mixes incorporating copper slag indicated a denser microstructure with reduced voids. With the low penetration of chloride ions in concrete, long term durability of concrete structures could be achieved.

5.3.4 Drying Shrinkage

The drying shrinkage of SCC mixes decreased on the addition of copper slag up to 60% at all curing ages. The least value of shrinkage was obtained for SCC mix incorporating 20% copper slag at all ages. The value of 28-day drying shrinkage of control SCC was 230 micro strain. The 28-day drying shrinkage of SCC made with 10, 20, 30, 40, 50 and 60% copper slag was 22.61, 32.61, 17.39, 13.04, 8.69 and 2.17% lower than that of control SCC mix. At 448 days, reduction in shrinkage strains were 10.19, 16.35, 7.69, 4.23, 1.92 and 0.96% for the same compositions of SCC mixes. This may be attributed to the loss of physically absorbed water from Calcium Silicate Hydrate (C–S–H), resulting in a shrinkage strain. The mutual effect of fly ash and copper slag was effective in lowering the shrinkage strains of copper slag SCC mixes. Long term drying shrinkage became stable for SCC mixes after 224 days. Shrinkage strains were comparable at early ages up to 28 days; while clear distinction was observed after 28 days of drying period.

5.3.5 Sulfate Resistance

The compressive strength of SCC mixes incorporating up to 60% copper slag showed almost similar/higher results in comparison with a concrete mix containing 100% sand after immersion in a sodium sulfate solution. The 28 days compressive strength of SCC mix incorporating 10, 20, 30, 40 and 50% copper slag achieved 6.15, 7.08, 4.62, 3.93 and 1.54% higher compressive strength as compared to control SCC mix (32.50 MPa). An

insignificant decrease of 0.14% was observed in SCC mix with 60% copper slag in comparison to control SCC mix at 28 days.

With respect to immersion in sulfate solution with curing ages, a marginal increase of about 11.05% (average) and 4.38% (average) in compressive strength of SCC mixes (0 to 60%) was established from 28 to 90 days and from 28 to 365 days, respectively. Peaks of Ca and Si under EDS analysis revealed the development of CSH layers leading to gain in compressive strength. No major phase change under XRD was observed for SCC mixes under normal curing as well as under sulfate attack at 28, 90 and 365 days.

The compressive strength of SCC exposed to sulfate showed a reduction when compared to the strength values of SCC mixes under normal curing at all ages. The average decrease in compressive strength of SCC mixes (0-60%) exposed to sulfate was around 19.07, 18.07 and 24.6% in comparison to respective SCC mixes (0-60%) under normal curing conditions at 28, 90 and 365 days.

Minute expansions (less than 0.02%) were observed in SCC mixes under sulfate environment for up to 365 days. SCC mixes containing (10-60%) copper slag showed lower expansions in comparison with control SCC mix. With respect to immersion in sulfate solution, an insignificant increase in the value of expansion (%) was observed in SCC prisms incorporating 0 to 60% copper slag exposed to sulfate solution after 90 days.

The gain in mass was less than 0.3% for mixes up to 365 days. SCC mix with 0% copper slag gave the lowest value of mass gain for up to 365 days; while the highest increase in mass was recorded for a mix with 60% slag.

Even after one year of sulfate exposure to SCC mixes, no major catastrophic damage was visible. Copper slag was successful in improving the overall sulfate resistance of SCC mixes. Depending on the strength requirements of the structures, SCC mixes could be designed using copper slag in selective percentages, especially in areas exposed to aggressive environments involving sulfate attack.

5.4 MICRO-STRUCTURAL PROPERTIES OF SCC

5.4.1 Scanning Electron Microscopy and Energy Dispersive Spectroscopy

The microstructure of SCC mixes improved and got denser with the addition of copper slag in SCC at all ages of curing. Reduction of voids and improved compressive strength of SCC gives a good effect to its durability properties. The formation of CSH layers in SCC can be closely related to its improved compressive strength and reduced permeability.

5.4.2 X-Ray Diffraction

SCC mixes showed a crystalline behaviour up to 365 days. No major phase change was indicated while increasing the percentages of copper slag in SCC. Major Peak of Quartz having hexagonal crystal structure was formed in SCC mixes up to 365 days. Other hydrated phases formed were that of Calcium Hydroxide, Anorthite, Aluminium Silicate Hydrate and Calcium Iron oxide at 90 days. In addition to these, traces of Gismondine, Calcium Silicide and Hedenbergite were formed in SCC mixes at 365 days.

5.5 RECOMMENDATIONS FOR FUTURE RESEARCH

The proposed research work involving the use of copper slag in self-compacting concrete can be further extended as:

1. Study of durability properties of SCC incorporating copper slag like alkali-silica reaction, resistance to freezing and thawing, accelerated corrosion, carbonation and resistance to acid attack.

2. Performance of SCC incorporating copper slag at structural level which includes its load-carrying capacity, failure mechanism and ductility.

REFERENCES

Afshinnia, K., Rangaraju, P.R., 2016. Impact of combined use of ground glass powder and crushed glass aggregate on selected properties of Portland cement concrete. Constr. Build. Mater. 117, 263–272. https://doi.org/10.1016/j.conbuildmat.2016.04.072

Afshoon, I., Sharifi, Y., 2017. Use of copper slag microparticles in self-consolidating concrete. ACI Mater. J. 114, 691.

Afshoon, I., Sharifi, Y., 2014. The IES Journal Part A : Civil & Structural Engineering Ground copper slag as a supplementary cementing material and its influence on the fresh properties of self-consolidating concrete. IES J. Part A Civ. Struct. Eng. 7, 37–41. https://doi.org/10.1080/19373260.2014.945622

Aggarwal, Y., Siddique, R., 2014. Microstructure and properties of concrete using bottom ash and waste foundry sand as partial replacement of fine aggregates. Constr. Build. Mater. 54, 210–223. https://doi.org/10.1016/j.conbuildmat.2013.12.051

Ahmad, S., Umar, A., 2018. Rheological and mechanical properties of self-compacting concrete with glass and polyvinyl alcohol fibres. J. Build. Eng. 17, 65–74. https://doi.org/10.1016/j.jobe.2018.02.002

Al-Bawi, R.K., Kadhim, I.T., Al-Kerttani, O., 2017. Strengths and Failure Characteristics of Self-Compacting Concrete Containing Recycled Waste Glass Aggregate. Adv. Mater. Sci. Eng. 2017. https://doi.org/10.1155/2017/6829510

Al-Jabri, K.S., Al-Saidy, A.H., Taha, R., 2011. Effect of copper slag as a fine aggregate on the properties of cement mortars and concrete. Constr. Build. Mater. 25, 933–938. https://doi.org/10.1016/j.conbuildmat.2010.06.090

Al-Jabri, K.S., Hisada, M., Al-Saidy, A.H., Al-Oraimi, S.K., 2009. Performance of high strength concrete made with copper slag as a fine aggregate. Constr. Build. Mater. 23, 2132–2140. https://doi.org/10.1016/j.conbuildmat.2008.12.013

Al-Swaidani, A.M., 2019. Use of micro and nano volcanic scoria in the concrete binder: Study of compressive strength, porosity and sulfate resistance. Case Stud. Constr. Mater. 11, e00294.

Ali, E.E., Al-Tersawy, S.H., 2012. Recycled glass as a partial replacement for fine aggregate in self compacting concrete. Constr. Build. Mater. 35, 785–791. https://doi.org/10.1016/j.conbuildmat.2012.04.117

Ambily, P.S., Umarani, C., Ravisankar, K., Prem, P.R., Bharatkumar, B.H., Iyer, N.R., 2015. Studies on ultra high performance concrete incorporating copper slag as fine aggregate. Constr. Build. Mater. 77, 233–240. https://doi.org/10.1016/j.conbuildmat.2014.12.092

Andrade, L.B., Rocha, J.C., Cheriaf, M., 2009. Influence of coal bottom ash as fine aggregate on fresh properties of concrete. Constr. Build. Mater. 23, 609–614. https://doi.org/10.1016/j.conbuildmat.2008.05.003

Andrade, L.B., Rocha, J.C., Cheriaf, M., 2007. Aspects of moisture kinetics of coal bottom ash in concrete. Cem. Concr. Res. 37, 231–241. https://doi.org/10.1016/j.cemconres.2006.11.001

Arabi, N., Meftah, H., Amara, H., Kebaïli, O., Berredjem, L., 2019. Valorization of recycled materials in development of self-compacting concrete: Mixing recycled concrete aggregates – Windshield waste glass aggregates. Constr. Build. Mater. 209, 364–376. https://doi.org/10.1016/j.conbuildmat.2019.03.024

Aslani, F., Khan, M., 2019. Properties of High-Performance Self-Compacting Rubberized Concrete Exposed to High Temperatures. J. Mater. Civ. Eng. 31, 1–15. https://doi.org/10.1061/(ASCE)MT.1943-5533.0002672

Aslani, F., Ma, G., Yim Wan, D.L., Tran Le, V.X., 2018. Experimental investigation into rubber granules and their effects on the fresh and hardened properties of self-compacting concrete. J. Clean. Prod. 172, 1835–1847. https://doi.org/10.1016/j.jclepro.2017.12.003

ASTM C 1012, 2010. Standard Test Method for Length Change of Hydraulic-Cement Mortars Exposed to a Sulfate Solution. ASTM International, West Conshohocken, PA.

ASTM C 1202, 2010. Standard test method for electrical indication of concrete's ability to resist chloride ion penetration. ASTM International, West Conshohocken, PA.

ASTM C 157, 2008. Standard Test Method for Length Change of Hardened Hydraulic-Cement Mortar and Concrete, ASTM International, West Conshohocken, PA.

ASTM C 1585, 2004. Standard Test Method for Measurement of Rate of Absorption of Water by Hydraulic-Cement Concretes, ASTM International. West Conshohocken, PA.

ASTM C 618, 2005. Standard Specification for Coal Fly Ash and Raw or Calcined Natural Pozzolan for Use in Concrete. ASTM International, West Conshohocken, PA.

ASTM C 642, 2013. Standard test method for density, absorption, and voids in hardened concrete, ASTM International, West Conshohocken, PA.

Ayano, T., Sakata, K., 2000. Durability of concrete with copper slag fine aggregate. Spec. Publ. 192, 141–158.

Azevedo, F., Pacheco-Torgal, F., Jesus, C., Barroso De Aguiar, J.L., Camões, A.F., 2012. Properties and durability of HPC with tyre rubber wastes. Constr. Build. Mater. 34, 186–191. https://doi.org/10.1016/j.conbuildmat.2012.02.062

Bai, Y., Darcy, F., Basheer, P.A.M., 2005. Strength and drying shrinkage properties of concrete containing furnace bottom ash as fine aggregate. Constr. Build. Mater. 19, 691–697. https://doi.org/10.1016/j.conbuildmat.2005.02.021

Bartos, P.J., Sonebi, M., Tamimi, A.K. (Eds.)., 2002. Report 24: workability and rheology of fresh concrete: compendium of tests–report of RILEM Technical Committee TC 145-WSM. RILEM publications.

Basar, H.M., Deveci Aksoy, N., 2012. The effect of waste foundry sand (WFS) as partial replacement of sand on the mechanical, leaching and micro-structural characteristics of ready-mixed concrete. Constr. Build. Mater. 35, 508–515. https://doi.org/10.1016/j.conbuildmat.2012.04.078

Batayneh, M.K., Marie, I., Asi, I., 2008. Promoting the use of crumb rubber concrete in developing countries. Waste Manag. 28, 2171–2176. https://doi.org/10.1016/j.wasman.2007.09.035

Behera, M., Minocha, A.K., Bhattacharyya, S.K., 2019. Flow behavior, microstructure, strength and shrinkage properties of self-compacting concrete incorporating recycled fine aggregate. Constr. Build. Mater. 228, 116819.

Bhat, S.T., Lovell, C.W., 1996. Design of flowable fill: Waste foundry sand as a fine aggregate. Transp. Res. Rec. 70–78. https://doi.org/10.3141/1546-08

Bignozzi, M.C., Sandrolini, F., 2006. Tyre rubber waste recycling in self-compacting concrete. Cem. Concr. Res. 36, 735–739. https://doi.org/10.1016/j.cemconres.2005.12.011

BIS: 383, 2016. Specification for coarse and fine aggreagtes from natural sources for concrete. Indian Standard. Bureau of Indian Standards, New Delhi, India.

BIS: 456, 2000. Plain and Reinforced Concrete, Indian Standard. Bureau of Indian Standards, New Delhi, India. https://doi.org/624.1834 TAY

BIS: 516, 1959. Method of Tests for Strength of Concrete, Indian Standard. Bureau of Indian Standards, New Delhi, India.

BIS: 5816, 1999. Splitting tensile strength of concrete, Indian Standard. Bureau of Indian Standards, New Delhi, India.

BIS: 8112, 2013. Ordinary portland cement, 43 grade-specification. Bureau of Indian Standards, New Delhi, India.

Boakye, A.D.M., Uzoegbo, H.C., 2014. Assessment of concrete pulverised with copper

slag as partial replacement of cement Assessment of concrete with pulverized copper slag as partial replacement of cement. J. Concr. Soc. South. Africa 139, 14–17.

Brindha, D., Nagan, S., 2011. Durability studies on copper slag admixed concrete. Asian J. Civ. Eng. 12, 563–578.

Cachim, P., Velosa, A.L., Rocha, F., 2010. Effect of Portuguese metakaolin on hydraulic lime concrete using different curing conditions. Constr. Build. Mater. 24, 71–78.

Canpolat, F., Yilmaz, K., Köse, M.M., Sümer, M., Yurdusev, M.A., 2004. Use of zeolite, coal bottom ash and fly ash as replacement materials in cement production. Cem. Concr. Res. 34, 731–735. https://doi.org/10.1016/S0008-8846(03)00063-2

Cheriaf, M., Rocha, J.C., Péra, J., 1999. Pozzolanic properties of pulverized coal combustion bottom ash. Cem. Concr. Res. https://doi.org/10.1016/S0008-8846(99)00098-8

Contrafatto, L., Danzuso, C.L., Gazzo, S., Greco, L., 2020. Physical, mechanical and thermal properties of lightweight insulating mortar with recycled Etna volcanic aggregates. Constr. Build. Mater. 240, 117917.

Dadsetan, S., Bai, J., 2017. Mechanical and microstructural properties of self-compacting concrete blended with metakaolin, ground granulated blast-furnace slag and fly ash. Constr. Build. Mater. 146, 658–667.

de Matos, P.R., Pilar, R., Bromerchenkel, L.H., Schankoski, R.A., Gleize, P.J.P., de Brito, J., 2020. Self-compacting mortars produced with fine fraction of calcined waste foundry sand (WFS) as alternative filler: Fresh-state, hydration and hardened-state properties. J. Clean. Prod. 252, 119871. https://doi.org/10.1016/j.jclepro.2019.119871

Dhir, R.K., Brito, J. de, Mangabhai, R., Lye, C.Q., 2016a. Copper Slag in Cement Manufacture and as Cementitious Material, in: Sustainable Construction Materials: Copper Slag. Woodhead Publishing, pp. 165–209. https://doi.org/10.1016/b978-0-

08-100986-4.00005-5

Dhir, R.K., Brito, J. de, Mangabhai, R., Lye, C.Q., 2016b. Use of Copper Slag as Concrete Sand, Sustainable Construction Materials: Copper Slag. https://doi.org/10.1016/b978-0-08-100986-4.00004-3

Dhir, R.K., Limbachiya, M.C., Paine, K.A., 2001. Recycling and Reuse of Used Tyres:, in: Proceedings of the International Symposium Organized by the Concrete Technology Unit, University of Dundee. Thomas Telford.

Domone, Jin, J., Chai, H., 1999. Optimum mix proportioning of self-compacting concrete, in: Proceedings of International Conference on Innovation in Concrete Structures: Design and Construction, Dundee. pp. 277–285.

dos Anjos, M.A.G., Sales, A.T.C., Andrade, N., 2017. Blasted copper slag as fine aggregate in Portland cement concrete. J. Environ. Manage. 196, 607–613. https://doi.org/10.1016/j.jenvman.2017.03.032

EFNARC, 2005. The European Guidelines for Self-Compacting Concrete: Specification, Production and Use, The European Guidelines for Self Compacting Concrete. https://doi.org/0 9539733 4 4

EFNARC, 2002. Specification and Guidelines for Self-Compacting Concrete. https://doi.org/0 9539733 4 4

Fathi, H., Lameie, T., Maleki, M., Yazdani, R., 2017. Simultaneous effects of fiber and glass on the mechanical properties of self-compacting concrete. Constr. Build. Mater. 133, 443–449. https://doi.org/10.1016/j.conbuildmat.2016.12.097

Gesoğlu, M., Güneyisi, E., 2011. Permeability properties of self-compacting rubberized concretes. Constr. Build. Mater. 25, 3319–3326. https://doi.org/10.1016/j.conbuildmat.2011.03.021

Gesoglu, M., Guneyisi, E., Ozbay, E., 2009. Properties of SCCs made with binary, ternary, and quaternary cementitious blends of fly ash, blast furnace slag, and silica fume. Constr. Build. Mater. 23, 1847-1854.

Glasser, F.P., Marchand, J., Samson., E., 2008. Durability of concrete—degradation phenomena involving detrimental chemical reactions. Cem. Concr. Res. 38, 226–246.

Gorai, B., Jana, R.K., Premchand, 2003. Characteristics and utilisation of copper slag - A review. Resour. Conserv. Recycl. 39, 299–313. https://doi.org/10.1016/S0921-3449(02)00171-4

Guney, Y., Sari, Y.D., Yalcin, M., Tuncan, A., Donmez, S., 2010. Re-usage of waste foundry sand in high-strength concrete. Waste Manag. 30, 1705–1713. https://doi.org/10.1016/j.wasman.2010.02.018

Güneyisi, E., Gesolu, M., Özbay, E., 2010. Strength and drying shrinkage properties of self-compacting concretes incorporating multi-system blended mineral admixtures. Constr. Build. Mater. 24, 1878–1887. https://doi.org/10.1016/j.conbuildmat.2010.04.015

Guo, S., Dai, Q., Si, R., Sun, X., Lu, C., 2017. Evaluation of properties and performance of rubber-modified concrete for recycling of waste scrap tire. J. Clean. Prod. 148, 681–689. https://doi.org/10.1016/j.jclepro.2017.02.046

Gurumoorthy, N., Arunachalam, K., 2016. Micro and mechanical behaviour of Treated Used Foundry Sand concrete. Constr. Build. Mater. 123, 184–190. https://doi.org/10.1016/j.conbuildmat.2016.06.143

Hari, R., Mini, K.M., 2019. Mechanical and durability properties of sisal-Nylon 6 hybrid fibre reinforced high strength SCC. Constr. Build. Mater. 204, 479–491. https://doi.org/10.1016/j.conbuildmat.2019.01.217

Hashemi, S.S.G., Mahmud, H. Bin, Ghuan, T.C., Chin, A.B., Kuenzel, C., Ranjbar, N., 2019. Safe disposal of coal bottom ash by solidification and stabilization techniques. Constr. Build. Mater. 197, 705–715. https://doi.org/10.1016/j.conbuildmat.2018.11.123

Hendi, A., Mostofinejad, D., Sedaghatdoost, A., Zohrabi, M., Naeimi, N., Tavakolinia,

A., 2019. Mix design of the green self-consolidating concrete: Incorporating the waste glass powder. Constr. Build. Mater. 199, 369–384. https://doi.org/10.1016/j.conbuildmat.2018.12.020

Hilal, N.N., 2017. Hardened properties of self-compacting concrete with different crumb rubber size and content. Int. J. Sustain. Built Environ. 6, 191–206. https://doi.org/10.1016/j.ijsbe.2017.03.001

Hwang, C.-L., Laiw, J.-C., 1989. Properties of Concrete Using Copper Slag as a Substitute for Fine Aggregate. Spec. Publ. 114. https://doi.org/10.14359/1986

Ibrahim, M.H.W., Hamzah, A.F., Jamaluddin, N., Ramadhansyah, P.J., Fadzil, A.M., 2015. Split Tensile Strength on Self-compacting Concrete Containing Coal Bottom Ash. Procedia - Soc. Behav. Sci. 195, 2280–2289. https://doi.org/10.1016/j.sbspro.2015.06.317

Indian Minerals Yearbook, 2019. Indian Minerals Yearbook 2018 (Part- III : Mineral Reviews) MINISTRY OF MINES INDIAN BUREAU OF MINES 2018.

International Copper Study Group, 2019. The World Copper Factbook 2016. Int. Copp. Study Gr. 63. https://doi.org/10.1007/s13398-014-0173-7.2

Ismail, M.K., Hassan, A.A.A., 2016. Use of metakaolin on enhancing the mechanical properties of self-consolidating concrete containing high percentages of crumb rubber. J. Clean. Prod. 125, 282–295. https://doi.org/10.1016/j.jclepro.2016.03.044

Jawahar, J.G., Sashidhar, C., Reddy, I.R., Peter, J.A., 2013. Micro and macrolevel properties of fly ash blended self compacting concrete. Mater. Des. 46, 696–705.

Kapoor, K., Singh, S.P., Singh, B., Singh, P., 2020. Effect of recycled aggregates on fresh and hardened properties of self compacting concrete. Mater. Today Proc.

Kavitha, O.R., Shanthi, V.M., Arulraj, G.P., Sivakumar, P., 2015. Fresh, micro-and macrolevel studies of metakaolin blended self-compacting concrete. Appl. Clay Sci. 114, 370–374.

Khanzadi, M., Behnood, A., 2009. Mechanical properties of high-strength concrete incorporating copper slag as coarse aggregate. Constr. Build. Mater. 23, 2183–2188. https://doi.org/10.1016/j.conbuildmat.2008.12.005

Kim, H.K., Jeon, J.H., Lee, H.K., 2012. Flow, water absorption, and mechanical characteristics of normal- and high-strength mortar incorporating fine bottom ash aggregates. Constr. Build. Mater. 26, 249–256. https://doi.org/10.1016/j.conbuildmat.2011.06.019

Kou, S.C., Poon, C.S., 2009. Properties of self-compacting concrete prepared with recycled glass aggregate. Cem. Concr. Compos. 31, 107–113. https://doi.org/10.1016/j.cemconcomp.2008.12.002

Li, N., Long, G., Ma, C., Fu, Q., Zeng, X., Ma, K., Xie, Y., Luo, B., 2019. Properties of self-compacting concrete (SCC) with recycled tire rubber aggregate: A comprehensive study. J. Clean. Prod. 236, 117707. https://doi.org/10.1016/j.jclepro.2019.117707

Ling, T.C., Poon, C.S., Kou, S.C., 2012. Influence of recycled glass content and curing conditions on the properties of self-compacting concrete after exposure to elevated temperatures. Cem. Concr. Compos. 34, 265–272. https://doi.org/10.1016/j.cemconcomp.2011.08.010

Liu, M., 2011. Incorporating ground glass in self-compacting concrete. Constr. Build. Mater. 25, 919–925. https://doi.org/10.1016/j.conbuildmat.2010.06.092

Lotfy, A., Hossain, K.M., Lachemi, M., 2016. Transport and Durability Properties of Self-Consolidating Concrete Using Three Types of Lightweight Aggregates. ACI Mater. J. 113, 679.

Lye, C.-Q., Koh, S.-K., Mangabhai, R., Dhir, R.K., 2015. Use of copper slag and washed copper slag as sand in concrete: a state-of-the-art review. Mag. Concr. Res. 67, 665–679. https://doi.org/10.1680/macr.14.00214

Madheswaran, C.K., Ambily, P.S., Dattatreya, J.K., Rajamane, N.P., 2014. Studies on use

of Copper Slag as Replacement Material for River Sand in Building Constructions. J. Inst. Eng. Ser. A 95, 169–177. https://doi.org/10.1007/s40030-014-0084-9

Makul, N., 2019. Combined use of untreated-waste rice husk ash and foundry sand waste in high-performance self-consolidating concrete. Results Mater. 1, 100014. https://doi.org/10.1016/j.rinma.2019.100014

Matos, A.M., Ramos, T., Nunes, S., Sousa-Coutinho, J., 2016. Durability enhancement of scc with waste glass powder. Mater. Res. 19, 67–74. https://doi.org/10.1590/1980-5373-MR-2015-0288

Mavroulidou, M., 2017. Mechanical Properties and Durability of Concrete with Water Cooled Copper Slag Aggregate. Waste and Biomass Valorization 8, 1841–1854. https://doi.org/10.1007/s12649-016-9819-3

Mehrinejad Khotbehsara, M., Mohseni, E., Ozbakkaloglu, T., Ranjbar, M.M., 2017. Durability characteristics of self-compacting concrete incorporating pumice and metakaolin. J. Mater. Civ. Eng. 29, 04017218.

Mehta, P.K., 1980. Durability of concrete in marine environment-A review. ACI Spec. Publ. 65, 1–20.

Mirhosseini, S.R., Fadaee, M., Tabatabaei, R., Fadaee, M.J., 2017. Mechanical properties of concrete with Sarcheshmeh mineral complex copper slag as a part of cementitious materials. Constr. Build. Mater. 134, 44–49. https://doi.org/10.1016/j.conbuildmat.2016.12.024

Mithun, B.M., Narasimhan, M.C., 2016. Performance of alkali activated slag concrete mixes incorporating copper slag as fine aggregate. J. Clean. Prod. 112, 837–844. https://doi.org/10.1016/j.jclepro.2015.06.026

Mohseni, E., Saadati, R., Kordbacheh, N., Parpinchi, Z.S., Tang, W., 2017. Engineering and microstructural assessment of fibre-reinforced self-compacting concrete containing recycled coarse aggregate. J. Clean. Prod. 168, 605–613.

Monshi, A., Asgarani, M.K., 1999. Producing portland cement from iron and steel slags

and limestone. Cem. Concr. Res. 29, 1373–1377. https://doi.org/10.1016/S0008-8846(99)00028-9

Murari, K., Siddique, R., Jain, K.K., 2015. Use of waste copper slag, a sustainable material. J. Mater. Cycles Waste Manag. 17, 13–26. https://doi.org/10.1007/s10163-014-0254-x

Naik, T.R., Singh, S.S., Ramme, B.W., 2001. Performance and leaching assessment of flowable slurry. J. Environ. Eng. 127, 359–368.

Najim, K.B., Hall, M.R., 2012. Mechanical and dynamic properties of self-compacting crumb rubber modified concrete. Constr. Build. Mater. 27, 521–530. https://doi.org/10.1016/j.conbuildmat.2011.07.013

Najimi, M., Sobhani, J., Pourkhorshidi, A.R., 2011. Durability of copper slag contained concrete exposed to sulfate attack. Constr. Build. Mater. 25, 1895–1905. https://doi.org/10.1016/j.conbuildmat.2010.11.067

Neville, A., 2004. The confused world of sulfate attack on concrete. Cem. Concr. Res. 34, 1275–1296.

Niewiadomski, P., Hoła, J., Ćwirzeń, A., 2018. Study on properties of self-compacting concrete modified with nanoparticles. Arch. Civ. Mech. Eng. 18, 877–886.

Nunes, S., Matos, A.M., Duarte, T., Figueiras, H., Sousa-Coutinho, J., 2013. Mixture design of self-compacting glass mortar. Cem. Concr. Compos. 43, 1–11. https://doi.org/10.1016/j.cemconcomp.2013.05.009

Obe, R.K.D., Brito, D.J., Mangabhai, R., Lye, C.Q., 2016. Sustainable Construction Materials: Copper Slag. Woodhead Publishing.

Okamura, H., 1997. Self-Compacting High Perfromance Concrete. Concr. Int. 19, 50–54.

Okamura, H., Ouchi, M., 2003. Self-Compacting Concrete. J. Adv. Concr. Technol. 1, 5–15.

Okamura, H., Ozawa, K., 1995. Mix design for self-compacting concrete. Concr. Libr.

JSCE 25, 107–120.

Ouchi, M., 2000. Self-compacting concrete-development, applications and investigations. Nord. Concr. Res. 23, 29–34.

Ouchi, M., Nakamura, S., Osterson, T., Hallberg, S.Lwin, M., 2003. Applications of self-compacting concrete in Japan, Europe and the United States., in: International Symposium on High Performance Concrete, Orlando, FL. p. 20.

Ouda, A.S., Gawwad, H.A., 2017. The effect of replacing sand by iron slag on physical, mechanical and radiological properties of cement mortar. HBRC J. 13, 255–261. https://doi.org/10.1016/j.hbrcj.2015.06.005

Ouldkhaoua, Y., Benabed, B., Abousnina, R., Kadri, E.H., Khatib, J., 2020. Effect of using metakaolin as supplementary cementitious material and recycled CRT funnel glass as fine aggregate on the durability of green self-compacting concrete. Constr. Build. Mater. 235, 117802. https://doi.org/10.1016/j.conbuildmat.2019.117802

Öz, H.Ö., Gesoglu, M., Güneyisi, E., Mahmood, S.F., 2016. Combined Use of Natural and Artificial Slag Aggregates in Producing Self-Consolidating Concrete. ACI Mater. J. 113, 599.

Ozawa, K., 1989. High-performance concrete based on the durability design of concrete structures., in: Proc. of the Second East Asia-Pacific Conference on Structural Engineering and Construction.

Parashar, A., Aggarwal, P., Saini, B., Aggarwal, Y., Bishnoi, S., 2020. Study on performance enhancement of self-compacting concrete incorporating waste foundry sand. Constr. Build. Mater. 251, 118875.

Poon, C.S., Kou, S.C., Lam, L., 2006. Compressive strength, chloride diffusivity and pore structure of high performance metakaolin and silica fume concrete. Constr. Build. Mater. 20, 858–865.

Prabhu, G.G., Hyun, J.H., Kim, Y.Y., 2014. Effects of foundry sand as a fine aggregate in concrete production. Constr. Build. Mater. 70, 514–521.

https://doi.org/10.1016/j.conbuildmat.2014.07.070

Prem, P.R., Verma, M., Ambily, P.S., 2018. Sustainable cleaner production of concrete with high volume copper slag. J. Clean. Prod. 193, 43–58. https://doi.org/10.1016/j.jclepro.2018.04.245

Rafieizonooz, M., Mirza, J., Salim, M.R., Hussin, M.W., Khankhaje, E., 2016. Investigation of coal bottom ash and fly ash in concrete as replacement for sand and cement. Constr. Build. Mater. 116, 15–24. https://doi.org/10.1016/j.conbuildmat.2016.04.080

Raharjo, D., Subakti, A., Tavio, 2013. Mixed concrete optimization using fly ash, silica fume and iron slag on the SCC's compressive strength. Procedia Eng. 54, 827–839. https://doi.org/10.1016/j.proeng.2013.03.076

Rajasekar, A., Arunachalam, K., Kottaisamy, M., 2019. Assessment of strength and durability characteristics of copper slag incorporated ultra high strength concrete. J. Clean. Prod. 208, 402–414. https://doi.org/10.1016/j.jclepro.2018.10.118

Rehman, S., Iqbal, S., Ali, A., 2018. Combined influence of glass powder and granular steel slag on fresh and mechanical properties of self-compacting concrete. Constr. Build. Mater. 178, 153–160. https://doi.org/10.1016/j.conbuildmat.2018.05.148

Resende, C., Cachim, P.B., Bastos, A.M., 2008. Copper slag mortar properties, in: Materials Science Forum. Trans Tech Publications Ltd, pp. 862–866.

Ridgley, K.E., Abouhussien, A.A., Hassan, A.A.A., Colbourne, B., 2018. Evaluation of abrasion resistance of self-consolidating rubberized concrete by acoustic emission analysis. J. Mater. Civ. Eng. 30, 1–9. https://doi.org/10.1061/(ASCE)MT.1943-5533.0002402

RILEM Technical Committe, 2006. Final report of RILEM TC 188-CSC-Casting of self compacting concrete, Materials and Structures. https://doi.org/10.1617/s11527-006-9186-9

Roy, D.M., Ldorn., G.M., 1982. Hydration, structure, and properties of blast furnace slag

cements, mortars, and concrete. J. Proc. 79, 444–457.

Roychand, R., Gravina, R.J., Zhuge, Y., Ma, X., Youssf, O., Mills, J.E., 2020. A comprehensive review on the mechanical properties of waste tire rubber concrete. Constr. Build. Mater. 237, 117651.

Saeedian, A., Dehestani, M., Asadollahi, S., Vaseghi Amiri, J., 2017. Effect of Specimen Size on the Compressive Behavior of Self-Consolidating Concrete Containing Polypropylene Fibers. J. Mater. Civ. Eng. 29, 04017208. https://doi.org/10.1061/(asce)mt.1943-5533.0002067

Şahmaran, M., Lachemi, M., Erdem, T.K., Yücel, H.E., 2011. Use of spent foundry sand and fly ash for the development of green self-consolidating concrete. Mater. Struct. Constr. 44, 1193–1204. https://doi.org/10.1617/s11527-010-9692-7

Saleh, H.M., El-Sheikh, S.M., Elshereafy, E.E., Essa, A.K., 2019. Mechanical and physical characterization of cement reinforced by iron slag and titanate nanofibers to produce advanced containment for radioactive waste. Constr. Build. Mater. 200, 135–145. https://doi.org/10.1016/j.conbuildmat.2018.12.100

Salhi, M., Ghrici, M., Bilir, T., Uysal, M., 2020. Combined effect of temperature and time on the flow properties of self-compacting concrete. Constr. Build. Mater. 240, 117914.

Sandhu, R.K., Siddique, R., 2019. Strength properties and microstructural analysis of self-compacting concrete incorporating waste foundry sand. Constr. Build. Mater. 225, 371–383. https://doi.org/10.1016/j.conbuildmat.2019.07.216

Savas, B.Z., Ahmad, S., Fedroff, D., 1997. Freeze-thaw durability of concrete with ground waste tire rubber. Transp. Res. Rec. 80–88. https://doi.org/10.3141/1574-11

Scherer, G.W., 1999. Crystallization in pores. Cem. Concr. Res. 29, 1347–1358.

Sharifi, Y., Houshiar, M., Aghebati, B., 2013. Recycled glass replacement as fine aggregate in self-compacting concrete. Front. Struct. Civ. Eng. 7, 419–428. https://doi.org/10.1007/s11709-013-0224-8

Sharma, R., Khan, R.A., 2017a. Fresh and mechanical properties of self compacting concrete containing copper slag as fine aggregates. J. Mater. Eng. Struct. 4, 25–36.

Sharma, R., Khan, R.A., 2017b. Durability assessment of self compacting concrete incorporating copper slag as fine aggregates. Constr. Build. Mater. 155, 617–629. https://doi.org/10.1016/j.conbuildmat.2017.08.074

Sheikh, M.R., Acharyab, B.S., Gartia, R.K., 2010. Characterization of iron slag of Kakching, Manipur by X-ray and optical spectroscopy. Indian J. Pure Appl. Phys. 48, 632–634.

Shi, C., Meyer, C., Behnood, A., 2008. Utilization of copper slag in cement and concrete. Resour. Conserv. Recycl. 52, 1115–1120. https://doi.org/10.1016/j.resconrec.2008.06.008

Shoya, M., Nagataki, S., Tomosawa, F., Sugita, S., Tsukinaga, Y., 1997. Freezing and thawing resistance of concrete with excessive bleeding and its improvement. Spec. Publ. 170, 879–898.

Siddique, R., 2013. Compressive strength, water absorption, sorptivity, abrasion resistance and permeability of self-compacting concrete containing coal bottom ash. Constr. Build. Mater. 47, 1444–1450. https://doi.org/10.1016/j.conbuildmat.2013.06.081

Siddique, R., 2007. Waste materials and by-products in concrete. Springer Science & Business Media.

Siddique, R., Aggarwal, Y., Aggarwal, P., Kadri, E.H., Bennacer, R., 2011. Strength, durability, and micro-structural properties of concrete made with used-foundry sand (UFS). Constr. Build. Mater. 25, 1916–1925.

Siddique, R., Sandhu, R.K., 2013. Properties of Self-Compacting Concrete Incorporating Waste Foundry. Leonardo J. Sci. 105–124.

Siddique, R., Schutter, G. De, Noumowe, A., 2009. Effect of used-foundry sand on the mechanical properties of concrete. Constr. Build. Mater. 23, 976–980.

https://doi.org/10.1016/j.conbuildmat.2008.05.005

Singh, G., Siddique, R., 2016a. Strength properties and micro-structural analysis of self-compacting concrete made with iron slag as partial replacement of fine aggregates. Constr. Build. Mater. 127, 144–152. https://doi.org/10.1016/j.conbuildmat.2016.09.154

Singh, G., Siddique, R., 2016b. Effect of iron slag as partial replacement of fine aggregates on the durability characteristics of self-compacting concrete. Constr. Build. Mater. 128, 88–95. https://doi.org/10.1016/j.conbuildmat.2016.10.074

Singh, G., Siddique, R., 2012. Effect of waste foundry sand (WFS) as partial replacement of sand on the strength, ultrasonic pulse velocity and permeability of concrete. Constr. Build. Mater. 26, 416–422. https://doi.org/10.1016/j.conbuildmat.2011.06.041

Singh, J., Singh, S.P., 2020a. Synthesis of alkali-activated binder at ambient temperature using copper slag as precursor. Mater. Lett. 262, 127169.

Singh, J., Singh, S.P., 2020b. Evaluating the alkali-silica reaction in alkali-activated copper slag mortars. Constr. Build. Mater. 253, 119189.

Singh, M., Siddique, R., 2015. Properties of concrete containing high volumes of coal bottom ash as fine aggregate. J. Clean. Prod. 91, 269–278. https://doi.org/10.1016/j.jclepro.2014.12.026

Singh, M., Siddique, R., 2014. Strength properties and micro-structural properties of concrete containing coal bottom ash as partial replacement of fine aggregate. Constr. Build. Mater. 50, 246–256. https://doi.org/10.1016/j.conbuildmat.2013.09.026

Singh, N., Mithulraj, M., Arya, S., 2019. Utilization of coal bottom ash in recycled concrete aggregates based self compacting concrete blended with metakaolin. Resour. Conserv. Recycl. 144, 240–251. https://doi.org/10.1016/j.resconrec.2019.01.044

Singh, R.B., Singh, B., 2018. Rheological behaviour of different grades of self-

compacting concrete containing recycled aggregates. Constr. Build. Mater. 161, 354–364.

Singh, D. V., Sachan, A.K., Rawat, A., 2016. Developments in Corrosion Detection Techniques for Reinforced Concrete Structures. Indian J. Sci. Technol 9.

Smarzewski, P., 2020. Mechanical Properties of Ultra-High Performance Concrete with Partial Utilization of Waste Foundry Sand. Buildings 10, 11.

Sormunen, P., Kärki, T., 2019. Recycled construction and demolition waste as a possible source of materials for composite manufacturing. J. Build. Eng. 24, 100742.

Su, N., Hsu, K.C., Chai, H.W., 2001. A simple mix design method for self-compacting concrete. Cem. Concr. Res. 31, 1799–1807. https://doi.org/10.1016/S0008-8846(01)00566-X

Sua-iam, G., Makul, N., Cheng, S., Sokrai, P., 2019. Workability and compressive strength development of self-consolidating concrete incorporating rice husk ash and foundry sand waste – A preliminary experimental study. Constr. Build. Mater. 228, 116813. https://doi.org/10.1016/j.conbuildmat.2019.116813

Sukontasukkul, P., 2009. Use of crumb rubber to improve thermal and sound properties of pre-cast concrete panel. Constr. Build. Mater. 23, 1084–1092. https://doi.org/10.1016/j.conbuildmat.2008.05.021

Taha, M.M.R., El-Dieb, A.., M.A, E.-W., Abdel-Hameed, M.., 2008. Mechanical, Fracture, and Microstructural Investigations of Rubber Concrete. J. Mater. Civ. Eng. 20, 640–649. https://doi.org/10.1061/(ASCE)0899-1561(2008)20

Tam, C.M., Tam, V.W., Ng, K.M., 2012. Assessing drying shrinkage and water permeability of reactive powder concrete produced in Hong Kong. Constr. Build. Mater. 26, 79–89.

Tang, W., Khavarian, M., Yousefi, A., Cui, H., 2020. Properties of self-compacting concrete with recycled concrete aggregates., in: Self-Compacting Concrete: Materials, Properties and Applications. Woodhead Publishing, pp. 219–248.

Thomas, B.S., Damare, A., Gupta, R.C., 2013. Strength and durability characteristics of copper tailing concrete. Constr. Build. Mater. 48, 894–900. https://doi.org/10.1016/j.conbuildmat.2013.07.075

Tian, B., Cohen., M.D., 2000. Does gypsum formation during sulfate attack on concrete lead to expansion? Cem. Concr. Res. 30, 117–123.

Topçu, İ.B., Bilir, T., 2009. Experimental investigation of some fresh and hardened properties of rubberized self-compacting concrete. Mater. Des. 30, 3056–3065.

Torres, A., Bartlett, L., Pilgrim, C., 2017. Effect of foundry waste on the mechanical properties of Portland Cement Concrete. Constr. Build. Mater. 135, 674–681. https://doi.org/10.1016/j.conbuildmat.2017.01.028

Wang, H.Y., Huang, W.L., 2010a. Durability of self-consolidating concrete using waste LCD glass. Constr. Build. Mater. 24, 1008–1013. https://doi.org/10.1016/j.conbuildmat.2009.11.018

Wang, H.Y., Huang, W.L., 2010b. A study on the properties of fresh self-consolidating glass concrete (SCGC). Constr. Build. Mater. 24, 619–624. https://doi.org/10.1016/j.conbuildmat.2009.08.047

Wong, A.C.L., Childs, P.A., R. Berndt, T.M., Peng, G.D., Gowripalan., N., 2007. Simultaneous measurement of shrinkage and temperature of reactive powder concrete at early-age using fibre Bragg grating sensors. Cem. Concr. Compos. 29, 490–497.

Wongkeo, W., Chaipanich, A., 2010. Compressive strength, microstructure and thermal analysis of autoclaved and air cured structural lightweight concrete made with coal bottom ash and silica fume. Mater. Sci. Eng. A 527, 3676–3684. https://doi.org/10.1016/j.msea.2010.01.089

Wu, W., Zhang, W., Ma, G., 2010. Optimum content of copper slag as a fine aggregate in high strength concrete. Mater. Des. 31, 2878–2883. https://doi.org/10.1016/j.matdes.2009.12.037

Youssf, O., Elgawady, M.A., Mills, J.E., Ma, X., 2014. An experimental investigation of crumb rubber concrete confined by fibre reinforced polymer tubes. Constr. Build. Mater. 53, 522–532. https://doi.org/10.1016/j.conbuildmat.2013.12.007

Youssf, O., Mills, J.E., Benn, T., Zhuge, Y., Ma, X., Roychand, R., Gravina, R., 2020. Development of Crumb Rubber Concrete for Practical Application in the Residential Construction Sector–Design and Processing. Constr. Build. Mater. 260, 119813.

Yu, C., Sun, W., Scrivener., K., 2013. Mechanism of expansion of mortars immersed in sodium sulfate solutions. Cem. Concr. Res. 43, 105–111.

Yüksel, I., Bilir, T., Özkan, Ö., 2007. Durability of concrete incorporating non-ground blast furnace slag and bottom ash as fine aggregate. Build. Environ. 42, 2651–2659. https://doi.org/10.1016/j.buildenv.2006.07.003

Yung, W.H., Yung, L.C., Hua, L.H., 2013. A study of the durability properties of waste tire rubber applied to self-compacting concrete. Constr. Build. Mater. 41, 665–672. https://doi.org/10.1016/j.conbuildmat.2012.11.019

Zhang, J., Han, Y.D., Gao, Y., 2014. Effects of water-binder ratio and coarse aggregate content on interior humidity, autogenous shrinkage, and drying shrinkage of concrete. J. Mater. Civ. Eng. 26, 184–189.

Zhang, X., Chen, J., Jiang, J.J., Li, J., Tyagi, R.D., Surampalli, R.Y., 2019. The potential utilization of slag generated from iron- and steelmaking industries: a review. Environ. Geochemistry Heal. 42, 1321–1334. https://doi.org/10.1007/s10653-019-00419-y

APPENDIX A

Multiple Comparisons between Compressive Strength of SCC using Post Hoc Tukey

Curing Age (days)	Copper Slag (%)	Copper Slag (%)	Significance (p-value)
28	0	10	.099
		20	.039*
		30	.556
		40	.999
		50	1.000
		60	1.000
	10	0	.099
		20	.998
		30	.883
		40	.198
		50	.102
		60	.093
	20	0	.039*
		10	.998
		30	.611
		40	.083
		50	.041*
		60	.037*
	30	0	.556
		10	.883
		20	.611
		40	.794
		50	.566
		60	.533
	40	0	.999
		10	.198
		20	.083
		30	.794
		50	1.000
		60	.999
	50	0	1.000
		10	.102
		20	.041*
		30	.566
		40	1.000
		60	1.000
	60	0	1.000
		10	.093
		20	.037*
		30	.533
		40	.999
		50	1.000

Curing Age (Days)	Copper slag (%)	Copper Slag (%)	Significance (p-value)
90	0	10	1.000
		20	.113
		30	.370
		40	1.000
		50	1.000
		60	1.000
	10	0	1.000
		20	.116
		30	.378
		40	1.000
		50	1.000
	20	60	1.000
		0	.113
		10	.116
		30	.983
		40	.160
		50	.136
		60	.098
	30	0	.370
		10	.378
		20	.983
		40	.481
		50	.426
		60	.332
	40	0	1.000
		10	1.000
		20	.160
		30	.481
		50	1.000
		60	1.000
	50	0	1.000
		10	1.000
		20	.136
		30	.426
		40	1.000
		60	1.000
	60	0	1.000
		10	1.000
		20	.098
		30	.332
		40	1.000
		50	1.000
*p value < 0.05 (significant)			

APPENDIX B

Multiple Comparisons between Splitting Tensile Strength of SCC using Post Hoc Tukey

Curing Age (Days)	Copper slag (%)	Copper Slag (%)	Significance (p-value)
7	0	10	1.000
		20	.285
		30	.082
		40	.077
		50	.022*
		60	.030*
	10	0	1.000
		20	.425
		30	.136
		40	.128
		50	.039*
		60	.052
	20	0	.285
		10	.425
		30	.984
		40	.979
		50	.738
		60	.822
	30	0	.082
		10	.136
		20	.984
		40	1.000
		50	.988
		60	.997
	40	0	.077
		10	.128
		20	.979
		30	1.000
		50	.991
		60	.998
	50	0	.022*
		10	.039*
		20	.738
		30	.988
		40	.991
		50	1.000
	60	0	.030*
		10	.052
		20	.822
		30	.997
		40	.998
		50	1.000

Curing Age (Days)	Copper slag (%)	Copper Slag (%)	Significance (p-value)
28	0	10	.711
		20	.143
		30	.004*
		40	.005*
		50	.010*
		60	.005*
	10	0	.711
		20	.863
		30	.074
		40	.090
		50	.152
		60	.076
	20	0	.143
		10	.863
		30	.488
		40	.550
		50	.732
		60	.494
	30	0	.004*
		10	.074
		20	.488
		40	1.000
		50	.999
		60	1.000
	40	0	.005*
		10	.090
		20	.550
		30	1.000
		50	1.000
		60	1.000
	50	0	.010*
		10	.152
		20	.732
		30	.999
		40	1.000
		50	.999
	60	0	.005*
		10	.076
		20	.494
		30	1.000
		40	1.000
		50	.999

Curing Age (Days)	Copper slag (%)	Copper Slag (%)	Significance (p-value)
90	0	10	.243
		20	.061
		30	.042*
		40	.039*
		50	.006*
		60	.002*
	10	0	.243
		20	.976
		30	.933
		40	.919
		50	.373
		60	.188
	20	0	.061
		10	.976
		30	1.000
		40	1.000
		50	.831
		60	.571
	30	0	.042*
		10	.933
		20	1.000
		40	1.000
		50	.915
		60	.695
	40	0	.039*
		10	.919
		20	1.000
		30	1.000
		50	.929
		60	.721
	50	0	.006*
		10	.373
		20	.831
		30	.915
		40	.929
		50	.999
	60	0	.002*
		10	.188
		20	.571
		30	.695
		40	.721
		50	.999

Curing Age (Days)	Copper slag (%)	Copper Slag (%)	Significance (p-value)
365	0	10	.193
		20	.032*
		30	.016*
		40	.006*
		50	.003*
		60	.001*
	10	0	.193
		20	.932
		30	.784
		40	.452
		50	.287
		60	.103
	20	0	.032*
		10	.932
		30	1.000
		40	.956
		50	.843
		60	.485
	30	0	.016*
		10	.784
		20	1.000
		40	.996
		50	.961
		60	.696
	40	0	.006*
		10	.452
		20	.956
		30	.996
		50	1.000
		60	.947
	50	0	.003*
		10	.287
		20	.843
		30	.961
		40	1.000
		50	.994
	60	0	.001*
		10	.103
		20	.485
		30	.696
		40	.947
		50	.994
*p value < 0.05 (significant)			

APPENDIX C

Multiple Comparisons between Water Absorption of SCC using Post Hoc Tukey

Curing Age (Days)	Copper slag (%)	Copper Slag (%)	Significance (p-value)
365	0	10	.430
		20	.014*
		30	.107
		40	.128
		50	.625
		60	.991
	10	0	.430
		20	.413
		30	.961
		40	.978
		50	1.000
		60	.817
	20	0	.014*
		10	.413
		30	.901
		40	.861
		50	.259
		60	.048*
	30	0	.107
		10	.961
		20	.901
		40	1.000
		50	.854
		60	.316
	40	0	.128
		10	.978
		20	.861
		30	1.000
		50	.895
		60	.364
	50	0	.625
		10	1.000
		20	.259
		30	.854
		40	.895
		50	.943
	60	0	.991
		10	.817
		20	.048*
		30	.316
		40	.364
		50	.943
*p value < 0.05 (significant)			

APPENDIX D

Multiple Comparisons between Sorptivity values of SCC using Post Hoc Tukey

Curing Age (Days)	Copper Slag (%)	Copper Slag (%)	Significance (p-value)
365	0	10	.428
		20	.004*
		30	.023*
		40	.090
		50	.498
		60	.994
	10	0	.428
		20	.139
		30	.571
		40	.939
		50	1.000
		60	.788
	20	0	.004*
		10	.139
		30	.939
		40	.571
		50	.112
		60	.011*
	30	0	.023*
		10	.571
		20	.939
		40	.984
		50	.498
		60	.072
	40	0	.090
		10	.939
		20	.571
		30	.984
		50	.900
		60	.254
	50	0	.498
		10	1.000
		20	.112
		30	.498
		40	.900
		50	.849
	60	0	.994
		10	.788
		20	.011*
		30	.072
		40	.254
		50	.849
*p value < 0.05 (significant)			

ANNEXURE E

Multiple Comparisons between RCPT values of SCC using Post Hoc Tukey

Curing Age (Days)	Copper Slag (%)	Copper Slag (%)	Significance (p-value)
28	0	10	.000*
		20	.000*
		30	.000*
		40	.000*
		50	.001*
		60	.497
	10	0	.000*
		20	.000*
		30	.001*
		40	.402
		50	.000*
		60	.000*
	20	0	.000*
		10	.000*
		30	.896
		40	.000*
		50	.000*
		60	.000*
	30	0	.000*
		10	.001*
		20	.896
		40	.000*
		50	.000*
		60	.000*
	40	0	.000*
		10	.402
		20	.000*
		30	.000*
		50	.012*
		60	.000*
	50	0	.001*
		10	.000*
		20	.000*
		30	.000*
		40	.012*
		60	.017*
	60	0	.497
		10	.000*
		20	.000*
		30	.000*
		40	.000*
		50	.017*

Curing Age (Days)	Copper Slag (%)	Copper Slag (%)	Significance (p-value)
90	0	10	.047*
		20	.000*
		30	.003*
		40	.043*
		50	.407
		60	.874
	10	0	.047*
		20	.026*
		30	.696
		40	1.000
		50	.813
		60	.341
	20	0	.000*
		10	.026*
		30	.357
		40	.029*
		50	.002*
		60	.001*
	30	0	.003*
		10	.696
		20	.357
		40	.724
		50	.114
		60	.025*
	40	0	.043*
		10	1.000
		20	.029*
		30	.724
		50	.788
		60	.318
	50	0	.407
		10	.813
		20	.002*
		30	.114
		40	.788
		60	.972
	60	0	.874
		10	.341
		20	.001*
		30	.025*
		40	.318
		50	.972

Curing Age (Days)	Copper Slag (%)	Copper Slag (%)	Significance (p-value)
365	0	10	.872
		20	.001*
		30	.011*
		40	.023*
		50	.087
		60	.967
	10	0	.872
		20	.006*
		30	.096
		40	.195
		50	.528
		60	1.000
	20	0	.001*
		10	.006*
		30	.697
		40	.452
		50	.157
		60	.003*
	30	0	.011*
		10	.096
		20	.697
		40	.999
		50	.895
		60	.054
	40	0	.023*
		10	.195
		20	.452
		30	.999
		50	.987
		60	.114
	50	0	.087
		10	.528
		20	.157
		30	.895
		40	.987
		50	.353
	60	0	.967
		10	1.000
		20	.003*
		30	.054
		40	.114
		50	.353
*p value < 0.05 (significant)			